Innovative Spectroscopic and Chromatographic Techniques for the Analysis of Complex Polyolefins Prepared by Metallocene Catalysis

Sven Markus Graef

M.Sc. Polymer Science

Dissertation presented for the degree of

Doctor of Philosophy in Polymer Science

at the

University of Stellenbosch

Promoter:

Prof. H. Pasch
Deutsches Kunststoff Institute
Darmstadt
Germany

Co-promoter:

Prof. R. D. Sanderson
Division of Polymer Science
Department of Chemistry
University of Stellenbosch
Stellenbosch
South Africa

Stellenbosch

December 2002

DECLARATION

I, the undersigned, hereby declare that the work contained in this thesis is my own original work and has not previously in its entire or in part been submitted at any university for a degree.

Signature Date

Innovative Spectroscopic and Chromatographic Techniques for the Analysis of Complex Polyolefins Prepared by Metallocene Catalysts

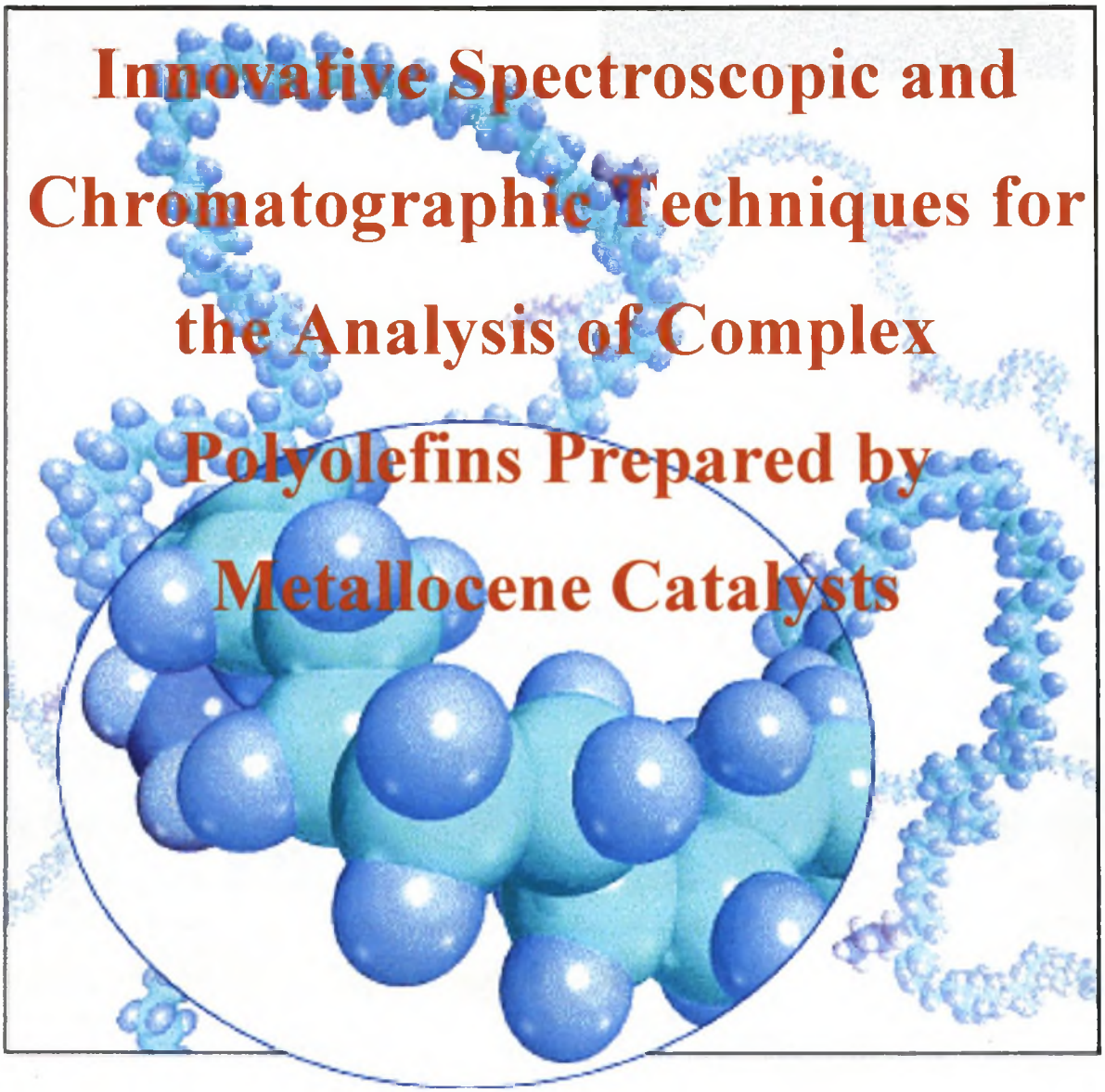

Sven M Graef

Summary

The study focused on the analysis of a variety of synthesised tailored copolymers. During the investigation of the samples new and innovative analytical techniques were developed to be able to identify the presence of certain predicted or expected copolymerisation products.

Emphasis was placed on the versatility of CRYSTAF as a method for the analysis of semi-crystalline copolymers. Changes in the crystallisation temperature were used as an indicator, while the type of method, solvent and sample weight served as variables in the system. The percentage comonomer content distribution for an unknown sample was determined from the standard curve plotted with the aid of copolymers with known comonomer content.

Ethylene/higher α-olefin and propylene/higher α-olefin copolymers were synthesised by means of a metallocene precatalyst. In both cases, NMR spectroscopy, DSC, GPC, and CRYSTAF were used as analytical tools. In the ethylene series it was shown that the sample mixture was homogenous in the molar mass axis (GPC) but not in the chemical composition axis (CRYSTAF) regarding the comonomer content. For the propylene series, an increase in stereoerrors was observed by NMR and this was correlated with crystallisation on heating a DSC for the range of copolymers.

In the case where ethylene/methyl methacrylate block copolymers were synthesised using metallocene precatalyst, novel detection and separation methods were used and developed. This included the use of CRYSTAF fitted with a carbonyl filter, high temperature gradient HPLC and high temperature liquid chromatography under critical conditions (LCCC). The last two techniques were the first where separation could be achieved with samples only dissolving at high temperature. All previous mentioned techniques, as well as the coupling of FTIR to GPC and high temperature gradient HPLC via LC-Transform revealed that the samples consisted of varying ethylene and MMA block lengths.

Opsomming

Die doelstelling van die navorsing was die analise van spesiaalvervaardigde kopolimere. Nuwe analitiese tegnieke is vir die bevestiging van sekere voorgestelde kopolimerisasie-produkte ontwikkel.

Klem is gelê op die veelsydigheid van CRYSTAF as 'n metode vir die analise van gedeeltelik-kristallyne kopolimere. Veranderinge in die kristallisasie-temperature is as respons gebruik, terwyl die metode van sintese, die oplosmiddel en die hoeveelheid monster as veranderlikes in die sisteem beskou is. 'n Standaardkurwe vir komonomeerinhoud is opgestel met behulp van kopolimere met 'n bekende komonomeerinhoud. Hierdie kurwe is gebruik om die komonomeerinhouds-verspreiding van onbekende monsters te bepaal.

Etileen/hoër α-olefien- en propileen/hoër α-olefien-kopolimere is met behulp van 'n metalloseen pre-katalis gesintetiseer. In beide gevalle is KMR spektroskopie, DSC, GPC en CRYSTAF gebruik om die analises uit te uitvoer. Met verwysing na komonomeerinhoud is daar in die geval van die etileenreeks bevind dat die monstermengsel homogeen is met betrekking tot die molêre massa, maar nie met betrekking tot die chemiese samestelling nie. Vir die propileenreeks is 'n verhoging in die stereofoute met behulp van KMR waargeneem. Dit is gekorrelleer met kristallisasie weens verhitting tydens DSC-bepalings vir die reeks kopolimere.

In die geval van die sinteses van etileen/metielmetakrilaat-blokkopolimere met metalloseen as pre-katalis, moes nuwe waarnemings- en skeidingstegnieke ontwikkel word. Dit het die gebruik van CRYSTAF met 'n karbonielfilter, hoë-temperatuurgradiënt-HPLC en hoë-temperatuurvloeistofchromatografie onder kritiese toestande ingesluit. Laasgenoemde twee tegnieke het vir die eerste keer skeiding van monsters wat net by hoë temperature oplos, moontlik gemaak. Bogenoemde tegnieke, sowel as die koppeling van FTIR met GPC en hoë-temperatuur-gradiënt-HPLC via LC-transformasie het getoon dat die monsters etileen- en MMA-blokke met verskillende lengtes bevat het.

List of contents

Chapter 1

Overview

Chapter 2

Historical and theoretical background

Chapter 3

Experimental

Chapter 4

Polyolefin crystallisation in solution measured by Crystallisation Analysis Fractionation (CRYSTAF)

Chapter 5

Copolymerisation of propylene with higher α-olefins in the presence of the syndiospecific catalyst *i*-Pr(Cp)(9-Flu)$ZrCl_2$ / MAO

Chapter 6

Copolymerisation of ethylene with higher α-olefins in the presence of the metallocene catalyst $Et(Ind)_2ZrCl_2$ / MAO

Chapter 7

Ethylene and Methyl Methacrylate block copolymers synthesised by the $Me_2CCpIndZrMe_2/B(C_6F_5)_3$ catalyst system

Chapter 8

Conclusions

List of Figures

Chapter 2

Chapter 3

Chapter 4

Chapter 5

Chapter 6

Chapter 7

List of Schemes

Chapter 2

Chapter 3

Chapter 5

Chapter 6

Chapter 7

List of Tables

Chapter 2

Chapter 3

Chapter 4

Chapter 5

Chapter 6

Chapter 7

List of Abbreviations

^{13}C	Carbon thirteen
^{1}H	Proton
ATR	Attenuated total reflection
Br	Backbone carbon from where side branches originate
CB	Chlorobenzene
CC	Comonomer-comonomer interaction
CCD	Chemical composition distribution
CF	Cross fractionation
CH	Cyclohexanone
CP	Critical point
CRYSTAF	Crystallisation analysis fractionation
DCB	1,2-Dichlorobenzene
DMA	Dynamic mechanical analysis
DMF	N,N-Dimethylformamide
DSC	Differential scanning calorimetry
FTD	Functionality type distribution
FTIR	Fourier transform infrared
GC	Gas chromatography
GPC	Gel permeation chromatography
HDPE	High density polyethylene
HPLC	High performance liquid chromatography
HTG-HLPC	High temperature gradient high performance liquid chromatography
ID	Internal diameter
i-PP	Isotactic polypropylene
IR	Infrared
LCCC	Liquid chromatography under critical conditions
LDPE	Low density polyethylene
LES	Longest ethylene sequence
LLDPE	Linear low density polyethylene
m	Meso (tacticity in NMR)

MAO	Methylalumoxane
MMA	Methyl methacrylate
MMD	Molar mass distribution
M_n	Number-average molar number (g/mol)
M_p	Molar mass peak maximum (g/mol)
MP	Melting point
M_w	Weight-average molar mass (g/mol)
NMR	Nuclear magnetic resonance
PC	Propylene-comonomer interaction
PE	Polyethylene
PMMA	Poly(methyl methacrylate)
PP	Polypropylene
r	Racemic (tacticity in NMR)
SCB	Short chain branching
SCBD	Short chain branch distribution
SEC	Size exclusion chromatography
s-PP	Syndiotactic polypropylene
T_c	Crystallisation point temperature (°C)
$T_{c\ (CRYSTAF)}$	Crystallisation point temperature in solution measured by CRYSTAF
$T_{c\ (DSC)}$	Crystallisation point temperature measured by DSC (°C)
$T_{c\ (DSC,\ heat)}$	Crystallisation temperature on heating in DSC (cold crystallisation) (°C)
TCB	1,2,4-Trichlorobenzene
TClEt	1,1,2,2-Tetrachloroethylene
T_g	Glass transition temperature (°C)
TLC	Thin layer chromatography
T_m	Melting point temperature (°C)
$T_{m\ (DSC)}$	Melting point temperature measured by DSC (°C)
TREF	Temperature rising elution fractionation
ΔH	Heat of fusion (J/g)

Acknowledgements

I would like to thank the following people and institutions that made this study possible:

1) Prof. H Pasch, for his leadership during the course of my study, showing me how best to approach analytical problems and the methods available for solving them. His unique insight into a problem and the critical manner in which he taught me to look at my data has proved to be very valuable.

2) Prof. R D Sanderson, for allowing me the opportunity to do part of my studies overseas to acquire the necessary skills and knowledge, not only to finish my Ph D but also enabling me to assist other students in their research.

3) SASOL Polymers, the National Research Foundation of South Africa, the Jülich fund in Germany, as well as the BMBF in Germany, for their financial support during my studies both in South Africa and Germany.

4) S Balk and H Keul at the Institut für Technische Chemie und Makromolekulare Chemie at RWTH Aachen, Germany. The ethylene/methyl methacrylate copolymer samples where obtained through collaboration with this group. Valuable information was exchanged in meetings regarding the reaction mechanism for the synthesis of ethylene/MMA with metallocene catalysts and the possible products formed during the reactions.

5) B Monrabal, from Polymer Char, Valencia Spain, who assisted me in method development on the CRYSTAF. Thanks to him I also had the opportunity to visit Spain and see the manufacturing process of the CRYSTAF. Further assistance was rendered in the analysis of the ethylene/methyl methacrylate copolymer samples by means of a special carbonyl detector on the CRYSTAF.

6) C Brinkmann, for assistance with the gel permeation chromatography, R Brüll, with the LC-Transform data analysis, and T Macko, for analyses of the ethylene/methyl methatcrylate copolymers by liquid chromatography under critical conditions at the Deutsches Kunststoff Institut in Darmstadt Germany. I also acknowledge all the other staff and students at the Institute who assisted me during my visits.

7) S de Goede at SASOL Polymers, my mentor for the duration of my studies, on whom I could always rely for advice.

8) I would like to thank my fellow students and friends at the Institute for Polymer Science that were there in the good as well as the bad times. In this regard, I would especially like to mention A van Zyl and J McLeary for their stimulating discussions regarding the obstacles I faced during the course of my study.

9) My friends, that made these years as memorable as they were.

10) A special thanks also goes to M Smit for her support during my studies and her assistance with correcting the manuscript.

11) Dr. A van Reneen, for advising me on changes that could be made in the method of the reaction setup, as well as the interpretation of the NMR data.

12) A Fourie and E Cooper for assistance with official matters.

13) Dr M J Hurndall, who assisted me with the grammatical corrections of both my articles and the final manuscript.

14) Last, but by no means least, I would like to thank my parents who always had confidence in my abilities and believed that I could achieve anything I set my mind to, despite my dyslexia. I would like to thank them for teaching me the moral of life, what is right and what is wrong, how to behave and to respect other people.

Publications and posters that have resulted from this research

1. *Copolymerization of Propylene with Higher a-Olefins in the Presence of the Syndiospecific Catalyst i-Pr(Cp)(9-Flu)ZrCl2/MAO*; SM Graef, U Wahner, R Brüll, AJ van Reenen, RD Sanderson and H Pasch; Journal of Polymer Science Part A; Polymer Chemistry; Volume 40, Number 1, issue dated January 1, 2002.

2. *Synthesis and Characterisation of Syndiotactic Polypropylene Copolymers with Higher α-Olefins*; SM Graef, H Pasch, U Wahner, R Brull, J van Reenen, RD Sanderson; 4th annual UNESCO school and IUPAC conference; 2001, Stellenbosch, South Africa.

3. *Synthesis and Characterisation of Syndiotactic Polypropylene Copolymers with Higher α-Olefins*; SM Graef, H Pasch, U Wahner, R Brull, J van Reenen, RD Sanderson; Europolymer Congress, 15-20 July 2001; Eindhoven University of Technology; Eindhoven; Netherlands.

4. *Synthesis and Characterisation of Syndiotactic Polypropylene Copolymers with Higher α-Olefins*; SM Graef, H Pasch, U Wahner, R Brull, J van Reenen, RD Sanderson; 222nd ACS National Meeting; 26-30 August 2001; Chicago; Illinois; United States of America.

5. *Polyolefinanalytik mit der Kristallisationsfraktionierung*; R Brüll, SM Graef, H Pasch, K Rode, U Wahner; GDCh Fachgruppen Tagung; 14 March; 2002; Darmstadt; Germany.

6. *Copolymers of Methyl Methacrylate and Ethylene Utilizing Methylated Metallocene Catalysis*; SM Graef, S Balk, H Keul, RD Sanderson, H Pasch; 5nd annual UNESCO school and IUPAC conference; 25-28 March; 2002; Stellenbosch; South Africa.

CHAPTER 1

Overview

1.1 Introduction

Developments in the polyolefin field have seen explosive growth over the last two decades for metallocenes catalysts, advancing from academic interest to industrial applications. Statistics recently published show that low density (LDPE)-, linear low density (LLDPE)-, high density polyethylene (HDPE) and polypropylene (PP) make up the bulk mass of the 120 million tonnes of polymers that are produced annually [1].

The exponential growth in the number and diversity of polyolefin products has not been met with the same technological advances in the field of analysis. Only in recent years have scientists developed advanced chromatographic methods for the tailor-made analysis of these semi-crystalline polymers i.e. high temperature gel permeation chromatography (HT-GPC), GPC-FTIR (Fourier transform infrared spectroscopy) coupling, temperature rising elution fractionation (TREF) and crystallisation analysis fractionation (CRYSTAF). Further advances in polyolefin research, with special reference to the once thought impossible copolymerisation of α-olefins with polar monomers [2], has lead to further challenges for the analyst in this field.

The potential of various chromatographic methods, with reference to the analysis of polyolefins and ethylene/ methyl methacrylate copolymers prepared by using metallocene catalysts, as well as their limitations are the focus of this study. CRYSTAF is a new technique that was developed for the determination of the crystallisation temperature of semi-crystalline polymers in solution. The effect of

different temperature programs on the crystallisation temperature of the samples under discussion was studied. By studying the crystallisation curves obtained by CRYSTAF and the spectra obtained by NMR spectroscopy, deductions regarding the reaction mechanisms could be made. We report here, for the first time in literature, the separation of ethylene/methyl methacrylate copolymers by gradient HPLC (high performance liquid chromatography) at elevated temperatures. High temperature gradient HPLC was used in the separation of ethylene/methyl methacrylate copolymers to determine the presence of block structures. Use of LC-Transform enabled for the unique coupling of the GPC or high temperature gradient HPLC to FTIR spectroscopy. This coupling allowed for the simultaneous detection of the different monomer units (ethylene/α-olefins and ethylene/methyl methacrylate) in a chromatogram.

1.2 Objectives

1. CRYSTAF is a new analytical technique with room for method improvement. This was to be addressed in terms of the following.
   - Instrumental parameter settings for analyses will be investigated to show which parameters should be improved for better and faster analysis.
   - The influence of the tared amount of samples used for analysis and the effect of solvent on the crystallisation temperature in CRYSTAF will be investigated.
   - By using copolymers of known comonomer composition and drawing up a standard calibration curve, the comonomer content distribution of an unknown copolymer will be determined.

2. The product of the copolymerisation of propylene/ higher α-olefins with the *i*-Pr(Cp)(9-Flu)$ZrCl_2$/ MAO catalyst will be analysed.
   - NMR spectroscopy will be used to the study the reaction mechanism of the catalyst system.

- DSC curves will be analysed to ascertain whether there is any relationship between the melting temperatures and the comonomer incorporation.
- Investigation will also focus on the different melting and crystallisation peaks that occur on heating and cooling in DSC, with regarding to the phenomenon of cold crystallisation.
- A relationship between the crystallisation in CRYSTAF and DSC results will be checked to see if the data show any correlations.

3. The product of the copolymerisation of ethylene/ higher α-olefins with $Et(Ind)_2ZrCl_2$ / MAO catalyst will be analysed.
   - The relationship between the crystallisation in CRYSTAF and DSC results will be followed for copolymers with different comonomer concentrations to see if the data show any correlation.
   - CRYSTAF diagrams will be studied to determine the heterogeneity in different copolymer samples.
   - By coupling FITR spectroscopy to GPC, this investigation will focus on the comonomer distribution according to molar mass.

4. Different analytical techniques will be employed to prove the presence of block copolymer formation during the synthesis of ethylene and MMA with the $Me_2C(Cp)(Ind)ZrMe_2$ / $B(C_6F_5)_3$ catalyst. These include:
   - GPC
   - DSC
   - GPC coupled to FITR spectroscopy via LC-Transfrom
   - High temperature gradient HPLC
   - High temperature LCCC

The latter two techniques need to be developed from scratch, as they are novel.

1.3 Layout of this dissertation

The range and limitations of the above-mentioned chromatographic methods will be discussed under the following headings while, for ease of reference, the experimental details are all given in Chapter 3.

1.3.1 Polyolefin crystallisation in solution measured by Crystallisation Analysis Fractionation (CRYSTAF)

The separation of polymer fractions, as a function of a temperature profile, was introduced by B. Monrabal in 1991 [3]. This method has been successfully used for the analysis of α-olefins, providing information regarding a particular polymer's chemical composition distribution. The purpose of this investigation is to assess the effect of instrumental parameters on experimental results obtained by this method, processing the obtained data and looking at further developing this method for the analysis of specific polymers (Chapter 4).

1.3.2 Copolymerisation of propylene with higher α-olefins in the presence of the syndiospecific catalyst *i*-Pr(Cp)(9-Flu)$ZrCl_2$/ MAO

Detailed analysis of propylene and higher α-olefin copolymers (1-hexene, 1-dodecene and 1-octadecene) by nuclear magnetic resonance (NMR) spectroscopy, differential scanning calorimetry (DSC) and CRYSTAF analysis is described. Special attention was given to the catalyst mechanism, resolved by NMR spectroscopy (Chapter 5).

1.3.3 Copolymerisation of ethylene with higher α-olefins in the presence of the metallocene catalyst Et$(Ind)_2ZrCl_2$/ MAO

This section can be regarded as supplementary to the LLDPE samples analysed by CRYSTAF, as seen in Chapter 4, as well as results of existing data as published in literature on ethylene copolymers [4]. Similarities between the results obtained in this section and that of the polypropylene analysis (in Chapter 5) will be highlighted. The

comonomer distribution heterogeneity of the samples will be investigated in terms of both the molar mass distribution (GPC-FTIR) and the chemical composition distribution (CRYSTAF) (Chapter 6).

1.3.4 Ethylene and methyl methacrylate block copolymers synthesised by metallocene catalysts

The unique copolymerisation of a polar monomer with an α-olefin by means of a metallocene precatalyst and a borate cocatalyst was first reported by Höcker *et al.* [2]. Polymer samples (ethylene/MMA copolymers) supplied by this research group were analysed via spectroscopic and chromatographic methods to obtain information regarding their chemical composition distribution and microstructure. The subsequent analysis of these polymers did not allow for the use of existing standard and high temperature chromatographic methods. For this reason new and innovative analytical methods had to be developed, namely high temperature gradient HPLC and high temperature liquid chromatography under critical conditions. These methods and results of analyses are described in Chapter 7.

1.4 References

1. DPI, *Annual report*, 2001.
2. Frauenrath H, Balk S, Keul H, Höcker H, Macromol. Rapid. Commun., 2001, **22**, 1147.
3. Monrabal B, US Patent 5 222 390, 1991.
4. Reddy S S, Sivaram S, Prog. Polym. Sci., 1995, **20** (2), 309.

CHAPTER 2

Historical and theoretical background

2.1 Introduction

The aim of this chapter is to introduce the field of transition metal catalysis and the theory behind these transition metal catalysed polyolefin systems, as well as to discuss the significance of analytical methods for polyolefm analysis.

2.2 Transition metal-based catalysts for polyethylene and polypropylene synthesis

2.2.1 Historical

Arguably, one of the most significant discoveries in the field of polymer science in the last 40 years was the polymerisation of olefins using transition metal-based catalysts. The details regarding the chronological development of these systems is summarised in Table 2.1 [1].

Karl Ziegler was the first person to discover that transition metal halides ($TiCl_4$, $TiCl_3$ and $ZrCl_4$), in combination with alkylaluminum compounds as cocatalysts, could be successfully used to synthesise linear high molar mass polyethylene and isotactic polypropylene [2, 3]. These catalysts were known as heterogeneous, multi active site catalysts.

Table 2.1. Development of metal based catalysts for the polymerisation of polyolefins in the past 50 years [1].

Year	Catalyst system	Polymer	Activity (kg-polymer / g-metal)	Tacticity [%]
1953-1955	$TiCl_4$-Et_3Al	Polyethylene	10-15	-
		Polypropylene	5-10	50-60
	$TiCl_3$-Et_3Al	Polyethylene	5-10	-
		Polypropylene	1-3	60-80
1955-1960	$TiCl_3$ electron donors-Et_3Al	Polyethylene	-	-
		Polypropylene	1-10	90-95
1970-Present	Supported $MgCl_2$	Polyethylene	500-1000	-
	$TiCl_4$-Et_3Al	Polypropylene	500-1000	560-70
	Supported $MgCl_2$ electron	Polyethylene	500-1000	-
	Donor $TiCl_4$-Et_3Al	Polypropylene	300-500	90-99
1980-Present	Homogeneous metallocene-methylaluminoxane	Polyethylene	400-500	-
1985-Present	Stereorigid metallocene-methylaluminoxane	Polypropylene	150-170	96-98
	Homogeneous aluminum free	Polypropylene	0-1	97-98
	Metallocene catalysts	Polypropylene		
	Supported metallocene	Polypropylene	10-20	80-90
	Catalysts/AlR_3 or MAO	Polypropylene		
1986-Present	$Ti(OR)_4$-MAO	Syndiospecific polystyrene	0.4-0.5	80-96
	$CpTi(OR)_3$-MAO	Syndiospecific polystyrene	3300	82
	$Mg(OH)_2$/$Ti(Obu)_4$- MAO	Syndiospecific polystyrene	0.3	100
1988-Present	Cp_2ZrCl_2-MAO	Ethylene-propylene copolymer	50-100	Aspecific
	Et[$IndH_2$]$ZrCl_2$-MAO	Ethylene-propylene copolymer	5-15	Isospecific
	i-Pr(Cp)(Flu)$ZrCl_2$-MAO	Ethylene-propylene copolymer		Syndiospecific
	Cp_2ZrCl_2-MAO	Ethylene-hexene copolymer	-	Aspecific
	Et[$IndH_2$]$ZrCl_2$-MAO	Ethylene-hexene copolymer		Isospecific
	i-Pr(Cp)(Flu)$ZrCl_2$-MAO	Ethylene-hexene copolymer		Syndiospecific
	Et[$IndH_2$]$ZrCl_2$-MAO	Ethylene-cyclic olefins copolymers	0.02-0.14	-

Shortly thereafter, Natta independently discovered the stereoregular nature of polymers of α-olefins such as propylene, 1-butene and styrene [4-7]. In 1963, the Noble Prize for chemistry was awarded to Ziegler and Natta for their contribution to the field of polymer science.

The transition metal catalyst range was broadened by the introduction of more transition metal compounds from groups IV-VII [8]. Improvement with regard to the efficiency of the current systems, as well as the economics of polyolefin processing through elimination of catalyst removal and solvent purification/removal steps, was later found with the introduction of $MgCl_2$ supported catalyst systems [9, 10].

The next revolution in polyolefin synthesis via transition metal catalysts was led by Breslow and Newburg [11] with the identification of the homogeneous $(Cp)_2TiCl_2$/alkylaluminum catalyst species. The significance of the homogenous character of a catalyst is its single site activity that produces polyethylenes of high molar masses and narrow molar mass distributions. However, the discovery of homogeneous catalyst systems did not attract widespread interest due to their poor catalytic activity, their short lifetime and lack of product stereospecificity.

The next milestone in the synthesis of polyolefins was the discovery of highly active and stereospecific catalyst species with methylalumoxane (MAO) as cocatalyst. Reichert and Meyer observed an increase in catalytic activity when water was added to the $Cp_2TiEtCl/AlEtCl_2$ catalytic system [12, 13]. This was followed by the discovery of a significantly higher polymerisation activity of 5 000 000 g PE/g Ti after the addition of Cp_2TiMe_2 to two equivalents of trimethylaluminium, previously treated with one equivalent of water [14]. Further studies by Sinn and Kaminsky showed that the increase in catalyst activity was a result of the presence of an oligomeric compound, known as methylaluminoxane (MAO).

The use of weakly bonded anion species to serve as cocatalysts in the activation of transition metal catalyst species renewed both commercial and scientific interest in homogeneous catalyst systems [15]. Another type of compound also used lately with great success to obtain cationic active metal species for olefin polymerisation is the borate species.

2.2.2 Effective cocatalysts for homogeneous polymerisation

Activation of the homogeneous precatalyst can be obtained with one of two compounds, as illustrated in Scheme 2.1.

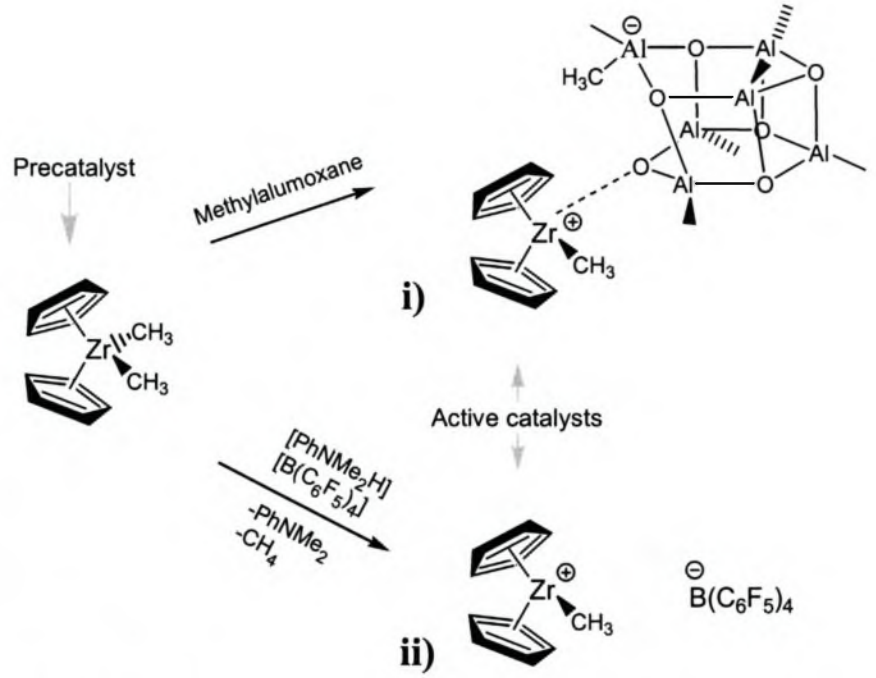

Scheme 2.1. Activation of precatalyst with (i) methylalumoxane and (ii) a borate species.

Activation by methylaluminoxane

Although the properties of MAO have been studied extensively since its discovery, quite a few questions still remain. It is known that MAO has a molar mass of 1500 g/mol. The exact structure is, however, not known. After various suggestions, the proposal by Sinn *et al.* [16] was accepted as the widely used model. The hypothesis is that MAO consists of a cage-like structure, with TMA dispersed within the molecule.

MAO is an ideal cocatalyst, as it serves as activator for transition metal catalyst species, as seen in Scheme 2.1. It scavenges the immediate surroundings of the active catalyst species for moisture and polar compounds, to prevent the deactivation of the catalyst. Its last function is the activation of inactive species during the polymerization process. The disadvantage of this system is that MAO is used in

molar ratios of at least 1000:1 with regard to the catalyst species. This makes it a very expensive cocatalyst to use in industry and resulted in a further search for other effective cocatalysts. The result was the introduction of the borate species as possible cocatalysts for transition metal based catalysts.

Activation by borate species

These species have the advantage that they are used in a 1:1 or 2:1 molar ratio with the desired precatalyst. (A precatalyst is the transition metal species before activation by a cocatalyst). The most simple borate species used is $B(C_6F_5)_3$. The drawback of borate activated systems is that they do not function as scavengers and, in most cases, an extra activator is required.

2.2.3 Polymerisation mechanism

Polyolefins are produced by multiple insertions of olefins into a metal-carbon bond. Olefin insertion occurs by the *cis*-opening of the double bond (both new bonds are on the same side of the inserting olefin) and with chain migratory insertion (it is the alkyl group on the metal that migrates to the olefin with a net exchange of two available coordination positions on the metal centre). See Scheme 2.2.

When we have primary insertion (1,2), then the 1-alkene enantioface that is inserted preferentially is the one which, in the transition state, places its substituent anti to the first C-C bond of the growing polymer chain (minimises non-bonded interactions).

The active metal centre bearing the growing alkyl chain must have an available co-ordination site for the incoming monomer. Insertion occurs via chain migration to the closest carbon of the olefin double bond, which undergoes *cis*-opening, with the formation of the new metal-carbon and carbon-carbon bonds. The new C-C bond is then on the site previously occupied by the co-ordinated monomer molecule.

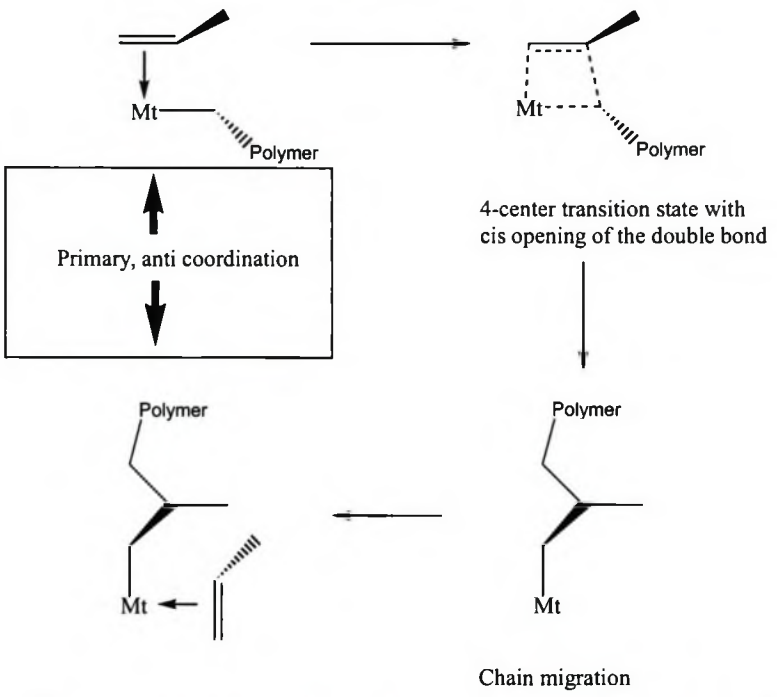

Scheme 2.2. Schematic representation of coordination and insertion during olefin polymerisation with transition metals. (Mt = metal atom).

Points of importance in transition metal catalysed polymerisation of olefins:

- The metal atom must have a site for coordination
- Insertion occurs via chain migration to the closest carbon of the olefin double bond.

The four proposed mechanisms for polymerisation are summarised in the work of Resconi *et al.* [17].

In short, the acceptable mechanisms all agree that:

- Monomer insertion is a two-step process, namely coordination followed by insertion;
- The active metal must have an available coordination site;
- Olefin insertion occurs by *cis*-opening of the double bond, followed by chain migratory insertion;
- The olefin has to coordinate face-on to the metal, with its double bond parallel to the metal-carbon bond.

The ligands and their substituents play an important role in the insertion of the monomer with reference to steric hindrance. The bite angle that the ligands form with each other is thus a vital variable and brings us to the concept of *ansa*-metallocenes. Control of the tacticity of the formed polymer is possible.

A distinction between the active centre and the active site of the catalyst precursor should be made: a metallocene type active centre has a minimum of two sites on which chain growth can take place. The nature of the active site is determined by the metal, the Cp ligands, the geometry and structure of the metal-bonded chain-end. Different types of last inserted monomer will thus increase the number of possible active sites. A difference in reactivity, regioselectivity and enantioface selectivity is therefore possible. The result is that the active centre itself changes during a single chain growth but, statistically, behaves the same from one chain to another. Such a species can therefore be described as a single-site catalyst [17].

2.2.4 Significance of catalyst system

The versatility of metallocene catalysts is seen in the various modifications one can make to the catalyst system in order to create polymers with specific properties that meet the needs of the scientist and industry. Two possible sources of enantioface selectivity in olefin insertion are possible (Scheme 2.3):

a) Stereoregularity of the metal active site is based on an enantiomorphic site control mechanism for stereoselection. The relationship of the chirality of the two co-ordination sites of the catalytic complex determines the stereochemistry of the polymer.

b) The last inserted monomer unit is based on a chain-end control mechanism for stereoselection. Every monomer insertion generates a new stereo centre.

Chiral induction/enantioface preference can come from the last inserted monomer unit.

A predictable relationship between complex symmetry and polymer tacticity exists. This can be seen from Ewen's symmetry rules (Figure 2.1), compiled by Ewen *et al.* [18-23] and Kaminsky *et al.* [24].

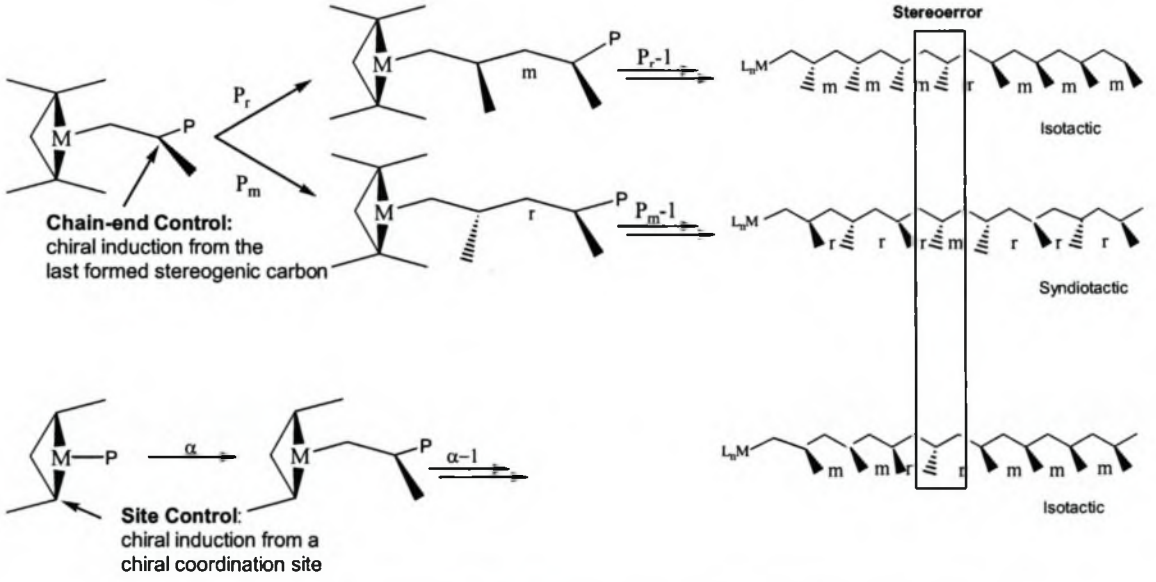

Scheme 2.3. Chain-end and enantiomorphic site mechanisms of stereocontrol [17].

Single-site polymerisation catalysts can be divided into five major symmetry categories. It is assumed that the polymer rapidly equilibrates with the available co-ordination site for the purposes of assigning symmetry. C_{2v} symmetric metallocene catalysts produce atactic polymers or moderately stereoregular polymers by chain-end control mechanisms. Catalysts exhibiting C_s symmetry, consisting of mirror planes containing two diastereotopic co-ordination sites, behave similarly and produce atactic polymers. C_s symmetric catalysts that have a mirror plane reflecting two enantiotopic co-ordination sites frequently produce syndiotactic polymers. C_2 symmetric complexes, both *racemic* and enantiomerically pure ones, typically

produce isotactic polymers via a site-control mechanism. The fifth symmetry category, not mentioned in Figure 2.1, is the "so-called" oscillating metallocenes.

The structure of the catalyst precursor also has a significant influence on the comonomer incorporation and molar mass of the obtained copolymer, as can be seen in Figures 2.2 and 2.3.

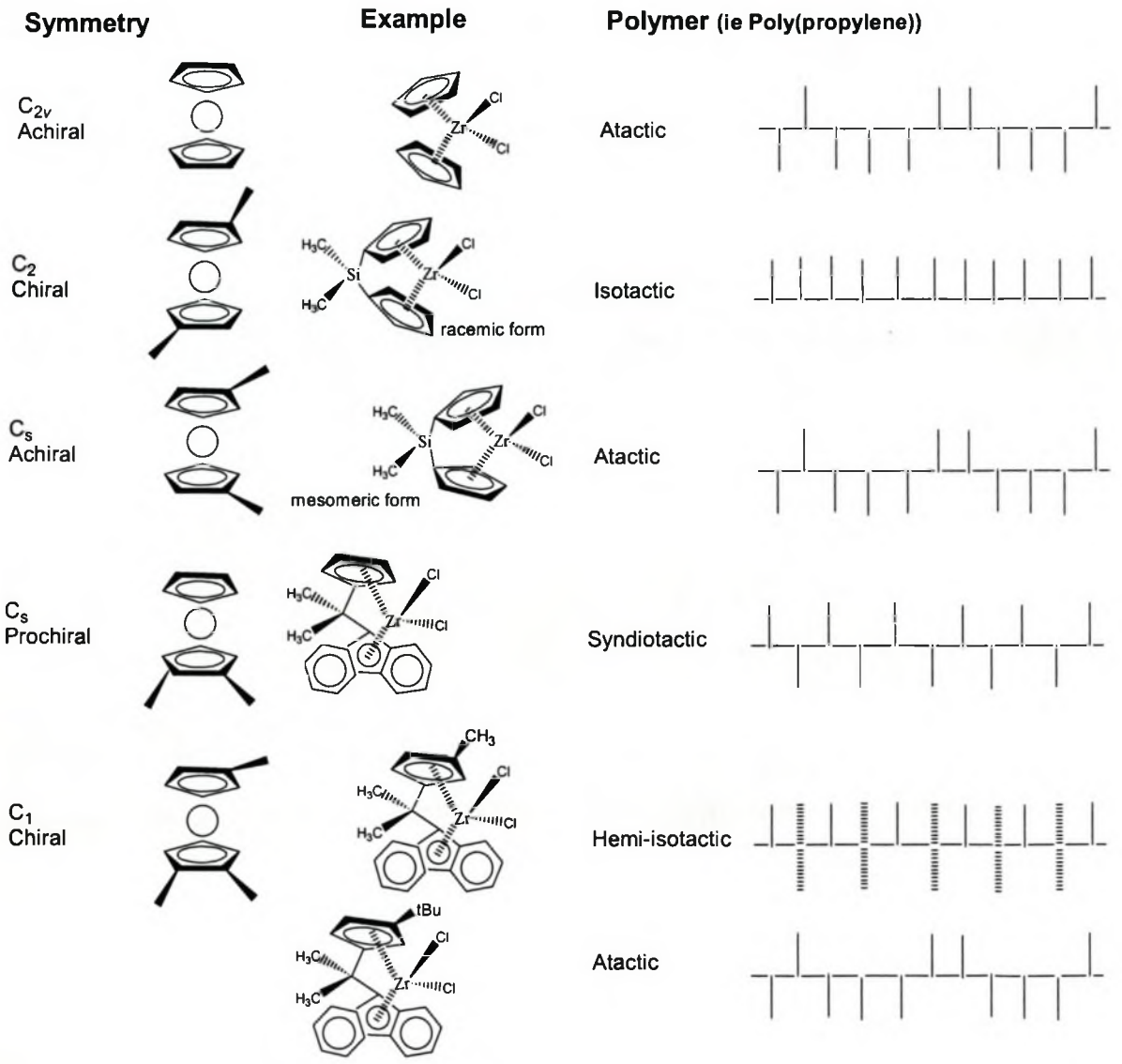

Figure 2.1. Steric control as a function of metallocene symmetry (Ewen's symmetry rules) [17, 25].

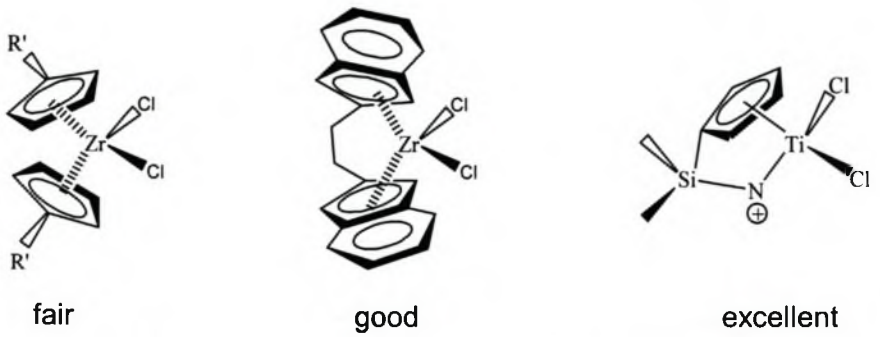

Figure 2.2. Control of comonomer incorporation in ethylene copolymers by the manipulation of catalytic structure [26] (fair-, good- and excellent activity).

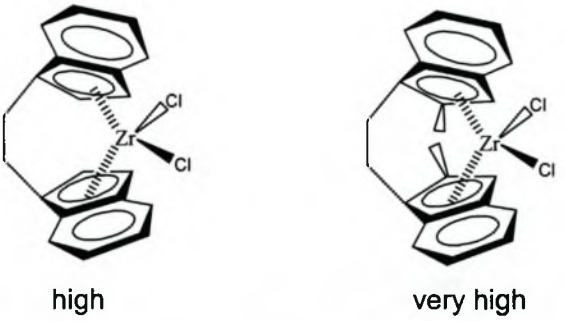

Figure 2.3. Control of molar mass (ethylene copolymers) by the manipulation of catalytic structure [26] (high- and very high reactivity).

2.3 Transition metal-based catalysts for the copolymerisation of ethylene and methyl methacrylate

In general, Ziegler-Natta catalysts such as $TiCl_4/AlR_3$ and the chlorinated Kaminsky catalysts such as Cp_2ZrCl_2/(MAO) do not polymerise polar monomers. However, Collins *et al.* [27] showed that some methylated Kaminsky species like Cp_2ZrMe_2 **2** and $[Cp_2ZrMe(THF)]^+[BPh_4]^-$ can be used to polymerise MMA. These polymers were syndiotactic and had molar masses between 62 900 g/mol and 158 300 g/mol with polydispersities between 1.19 and 1.40. Soga *et al.* [28] reported on the synthesis of mostly syndiotactic poly(methyl methacrylate) (PMMA) with $Cp_2Zr(CH_3)_2/Ph_3CB(C_6F_5)_4/B(C_6F_5)_3$ as catalyst system, as well as isotactic PMMA

with *rac*-Et[$Ind_2Zr(CH_3)_2$] as catalyst precursor. It was determined that the syndiospecific polymerisation proceeds via a chain-end controlled mechanism, while the isospecific polymerisation proceeds via an enantiomorphic site controlled mechanism.

The lanthanide elements can be used as metal ions in a metallocene catalyst for the synthesis of both polar and nonpolar monomers (acrylate and olefin based polymers). Yasuda *et al.* [29, 30] examined the existence of an eight-membered structure, in the MMA polymerisation with $Sm(C_5Me_5)_2(MMA)_2H$ **1** as catalyst precursor, via single crystal X-ray analysis. They found that one MMA unit links to the metal in an enolate form, while at the other end the penultimate MMA unit is attached to the metal through its C=O group. Two MMA units are thus used in this reaction mechanism. The assumption for the initiation step was that the hydride attacks the CH_2 group of the MMA and a transient $SmOC(OCH_3)=C(CH_3)_2$ is formed, as illustrated in Scheme 2.4. The next MMA unit to be inserted at the reactive catalyst site attaches in a 1,4-addition, to produce an eight-membered cyclic intermediate species. Marks *et al.* [31] used a chiral *ansa*-lanthanide metallocene to obtain isotactic PMMA.

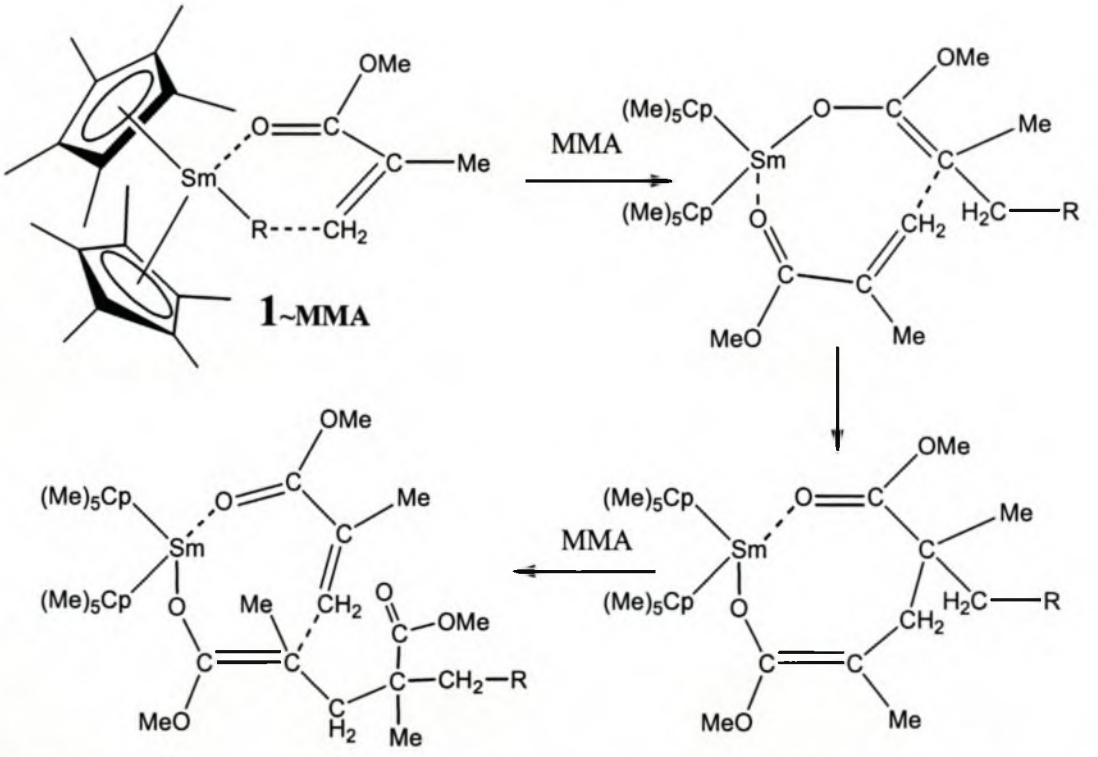

Scheme 2.4. Reaction diagram of the ring formation mechanism resulting from two MMA monomers during polymerisation with **1.**

Collins *et al* [32, 33] have done extensive research on the initiation and propagation mechanisms of the two-component catalyst systems **2** and **3**. It was found that the mechanism involves two types of zirconocene complexes: a cationic methyl complex that activates a monomer as an acceptor and, secondly, the growing chain methyl ester enolate complex as a donor. The formation of the carbon bond proceeds via a Michael-type addition between the activated monomer and activated growing chain, far away from the zirconium centre (Scheme 2.5). The marked methyl (* in Scheme 2.5) is the one end of the propagating PMMA chain, while **4** and **5** are the enolate complexes which are formed in the intermediate stages of polymerisation. The reactions were carried out at 0 °C, where this specific catalyst lends itself for the production of syndiotactic PMMA.

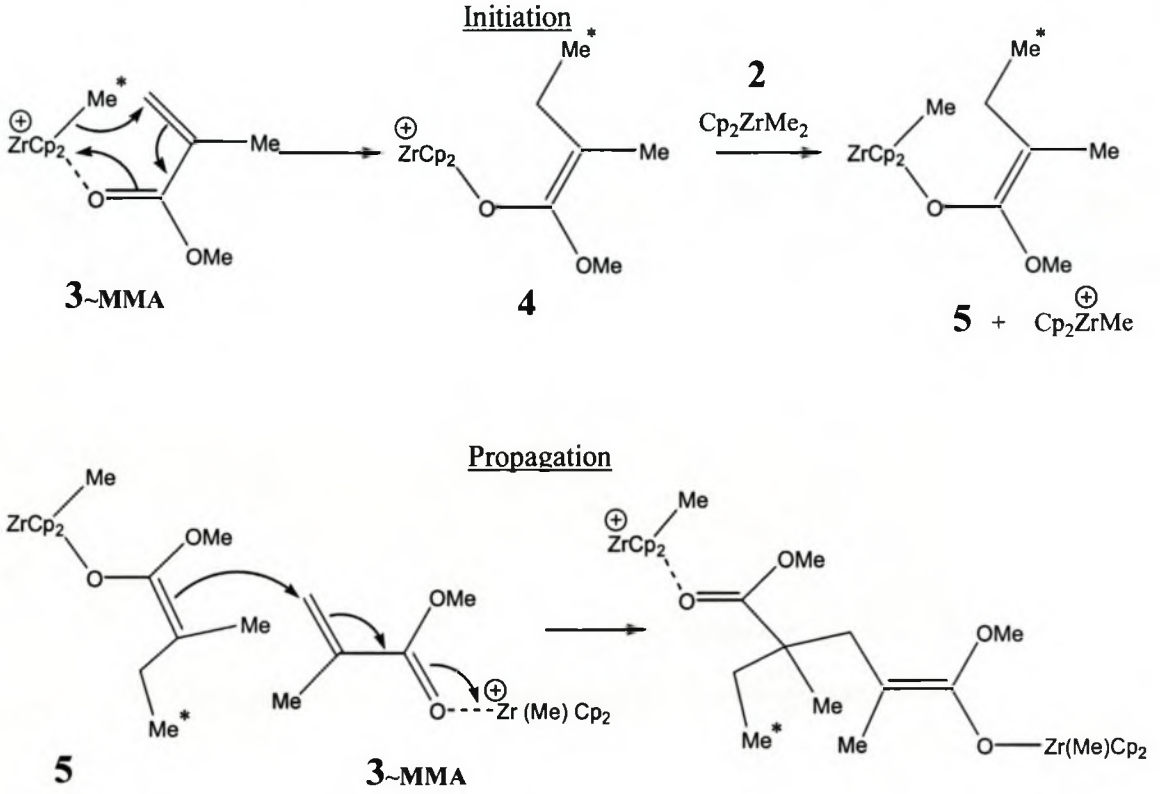

Scheme 2.5. Reaction mechanism for a two-component catalyst system for the polymerisation of MMA.

Höcker *et al.* [34] investigated different types of catalyst systems with respect to their reactivity with MMA. Polymerisation with **6** yields highly isotactic PMMA, whereas

7 yields syndiotactic PMMA at low reaction temperature (Figure 2.4). These results are in agreement with the findings of Cameron *et al.* [35], who used *in situ* generated catalysts. Cameron *et al* [35] were, however, also able to generate active catalysts similar to **8** (*in situ*), while Höcker *et al.* [34] reported cations **8-10** to be inactive for polymerisation. Höcker *et al.* [34] proposed that the inactivity could be related to the nature of the angle of the ligands around the zirconium centre. This change in angle can entail a change in the steric demand of the complexes or their electronic properties. The activity of the site is also influenced by the sterical dimensions of the acrylate monomer (the bulkier the side groups the lower the reactivity).

Sustmann *et al.* [36] considered the reaction mechanism proposed by Collins *et al.* [27, 32, 33] and Soga *et al.* [28, 37] in the polymerisation of acrylic acid, instead of MMA. The energies for the different reaction coordinates were also measured to see which mechanism has the best energy configuration. It was found that all mechanisms have the ability to polymerise, although some of the intermediate species showed higher activation energies than others.

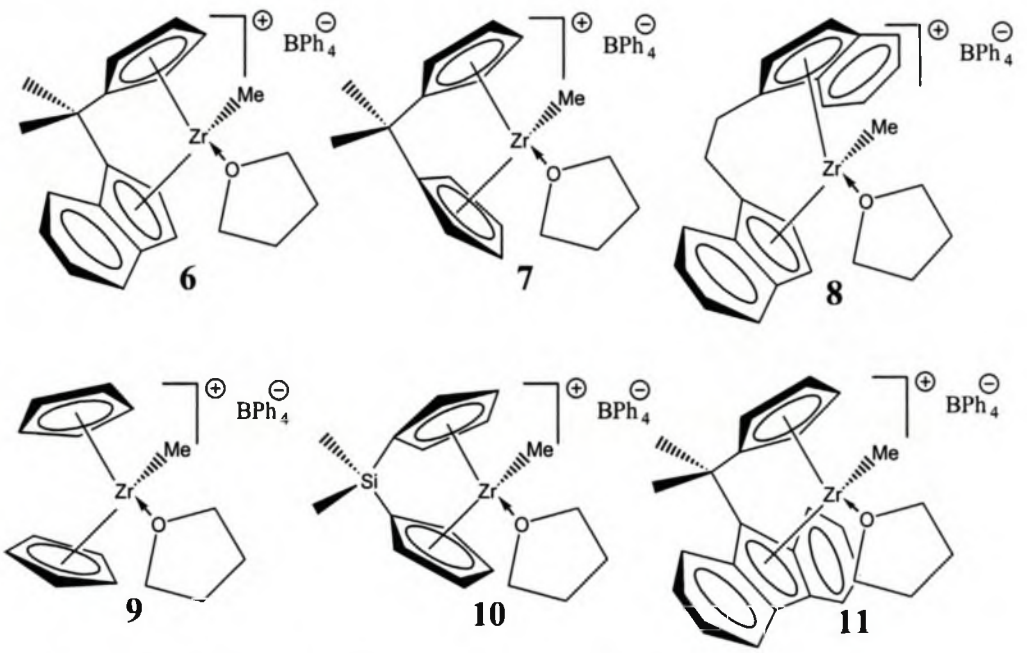

Figure 2.4. Catalysts used for activity studies by Höcker et al. [34].

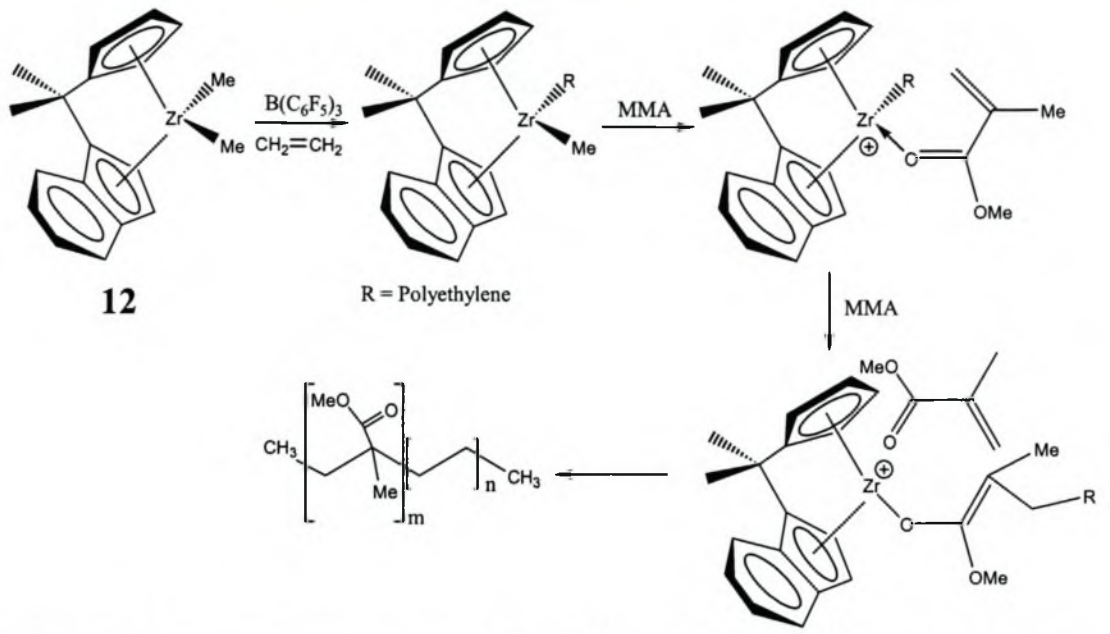

Scheme 2.6. Reaction scheme as proposed by Höcker *et al.* [34], for the copolymerisation of ethylene and MMA with **12.**

The model for the formation of isotactic PMMA by means of the metallocene catalyst **6** [34] can be related to that of the metallocene catalyst $Me_2C(Cp)(Ind)ZrMe_2$ **12**. The two catalysts **6** and $Me_2C(Cp)(Ind)ZrMe_2$ **12** have the same ligands, the only difference being that one methyl group in $Me_2C(Cp)(Ind)ZrMe_2$ is replaced by a tetrahydrofurane (THF) in **6**.

The polymerisation mechanism of $Me_2C(Cp)(Ind)ZrMe_2$, as proposed by Höcker *et al.* [34], will be discussed in further detail in Chapter 7 where the analysis of the poly(ethylene-co-MMA) samples will be reported on. Scheme 2.6 gives only a brief outline of this reaction.

2.4 Chromatographic techniques for polyolefin analysis

The main analytical tools used in this study were based on chromatographic methods. It is therefore vital to understand, firstly, the development and the theory behind these

methods of analysis and, secondly, that polyolefins are semi-crystalline polymers that do not dissolve in any solvent at room temperature.

Special attention will be given to the theory behind the development of Crystallisation Analysis Fractionation (CRYSTAF), gradient High Performance Liquid Chromatography (HPLC) and GPC coupled to FTIR spectroscopy (LC-Transform).

2.4.1 Historical development of chromatographic techniques

In 1964 J.C. Moore [38] discussed the use of cross-linked polystyrene gels for the separation of polymer molecules that are soluble in organic solvents, this was the birth of GPC. By use of this technique information could be obtained on the molar mass and MMD of a polymer sample. Prior to this, Cortis-Jones [39] had already separated samples on a column packed with slightly cross-linked polystyrene, but he only investigated small molecules.

Gradient elution chromatography was developed by Alm *et al.* [40]. In their work they used a step gradient to obtain separation. With gradient elution, almost every form of elution chromatography, which uses a liquid as mobile phase can be used. In gradient elution chromatography separation results when a weak displacing eluent dissolves the sample that is least retained at the start of elution while, as the gradient enriches, the stronger displacing eluent will progressively elute the stronger retained samples. As early as 1963 Snyder already started to investigate the phenomena related to the adsorption of molecules to the column packing material in gradient elution [41, 42]. In his work he used both linear and convex gradients to achieve the best possible separations but he only worked with small molecules.

There are certain advantages of using a linear gradient in elution chromatography compared to a stepwise gradient. These advantages include 1) optimum peak spacing, meaning that the weakly adsorbed components are sufficiently separated from the strongly adsorbed components, 2) the elution bands are approximately equal in width and 3) no band splitting with development of spurious peaks occurs.

In 1979, Teramachi *et al.* [43] were the first to analyse copolymers by means of adsorption chromatography in order to elucidate the chemical composition of the copolymers. Prior to the use of this technique, TLC was used to separate copolymers. Unfortunately, TLC will only give qualitative results and the technique cannot be operated automatically.

During the 1980's a number of articles on gradient HPLC were published by various groups around the world, amongst which were Glöckner *et al.* [44-46], Mori *et al.* [47, 48], Snyder *et al.* [49, 50] and Sato *et al.* [51-53]. They all used this technique to characterise copolymers and oligomers. The chemical composition distribution (CCD) of the polymers could be studied without any significant interference of molar mass and, in an oligomer separation, they were able to separate complex samples into their different oligomers.

The CCD of a polymer sample can, however, not only be determined by changing the solvent gradient in a chromatographic run, but it can also be accomplished by changing the temperature of the system while keeping the solvent composition of the system constant. This method of analysis was used by Hee Cheong Lee and Taihyun Chang to analyse polystyrene and poly(methyl methacrylate) under temperature gradient conditions [54-56].

Besides gradient HPLC, another method was developed for the analysis of polymers. This method employs an isocratic HPLC mode and is called liquid chromatography under critical conditions (LCCC). This liquid chromatographic method, at the critical point of adsorption, was developed by Gorshkov *et al.* [57], Entelis *et al.* [58] and Belenkii *et al.* [59, 60]. LCCC can be used to look at the functionality type distribution (FTD) of a sample, independent of its molar mass. In all other separations, the functionality distribution is accompanied by separation according to molar mass, which complicates the processing of the obtained chromatograms.

In all the analytical techniques mentioned in the previous section, the molar mass has an influence on the separation of the chemical composition, or the chemical structure of the polymer has an influence on the molar mass separation. Looking ahead, if one could combine two analytical methods then it might be possible to obtain better results from the chromatograms, due to the fact that both the effect of molar mass and the chemical composition can be seen on one chromatogram. By combining two chromatographic systems it might also be possible to almost completely eliminate the opposing factors of molar mass and chemical composition. Inagaki and Tanaka [61] used the combination of column adsorption chromatography and gel permeation chromatography (GPC), and Taga and Tagaki used TLC and GPC for their separations. Belenkii and Gankina [62] mentioned the combination of first using GPC and then TLC. Balke *et al.* [63, 64] performed their analysis on two GPC instruments in which different mobile phases were used and Glöckner [65] combined gradient HPLC and GPC. All these methods in which two different separation systems are used are referred to as cross-fractionation (CF).

Little work on CF has been published as the equipment for such studies is expensive and it takes a long time to complete one analysis [66-70]. The reason for the long time intervals for analyses is that the fractions of the first dimension have to be collected separately before they are injected into the second dimension. It may also be necessary for the collected set in the first dimension to be repeated several times to obtain a high enough concentration in order for the detector in the second dimension to adequately detect the sample. Kilz was the first to couple gradient HPLC and GPC so that the effluent of the first dimension is automatically injected into the second dimension [71-73].

2.4.2 Gradient High Performance Liquid Chromatography (gradient-HPLC) and Liquid Chromatography under Critical Conditions (LCCC)

The use of gradient HPLC as an analytical technique is well established in the modern day analytical laboratory. The chromatographic separation of large molecules (10^3-10^7 Dalton) began in the early 1950's when the first separations of proteins were done by ion exchange in a gradient system [74]. Snyder *et al.* did extensive work on gradient elution systems, especially with small molecules, and he also derived some of the fundamental principles of gradient elution [41, 42]. In 1979 Teramachi *et. al.* [43] were the first to use gradient HPLC as an analytical technique for the analysis of copolymers. At the same time, the separation of low molar mass polymers into a large number of oligomers was done by van der Maeden *et al.* [75]. This work was also done with the aid of gradient HPLC but in a reversed phase mode. Oligomers and copolymers (random copolymers of high molar mass) were analysed by a number of different people, for example, Glöckner *et al.* [44-46, 76-78], Mori *et al.* [47, 48, 69, 79], Teramachi *et al.* [80-83] and Snyder *et al.* [49]. The most common polymers that were investigated were polystyrene, polymethyl methacrylate, polyglycols, polybutadiene and copolymers of poly (styrene-co-methyl methacrylate), poly (styrene-co-butadiene) and poly (styrene-co-acrylonitrile). These chromatographic techniques are however of little use for the analysis of polyethylene, since this polymer only dissolves at high temperatures in certain solvents. All the above mentioned separations were carried out at room temperature. Only H. C. Lee and T. Chang used a temperature gradient for their analyses [54-56]. J.W. Lyons *et al.* [84] were the first to report on the separation of ethylene styrene copolymers via solvent gradient adsorption conditions at temperatures up to 100 °C.

Critical conditions in the chromatography of polymers are defined as those conditions under which entropic exclusion effects are exactly compensated by enthalpic effects from the adsorption. Here the retention is solely governed by small differences in the chemical structure of the polymer chains. These differences in chemical structure can be due to different end-groups or a different sequence of the monomer units along the

polymer chain. Most of the work done, to date, has been on block copolymers [85, 86] and end-groups [87].

Liquid chromatography under critical conditions (LCCC) of adsorption has been shown to be a useful method for the determination of functional type distribution (FTD) [57, 59]. Entelis *et al.* [58] were one of the first groups to develop a theory for this method. Much work has been done in the area of critical chromatography by Pasch *et al.* [88, 89].

2.4.3 GPC coupled to FTIR spectroscopy

Characterisation of graft or block copolymers has been mainly carried out by size-exclusion chromatography [90-92], although no information regarding the chemical components as a function of MM could be obtained. By coupling selective separation methods e.g. critical, adsorption or size exclusion chromatography coupled with selective detectors e.g. UV or FTIR, not only is it possible to separate complex polymers into their constituting components (i.e. molar mass or chemical composition), but also to selectively analyse specific functional groups as a function of these distributions.

In 1971 Ross and Shank [93] introduced infrared (IR) spectroscopy coupled to GPC, while in 1975 the coupling was performed by use of a flow-through cell [94]. In the case of liquid chromatography coupling, the large amounts of solvents required have a negative influence on the IR spectra. The solvents are IR active, hence the spectra obtained with the GPC-FTIR flow-through coupling gave inferior signal-to-noise ratios. Additionally, solvents that have absorption bands in the same region as the polymer sample make accurate analyses impossible [95, 96].

The latest method for the analysis of GPC fractions by means of FTIR was proposed in 1986 by Gagel and Biemann [97]. In this method an intermediate step is introduced during which the eluent is evaporated from the sample after it leaves the

chromatographic system. As the solvent is no longer present, the entire IR spectrum can now be analysed.

The FTIR interface allows the combination of high resolution GPC or gradient HPLC together with the good identification capabilities of FTIR. Further improvements were made to the nebulisation of the aerosol [98, 99] and later Lab Connections started manufacturing and selling analytical instruments that operate on this concept under the name LC-Transform ® [100].

2.4.4 Crystallisation Analysis Fractionation (CRYSTAF)

The demand by industry for innovative and more cost effective polymer products has lead to the development of a considerable diversity of polymers. Extensive characterisation of these polymers is required to obtain a better understanding of their properties and subsequently their potential application. The solubility of a semi-crystalline polymer is however one of the limiting factors when doing chromatography. Polymers soluble at room temperature can be analysed by various techniques (ie. Chromatography) [66, 101]. Polymers of high crystallinity, on the other hand, are more complex to analyse as they are only soluble at high temperatures and there are only a few effective analytical methods that have been developed for the use at elevated temperatures [102-104]. Most polyolefins fall in the last mentioned category. Only 1-pentene and higher α-olefin (ie. 1-hexene, 1-decene, 1-dodecene, 1-tetradecene and 1-octadecene) homo- and copolymers, with large amounts of higher α-olefins incorporated, will be soluble at room temperature [105].

The common and most basic chromatographic technique used for analysis of the polyolefins (soluble at elevated temperature) is High Temperature Gel Permeation Chromatography (HT-GPC) [106, 107]. This method provides information regarding the average molar mass (MM) and molar mass distribution (MMD) of the particular polymer sample. It must be noted that this method provides inadequate information regarding the chemical composition of the polymer.

The concept of Temperature Rising Elution Fractionation (TREF) was first used by Shirayama *et al.* [108] to describe the method of fractionating low density polyethylene samples according to the degree of short-chain branching (SCB). Desreux and Spiegels [109] were the first to describe the mechanism of this technique. TREF is a technique by which semi-crystalline polymers are fractionated according to their solubility-temperature relationship and thus to their molecular structure [102, 110].

The scientific community, as well as industry, is always striving for better and more innovative techniques by which to analyse their products. Crystallisation Fractionation Analysis (CRYSTAF), developed by Monrabal [111, 112], is a method that complements the analysis results as obtained from TREF. The former technique, however, can provide data up to 24 hours faster than the latter mentioned technique due to the analysis method involved. A second advantage of CRYSTAF is its ability to analyse five samples simultaneously.

In TREF the samples are dissolved in a suitable solvent at high temperatures, where after the solution is placed into a column with an inert stationary phase. The filled column is then cooled down to room temperature at cooling rates of 0.01-0.05 °C/min, in an oven. After the cooling cycle the column is coupled to the GPC pump for elution of the samples in the heating cycle (Figure 2.5(A)). In the heating cycle the column is flushed with a solvent while the oven is heated at a rate of 0.1 °C/min. The eluent concentration is monitored by a refractive index detector. In CRYSTAF only the cooling cycle is used for sample analysis (Figure 2.5(B)). Infrared detection is used to measure the decrease of polymer concentration in the solution during the cooling cycle (0.1 °C/min). During the cooling cycle the crystallised polymer is separated from the solution by a sintered-glass filter inside the reactor.

The unique set-up of the CRYSTAF system makes it possible to calculate the short chain branching, SCB, of LLDPE from a standard calibration curve [113]. CRYSTAF analyses of PP and LLDPE have been reported to be much more effective than the analysis done by TREF [114, 115]. Most work done on CRYSTAF to date

involved basic analysis of standard polyolefin copolymers [112, 116-120] and blend separation [112, 113, 121].

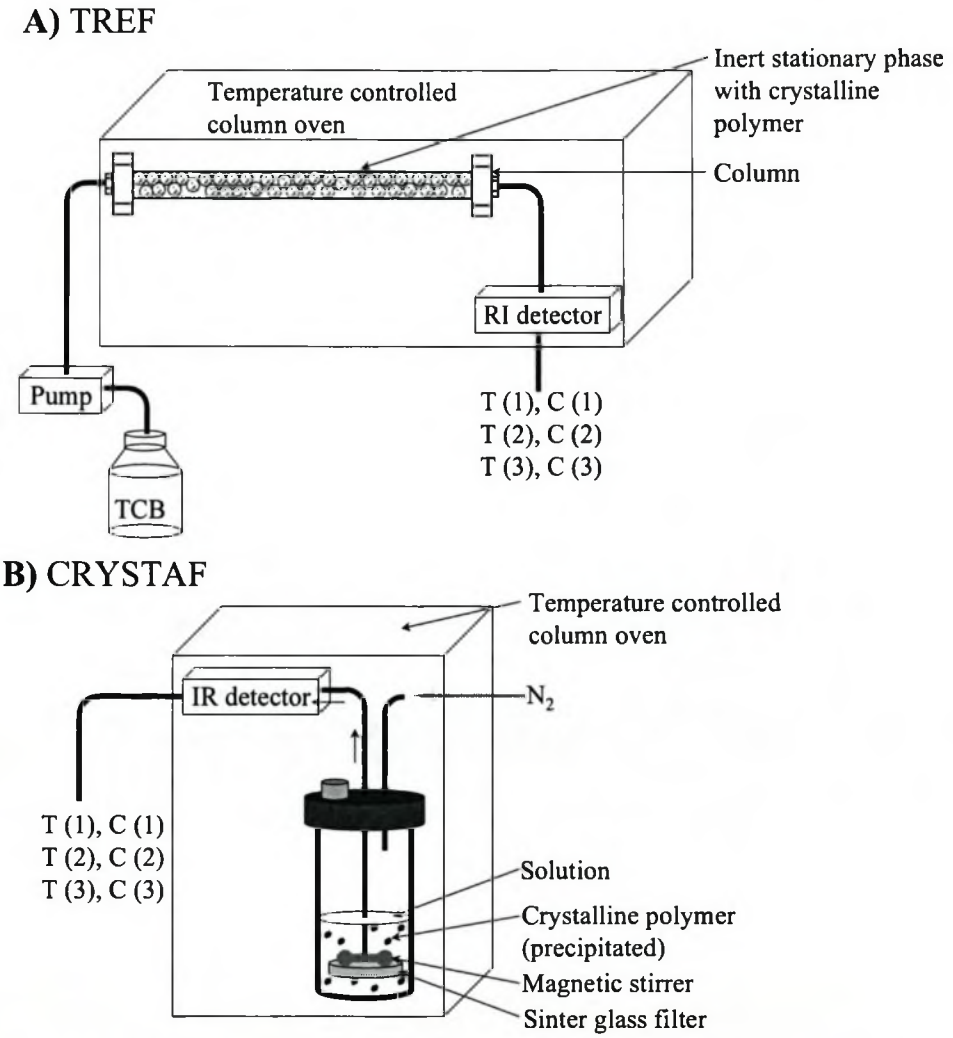

Figure 2.5. Schemes illustrating the build up of TREF (A) and CRYSTAF (B) instruments, where T and C denotes the different temperatures and concentrations respectively were analysis data are collected.

It has been reported that a good correlation exists between the melting point (T_m), as determined by Differential Scanning Calorimetry (DSC), and the crystallisation point (T_c) in solution [122, 123]. The latest research addresses the Monte Carlo simulation of the longest ethylene sequence length (LES) for single-site type catalysts and relates this directly to the fractionation process in the crystallisation distribution chromatogram [124, 125].

Calorimetric measurements, for which the samples are prepared in a solvent before analysis, is the newest and least expensive technique for the investigation of SCB in LLDPE and polyolefin blends. This method is based on DSC analysis, using a special sample preparation procedure where the samples are precipitated from solution. Numerous researchers have shown that results obtained from DSC analysis are comparable with those obtained from CRYSTAF and TREF methods [126-128]. The only disadvantage of analysis by DSC is that the distribution curve cannot be directly converted into a weight percentage of the components of the different branching structures.

The present study focuses on the parameters that can change the T_c of polymers in solution as measured by CRYSTAF. Insight into instrument limitation and analytical optimisation possibilities are thus obtained.

2.5 References

1. Reddy S S, Sivaram S, Prog. Polym. Sci., 1995, **20** (2), 309.
2. Ziegler K, Belgian Pat., 1954, **533**, 362.
3. Ziegler K, Holzkamp E, Martin H, Breil H, Angew. Chem., 1955, **67**, 541.
4. Natta G, Pasquon I, Zambelli A, J. Am. Chem. Soc., 1962, **84**, 1488.
5. Natta G, Angew. Chem., 1956, **68**, 393.
6. Natta G, Mod. Plast., 1956, **34**, 169.
7. Natta G, Angew. Chem., 1964, **76**, 553.
8. Boor J, *Ziegler-Natta Catalysts and Polymerizations*, 1979, New York, Academic Press.
9. Natta G, Mazzanti G, Deluca D, Gainnini U, Bandini F, Makromol. Chem., 1964, **76**, 54.
10. Gardner K, Parsons I W, Haward R N, J. Polym. Sci. Part A, 1978, **16**, 1683.
11. Breslow D S, Newburg N R, J. Am. Chem. Soc., 1957, **79**, 5072.
12. Dyachkovskii F S, Vysokomol Soedin, 1965, **7**, 114.
13. Meyer K, *Ph D dissertation*, 1970, T.U. München.
14. Anderson A, Cordes H G, Herwig J, Kaminsky W, Merck A, Mottweiler R, Pein J, Sinn H, Vollmer H J., 1977, Ger. Offen. 2608933 to BASF A.G., C.A. No. 87:152744e and Ger. Offen. 2608863 to BASF A.G., C.A. No. 87:152743d.
15. Kaminsky W, *Transition Metal Catalyzed Polymerization*. MMI press, Ed. Quirk R P, 1985, New York, Harwood Academic Publications, 225.
16. Sinn H, Macromol. Symp., 1995, **97**, 27.
17. Resconi L, Cavallo L, Fait A, Piemontesi F, Chem. Rev., 2000, **100**, 1253.
18. Ewen J A, J. Am. Chem. Soc., 1984, **106**, 6355.
19. Ewen J A, Jones R L, Razavi A, Ferrara J D, J. Am. Chem. Soc., 1988, **110**, 6255.
20. Ewen J A, Elder M J, Jones R L, Curtis S, Cheng H N, *In catalytic olefin polymerisation, Studies in surface science and catalysis*, Ed. Keit T, Soga K, 1990, New York, Elsevier, 439.

21. Ewen J A, Hasreslach L, Ejder M J, Atwood J T, Zhang H, Cheng H N, *Transition metals and organometallics as catalysts for olefin polymerization*, Ed. Kaminsky W, Sinn H, 1988, Berlin, Springer Verlag, 281.
22. Cheng H N, Ewen J A, Macrmol. Chem., 1989, **190**, 1931.
23. Ewen J A, Elder M J, Jones R L, Curtis S, Cheng H N, Stud. Surf. Sci. Catal., 1990, **56**, 439.
24. Kaminsky W, Külper K, Brintzinger H H, Wild R R W P, Angew. Chem. Int. Ed. Engl., 1985, **24**, 507.
25. Coates G W, Chem. Rev., 2000, **100**, 1223.
26. Kristen M O. *Article about Metallocenes for publication in the Emerging Technology Series: New & Advanced Materials: Metallocenes - From a Laboratory Curiosity to Industrial Scale Applications*. in *2nd Annual UNESCO Training School & Poster Symposium*. 1999. Rosebank, Johannesburg.
27. Collins S, Ward G, J. Am. Chem. Soc., 1992, **114**, 5460.
28. Soga K, Deng H, Yano T, Shiono T, Macromolecules, 1994, **27**, 7938.
29. Yasuda H, Yamamoto H, Yamashita, Yokota K, Nakamura A, Miyake S, Kai Y, Kanehisa Y, Macromolecules, 1993, **26**, 7134.
30. Yasuda H, Yamamoto H, Yokota K, Miyake S, Nakamura A, J. Am. Chem. Soc., 1992, **114**, 4908.
31. Giardello M A, Yamamoto Y, Brard L, Marks T J, J. Am. Soc., 1995, **117**, 3276.
32. Collins S, Ward D G, Suddaby K H, Macromolecules, 1994, **27**, 7222.
33. Li Y, Ward D G, Reddey S S, Collins S, Macromolecules, 1997, **30**, 1875.
34. Frauenrath H, Keul H, Höcker H, *Single component Zirconocene catalysts for the stereospecific polymerization of MMA*. in Organometallic Catalysts and Olefin Polymerization, Ed. Blom R, Follestad A, Rytter E, Tilset M, Ystenes M, 2000, Berlin, Springer Verlag, 97.
35. Cameron P A, Gibson V C, Graham A J, Macromolecules, 2000, **33**, 4329.
36. Sustmann R, Sicking W, Bandermann F, Ferenz M, Macromolecules, 1999, **32**, 4204.
37. Deng H, Shiono T, Soga K, Macromol. Chem. Phys., 1995, **196**, 1971.
38. Moore J C, J. Polym. Sci.: Part A, 1964, **2**, 835.
39. Cortis-Jones B, Nature, 1961, **191**, 272.

40. Alm R S, Williams R J P, Tiselius A, Acta Chem. Scand., 1952, **6**, 826.
41. Snyder L R, J. Chromatogr., 1964, **13**, 415.
42. Snyder L R, Warren H D, J. Chromatogr., 1964, **15**, 344.
43. Teramachi S, Hasegawa A, Shima Y, Akatsuka M, Nasahiko N, Macromolecules, 1979, **12** (5), 992.
44. Glöckner G, J. Chromatogr., 1987, **403**, 280.
45. Glöckner G, van-der-Berg J H M, J. Chromatogr., 1986, **352**, 511.
46. Glöckner G, Chromatographia, 1988, **25** (10), 854.
47. Mori S, Mouri M, Anal. Chem., 1989, **61**, 2171.
48. Mori S, J. Appl. Polym. Sci., 1989, **38**, 95.
49. Snyder L R, Stadalius M A, Quarry M A, Anal. Chem., 1983, **55** (14), 1413.
50. Quarry M A, Stadalius M A, Mourey T H, Snyder L R, J. Chromatog., 1986, **358**, 1.
51. Sato H, Ogino K, Maruo S, Sasaki M, J. Polym. Sci.: Part B: Polym. Phys., 1991, **29**, 1073.
52. Sato H, Takeuchi H, Suzuki S, Tanaka Y, Makromol. Chem. Rapid Commun., 1984, **5**, 719.
53. Sato H, Takeuchi H, Tanaka Y, Am. Chem. Soc., 1986, **19** (10), 2613.
54. Chang T, Lee H C, Lee W, Macromol. Symp., 1997, **118**, 261.
55. Lee H C, Chang T, Macromolecules, 1996, **29**, 7294.
56. Lee H C, Chang T, Polymer, 1996, **37** (25), 5747.
57. Gorshkov A V, Purdakova T N, Gur'yanova R, Evreinov V V, Poly. Bull., 1986, **15**, 465.
58. Entelis S G, Evreinov V V, Gorshkov A V, Adv. Polym. Sci., 1986, **76**, 129.
59. Belenkii B G, Gankina E S, Tennikov M B, Vilenckik B, J. Chromatogr., 1978, **147**, 99.
60. Zimina T M, Kever Y Y, Melenevskaya Y Y, Zgonnik V N, Belenkii B G, J. Polym. Sci., 1991, **6** (33), 1250.
61. Inagki H, Tanaka T, Pure Appl. Chem., 1980, **54** (2), 309.
62. Gankina E S, Belenkii B G, Chromatogr. Sci., 1991, **55**, 807.
63. Balke S T, J. Am. Chem. Soc., 1987, **4**, 59.
64. Balke S T, Patel R D, Adv. Chem. Ser., 1983, **203**, 281.
65. Glöckner G, van-der-Berg J H M, Meijrink N L J, Scholte T G, Koningsveld R, J. Chromatogr., 1984, **31**, 615.

66. Glöckner G, *Gradient HPLC of Copolymers and Chromatographic Cross-Fractionation*, 1991, Berlin, Heidelberg, New York, Springer-Verlag.
67. Glöckner G, van-der-Berg J H M, Meijerink N L J, Scholte T H G, *Integration of Fundamental Polymer Science and Technolog.* Ch. 2, 1986, 85.
68. Augenstein M, Stickler M, Makromol. Chem., 1990, **191**, 415.
69. Mori S, J. Chromatogr., 1990, **503**, 411.
70. Mori S, Anal. Chem., 1988, **60**, 1125.
71. Kilz P, Labor Praxis, 1993, **6**, 64.
72. Kilz P, Krüger R P, Much H, Schulz G, PMSE Preprints, 1993, **69**, 114.
73. Kilz P, Krüger R P, Much H, Schulz G, ACS Adv. Chem., 1995, **247**, 223.
74. Peterson E A, Sober H A, Fed. Proc., 1954, **13**, 273.
75. van-der-Maeden F P B, Biemond M E F, Janssen P C G M, J. Chromatogr., 1978, **149**, 539.
76. Glöckner G, Spectra 2000, 1989, **17** (140), 41.
77. Glöckner G, Müller A H E, J. Appl. Polym. Sci., 1989, **38**, 1761.
78. Glöckner G, van-der-Berg J H M, J. Chromatogr., 1991, **550**, 629.
79. Mori S, J. Liquid Chrom., 1990, **13** (15), 3039.
80. Tanaka S, Uno M, Tramachi S, Tsukahara Y, Polymer, 1995, **36** (11), 2219.
81. Teramachi S, Hasegawa A, Matsumoto T, Kitahara K, Macromolecules, 1992, **25**, 4025.
82. Teramachi S, Sato S, Shimura H, Watanabe S, Macromolecules, 1995, **28**, 6183.
83. Kawai T, Akasuima M, Teramachi S, Polymer, 1995, **36** (14), 2851.
84. Lyons J W, Poche D, Wang F C-Y, Smith P B, Adv. Mater., 2000, **12** (123), 1847.
85. Zimina T M, Fell A F, Castlendine J B, J. Chromatogr. Sci., 1993, **31** (11), 455.
86. Pasch H, Much H, Schulz G, J Appl Polym Sci: Appl Polym Symp, 1993, **52**, 79.
87. Gorshkov A V, Verenich S S, Evreinov V V, Entelis S G, Chromatographi., 1988, **26**, 338.
88. Pasch H, Zammert I, J. Liquid Chrom., 1994, **17** (14&15), 3091.
89. Pasch H, Brinkmann C, Gallot Y, Polymer, 1993, **34** (19), 4100.

90. Schröder E, Franz J, Hagen E, *Ausgewählte Methoden der Plastanalytik*, 1976, Berlin, Akademie-Verlag.
91. Cantow H J, Probst J, Stojanov C, Kautschuk u. Gummi, 1968, **21**, 609.
92. Balke S T, Sep. Purif. Methods, 1982, **11**, 1.
93. Ross J H, Shank R L, Polymer Preprints, 1971, **12**, 812.
94. Kiser K L, Mantz A W, Bonar L C, Am. Lab., 1975, **7** (5), 85.
95. Brown R S, Hausler D W, Taylor L T, Carter R C, Anal. Chem., 1981, **53** (2), 197.
96. Hellgeth J W, Taylor L T, Anal. Chem., 1987, **59**, 295.
97. Gagel J J, Biemann K, Anal. Chem., 1986, **58**, 2184.
98. Dekmezian A H, Morioka T, Camp C E, J. Polym. Sci. Part B: Polym. Phys., 1990, **28**, 1903.
99. Kalasinsky V F, Whitehead K G, Kenton R C, Smith J A S, Kalasinsky S S, J. Chromatogr. Sci., 1987, **25**, 273.
100. Willis J N, Dwyer J L, Wheeler L M, Polym. Mater. Sci. Eng., 1993, **69**, 120.
101. Pasch H, Trathnigg B, *HPLC of Polymers*, 1998, Berlin, Heidelberg, New York, Springer-Verlag, Ch. 7.
102. Wild L, Adv. Polym. Sci., 1990.
103. Grinshpun V, O'Driscoll K F, Rudin A, J. Appl. Polym. Sci., 1984, **29**, 1071.
104. Housaki T, Satoh K, Makromol. Chem. Rapid. Commun., 1988, **9**, 525.
105. Grumel V, Brüll R, Pasch H, Raubenheimer H G, Sanderson R D, Wahner U M, Macromol. Chem. Phys., 2001, **286** (8), 480.
106. Salovey R, Hellman M Y, J. Polym. Sci. Part A-2, 1967, **5**, 333.
107. Lecacheux D, Lesec J, Quivoron C, J. Appl. Polym. Sci., 1982, **27**, 4867.
108. Shirayama K, Okada T, Kista S, J. Polym. Sci., Part A-2, 1965, **3**, 907.
109. Desreux A, Spiegels M L, Bull. Soc. Chim. Belg., 1950, **59**, 470.
110. Soares J B P, Haimielec A E, Polymer, 1995, **36** (8), 1639.
111. Monrabal B, US Patent 5 222 390, 1991.
112. Monrabal B, J. Appl. Polym. Sci., 1994, **52**, 491.
113. Pasch H, Brüll R, Wahner U, Monrabal B, Macromol. Mater. Eng., 2000, **279**, 46.
114. Monrabal B, *Chemical composition distribution analysis in polyolefins. Introduction to crystallization analysis fractionation. CRYSTAF.* Research

Signpost, Ed. Hosoda S, 1996, New trends in polyolefin science and technology, 119.

115. Monrabal B, *Temperature rising elution fractionation and crystallization analysis fractionation*. Encyclopaedia of Analytical Chemistry, 2000, Chichester, John Wiley & Sons Ltd, 8074.
116. Kim D J, Soares J B P, Macromol. Rapid. Commun., 1999, **20**, 347.
117. Chu K J, Soares J B P, Penlidis A, Macromol. Chem. Phys., 2000, **201**, 340.
118. Chu K J, Soares J B P, Penlidis A, Ihm S K, Macromol. Chem. Phys., 1999, **200**, 1298.
119. Chu K J, Shan C L P, Soares J B P, Penlidis A, Macromol. Chem. Phys., 1999, **200**, 2372.
120. Soares J B P, Abbott R F, Kim D J, J. Polym. Sci., Part B: Polym. Phys., 2000, **38**, 1267.
121. Brüll R, Grumel V, Pasch H, Raubenheimer H G, Sanderson R D, Wahner U, Macromol. Symp., 2002, **55**, 178.
122. Graef S M, Wahner U M, van-Reenen A J, Brüll R, Sanderson R D, Pasch H, J. Polym. Sci. Part A: Polym. Chem., 2002, **40**, 128.
123. van-Reenen A J, Brull R, Wahner U W, Raubenheimer H G, Sanderson R D, Pasch H, J. Polym. Sci., Part A: Polym. Chem., 2000, **38** (22), 4110.
124. Beigzadeh D, Soares J B P, Duever T A, J. Appl. Polym. Sci., 2001, **80**, 2200.
125. Costeux S, Anantawaraskul S, Wood-Adams P M, Soares J B P, Macromol. Theory. Simul., 2002, **11**, 326.
126. Starck P, Lehmus P, Seppälä J V, Polym. Eng. Sci., 1999, **39** (8), 1444.
127. Britto L J D, Soares J B P, Penlidis A, 2000, **8** (2), 159.
128. Gabriel C, Lilge D, Polymer, 2001, **42**, 297.

CHAPTER 3

Experimental

3.1 Introduction

This chapter will cover all the materials, instrumentations and parameter settings for all the instruments used in this study. This is done to avoid repetition in the subsequent chapters. Detailed information will be given on the synthesis of the different materials ethylene/higher α-olefins, propylene/higher α-olefins and ethylene/methyl methacrylate copolymers via metallocene catalysts. Detailed information on the working of certain techniques is given since these are not standard analytical techniques used in laboratories.

3.2 Materials

3.2.1 Solvents

The following solvents used for the solubility tests in CRYSTAF were received from Sigma-Aldrich: 1,2,4-trichlorobenzene (TCB); 1,2-dichlorobenzene (DCB); chlorobenzene (CB) and 1,1,2,2-tetrachloroethene (TClEt). HLPC-Grade 1,2,4-trichlorobenzene (TCB) and N,N-dimethylformamide (DMF) from Acros were used for analytical work done on gradient HPLC and SEC. 1,1,2,2-Tetrachloroethene used for the detection of MMA concentration via CRYSTAF analysis was supplied by a local supplier in Spain. Deuterated benzene (C_6D_6) (Sigma Aldrich) was used in

combination with TCB as internal standard in NMR spectroscopy. Toluene (obtained from Aldrich) was dried by refluxing over sodium. Cyclohexanone (CH) used for the liquid chromatography under critical conditions was purchased from Merck, Germany.

3.2.2 Monomers

Propylene was obtained from Fedgas and purified by passing it through copper-based catalysts R3-11G and R3-12, as obtained from BASF at 110 °C, and a column of 4 Å molecular sieve (obtained from Merck), to removes traces of water and oxygen. Ethylene was used as supplied by Fedgas. The higher α-olefins (1-hexene, 1-decene, 1-dodecene, 1-tetradecene and 1-octadecene) were purchased from Sigma-Aldrich, dried over $LiAlH_4$ and stored under an inert atmosphere until used.

3.2.3 Catalysts

Synthesis of polyethylene

The transition metal pre-catalyst $Et(Ind)_2ZrCl_2$ [**1**] in Scheme 3.1, was purchased form Sigma Aldrich, South Africa.

Synthesis of isotactic polypropylene

The transition metal pre-catalyst, $(CH_3)_2Si$(2-methylbenz[e]indenyl)$_2ZrCl_2$ [**2**] in Scheme 3.1, was kindly donated by H. H. Brintzinger from the University of Konstanz, Germany.

Synthesis of syndiotactic polypropylene

The syndiospecific pre-catalyst *i*-Pr(Cp)(9-Flu)$ZrCl_2$ [**3**] in Scheme 3.1, was purchased from Boulder Scientific.

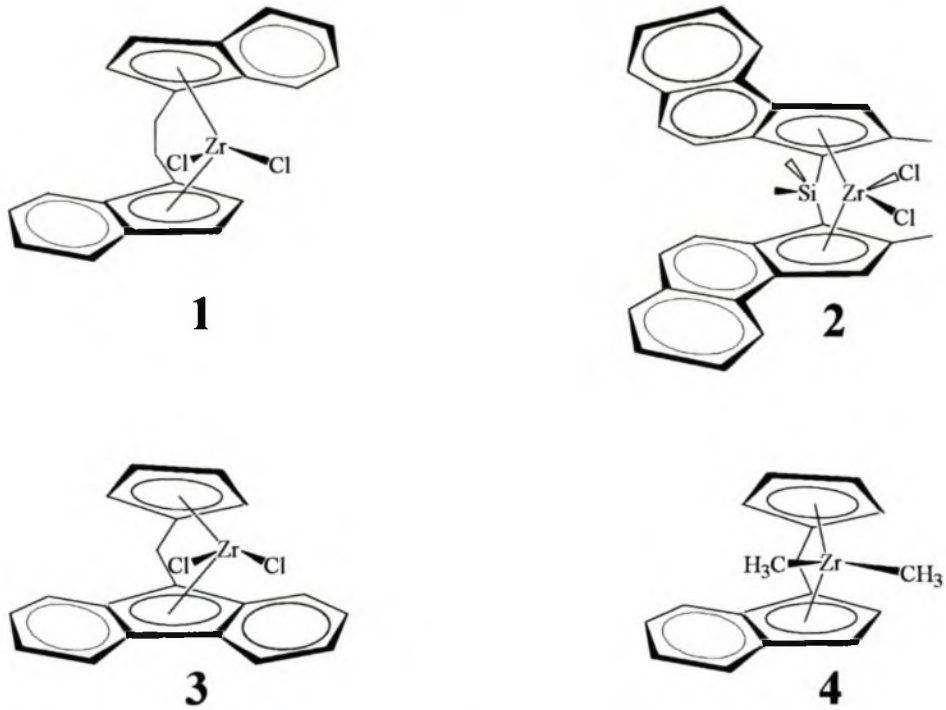

Scheme 3.1. Pre-catalysts used in the polymerisations of monomers considered in this study: $Et(Ind)_2ZrCl_2$ [**1**], $(CH_3)_2Si$(2-methylbenz[e]indenyl)$_2ZrCl_2$ [**2**], *i*-Pr(Cp)(9-Flu)$ZrCl_2$ [**3**] and $Me_2C(Cp)(Ind)ZrMe_2$ [**4**].

Synthesis of ethylene/MMA copolymer

The syntheses of the ethylene/MMA copolymers were carried out with the $Me_2C(Cp)(Ind)ZrMe_2$ [**4**] (Scheme 3.1) pre-catalyst. **4** was synthesised in-house by the research group in the Institut für Technische Chemie und Makromolekulare Chemie at RWTH Aachen, Germany.

3.2.4 Cocatalysts

Methylaluminoxane (MAO) (10% w/v in toluene) was obtained from Aldrich. MAO was used as scavenger in polymerisations initiated by the active forms of pre-catalysts **1**, **2** and **3**.

In the synthesis of the ethylene and MMA copolymers with **4**, $B(C_6F_5)_3$ was employed to activate the pre-catalyst. $B(C_6F_5)_3$ was synthesised in-house by the research group

at the Institut für Technische Chemie und Makromolekulare Chemie der RWTH Aachen, Germany.

3.3 Polymerisations

3.3.1 Polymerisation of ethylene and propylene with higher α-olefins

The polymerisation reactions were carried out in a 350 cm^3 Teflon®-stainless steel Parr autoclave with a glass insert (Figure 3.1(A) and (B)) at room temperature

Table 3.1. Comonomer contents as calculated from ^{13}C NMR spectroscopy. Quantities of ethylene and comonomer added under feed conditions.

Sample code	Comonomer content in polymer (mol-%)	Volume comonomer (mL)	Ethylene weight (g)	Comonomer content in feed (mol-%)
Polyethylene				
PE	0	0	17.6	0
1-Hexene				
EH1	0.57	2	17.6	1.66
EH2	1.05	6	15.5	5.43
EH3	1.79	12	16.2	9.89
EH4	2.83	18	12.6	17.47
EH5	3.57	6	6.9	11.42
1-Tetradecene				
ET1	2	12	14.5	8.39
ET2	2.02	6	12.0	5.25
ET3	2.23	6	6.5	9.27
ET4	2.83	18	12.2	14.04
ET5	3.27	24	13.7	16.24
ET6	4.56	12	5.9	18.38
ET7	5.86	18	6.4	23.74
1-Octadecene				
EO1	1.43	6	15.2	3.34
EO2	1.66	18	14.2	10.00
EO3	1.77	6	7.0	6.99
EO4	2.33	24	15.7	11.82
EO5	3.55	12	5.3	16.56
EO6	4.03	24	6.4	24.74

Reaction conditions: a) pre-catalyst **1**
b) [Zr]/[Al] = 1:6 000
c) reaction temperature 25 °C

(25 °C). The reactors, glass inlets, glass funnel, magnetic stirrer bar and syringes were super-dried overnight in an oven at 120 °C and cooled down under a nitrogen atmosphere prior to use. After the assembly of the autoclave, three consecutive vacuum and nitrogen purge cycles were carried out, to remove all moisture still present in the reactor. The catalyst, still in powder form, was weighed off in a dry box (glove box) under nitrogen atmosphere. The dry box, with the necessary equipment, was prepared with four vacuum and nitrogen purge cycles. All the reactants were prepared and combined under an inert gas atmosphere using standard Schlenk techniques. All polymerisation reactions were carried out at [Zr] = 8 μmol/L in 50 mL toluene. Tables 3.1 and 3.2 depict the volumes of liquid comonomers used and the weights of ethylene and propylene gasses employed for the polymerisations. Table 3.3 only gives the comonomer content of the polymer. In the case of propylene, the reactor was pressurised at 0 °C to ensure maximum intake of the monomer. In all these reactions, 3.7 mL of the MAO solution was used. The reactor was weighed before the addition of gaseous monomers and weighed again after the addition. After 3 hours the reaction was stopped, the polymer precipitated with acidic methanol (10 % HCl), washed and subsequently dried in a vacuum oven at 60 °C for three days. ^{1}H-NMR spectroscopy showed that the propylene copolymers did not contain residual higher 1-olefins after work up.

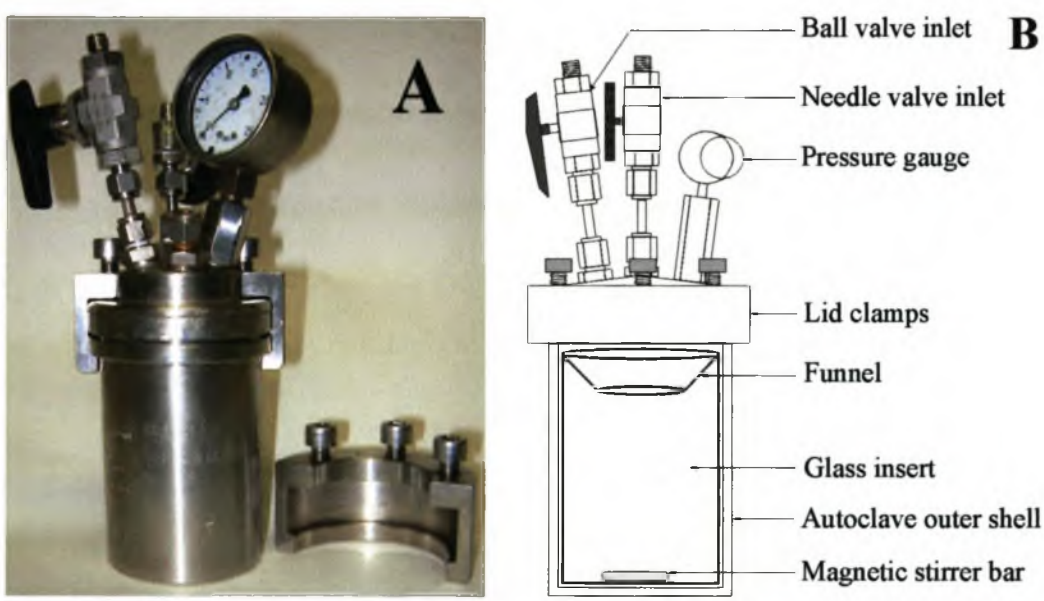

Figure 3.1. A) Photograph of the autoclave reactor and B) Schematic illustration of the different components of the autoclave reactor.

Table 3.2. Comonomer contents as calculated from ^{13}C NMR spectroscopy. Quantities of propylene and comonomer added under feed conditions.

Sample code	Comonomer content in polymer (mol-%)	Volume comonomer (mL)	Propylene weight (g)	Comonomer content in feed (mol-%)
Polypropylene				
s-PP	0	0	23.1	0
1-Hexene				
H1	0.61	1	29.7	1.14
H2	0.96	2	29.0	2.34
H3	1.02	2	25.0	2.71
H4	1.76	3	22.1	4.60
H5	1.88	3	23.0	4.44
H6	1.95	6	25.0	8.14
H7	2.03	4	19.0	7.14
H8	2.12	4	28.0	4.84
H9	4.19	4	10.0	13.56
H10	8.15	15	24.0	21.19
1-Dodecene				
D1	0.24	1	21.3	0.31
D2	0.27	1	60.6	0.47
D3	0.3	1	24.7	0.77
D4	0.35	1	30.2	0.63
D5	0.38	1	18.2	1.04
D6	0.49	2	25.0	1.52
D7	0.52	3	34.0	1.67
D8	0.8	1	10.4	1.82
D9	0.83	3	23.0	2.47
D10	0.89	4	22.0	3.45
D11	1.52	5	22.0	4.31
D12	6.65	20	34.0	11.15
1-Octadecene				
O1	0.27	1	22.7	0.58
O2	0.39	2	24.1	1.09
O3	0.58	1	11.2	1.17
O4	0.75	3	23.7	1.66
O5	0.78	2	13.6	1.93
O6	0.84	4	21.0	2.50
O7	0.87	4	19.0	2.77
O8	0.95	3	15.9	2.48
O9	2.14	4	11.6	4.53
O10	2.65	3	9.4	4.2
O11	4.48	20	25	10.52

Reaction conditions: a) pre-catalyst **2**
b) [Zr]/[Al] = 1:1 000
c) reaction temperature 25 °C

Table 3.3. Comonomer content as calculated from ^{13}C NMR spectroscopy for the isotactic propylene/1-hexene copolymers.

Sample code	Comonomer content in polymer (mol-%)
PH1	0,30
PH2	0,32
PH3	0,46
PH4	1,03
PH5	1,24
PH6	1,39
PH7	1,80
PH8	2,35
PH9	2,41

Reaction conditions: a) pre-catalyst **3**
b) [Zr]/[Al] = 1:6 000
c) reaction temperature 25 °C

3.3.2 Ethylene/MMA copolymerisation

The poly(ethylene-co-MMA) samples were synthesised through the collaboration with colleagues (S. Balk and H. Keul) at the Institut für Technische Chemie und Makromolekulare Chemie der RWTH Aachen, Germany.

All copolymerisation reactions were carried out in a 1L glass autoclave (Büchi), seen in Figure 3.2. In the first step of the reaction sequence the reactor was placed under vacuum for 3 hours, to ensure a moisture-free surface. Toluene (400 mL) was then added and the reactor was left for a few minutes to equilibrate at a temperature of 8 °C. Temperature control of the reactor was maintained by means of an external cooling bath from which the water was circulated through the outer mantel of the reactor, as seen in Figure 3.2. The co-catalyst and **4** (amounts as depicted in Table 3.4) were each dissolved in 5-10 mL of toluene. After the temperature equilibration the co-catalyst was added, followed by the addition of **4**. This was done so that the co-catalyst can scavenge any unwanted molecules that could have entered the reactor together with the toluene. A constant pressure of 2 bar ethylene gas was applied to the reactor for predetermined times (Table 3.4). After this predetermined time ±10 mg of MMA was added at a pressure of 2 bar. The ethylene gas was turned off and the reaction left for 2 hours at 8 °C. For termination of the reaction, methanol

and HCl were used. This resulted in the precipitation of the polymer from the solution. The polymer was dried in a vacuum oven at a temperature of 45 °C for a day.

Table 3.4. Reaction conditions for the synthesis of poly(ethylene-co-MMA), with reference to the monomers, $B(C_6F_5)_3$ as cocatalyst and the pre-catalyst **4** added, as well as the polymerisation times for each reaction.

Sample code	Duration of ethylene added (min)	MMA (mg)	$B(C_6F_5)_3$ (g)	$Me_2C(Cp)(Ind)ZrMe_2$ [**4**] (g)	Polymerisation time (min)
T0	-	28.08	0.80	0.45	120
T1	1	9.92	0.77	0.32	120
T8	12.5	9.71	0.96	0.48	120
T9	15	9.61	1.38	0.36	120
T11	20	9.61	1.53	0.34	120

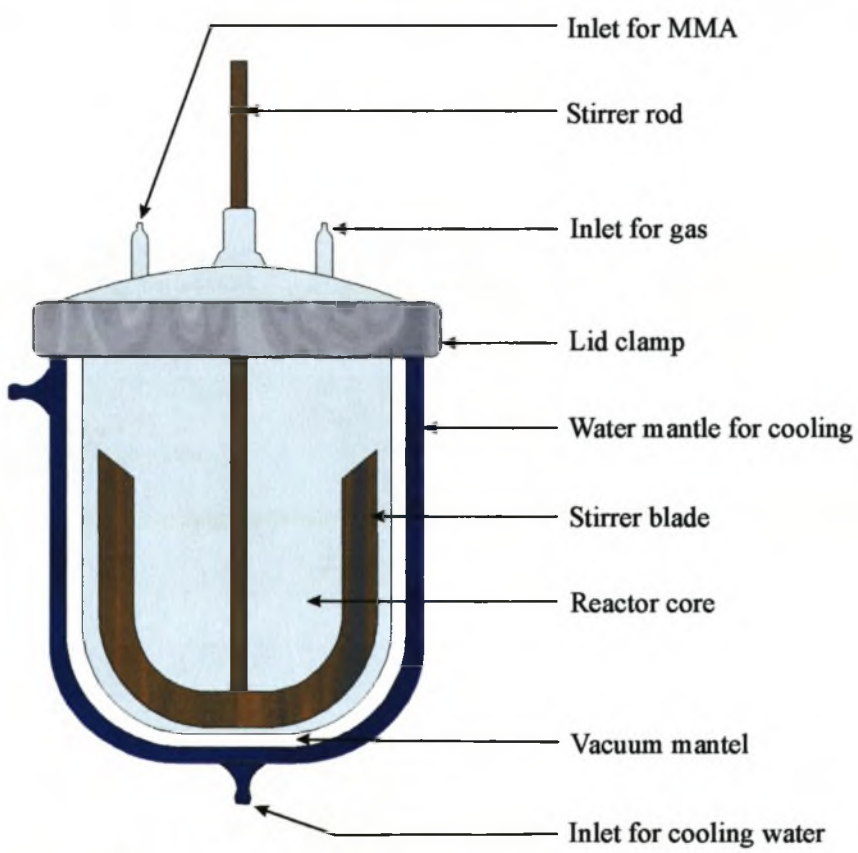

Figure 3.2. Schematic illustration of the reactor set-up used for the synthesis of ethylene/MMA copolymers, as employed at the University of Aachen.

3.4 Commercial polymers

Lupolen 3020D, a LDPE polymer from BASF, with a $M_n = 4.6 \times 10^4$ g/mol, was used as standard for the tests involving the parameter changes in CRYSTAF, except when specified otherwise. In the latter cases, Lupolen 5162Z, a high density polyethylene HDPE, with a $M_n = 5.7 \times 10^4$ g/mol, was used. The standards used for the calibration of the high temperature gradient HPLC (HTG-HPLC) system and the determination of the critical point in liquid chromatography under critical conditions (LCCC) are shown in Table 3.5. These standards were obtained from Polymer Standards Service (PSS), Mainz, Germany.

Table 3.5. PMMA and PE standards used for the calibration of the HTG-HPLC and the LCCC systems.

Standard	[a] M_p (g/mol)	[b] M_n (g/mol)	Standard	[a] M_p (g/mol)	[b] M_n (g/mol)
PE	1080	1110	PMMA	1020	
PE	2030		PMMA	1960	1730
PE	22000	12000	PMMA	4250	
PE	33500		PMMA	10900	
PE	66000		PMMA	24400	22200
PE	77500		PMMA	56900	
PE	126000	114000	PMMA	85100	
PE	145500		PMMA	175000	
PE	260000		PMMA	263000	
PE	500000		PMMA	296000	
			PMMA	675000	
			PMMA	903000	829000

[a] Peak maximum MM was used in LCCC
[b] Number average molar mass was used in HTG-HPLC

3.5 Extractables

For all analytical purposes, in chapter 6, all ethylene/higher α-olefm copolymers synthesised by **1** were extracted according to the method explained there. The extracted and the non-extracted samples (as used in Chapter 4) were taken from the

same reaction batch for a comparative analysis by CRYSTAF. The samples to be extracted were placed into a reflux extraction set-up, by which most of the monomer and catalyst could be solvent extracted. Extractions were run over a period of 6 hours, using petroleum ether (b.p. 80-100 °C). The samples were subsequently dried in a vacuum oven for 24 hours at 70 °C. After completion of the extraction process these samples were then analysed by CRYSTAF analysis with the TCB method set-up, as explained in Table 3.6.

3.6 Analytical equipment

3.6.1 Thermal analysis

Differential scanning calorimetry (DSC)

The thermal properties of the ethylene/MMA copolymers were determined, under an inert atmosphere, with the aid of a SII Seiko Instruments DSC 22C and controlled by a SII Seiko Instrument SSC 5100. All other samples were measured with the Pyris 1 from Perkin Elmer, also under an intert atmosphere. The samples (5 mg) were heated from –50°C to 180 °C, cooled from 180 °C to –50 °C, and subsequently heated from -50 °C to 180 °C at heating and cooling rates of 10 °C/min. In the propylene/α-olefin copolymer and ethylene/α-olefin copolymer experiments, the cooling- and heating rate parameters were changed to test certain properties (with rates set at 5 °/min on the Pyris 1 (PP samples; chapter 5) and 1 °C/min on the SII Seiko Instruments DSC 22C (PE samples; chapter 6)). Only the second heating profile was used for analysis, in order to ensure the same thermal history for all samples. The DSC was used to obtain the melting point temperature, $T_{m\ (DSC)}$, crystallization temperature on heating, $T_{c\ (DSC,\ heat)}$ (cold crystallization) [1-3], crystallization temperature on cooling, $T_{c\ (DSC)}$, and the heat of fusion ΔH.

Dynamic mechanical analysis (DMA)

The Perkin Elmer DMA 7e with Intracooler II (for the cooling of the samples) was used for the additional determination of the glass transition temperature (T_g) of the samples. Pyris© Manager software for windows version 3.81 was used for the control of the instrument, data collection and data manipulation. Samples (5 mg) were cooled down from room temperature to –55 °C after which the sample was heated up at a rate of 5 °C/min to an final temperature of 140 °C. Analysis of the samples was done with a parallel plate measuring system, meaning that the analysis was done in compression mode.

3.6.2 Molar mass determination

The molar masses and the polydispersities of the polymers were determined with a Waters 150C high temperature GPC instrument. 12 mg of each polymer sample were dissolved in 3 mL of 1,2,4-trichlorobenzene at 140 °C and 100 µL of the solution were used for analysis at a flow rate of 1 mL/min. Columns HT 6, 5, 4, 3 and 2 (as obtained from Waters) were used. GPC software from Polymer Standards Service (PSS, Mainz, Germany) was used for data collection. The same instrumental settings were used as for the separation of samples analysed by LC-Transform coupled to high temperature GPC. The injection volume was however increased to 150 µL for the samples run in both the ethylene/MMA copolymers and ethylene/α-olefin copolymers experiments. In the ethylene/α-olefin copolymers experiments, the solution concentration was increased to 3 mg/mL.

3.6.3 Crystallisation Analysis Fractionation (CRYSTAF)

General procedure

CRYSTAF is a new technique for the analysis of semi-crystalline polymers containing various amounts of short chain branching distribution (SCBD). The

CRYSTAF Model 200 with liquid nitrogen cooling unit, as obtained from Polymer Char (Valencia Spain), was used to measure the crystallisation temperature in solution. TCB was selected as solvent for the analysis of the poly(ethylene-co-MMA), PE copolymers, isotactic poly(propylene-co-1-hexene) and commercial polymers (Lupolen 3020D and Lupolen 5162Z). The limiting factor of TCB as solvent is its melting point at 16 °C. For this reason, DCB (MP = -17 °C) was used in the analysis of syndiotactic PP copolymers. The isotactic poly(propylene-co-1-hexene) samples were additionally analysed in DCB, CB and TClEt. 20 mg samples were dissolved in 30 mL of solvent, unless specified otherwise. Two general analytical methods were used in all CRYSTAF measurements, except when specified otherwise (Table 3.6). Fractions were taken automatically and the polymer concentration in solution was determined by an infrared detector, using 3.5 μm as measuring wavelength.

Table 3.6. Parameter changes for the TCB and DCB temperature programs in CRYSTAF analysis.

Method procedure	TCB method values	DCB method values
Dissolution temperature (°C)	150	140
Dissolution time (min)	60	30
Stabilization temperature (°C)	100	80
Stabilization time (min)	60	45
Cooling rate (°C/min)	0.1	0.1
Final analysis temperature (°C)	20	-10
Number of data points set	36	36

MMA detection

For the determination of MMA concentration in the poly(ethylene-co-MMA) samples via CRYSTAF a different set-up to the standard detector was needed. The technology required for the analysis of the above-mentioned polymers was not available at Deutsches Kunststoff-Institut in Darmstadt (Germany), nor in our laboratory at the University of Stellenbosch (South Africa). These samples were subsequently kindly analysed by B. Monrabal from Polymer Char in Spain. Perchlorethylene was used as solvent. The IR detector was equipped with a 5.82 micron filter, with a bandwidth of 95 nanometers (per definition, a filter that can only measure adsorption in the

carbonyl region around 1700 cm^{-1} to 1760 cm^{-1}). The temperature program was run from 80 °C to –10 °C, with a cooling rate of 0.1° C/min.

3.6.4 ^{13}C- and ^{1}H-NMR Spectroscopy

Experiments were carried out at 300 MHz (^{1}H spectra) and 75.42 MHz (^{13}C spectra) on a Varian VXR-300 NMR spectrometer using broadband proton decoupling at 100 °C. A 9:1 mixture of TCB/C_6D_6 was used as solvent for the analysis of all polymer samples. C_6D_6 (observed at 128.6 ppm in the ^{13}C spectra) served as a secondary, internal reference. The pulse delay (D1) was 0.0012 sec, the total acquisition time was 0.810 seconds per scan, the number of scans was 4 000 and the pulse angle was 45°. The comonomer content as calculated by NMR spectroscopy, in the following chapters, is given as the percentage comonomer (methyl methacrylate, 1-hexene, 1-decene, 1-dodecene, 1-tetradecene and 1-octadecene) to ethylene or propylene.

3.6.5 High temperature gradient HPLC

To our knowledge, this is the first successful separation of polymers by means of gradient chromatography at high temperatures. The separation was achieved by combining different chromatographic units. The Spectra Series P200 was used as a gradient pump, for a gradient of 100 % DMF to 100 % TCB, as shown in Figure 3.3. The total run time for the gradient was 45 minutes, with a flow rate of 0.5 mL/min. Separation was carried out with a Nucleosil 300 C_{18} column (250x4.6 mm I.D.), which was placed into the column oven of the Waters 150C at 140 °C. The Waters 150C injector was used to inject 70 µL of polystyrene standards for the calibration curve and 150 µL of sample into the column at 140 °C. The sample concentration for the analysis was 1 mg/mL. The evaporative light scattering detector ELSD-PL 1000 (with gas flow speed at 1 mL/min, nozzle temperature at 270 °C and chamber temperature of 200 °C) was obtained from Polymer Laboratories, United Kingdom.

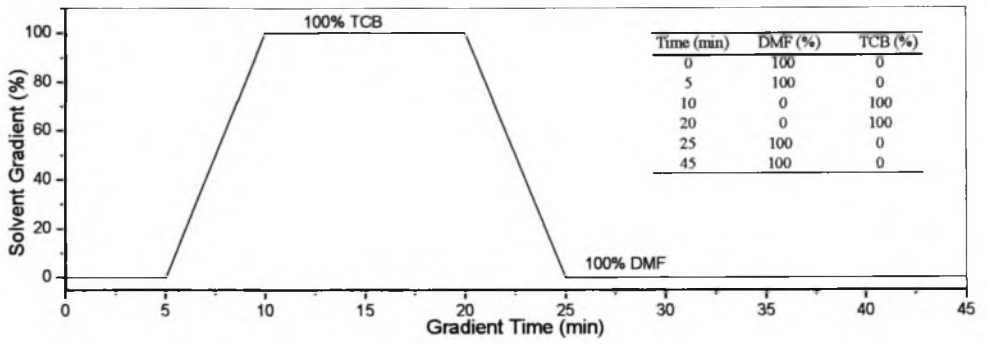

Time (min)	DMF (%)	TCB (%)
0	100	0
5	100	0
10	0	100
20	0	100
25	100	0
45	100	0

Figure 3.3. Solvent profile, as obtained for high temperature gradient HPLC separation.

3.6.6 Fourier Transformed Infra-Red (FTIR) spectroscopy

Polyolefin samples used in this study were either powders or solids and subsequently only soluble at high temperatures in TCB. A special optical sample press module from Sensir Technologies (type: Dicomp) was used for solute or powdery samples. This allowed the analysis of samples without tedious sample preparation. The sample press was placed in the Nicolet (NEXUS) Fourier Transform Infrared (FTIR) spectroscope sample holder compartment, see Figure 3.4, where the IR spectra can be collected through attenuated total reflectance (ATR). 50 scans were done per spectra. Data collection as well as manipulation were done with the aid of Omnic E.S.P. 5.1 software.

3.6.7 GPC coupled to FTIR spectroscopy (LC-Transform)

Instrumental set-up

The use of the GPC coupled to FTIR spectroscopy through LC-Transform is a unique analytical method, as samples are retained permanently on a Germanium disc (IR

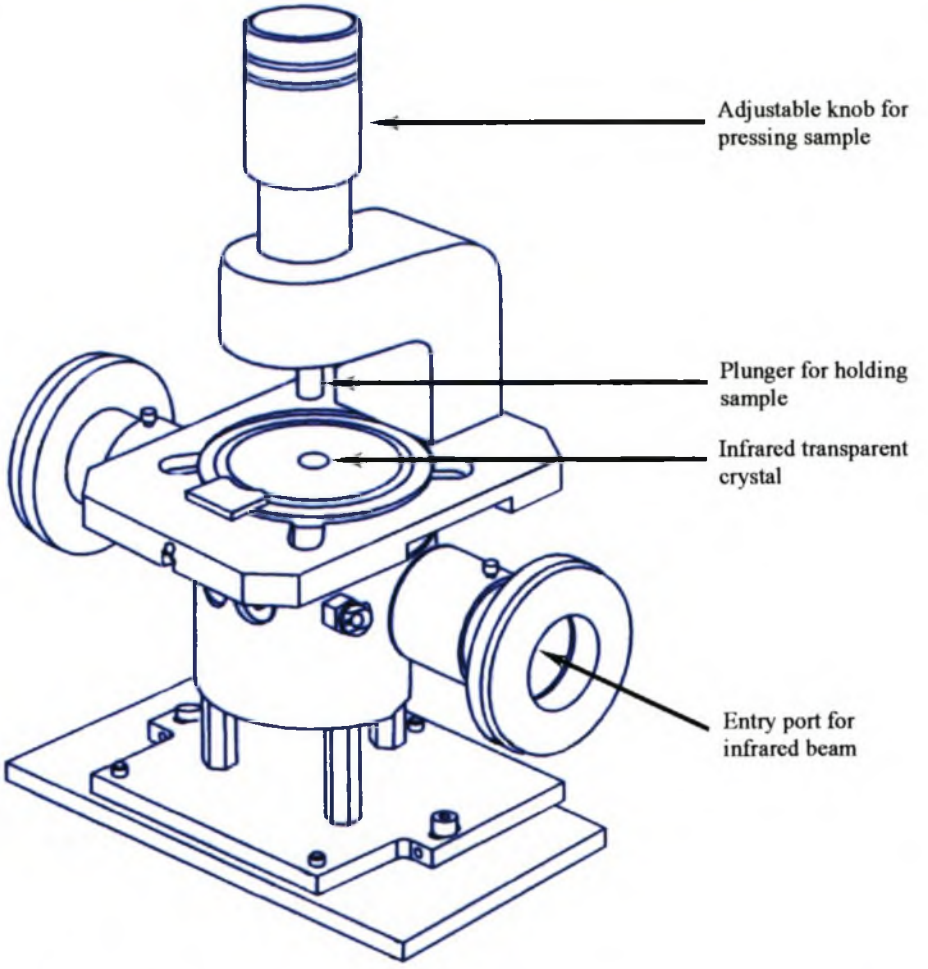

Figure 3.4. Schematic illustration of the optical sample press used for the IR analysis of all powdery and solute samples.

transmission in the range of 450-6000 cm^{-1}). The combination of an ultrasonic nozzle, elevated temperatures and vacuum (of 8-12 torr) permits the use of solvents with high boiling points as eluents. By spraying the solution separated by a chromatographic technique directly onto the rotation disc, samples can be deposited solvent-free onto the disc (Figure 3.5(A) and 3.6). Reflective transmission infrared spectroscopy, measured by a FTIR, is only possible due to the aluminium coated backside of the disc (Figure 3.5(B)). The optical module placed inside the FTIR apparatus also rotates the disc while scanning continuously, thus collecting a series of infrared spectra. This series of spectra can be converted to a total intensity- (Gram Schmidt) or selective wavenumber-chromatogram (chemigram) respectively. The Gram Schmidt is thus the sum of all the intensities in a spectrum during the retention

or elution time whereas the chemigram is only the sum of a certain peak height or peak area during the elution time.

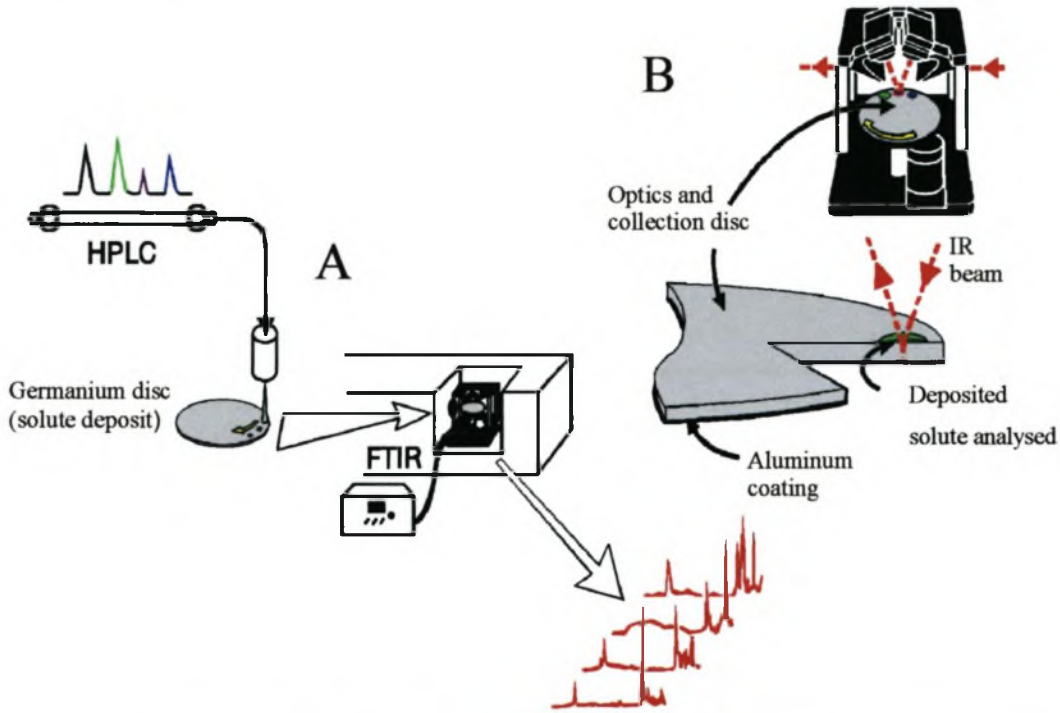

Figure 3.5. Illustration of the (A) collection module, after the separation by the HPLC system, and (B) the optical module in a FTIR spectrometer to allow the scanning of the disc.

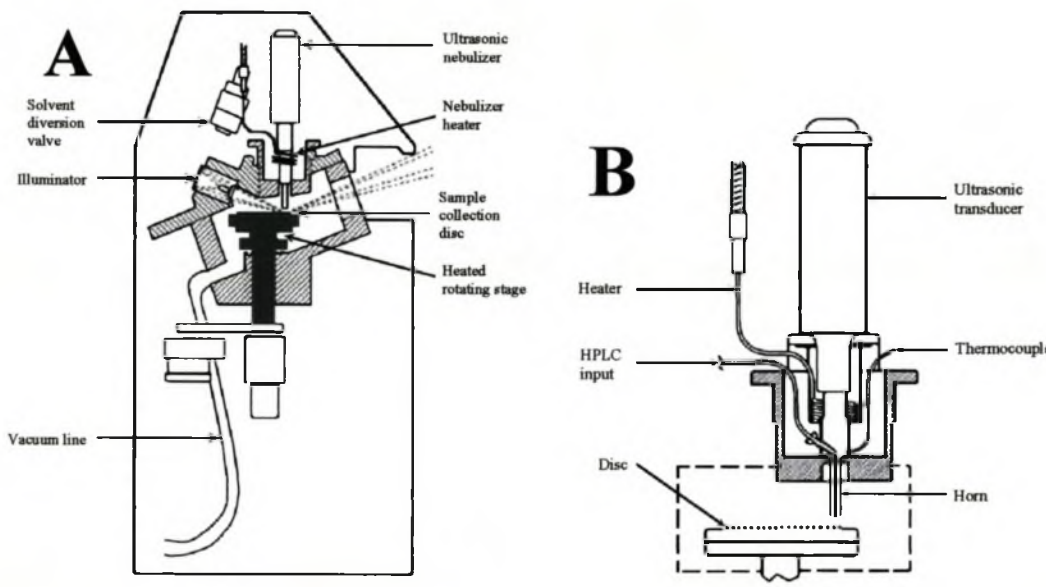

Figure 3.6. The heating chamber of the LC-Transform (A), with an enlargement of the ultrasonic transducer (B).

A more detailed schematic illustration of the LC-Transform collection module is given in Figure 3.6. The heating chamber, in the collection module (Figure 3.6 (A)), contains the heated rotating stage, an outlet to the vacuum pump, the ultrasonic nozzle and an observation light. The ultrasonic nozzle consists of an ultrasonic transducer, heater unit, thermocouple and heated transfer line from the HPLC instrument (Figure 3.6(B)). The function of the ultrasonic nozzle is to generate an aerosol from the eluent.

Experimental set-up

Sample collection was done on the Lab Connections 300 series LC-Transform®. All settings related to the samples collection for the ethylene/MMA copolymer and ethylene/α-olefin copolymers are given in Table 3.7.

Table 3.7. Instrumental settings as used for sample collection, using different samples and separation methods.

	Ethylene/MMA Copolymer		Ethylene/α-olefin copolymer
Instrumental settings	Gradient HPLC	GPC	GPC
Transfer line (°C)	140	120	145
Stage temperature (°C)	155	175	162
Ultrasonic nozzle (°C)	75	110	124
Rotation speed (°/min)	10	10	10

The optic module was set at a rotation speed of 10°/min for size exclusion separation and 5°/min for gradient separation. Slower rotation was used for the gradient separation to ensure better resolution in the IR. Samples were conditioned for 1 hour under an inert atmosphere inside the FTIR sample compartment to remove all moisture from the surrounding atmosphere. FTIR analysis was carried out on a Nicolet Instrument Protege 460. Infrared instrumentation control and data collection were done with Omnic 5.1b software and its extension software (Series 5.1b). Twenty background scans were collected on a part of the disc where no sample was

deposited. For gradient HPLC 80 background scans were done. IR spectra were taken at a scanning rate of 20 scans per spectrum.

3.6.8 Liquid Chromatography under Critical Conditions (LCCC)

This is the first successful separation of polymers by means of LCCC at high temperatures. The separation was achieved by combining different chromatographic units. The Waters 150C was used, and the column oven and injector compartment were kept at a constant temperature of 140 °C. Separation was done on a Nucleosil 300 (250×4 mm I.D.) silica gel column. Both standards and samples were made up to a concentration of 1 mg/mL and 40 μL of the solution was injected. The critical solvent composition was determined as 34,5/65,5 (V/V%) of TCB to cyclohexanone. The exact determination of this critical point will be discussed in Chapter 7. The flow speed was 1 mL/min. The evaporative light scattering detector, ELSD-PL 1000 was obtained from Polymer Laboratories, United Kingdom. Conditions used were gas flow speed 0.8 mL/min, nozzle temperature 270 °C and chamber temperature 200 °C.

3.7 References

1. Tanaka M, Motomura T, Ishii N, Shimura K, Onishi M, Mochizuki A, Hatakeyama T, Polymer International, 2000, **49** (12), 1709.
2. Cho J W, Woo K S, J. Polym. Sci. Part B: Polym. Phys., 2001, **39** (16), 1920.
3. Qiu Z, Mo Z, Zhang H, Shouri S, Song C, J. Appl. Polym. Sci., 2000, 77 (13), 2865.

CHAPTER 4

POLYOLEFIN CRYSTALLISATION IN SOLUTION MEASURED BY CRYSTALLISATION ANALYSIS FRACTIONATION (CRYSTAF)

4.1 Abstract

Crystallisation Analysis Fractionation (CRYSTAF) is a new technique for the compositional analysis of semi-crystalline polymers. For instance, it can determine various degrees of short chain branching distribution (SCBD). This is based on the segregation of crystals with different comonomer content by a stepwise crystallisation precipitation approach in the form of crystallisation. By monitoring the polymer solution concentration during the crystallisation process a collective and differential SCBD can be observed without the need of physical separation of the fractions. The homogeneity of polyolefins synthesised by different techniques can thus be analysed according to their chemical composition distribution (CCD). This technique was studied for the optimisation of the parameters to obtain results in the shortest time. Influence of the crystallisation temperature in solution was observed when changing both the amount of samples and the type of solvents used. By use of copolymers with known comonomer content the comonomer concentration distributions of unknown samples were determined. A correlation was indeed achieved between SCBD and the temperature profile.

4.2 Introduction

Crystallisation Analysis Fractionation (CRYSTAF) is a new technique for the analysis of semi-crystalline polymers containing various amounts of short chain branching distribution (SCBD). The method was developed by B. Monrabal [1, 2]. The technique is based on the segregation of crystals with different comonomer content by a stepwise precipitation approach (through a slow cooling cycle) in the form of crystallisation. By monitoring the polymer solution concentration during the crystallisation process a collective and differential SCBD can be observed without the need for physical separation of the fractions. The homogeneity of the polyolefins can thus be analysed according to their chemical composition distribution (CCD).

The analysis of SCBD in polyolefins is not a simple task and therefore special attention has to be given to resolution of the data as well as fractionation of these polymer samples during the analysis step. The most common technique used for this type of separation was Temperature Rising Elution Fractionation (TREF). Wild *et al.* [3-5] did a great deal of work in this field. TREF is however a slow and time consuming technique compared to CRYSTAF, where the sample preparation was simplified and analysis time was significantly reduced.

The goal of this chapter is to show the analytical potential of CRYSTAF by using a variety of polyolefin samples. The advantages, disadvantages and limitations of CRYSTAF were looked at and are commented on. A new method by which the comonomer distribution could be calculated from linear low density polyethylene samples with unknown comonomer composition was introduced.

4.3 Theoretical background

CRYSTAF and TREF are separation techniques based on the fractionation of species, at a slow cooling rate, as a function of crystallisation in solution. The chemical composition distribution (CCD) of a polymer can be obtained by CRYSTAF, in a

single crystallisation step. This is achieved by monitoring the decrease of polymer concentration in solution as a function of temperature decrease. In the case of TREF, the elution step is an additional step in which information is obtained on the polymer composition through the heating of the sample crystallised in the column and the elution thereof from the column.

Free energy change for mixing two substances at temperature T is given by the relationship:

$$\Delta G_{mix} = \Delta H_{mix} - T\Delta S_{mix} \qquad \textbf{(4.1)}$$

The heat of mixing (ΔH_{mix}) is mostly a positive value for solutions, as the dissolution process is usually endothermic. The entropy of mixing (ΔS_{mix}) is also a positive value, relating to the higher random motion of the solutions compared to the unmixed state. In order for a polymer to dissolve, $\Delta G_{mix} \leq 0$. This implies that the value of ΔH_{mix} must be small.

In the case of highly crystalline polymers, which are insoluble at room temperature, Equation 4.1 has to be changed to accommodate the heat of fusion:

$$\Delta G_{mix} = (\Delta H_{mix} + \Delta H_f) - T(\Delta S_{mix} + \Delta S_f) \qquad \textbf{(4.2)}$$

where the subscripts *mix* and *f* denote mixing and fusion, respectively. Highly crystalline polymers comply with the solubility parameter rules at $T \geq T_m$, where T_m is the melting temperature of the polymer. Crystalline polyethylene becomes soluble at elevated temperatures ($T \geq 80$ °C), depending on the choice of solvent. At room temperature these polymers swell.

Polymer fractionation or crystallisation in solution can be explained on the basis of the Flory-Huggins statistical thermodynamic treatment, that accounts for melting point decline in the presence of diluent:

$$\frac{1}{T_m} - \frac{1}{T_m^o} = \frac{R}{\Delta H_u}\frac{V_u}{V_1}(v_1 - \chi_1 v_1^2) \qquad \textbf{(4.3)}$$

where T_m^o is the melting temperature of the homopolymer; T_m the equilibrium melting temperature of the diluent; ΔH_u the heat of fusion per polymer repeating unit; V_u and V_1 the molar volumes of the polymer repeating unit and the diluent respectively; v_1 the volume fraction of the solvent and χ_1 the Flory-Huggins thermodynamic interaction parameter.

The classical Flory equation can be applied for random copolymers:

$$\frac{1}{T_m} - \frac{1}{T_m^o} = -\frac{R}{\Delta H_u}\ln(p) \qquad \textbf{(4.4)}$$

where T_m^o is the melting temperature of the homopolymer; ΔH_u the heat of fusion for the homopolymer repeating unit and p the molar fraction of the crystallising units. If the concentration of the individual species is low and if they are not incorporated into the crystalline lattice, then the comonomer units and the polymer chain ends all have the same effect on the melting point decline. Flory proved that Equation 4.3 can be reduced to the same form as Equation 4.4 [6].

By replacing the term p with $(1 - N_2)$ in Equation 4.4, simplifications can be made to the equation, where N_2 is the molar fraction of the comonomer that is not incorporated into the crystalline lattice structure. In the case where N_2 is a small value, the following holds: $\ln(1 - N_2) \cong -N_2$, hence:

$$\frac{1}{T_m} - \frac{1}{T_m^o} \cong \frac{R}{\Delta H_u} N_2 \qquad \textbf{(4.5)}$$

Polyethylene with a MM of 15 000 g/mol and higher crystallises independently of MM in the solvent system [7]. Experiments have shown that samples containing PE with MM as low as 1 000 g/mol can be fractionated with TREF, in the case where end groups are considered as non-crystalline units [8].

4.4 Experimental and results

4.4.1 Basic CRYSTAF analysis

An example of a basic method setup is shown in Figure 4.1. Dissolution temperature, dissolution time, stabilisation temperature, stabilisation time and cooling rate during analysis are the parameters considered in this study. These parameters were selected due to the fact that they are the only changes that could have an influence on the crystallisation temperature $T_{c\ (CRYSTAF)}$ from solution. The CRYSTAF unit is shown in Figure 4.2(A), where the five reactors are clearly visible in the main oven. An individual reactor is shown in Figure 4.2(B). The sintered glass filter (1) separates the soluble polymer from the crystalline polymer in the reactor, while the magnetic stirrer (2) maintains a homogenous solution. A diagram layout of the CRYSTAF instrumentation is given in Figure 4.3. The latter gives an overview of the procedures carried out by the instrument during a run.

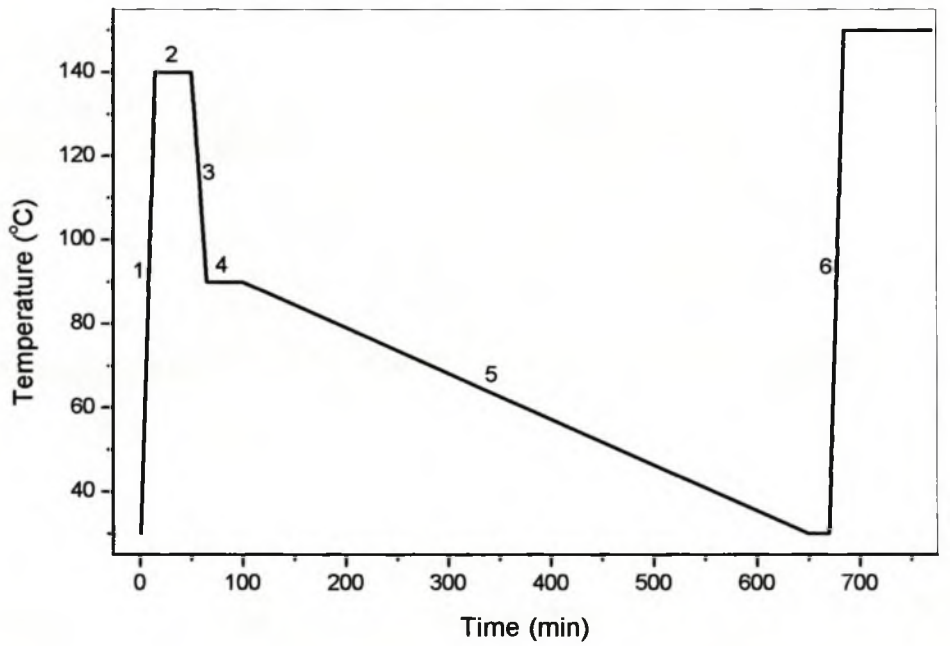

Figure 4.1. Schematic representation of the various steps in CRYSTAF analysis.
(1 = dissolution temperature and the rate of heating, 2 = dissolution time, 3 = stabilisation temperature and cooling rate, 4 = stabilisation time, 5 = cooling rate for analysis and 6 = heating rate for cleaning cycle).

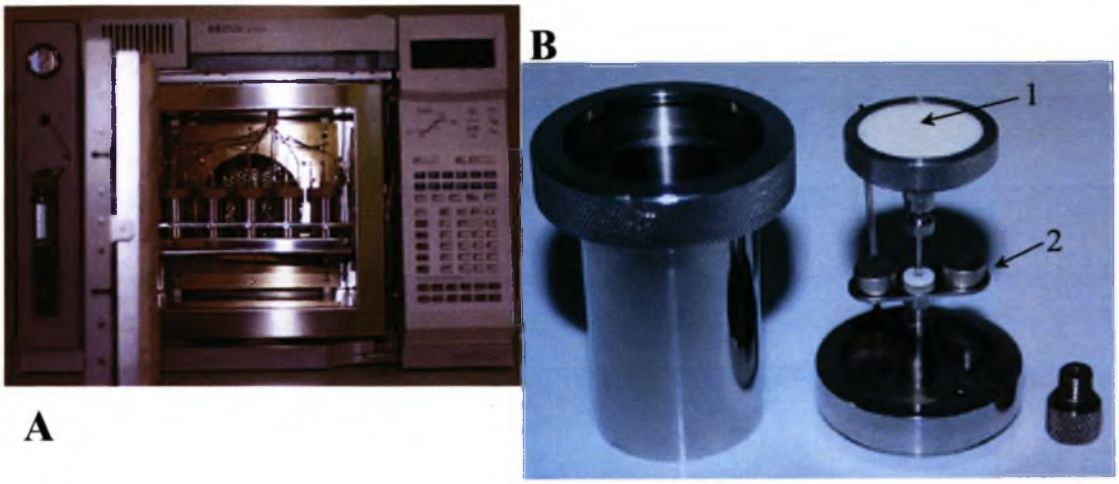

Figure 4.2. Photos of the CRYSTAF instrument's main oven unit with its five reactors (A) and a single reactor (B) with the sintered glass filter (1) and the magnetic stirrer (2).

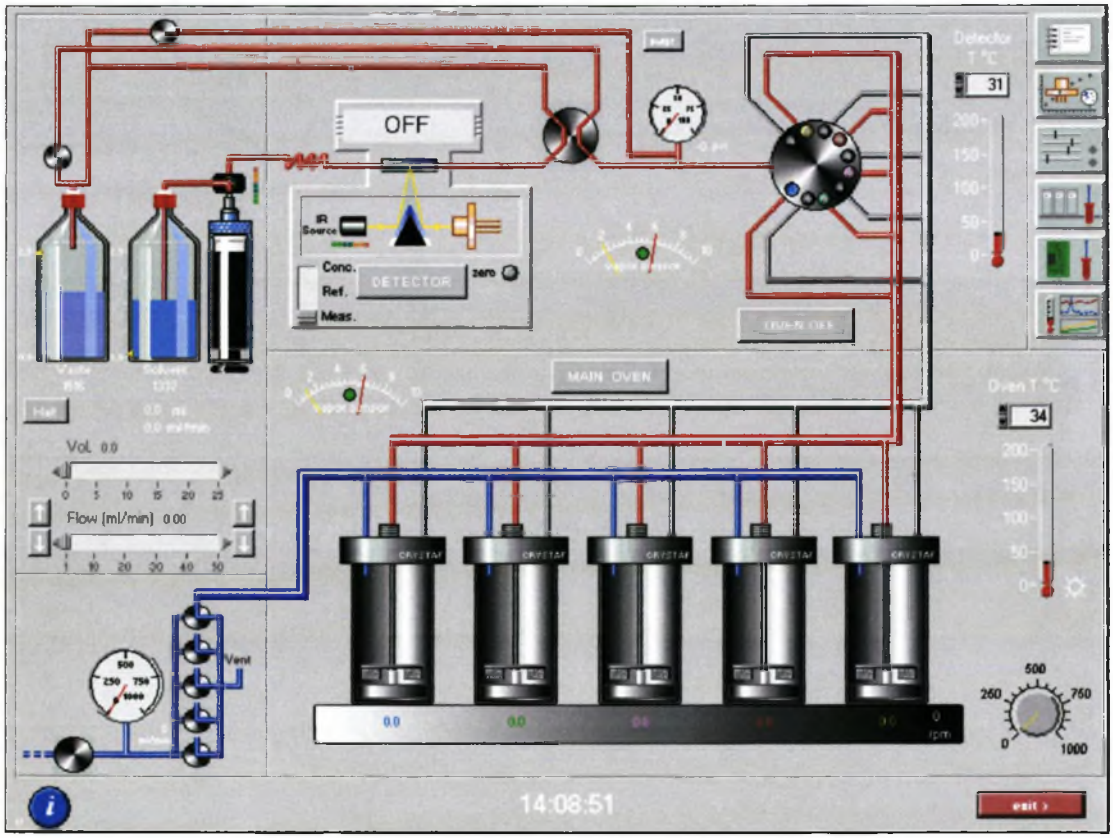

Figure 4.3. Schematic layout of the CRYSTAF instrument showing all the valves, the five reactors, the infrared cell and the procedure currently being performed by the instrument.

Figure 4.4 is a general representation of the data obtained with CRYSTAF. The black line represents the intensity of the infrared signal, whereas the red line is the first derivative of the infrared signal. The first data points are taken at a temperature above the crystallisation point, where all polymers are still in solution. This provides a constant concentration measurement, equal to the total polymer solution concentration in the reactor (Figure 4.4, Zone 1). With a drop in temperature, the most crystalline fraction (polymers with no or very little branching) will precipitate first from solution. The precipitation occurs due to the formation of polymer crystals, resulting in a steep decline in the solution concentration (Figure 4.4, Zone 2). Polymer fractions with lower crystallinity (more branching) will precipitate out of solution after this point. If these polymers are present, then they will crystallise in Zone 3. The part marked *soluble fraction* (a graphical value generated by the CRYSTAF apparatus) is mostly polymer that can either not crystallise in the temperature range or represents amorphous polymer that cannot crystallise at all. CRYSTAF results give information regarding the maximum T_c, the percentage of crystalline material under the peak(s) and the percentage soluble fraction.

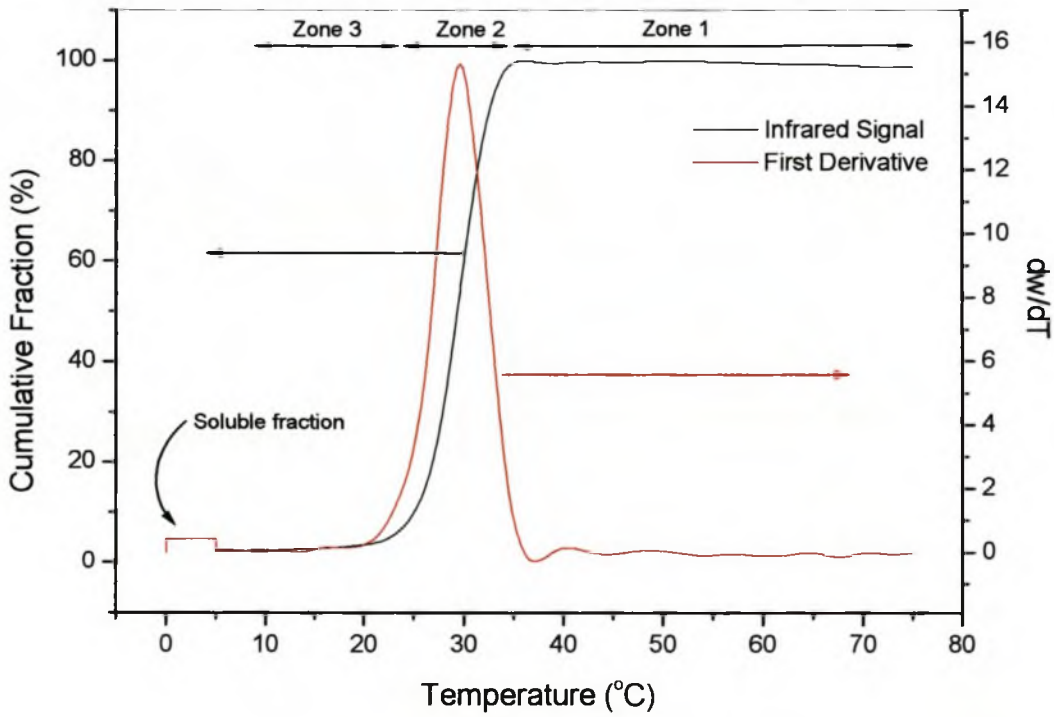

Figure 4.4. Basic CRYSTAF diagram, with the infrared signal presented in percentage points and the first derivative forming the peak.

4.4.2 Troubleshooting

Samples with medium MM can give problems in CRYSTAF analysis due to the presence of high MM shoulders. An example of such a sample is Lupolen 5162Z. The molar mass of this species is identical to that of the other industrially provided sample Lupolen 3020D (see specifications of industrial samples in section 3.4). Figure 4.5 illustrates the phenomenon observed above. The only major difference between the two samples is shown in Figure 4.5, where the chromatogram of the Lupolen 5162Z sample has a high MM shoulder (1) that appeared at 1.5×10^6 g/mol. The shoulder prevented the analysis of these samples at a standard sample weight of 20 mg. At a sample weight of 20 mg the CRYSTAF instrument shut down the run automatically. This resulted from the filters clogging inside the reactor, thus preventing the solution from reaching the infrared cell. This problem was resolved by using less sample. 10 mg of the samples did not cause filter clogging and the instrument was able to draw-up solution even at low analysis temperatures.

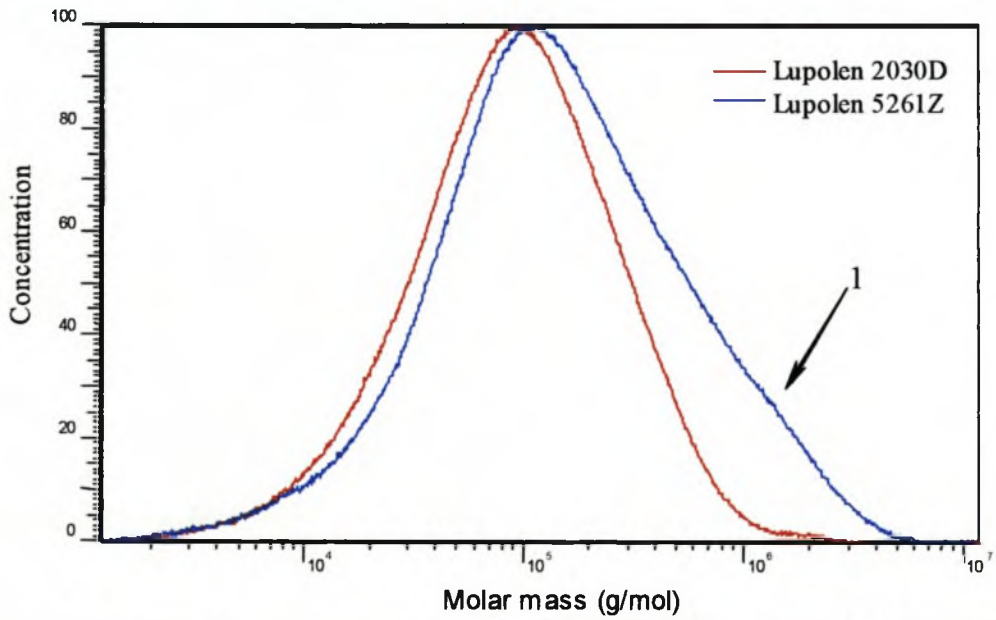

Figure 4.5. GPC chromatograms of Lupolen 3020D (LDPE) and Lupolen 5261Z (HDPE) with a shoulder at 1.5×10^6 g/mol.

Care has to be taken to place the reactors in an upright position. If this is not done, air bubbles can reach the infrared cell, which in turn can cause a negative concentration reading. The same thing can happen at the end of a run when the solution is reduced to the point where air is drawn up instead of solution.

4.4.3 Average T_c

An important aspect is the reproducibility of the T_c of a sample obtained by CRYSTAF analysis. The runs were repeated four times and in every run three reactors were filled with the same amount of Lupolen 2030D sample. This was done to see if there was any significant difference between the runs and/or the reactors. The sample weights were kept constant to ensure a minimum concentration effect in solution.

There were no significant changes in the T_c from one reactor to the next and the average T_c of the sample was 68.0 °C. The T_c from the 12 runs did not change by more than ±0.4 °C from the average temperature. Some of the results are shown in the 20 mg sample column in Table 4.1. A deviation of 0.4 °C is acceptable for the CRYSTAF, which can only measure thermal intervals of 0.1 °C.

4.4.4 Sample weight

Weight increase

Three different sample weights were analysed for changes in their T_c. The volume of solvent was held constant at 30 mL of TCB. The sample weights were 20 mg, 40 mg and 60 mg, respectively. These sample weights were also used with different methods to see whether changes in T_c with change in method could be observed. Experimental results showed an average change of 0.76 °C for every 20 mg of sample added to the reactor, as seen in Table 4.1. This corresponds well to the DSC data, where a shift to a higher melting temperature on heating was also obtained with an increase in sample weight [9]. The average T_c for each of the three sample weights was as follows: 67.94 °C (20 mg), 68.70 °C (40 mg) and 69.46 °C (60 mg). It can thus be noted that there is an increase in the T_c with a rise in sample weight, although changes in method have no influence on the T_c (Table 4.1).

Table 4.1. T_c measurements for different samples weights, where the method of the runs was changed for every second row.

Method Change	20mg Sample (°C)	40mg Sample (°C)	60mg Sample (°C)
Dissolution temperature	68.0	68.5	69.4
	67.6	68.8	69.1
Dissolution time	67.6	68.7	69.1
	67.6	68.8	69.5
Stabilisation temperature	67.9	68.7	69.7
	68.4	68.7	69.7
Stabilisation time	68.4	68.6	69.7
	68.4	68.8	69.5
Average temperature (°C)	68.0	68.7	69.5

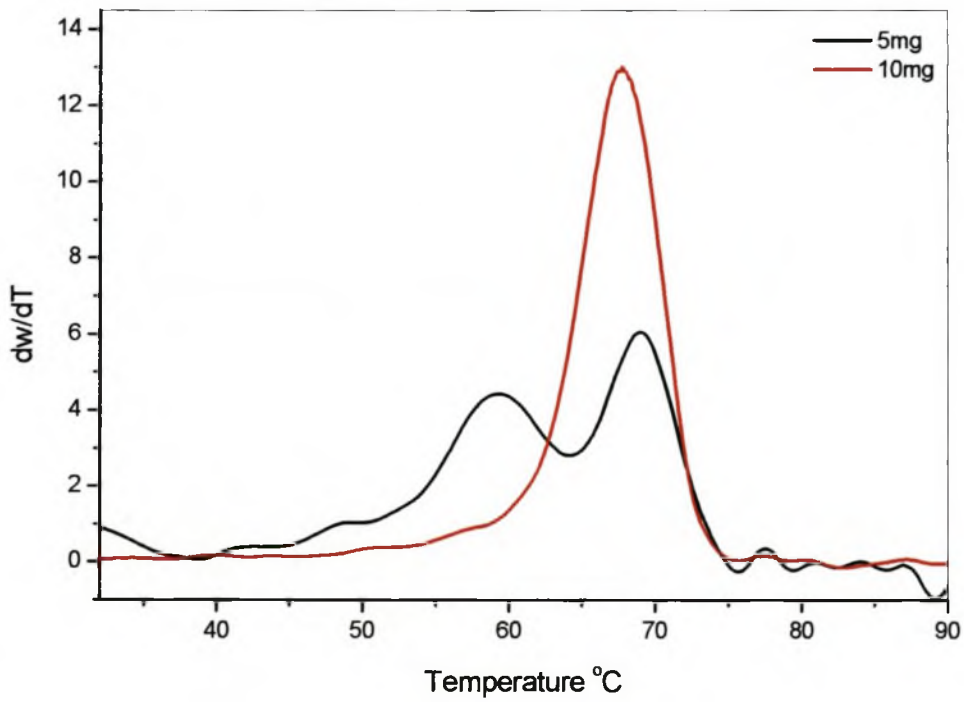

Figure 4.6. The same LDPE (Lupolen 3020 D) sample run at two different sample weights, showing the formation of a double peak.

Modest amounts of LDPE

LDPE samples (with sample weights below 10 mg) were the only samples that showed the phenomenon of a double peak. All other polyolefin samples investigated gave single peaks. Figure 4.6 demonstrates the change from a single peak for a 10 mg sample to a double peak for a 5 mg sample. An explanation for the second

crystallisation with low sample weights can be given by co-crystallisation. A number of research groups have shown (with the aid of DSC) that higher α-olefin homopolymers produce two melting points [10-12]. These two endothermal peaks could be related back to main and side chain melting. Monrabal [13], the designer of the CRYSTAF, suggested that this could be due to the filter porosity inside the reactor and not due to co-crystallisation of the side chains. RD Sanderson [14] mentioned that it is known that preformed polyolefin crystals act as nuclei or loci for further crystallisation of lower melting point material. As the solution concentration decreases there may be too few nuclei present for this to take place and some supercooling or supersaturation occurs, followed by self-nucleation, hence the second peak.

4.4.5 Method set-up

Dissolution temperature

In this part of the test, a temperature change from 140 °C to 100 °C in 20 °C intervals was considered. No significant changes could be seen in the T_c with a decrease in temperature. It has to be kept in mind that the dissolution temperature is dependent on the type of polymer that is used. If the polymers are difficult to dissolve, changes in the dissolution temperature will lead to undissolved polymer in the reactor while analysis is in progress.

Dissolution time

This is the time that the instrument will stay at the dissolution temperature. The dissolution time was decreased in 20 minute intervals starting at 90 minutes and ending at 10 minutes. It was found that the dissolution time gives no change in T_c with a decrease in time. However, it was observed that polymers analysed at sample weights of 60 mg were still dissolving while the analysis was taking place. Dissolution time should always be longer than 30 minutes, except for polymers that degrade rapidly or in a fast analysis.

Stabilisation time

Stabilisation time is the time needed to stabilise the reactors at a temperature lower than the dissolution temperature before an analysis can commence. The setting changes in the time interval were set at 20 minutes, starting from 70 minutes, and ending at a stabilisation time of 10 minutes. The stabilisation time, as in the case of the dissolution time, also showed no changes in T_c with an increase in time.

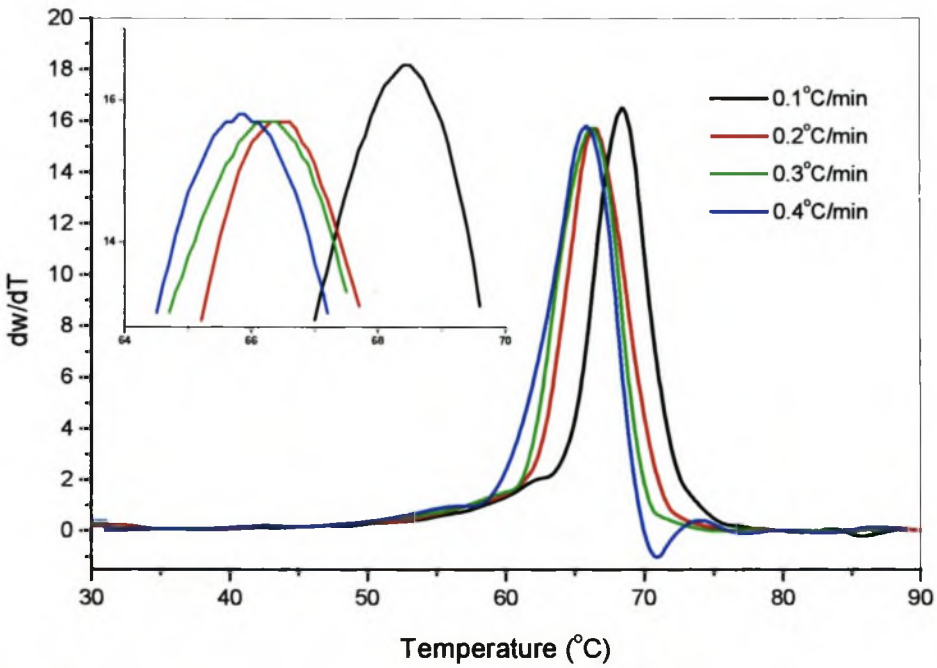

Figure 4.7. Change in T_c, for 20 mg samples, with change in the cooling rate.

Cooling rate during analysis

This is the rate at which the main oven is cooled. During this process samples are drawn from the reactors for analysis. The cooling rate was increased with 0.1 °C/minute increments, from 0.1 °C/minute to 0.4 °C/minute. The T_cs for different cooling rates for a 20 mg sample were observed to be as follows (Figure 4.7): 67.6 °C (0.1 °C/min), 66.4 °C (0.2 °C/min), 66.3 °C (0.3 °C/min) and 65.8 °C (0.4 °C/min). The decrease in T_c with increase in cooling rate is due to the higher heat capacity of the reactors compared to the rest of the oven. This simply means that the reactors are at higher temperature than registered by the thermocouple in the oven [13]. It is for

this reason that the T_c of the sample seems to be lower than it really is. Figure 4.8 shows propylene/1-hexene copolymers with different comonomer contents as a function of temperature, cooling rates of 0.1 °C/min and 0.4 °C/min were used, with DCB as solvent. Here too, a drop in T_c is observed with an increase in the cooling rate.

An important factor to consider, while setting up a method, is the time interval that the instrument needs to draw up a sample for detection by the infrared detector. These time intervals can be influenced by setting up too many points for data collecting or by making the cooling rate too fast in relationship to the data point collection rate. If these time intervals are too short, resolution will be lost in quality of the first derivative graphs due to the fact that not all the data points, as specified in the method, can be analysed.

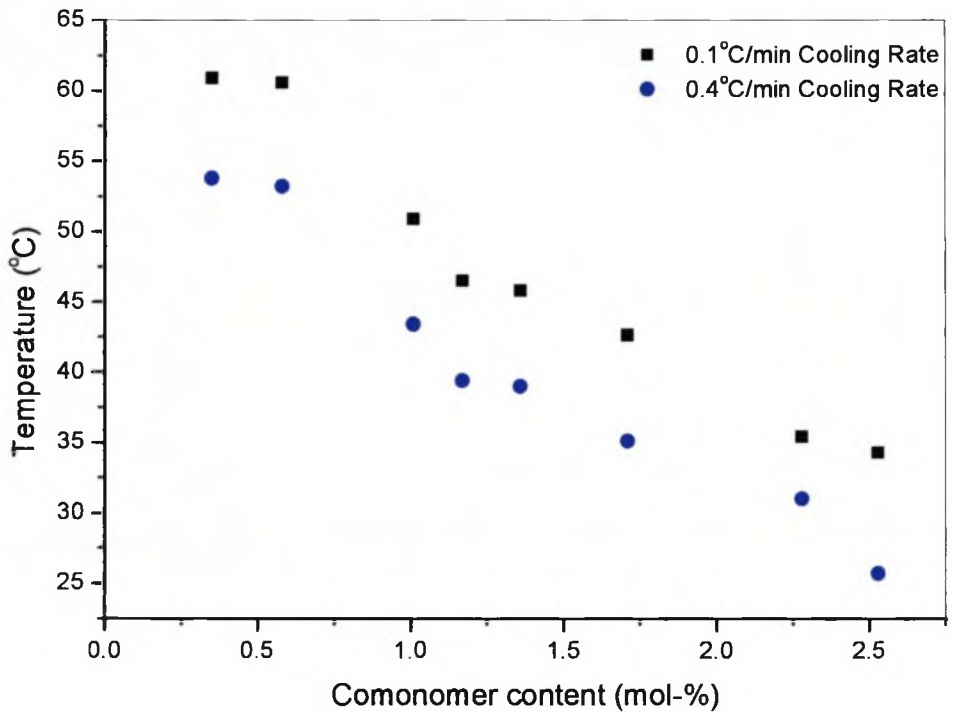

Figure 4.8. Comonomer content of propylene/ 1-hexene copolymers, as a function of temperature (at cooling rates of 0.1 °C/minute and 0.4 °C/minute). Solvent: DCB.

4.4.6 Difference in solvents

Propylene/1-hexene copolymers, with comonomer contents ranging between 0.35 and 2.53 mol%, and molar masses (MM) between 3.3×10^{-5} g/mol and 5.7×10^{-5} g/mol, were used (Table 4.2). Solvents with poor solvent strength are thermodynamically less favourable to keep a crystalline polymer in solution than solvents with higher solvent strength. This implies that a crystalline polymer will give a lower T_c in a stronger solvent as compared to a weaker solvent.

The changes in T_c from a set of samples crystallising in different solvents can clearly be seen in Figure 4.9. T_c for a given sample decreases progressively in the order TCB, DCB, CB to TClEt. This corresponds to information already known about the individual solvent strengths [15]. Linear fits through the data points of a certain solvent will yield a line that is parallel to the other linear line fits. These parallel fits prove that there is no change in the crystallisation process of polymers with different comonomer contents in a series of solvents having varying solvent strength. In the case of a change in the crystallisation process, the linear fits would not have been parallel.

Table 4.2. $T_{c\,(CRYSTAF)}$ for propylene/1-hexene copolymers as obtained in trichlorobenzene (TCB), dichlorobenzene (DCB), chlorobenzene (CD) and tetrachlorobenzene (TClEt) as solvents. M_w and polydispersity of these samples are also shown.

Sample code	Comonomer content (mol-%)	TCB $T_{c\,(CRYSTAF)}$ (°C)	DCB $T_{c\,(CRYSTAF)}$ (°C)	CB $T_{c\,(CRYSTAF)}$ (°C)	TClEt $T_{c\,(CRYSTAF)}$ (°C)	$M_w\times10^{-5}$ (g/mol)	M_w/M_n
PH1	0,30	67,2	60,9	54,5	34,7	422100	2,1
PH2	0,32	67,6	60,6	53,2	36,2	339900	2,1
PH3	0,46			49,2	31,5	356000	2,2
PH4	1,03	57,7	50,9	42,4	22,0	343000	2,2
PH5	1,24	54,7	46,5	41,6	20,3	331600	2,0
PH6	1,39	53,2	45,8	38,7	19,3	520100	2,2
PH7	1,80	48,4	42,6	33,7	13,5	395100	2,2
PH8	2,35	40,6	35,4			572800	2,3
PH9	2,41	39,4	34,3	25,6	7,1	574400	2,2

The solubility parameters for the solvents were determined by J.-L. M. Abboud and R. Notario [15] and were as follows TCB (δ_S = 20.3 $J^{1/2}/cm^{3/2}$), DCB (δ_S = 20.1 $J^{1/2}/cm^{3/2}$), CB (δ_S = 19.4 $J^{1/2}/cm^{3/2}$) and TClEt (δ_S = 19.0 $J^{1/2}/cm^{3/2}$). The solubility parameter of a polypropylene was given as δ_P = 7.9 $J^{1/2}/cm^{3/2}$. For polymers to be soluble in solution the solubility parameters of the polymers and the solvent must normally be similar in dimensions or as close as possible ($\delta_S \approx \delta_P$). In the case of polyolefins the temperature of the system has to be increased significantly to narrow the gap in solubility parameter values. The solubility limit of a given polymer in a solution is closely related to the Flory-temperature (Θ_F). The Θ_F is defined as the temperature at which the partial molar free energy due to polymer-solvent interaction energy is zero. In this state the system shows ideal solution behaviour and the polymer will dissolve. If the temperature of the system is lower than Θ_F the intramolecular attraction will increase and the polymer will precipitate from solution. An increase in comonomer content will lead to an increase in the solubility parameter in the copolymers thus giving a negative slope for a given solvent (Figure 4.9).

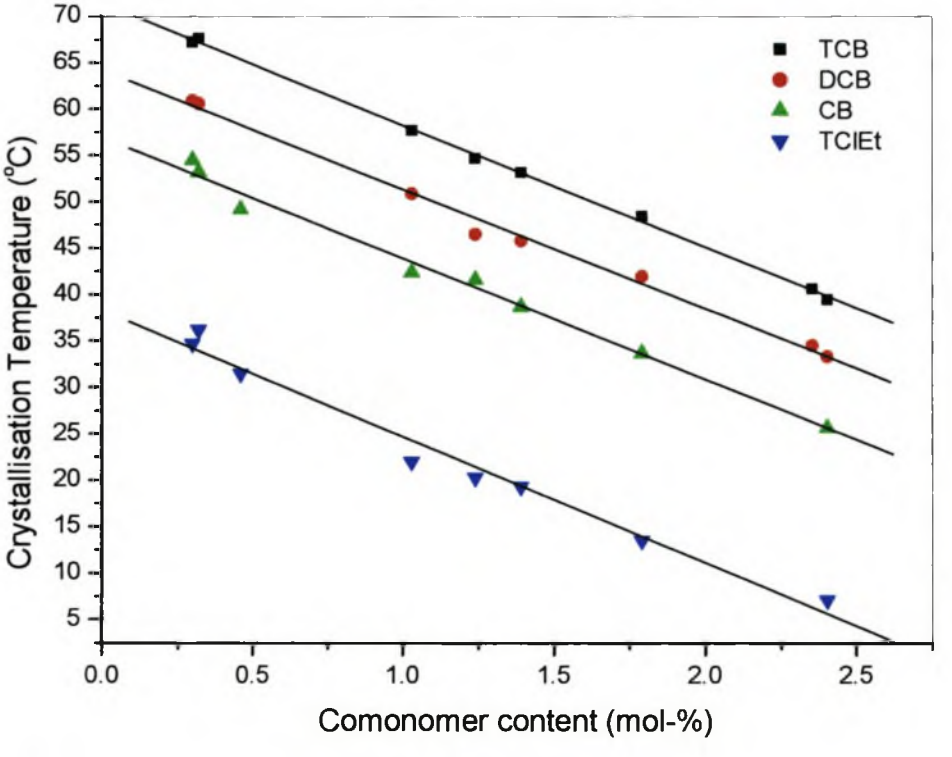

Figure 4.9. Propylene/1-hexene copolymers crystallised from different solvents (TCB, DCB, CB and TClEt).

Propylene copolymers will have a solubility parameter $\delta_P > 7.9$ $J^{1/2}/cm^{3/2}$, thus giving them a higher solvent compatibility at lower temperature. Differences in the T_c between solvents are related to the solubility parameter, solvents with lower δ will need lower system temperatures to precipitate the polymer from solution.

4.4.7 Extraction of sample

A difference in the solutions of the extracted and non-extracted samples is observed at low temperature (around 30 °C), as illustrated in Figure 4.10(A). One representative example of an extracted and one of a non-extracted sample are shown here, as all other results match the data obtained here. The non-extracted polymer had a higher infrared absorption signal than the extracted polymer at similar temperature. The higher IR signal is due to the higher soluble part of the sample at the lower analysis temperatures. Monomer and mostly amorphous polymer are present in the non-extracted samples and are unable to crystallise under these analytical conditions. The peak at the low MM region of the size exclusion chromatogram for the non-extracted sample of the polymer with 1-octadeceneas comonomer corresponds to the MM (peak maximum at 252 g/mol) of 1-octadecene from an ethylene/1-octadecene copolymer (Figure 4.11). This proves that in the case of these copolymers the soluble fraction in the CRYSTAF is mostly due to the residual 1-octadecene.

Figure 4.10(B) shows that the non-crystalline part (mainly 1-octadecene) can influence the crystallisation process, when looking at the lower but large tail of the crystallisation peak of the non-extracted sample. This lower T_c can be attributed to 1-octadecene acting either as an impurity during the crystallisation or as a solvent. The similarity between the 1-octadecene chain and the PE backbone makes the incorporation of 1-octadecene into the latter structure possible, thereby decreasing the T_c. In the case where 1-octadecene acts as a solvent it will increase the solvent strength of the TCB solvent thus leading to a lower T_c. This is similar to the results discussed in the previous section 4.4.6 regarding differences in solvents, where pure solvents were used.

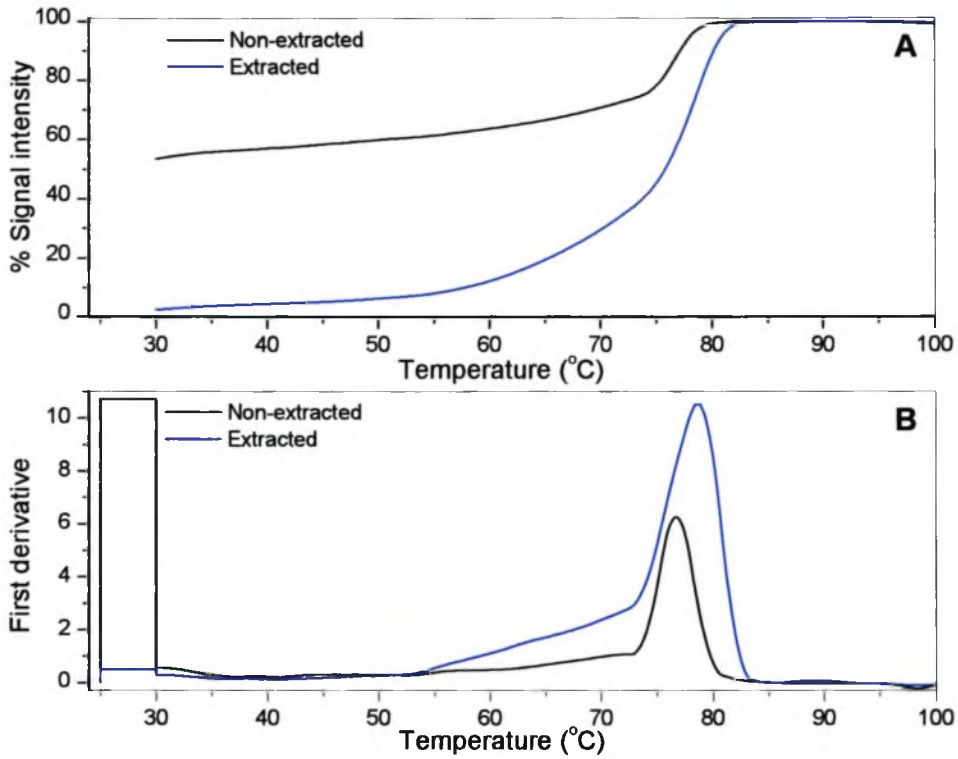

Figure 4.10. A) CRYSTAF plots and B) the first derivative curves of an extracted (blue line) and a non-extracted (black line) ethylene/1-octadecene copolymer sample.

CRYSTAF can thus indicate the presence of impurities which are not crystalline (Figure 4.10(A)). These results show the significance of proper sample preparation before analysis in order to obtain correct information on the samples. It can also be seen (Figure 4.10(B)) how the crystallinity in both the extracted and non-extracted samples is not homogeneous. One can also use this method to identify a difference in crystallinity within a single sample.

4.4.8 Comonomer content distribution

A diagram as obtained by CRYSTAF gives no direct information about the chemical composition of a polymer sample. The only information received from the

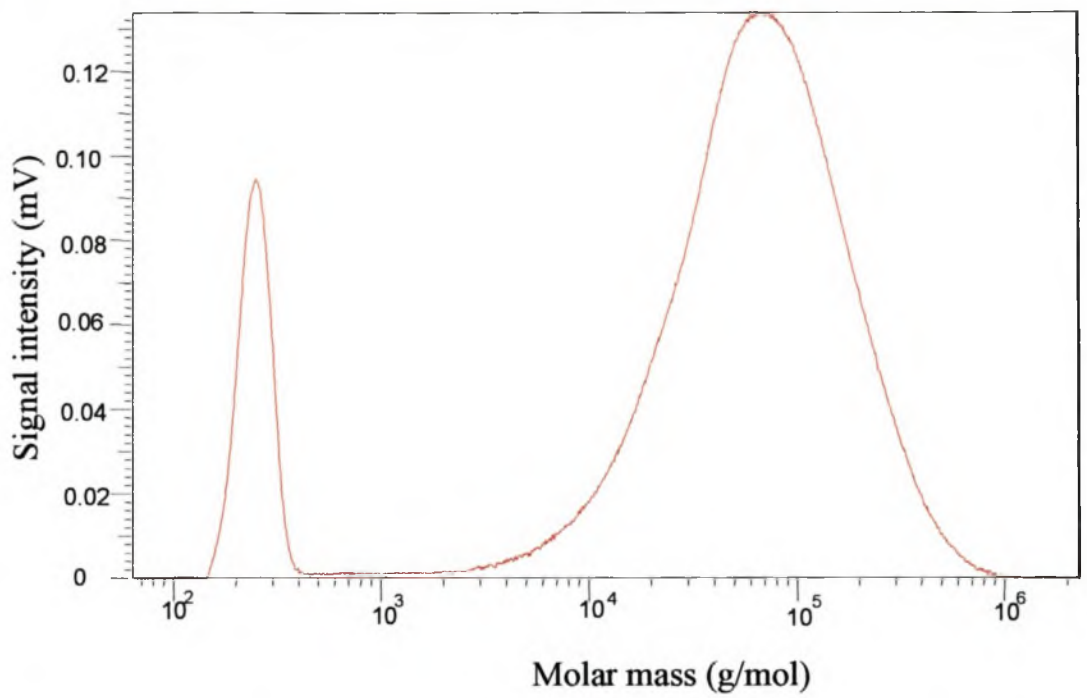

Figure 4.11. Size exclusion chromatogram of the ethylene copolymer containing unreacted 1-octadecene as comonomer (M_n = 252 g/mol).

chromatograms is the relationship between the change of concentration with temperature. More significant would be the conversion of the temperature scale (x-axis) to a comonomer concentration scale, similar to the conversion in GPC from the retention time scale to a molar mass axis. This conversion would allow direct interpretation of the structural build-up of a sample versus concentration regarding the comonomer distribution.

New calibration curves have to be drawn up for every copolymer series, as well as every new solvent used in the determination of the comonomer content distribution. As shown above, different solvents give different T_c values and by changing the comonomer type the T_c can also be changed [16]. The calculation of a standard calibration curve from a series of copolymers will give a linear relationship. The comonomer distribution for any unknown copolymer can thus be derived from the linear calibration curve.

The standard calibration curve was drawn up from propylene/1-hexene copolymers, where the comonomer content was determined by means of ^{13}C NMR (Table 4.2).

These copolymer samples were measured by CRYSTAF in DCB. Figure 4.12(A) shows, on the right hand y-axis, the percentages comonomer content for the different copolymer compounds from which the calibration line was drawn up. The square dots are the individual $T_{c\ (interval)}$ values as measured by CRYSTAF. The linear fit through these data points gave the equation

$$C_c = 5.13 - 0.08\ T_{c\ (interval)} \qquad \textbf{(4.6)}$$

C_c is the unknown comonomer content and $T_{c\ (interval)}$ is the crystallisation temperature of a polymer sample at different temperature intervals.

The CRYSTAF curve in Figure 4.12(A) belongs to a propylene/1-hexene copolymer with an unknown comonomer content, analysed by CRYSTAF in DCB. The crystallisation temperature chromatogram lies in the range of the calibration line, hence for this reason the chromatogram can be converted to a comonomer distribution chromatogram. If this had not been the case an area of unknown composition would be calculated. A similar example is GPC, where accurate MMD curves can only be given within the calibration limits.

In the conversion process the unknown CRYSTAF curve (Figure 4.12 (A)) was recalculated to the comonomer content distribution curve (Figure 4.12(B)). The $T_{c\ (intervals)}$ could be read from Figure 4.12(A) and with aid of Equation 4.6 C_c could be calculated. The C_c data obtained from the calculation was then plotted against the signal intensity as given by the CRYSTAF chromatogram.

As expected for a homogeneous catalyst, the comonomer incorporation followed a statistical distribution model (Gaussian distribution). The chemical composition (content) distribution is thus homogeneous for the metallocene under these reaction conditions.

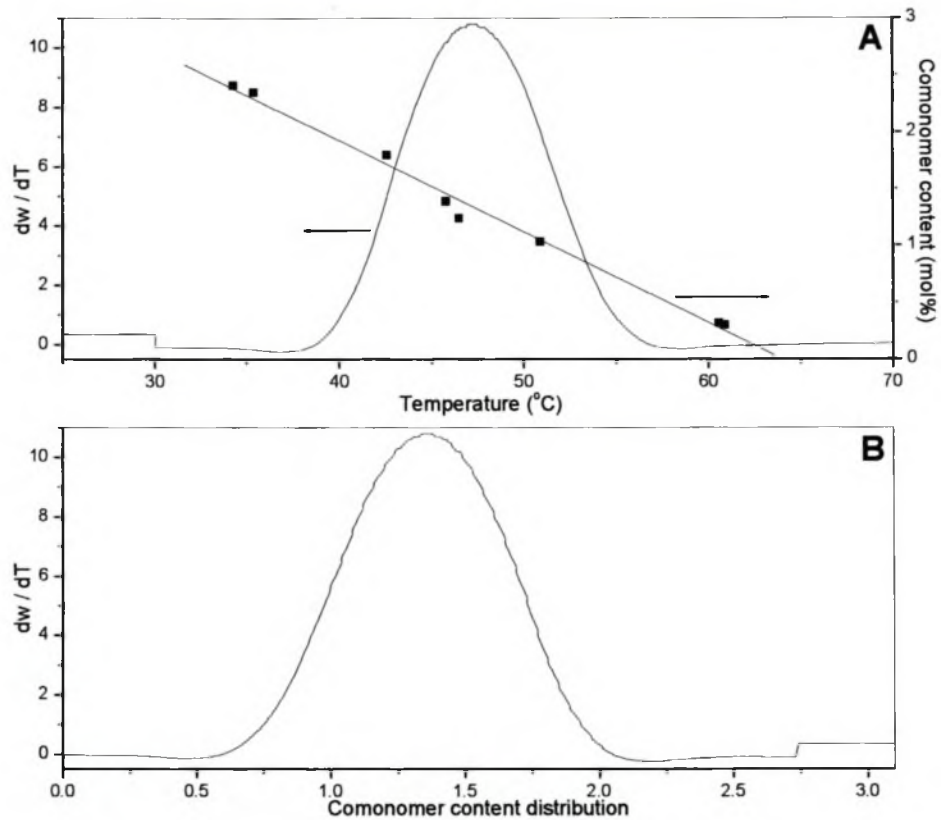

Figure 4.12. A) The linear calibration curve for a propylene/1-hexene copolymer series and a CRYSTAF chromatogram of such copolymer on the same temperature scale, B) Comonomer content distribution curve calculated for the CRYSTAF curve using the calibration curve.

4.5 Summary

The focus of this chapter was on the analysis standard polyolefin copolymers by CRYSTAF. CRYSTAF instrumentation and method of separation was discussed. The results of a standard run were broken down into its individual parts to explain the data obtained by this technique.

Standard commercial LDPE samples were used to study various parameter changes. These parameter changes included: amount of tared samples; dissolution time and temperature; stabilisation time and temperature; cooling rate; and the use of different

solvents. It was found that an increase in the of sample mass and in the cooling rate resulted in an increase and decrease in T_c respectively. The T_c remained constant throughout the changes made to the dissolution time/temperature and the stabilisation time/temperature parameters. It was also seen that samples with high MM fractions could only be analysed at lower amounts of sample weight due to blockage of the filter by high molar masses fractions. With low samples weights (5 mg) a second peak could be observed which could be related to either a filter problem or a secondary crystallisation. Different solvents also gave different T_c values for the same sample. These differences in T_c could be explained by the solubility strength of these solvents.

By comparing an extracted and non-extracted sample, differences in the CRYSTAF diagrams could be related to the comonomer that was present in the non-extracted sample. The lower T_c of the non-extracted sample compared to that of the extracted sample resulted from the comonomer acting as a solvent in the non-extracted sample.

By using copolymers of known comonomer composition a standard calibration curve could be drawn up. With the aid of this calibration curve a comonomer content distribution curve could be drawn up for a sample unknown comonomer content.

4.6 References

1. Monrabal B, US Patent 5 222 390, 1991.
2. Monrabal B, J. Appl. Polym. Sci., 1994, **52**, 491.
3. Wild L, Ryle T, Knobeloch D, Peat I R, J. Polym. Sci. Polym. Phys. Ed., 1982, **20**, 441.
4. Wild L, Ryle T, Polym. Prepr. Am. Chem. Soc. Polym. Chem. Div., 1977, **18**, 182.
5. Wild L, Ryle T, Knobeloch D, Polym. Prepr. Am. Chem. Soc. Polym. Chem. Div., 1982, **23**, 133.
6. Flory P J, *Principles of Polymer Chemistry*. Chaps. XII, XIII, Ed. Ithaca, 1953, New York, Cornel University Press.
7. Fatou J G, *Encyclopedia of Polymer Science and Engineering*. H F Mark and J I Korschwitz ed, Ed. 2nd. Vol. Suppl., 1989, New York, John Wiley & Sons Ltd, 231.
8. Monrabal B, *Temperature rising elution fractionation and crystallization analysis fractionation*. Encyclopaedia of Analytical Chemistry, 2000, Chichester, John Wiley & Sons Ltd, 8074.
9. Mathot V B F, *Calorimetry and thermal analysis of polymers*. Chapter 4, Ed. Mathot V B F, 1994, New York, Vienna, Munich, Hanser/Gardner Publications, 91.
10. Wang J, Porter R S, Knox J R, Polym. J., 1978, **10** (6), 619.
11. Brüll R, Pasch H, Raubenheimer H G, Sanderson R D, Wahner U W, J. Polym. Sci., Part A: Polym. Chem., 2000, **38** (21), 2333.
12. Trafara G, Koch R, Blum K, Hummel D, Makromol. Chem., 1976, **177**, 1089.
13. Monrabal B, personal communications, 2001 (Polymer Char), Spain.
14. Sanderson R D, Personal communications, 2002.
15. Abboud J L M, Notario R, Pure Appl. Chem., 1999, **71** (4), 645.
16. Brüll R, Graef S M, Pasch H, Rode K, Wahner U, Fachgrupentagung Makromolekulare Chemie GDCH, 2002 (Poster).

CHAPTER 5

COPOLYMERISATION OF PROPYLENE WITH HIGHER α-OLEFINS IN THE PRESENCE OF THE SYNDIOSPECIFIC CATALYST *i*-Pr(Cp)(9-Flu)$ZrCl_2$ / MAO

5.1 Abstract

The catalyst system *i*-Pr(Cp)(9-Flu)$ZrCl_2$/MAO was utilised to synthesise random syndiotactic copolymers of propylene with 1-hexene, 1-dodecene and 1-octadecene as comonomers. Investigation of the microstructure by ^{13}C-NMR spectroscopy revealed that the stereoregularity of the copolymers decreased due to an increase of skipped insertions in the presence of the higher α-olefins. The melting temperature of the copolymers, as measured by DSC, decreased linearly with increasing comonomer content (independent of the nature thereof). During the heating cycle of the DSC, an exothermic peak indicating a crystallisation process was observed. The decrease in the crystallization temperature with higher α-olefin content, measured by CRYSTAF, indicated a small but significant dependence on the nature of the comonomer.

5.2 Introduction

In the early 1960's, Natta *et al.* accomplished the synthesis of syndiotactic polypropylene (at low reaction temperature) with hydrocarbon-soluble vanadium compounds and alkylaluminium halides [1]. However, this first generation syndiotactic polypropylene was of low molar mass and exhibited low regio- and stereoregularity [2]. In 1988, Ewen *et al.* reported the synthesis of syndiotactic polypropylene utilising *i*-Pr(Cp)(9-Flu)$ZrCl_2$ (**1**) [3]. The C_s-symmetric metallocene allowed an easier access to highly regioregular and stereoregular, syndiotactic polypropylene. The improved properties of these materials has led to the bulk production of syndiotactic polypropylene by industry in recent years.

Fundamental properties of polyolefms, such as crystallinity, are strongly affected by the distribution of short- and long- chain branches. The polymerisation conditions allow control of the nature and distribution of branches in polyolefms. The copolymerisation of ethylene with higher α-olefins by metallocene catalysts with constrained geometry leads to essentially linear polyethylenes with low density (LLDPE) and homogeneous short chain branching distribution (SCBD). Recently, crystallisation analysis fractionation (CRYSTAF) was developed as a new technique for the composition analysis of semi-crystalline polymers. Monrabal and co-workers [4, 5] showed that CRYSTAF is especially useful for determining the SCBD in LLDPE.

In contrast to LLDPE, copolymers of propylene with higher α-olefins have received far less attention and the number of reports concerning their synthesis is quite limited [6-14]. In this work, we report on the synthesis and properties of syndiotactic copolymers of propylene with 1-hexene, 1-dodecene and 1-octadecene as comonomers. The microstructure and thermal properties of the copolymers, as well as their analysis by CRYSTAF, were investigated.

5.3 Results and Discussion

Copolymers of propylene with various amounts of higher linear α-olefins, including 1-hexene, 1-dodecene and 1-octadecene, were synthesised with the single site precatalyst *i*-Pr(Cp)(9-Flu)$ZrCl_2$ (**1**) in a batch mode (Scheme 5.1 and Figure 5.1). The conversion was kept below 20 % in all cases so that statistical random copolymers could be synthesised. All of the copolymers had molar mass between 60 000 and 110 000 g/mol and exhibited polydispersities around 2, as expected for metallocene catalysts (Table 5.1).

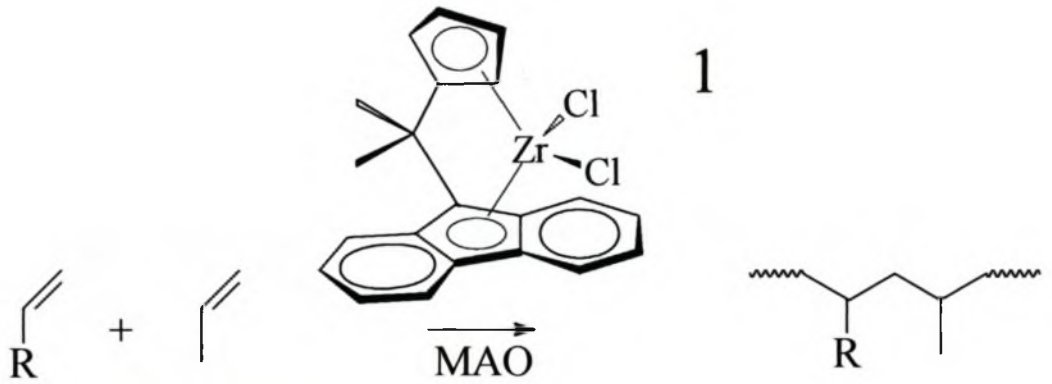

R = *n*-Butyl, *n*-Decyl or *n*-Hexadecyl

Scheme 5.1. Synthesis of copolymers of propylene with 1-hexene, 1-dodecene or 1-octadecene, respectively, using the catalyst system **1**/MAO.

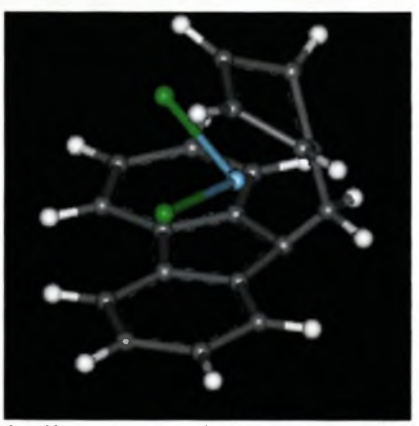

Figure 5.1. 3-Dimensional illustration of *i*-Pr(Cp)(9-Flu)$ZrCl_2$ pre-catalyst (white = hydrogen atoms, grey = carbon atoms, cyan = zirconium and green = chlorine atoms).

Table 5.1. Comonomer content in the feed and in the copolymer for propylene/higher α-olefin copolymers synthesised with **1**. The abundance of the [rrrr] pentad and the main [rmmr] and [rrmr] error pentads are listed in percent. M_n is the number average molar mass in g/mol and M_w/M_n the polydispersity.

Sample	Comonomer content in polymer (mol-%)	Comonomer content in feed (mol-%)	[rrrr]	[rmmr]	[rrmr]	M_n	M_w/M_n
Polypropylene							
s-PP	n.a.	n.a.	88.9	0.9	1.0	101200	1.78
1-Hexene							
H1	0.61	1.14	81.7	0.7	3.9	79400	1.71
H2	0.96	2.34	82.9	1.1	4.5	89100	1.81
H3	1.02	2.71	85.2	0.7	3.7	98200	1.78
H4	1.76	4.60	75.9	n.d.[a]	8.0	65800	1.75
H5	1.88	4.44	82.0	0.7	6.6	89900	1.83
H6	1.95	8.14	77.1	n.d.	3.6	62200	1.76
H7	2.03	7.14	78.0	0.7	6.5	100100	1.80
H8	2.12	4.84	78.9	n.d.	9.7	87500	1.76
H9	4.19	13.56	78.9	n.d.	17.5	58300	1.91
H10	8.15	21.19	69.3	0.9	22.4	68500	1.78
1-Dodecene							
D1	0.24	0.31	84.8	1.2	2.4	68800	1.90
D2	0.27	0.47	87.3	0.7	2.4	73800	1.91
D3	0.30	0.77	82.7	1.1	4.7	63800	1.86
D4	0.35	0.63	83.5	0.7	3.5	60700	1.88
D5	0.38	1.04	86.9	1.0	2.4	79300	1.88
D6	0.49	1.52	84.4	1.0	3.1	110000	1.79
D7	0.52	1.67	84.1	0.8	3.3	103100	1.79
D8	0.80	1.82	81.4	0.9	6.1	64100	1.66
D9	0.83	2.47	83.4	0.8	4.7	100600	1.78
D10	0.89	3.45	81.7	1.0	4.3	101400	1.71
D11	1.52	4.31	82.1	1.0	6.5	102400	1.72
D12	6.65	11.15	76.7	2.0	15.8	78400	1.89
1-Octadecene							
O1	0.27	0.58	85.3	1.2	2.8	74800	1.84
O2	0.39	1.09	79.8	1.3	4.3	82800	1.79
O3	0.58	1.17	81.5	0.8	5.3	64900	1.81
O4	0.75	1.66	79.1	1.0	5.2	58700	1.91
O5	0.78	1.93	81.3	0.5	5.0	60800	1.82
O6	0.84	2.50	85.5	0.5	3.0	100400	1.78
O7	0.87	2.77	82.6	1.0	5.6	92000	1.77
O8	0.95	2.48	81.5	0.7	5.3	97000	1.75
O9	2.14	4.53	72.9	0.9	10.1	78200	1.78
O10	2.65	4.20	73.7	0.9	8.8	51600	1.81
O11	4.48	10.52	85.5	0.8	7.9	62300	1.88

[a] not determined

5.3.1 Microstructure

The amount of comonomer incorporated was determined by ^{13}C-NMR spectroscopy [15]. Detailed information on the calculation of the comonomer content will be given in section 6.3.2. In contrast to polypropylene synthesised with isospecific metallocene catalysts, syndiotactic polypropylene obtained with **1** is well known to be highly regioregular and the number of regio-irregular enchainments due to 2,1-misinsertions is low [16]. According to Zambelli *et al.* [2], resonance signals in the region of 12.8 - 15.6 ppm and 32.9 - 33.4 ppm are diagnostic for methyl-groups of tail-to-tail and methylene-groups of head-to-head enchained units, respectively. The ^{13}C-NMR spectra of the investigated propylene copolymers with higher α-olefins showed no signals for such regio-irregular inserted monomer units, whereas Busico *et al.* proved, by analysis of the copolymer of propylene with low amounts of ethylene, that 2,1 misinsertions occurred [17].

Table 5.2. Assignment of signals (^{13}C NMR) to the respective C-atoms of propylene/higher α-olefin copolymers synthesised with **1**. The indices PP, PC and CC indicate propylene-propylene, propylene-comonomer and comonomer-comonomer dyads. Numbers refer to C-atoms of the long chain branches, as designated in Figure 5.2.

type	1-hexene (ppm)	1-dodecene (ppm)	1-octadecene (ppm)
$(CH_2)_{PP}$	47.05	47.07	47.05
$(CH_2)_{PC}$	44.12	44.17	44.17
$(CH_2)_{CC}$	41.15	41.18	n.o.
$(CH)_C$	32.91	32.97	33.16
$(CH)_P$	28.17	28.23	28.32
$(CH_3)_P$	20.28	20.29	20.28
$^{1}CH_3$	14.41	14.38	14.18
$^{2}CH_2$	23.72	23.12	22.95
$^{3}CH_2$	-	32.38	32.26
$^{4}CH_2$	-	29.83	29.65
$^{5\text{-}6}(CH_2)_n$	-	30.23	30.09
$^{7}CH_2$	-	30.78	30.67
$^{8}CH_2$	28.79	26.61	26.62
$^{9}CH_2$	34.12	34.50	34.61

Earlier we reported the assignment of signals obtained by ^{13}C-NMR spectroscopy of the respective carbon atoms for higher α-olefins [18]. On this basis, assignment of

the principal resonance signals of the side chain carbon atoms was possible (Figure 5.2, Table 5.2). The index $(CH_2)_{CC}$ is not shown in Figure 5.2 since no coupling between two comonomers (1-octadecene) could be detected, thus no comonomer clustering. The favored formation of syndiotactic copolymers was confirmed by analysis of the chemical shift and the pentad distribution of the methyl group of the propylene building block according to the detailed ^{13}C-NMR spectral assignment for polypropylene carried out by Busico *et al.* [19].

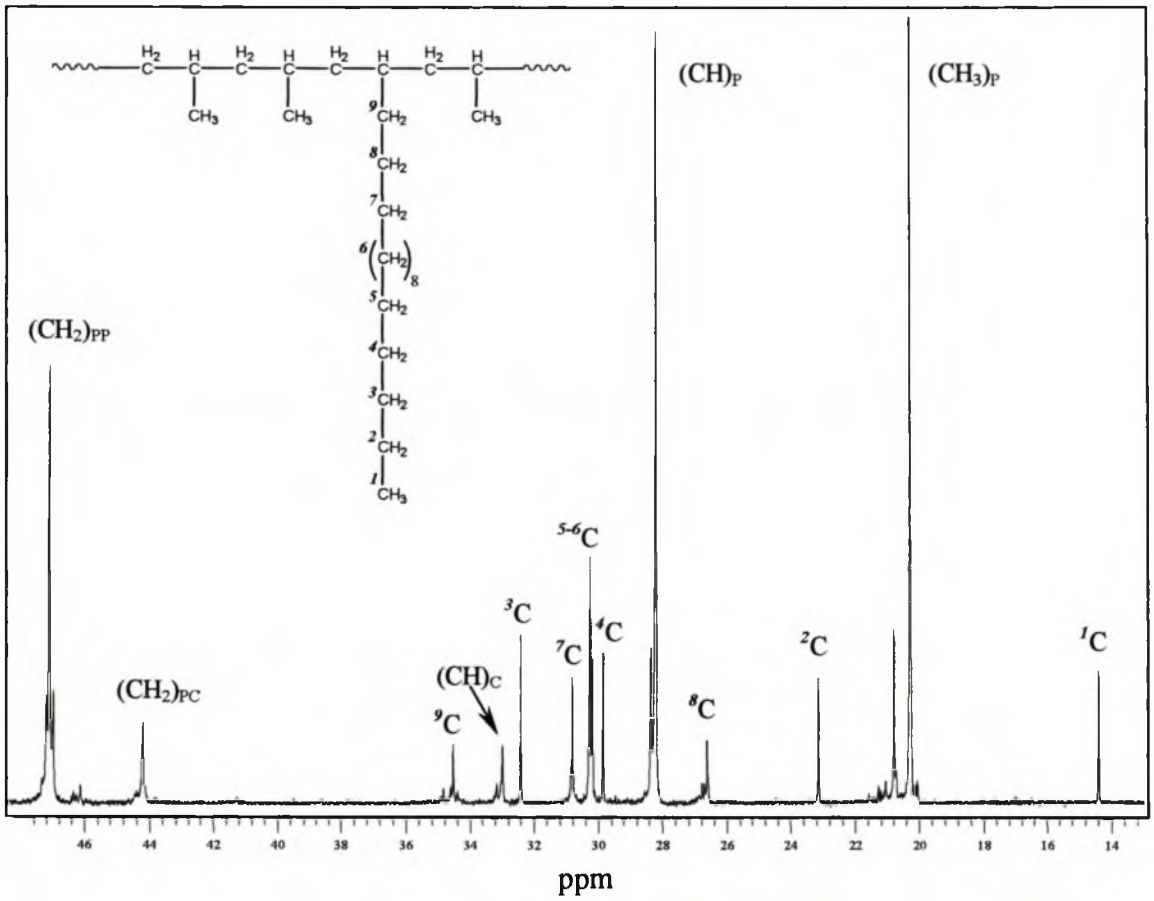

Figure 5.2. ^{13}C-NMR spectrum of the propylene/1-octadecene copolymer O11 synthesised with **1**. The indices PP and PC indicate propylene-propylene and propylene-comonomer dyads. Numbers refer to C-atoms of the long chain branches as designated.

The ratio of the integral rrrr pentad to the integral sum of all pentad signals (designated [rrrr]) at the methyl carbon of the propylene building block was used to determine the degree of syndiotacticity of the copolymer. The stereoregularity of the copolymer decreased from [rrrr] = 0.89 to 0.74, with increasing amounts of comonomer incorporated (Figure 5.3). In the chiral active catalyst derived from

C_s-symmetric **1**, one catalytic site favors the insertion of a specific propylene enantioface and the so generated alternative catalytic site preferably inserts the opposite enantioface [20, 21]. It is thus a crucial requirement for a syndiotactic polymerisation with **1**/MAO that each olefin insertion takes place at the coordination site opposite to the previous one. In order to meet this requirement the growing polymer must not move to the opposite coordination site before the next monomer unit inserts. Skipped insertions lead to stereoerrors with single m dyads, which are identical to those produced by a chain-end control and therefore an ambiguity for the source of rrmr pentads remains (Scheme 5.2) [20]. However, skipped insertions will become more likely when the rate of olefin insertion is decreased. Ewen *et al.* [22], Herfert and Fink [23] reported an increase of rmrr errors when the olefin or MAO concentrations are decreased. The same arguments can be used for bulky monomers and, therefore, the observed error can be readily explained (Figure 5.4A).

Site-chain control
Reversal of the enantioface selectivity

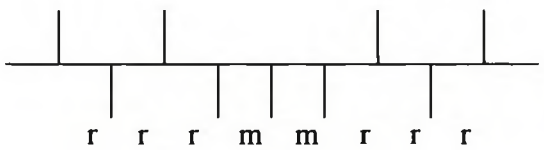

rrrm : <u>rrmm</u> : rrmr : <u>rmmr</u> = 2 : 2 : 0 : 1

Chain migration without olefin insertion

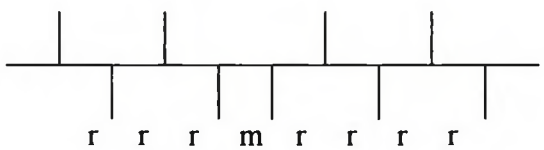

rrrm : rrmm : <u>rrmr</u> : rmmr = 2 : 0 : 2 : 0

Scheme 5.2. Pentad distribution of stereoerrors in syndiotactic polypropylene characteristic for catalytic-site control (top) and for chain-end stereocontrol (bottom).

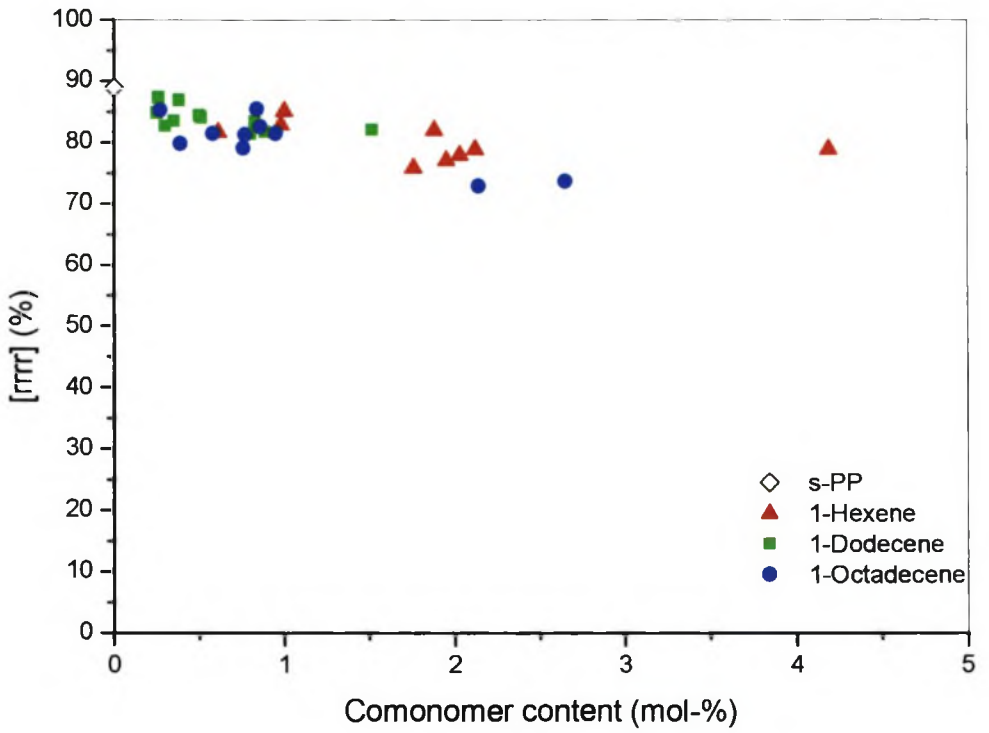

Figure 5.3. Abundance of the rrrr pentad as a function of the comonomer content for copolymers of propylene with higher α-olefins synthesized with **1**.

If propylene is polymerised with **1,** in the absence of a higher α-olefm comonomer, regular stereochemical defects are the rmmr, the mmrr and the rrrm pentads (Figure 5.4B.). The observed error pentad distribution rmmr : mmrr : rrrm = 1 : 2 : 2 for the syndiotactic polypropylene is in accord with an enantiomorphic site-control of the propagation step (Scheme 5.2). These stereoerrors are the result of a reversed enantioface insertion of the monomer. As expected, the rmmr pentad remains fairly constant in all copolymerisation reactions, whereas the rrmr pentad shows a significant increase with increasing amounts of comonomer and subsequently becomes the predominant stereoerror (Figure 5.5).

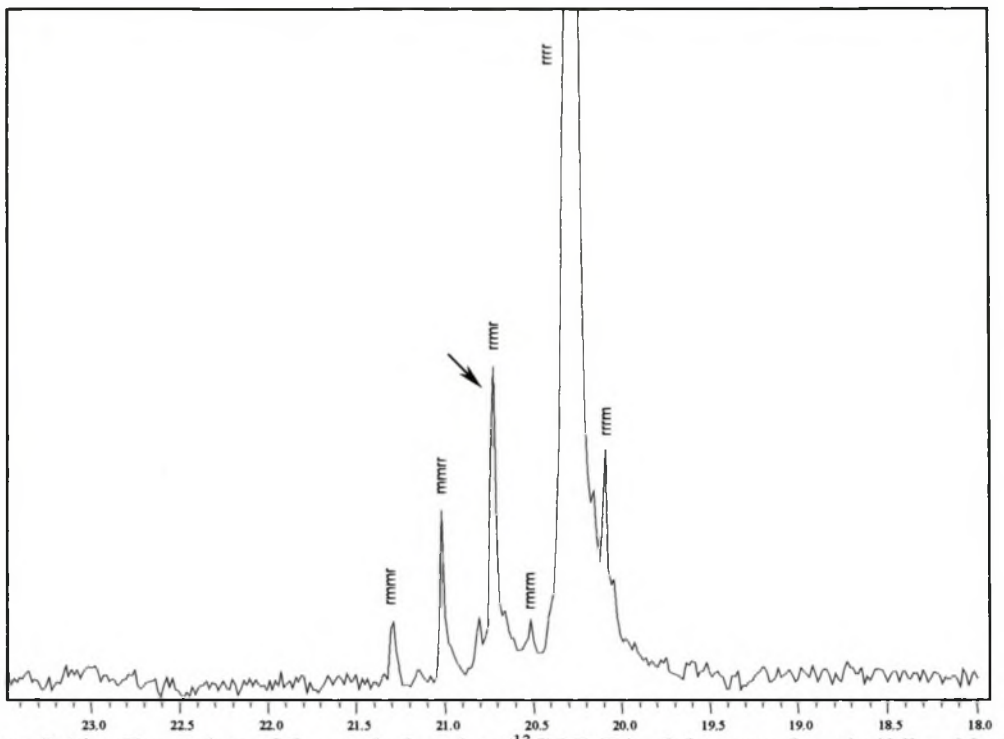

Figure 5.4A. Expansion of the methyl region (^{13}C NMR) of the propylene building block in the propylene/1-hexene copolymer H5 with 1.88 mol-% comonomer content, synthesised with **1**.

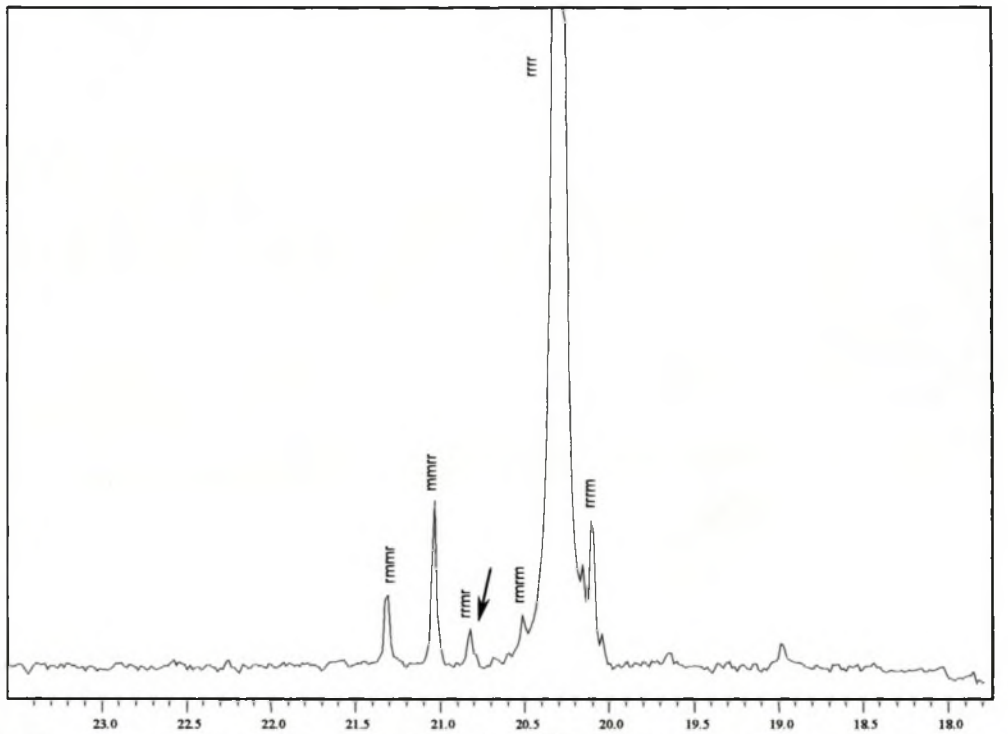

Figure 5.4B. Expansion of the methyl region (^{13}C NMR) of the reference polypropylene sample (s-PP) synthesised with **1**. The pentad assignment as carried out according to Busico *et al* [19].

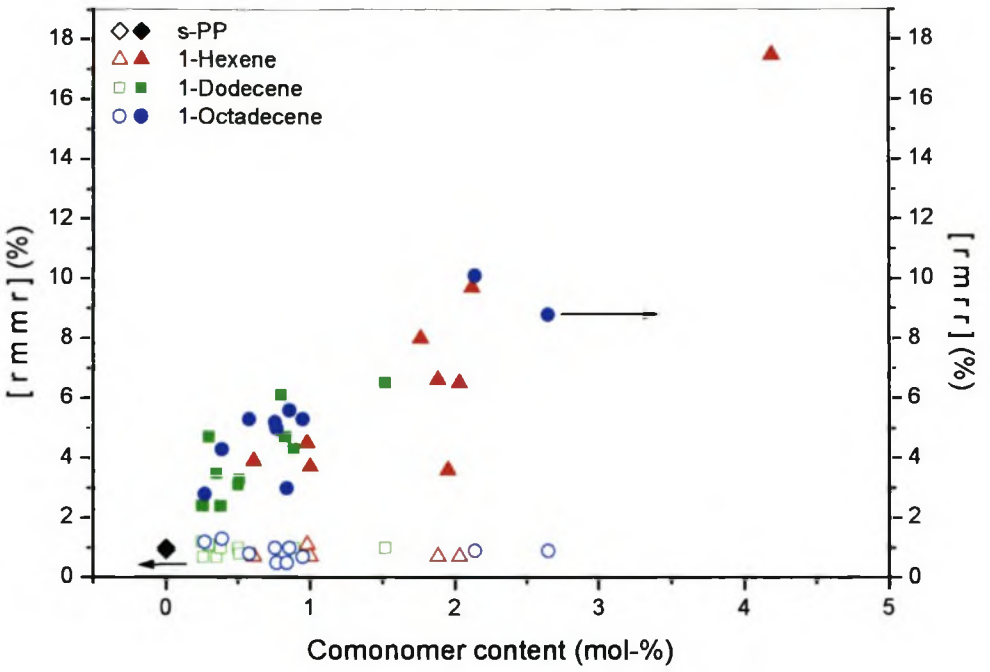

Figure 5.5. Abundance of the error pentads rmmr and rrmr (%) as a function of the comonomer content.

The occurrence of both skipped insertions through chain migration and site-control misinsertion can be better understood when looking at a 3-dimensional diagram of the reaction mechanism. Figure 5.6A-D shows the start of syndiotactic polymerization at the active site of the catalyst, where the propylene monomers attach, alternating on either site of the zirconium center. Only rrrr pentads are formed during this reaction step. In the case where one of the two sites on the zirconium center is not occupied by a propylene monomer unit, the growing polymer chain will migrate to the unoccupied site without monomer insertion (Figure 5.7A-D). This movement of the chain without monomer insertion is called skipped insertion and leads to rmrr pentad stereoerrors. Reversed enantioface insertion results from propylene monomer units, which do not have the right orientation towards the ring structure of the catalyst and are thus sterically hindering (Figure 5.8A-D). If the next propylene monomer unit is inserted in the right way, once again the rmmr pentad stereoerror is created. This is a chain end controlled error.

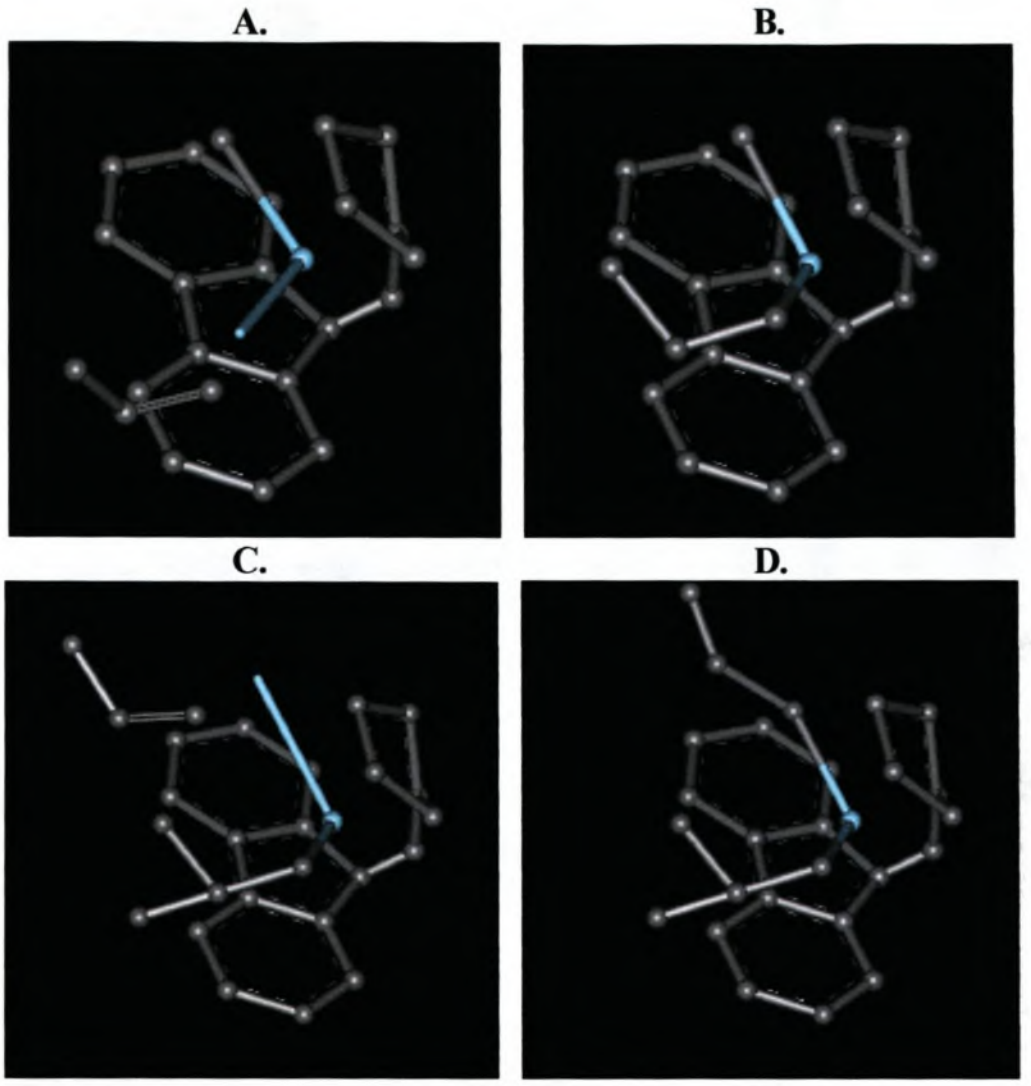

Figure 5.6A-D. Monomer insertion at alternative sites of the active catalyst centre **1**.

The samples H10 and D12 with significantly higher comonomer content (8.15 mol-% of 1-hexene, 6.65 mol-% of 1-dodecene) than all other copolymers in these series were specially prepared in order to determine the reactivity ratios from the methylene sequence distribution determined by ^{13}C-NMR spectroscopy. With the aid of the reactivity ratios it can be determined whether **1** synthesises random copolymers. The propylene-propylene [PP], propylene-comonomer [PC] and comonomer-comonomer [CC] methylene shifts for these samples were assigned according to the Grant and Paul rules [24] (Table 5.2). The assignments are in agreement with those reported by Zhi-Qiang *et al.* [9].

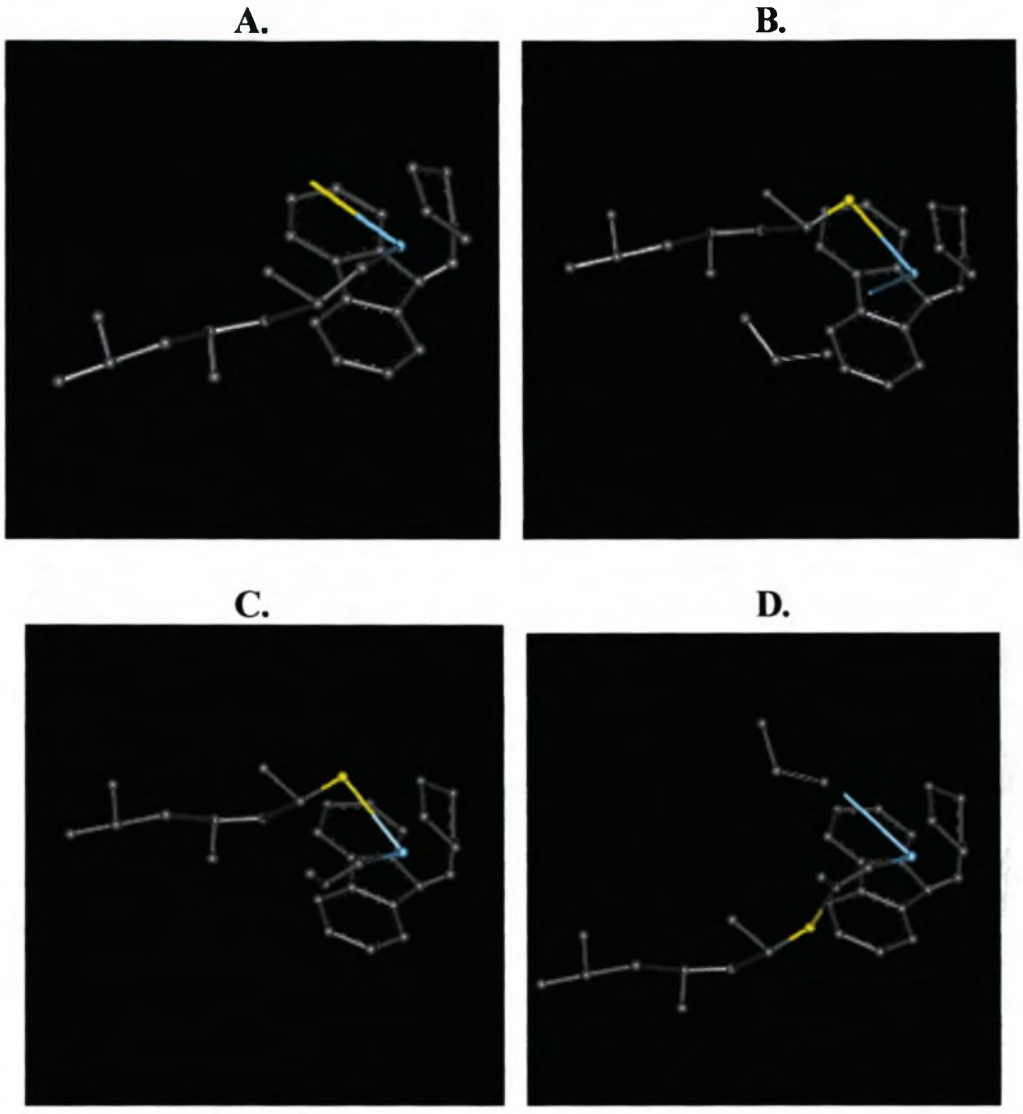

Figure 5.7A-D. Chain migration to the unoccupied site without monomer insertion, leading to skipped insertion error.

The equation for the Grant and Paul rules is as follows:

$$\delta_i = -2.3 + \sum_k A_k n_k + S_{i\alpha} \qquad \textbf{(5.1)}$$

The increments $A_k\, n_k$ are added to the chemical shift of methane δ = -2.3 in order to obtain the chemical shift for an unknown C_i carbon atom in the ^{13}C-spectra. The index k is the summary of the carbon atom positions in sequence adjacent to the

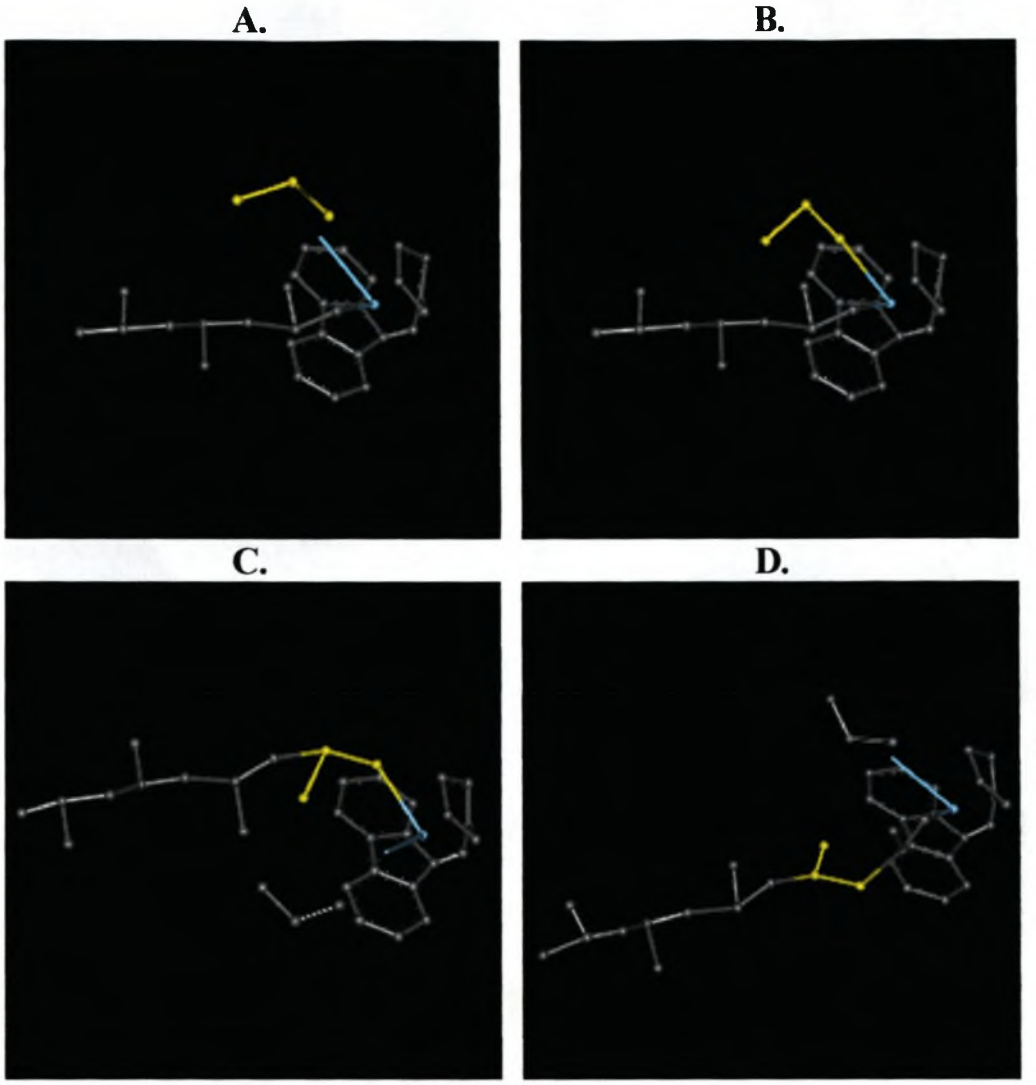

Figure 5.8A-D. Monomer units, with wrong orientation towards the ring structure, are sterically hindered and will lead to reversed enantioface insertion.

C_i atom (k = α,β, γ, δ and ε) and n_k represents the number of carbon atoms that are at a position k. Increments A_k have the following values:

$A_\alpha = +9.1$ $A_\gamma = -2.5$ $A_\varepsilon = +0.2$

$A_\beta = +9.4$ $A_\delta = +0.3$

In the case of tertiary and quaternary C-atoms and their adjacent neighbours, an additional sterical correction has to be introduced ($S_{i\alpha}$). For this, the highest substituted C-atom neighbouring the calculated C_i atom has to be found and the correction factor can be obtained from Table 5.3.

Table 5.3. Correction values $S_{i\alpha}$ as used for the application for the Grant and Paul rule.

C_i (calculated C atom)	Higher substituted neighbouring C atoms			
	—CH_3	—CH_2—	—CH<	—C<
Primary —CH_3	0	0	-1.1	-3.4
Secondary —CH_2—	0	0	-2.5	-7.5
Tertiary —CH<	0	-3.7	-9.5	(-15.0)
Quaternary —C<	-1.5	-8.4	(-15.0)	(-25.0)

The r_1 and r_2 ratios were calculated according to Equations 5.2 and 5.3.

$$r_P = \frac{2[PP]}{[PC]X} \tag{5.2}$$

$$r_C = \frac{2[CC]X}{[PC]} \tag{5.3}$$

where X is the concentration ratio of the comonomer to propylene in the feed. The reactivity ratios for the sample H10 were $r_P = 30.7$ and $r_H = 0.032$ (r_H is the reactivity ratio for 1-hexene) and for the sample D12 were $r_p = 93.3$ and $r_D = 0.010$ (r_D reactivity ratio for 1-dodecene). Since the product $r_1 \cdot r_2$ is close to 1, the higher α-olefins can be assumed to be randomly distributed throughout the copolymers. The product for the reactivity ratios of the 1-hexene copolymer was 0.98 and that of the 1-dodecene copolymer was 0.93. As an example, a copolymer of propylene and 1-hexene with a comonomer content of 11.67 mol% is shown in Figure 5.9. The triplet at 41.28 ppm (HH) is the methylene peak of two 1-hexene units that lie adjacent to each other in the copolymer.

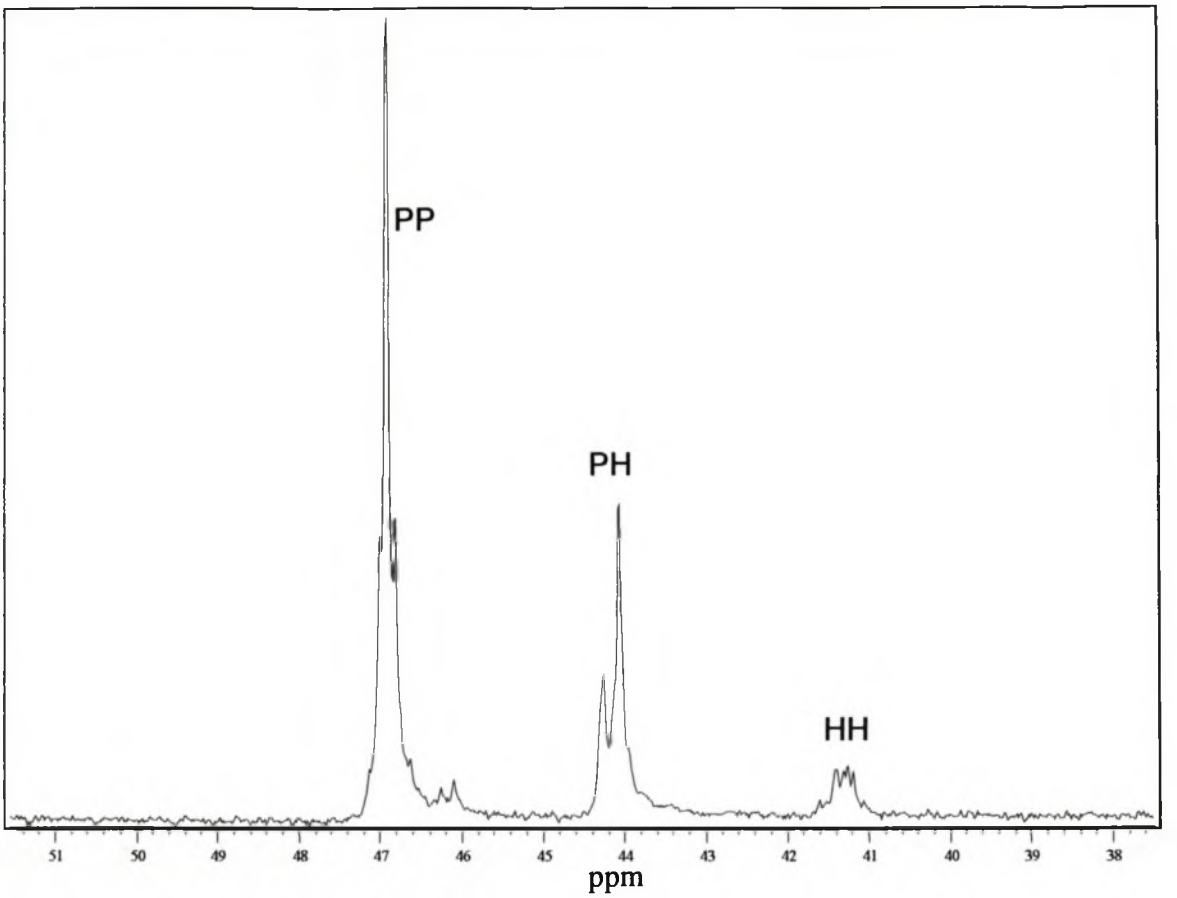

Figure 5.9. ^{13}C-NMR spectrum of a copolymer of propylene and 1-hexene, with a 1-hexene content of 11.67 mol-%.

5.3.2 Thermal Analysis

The thermal behavior of the syndiotactic copolymers was investigated by DSC at a heating and cooling rate of 10 °C/min, unless otherwise indicated. In order to obtain samples with a comparable thermal history, only the results of a second heating cycle were considered for the discussion of the thermal behavior on heating. The curves recorded by DSC for the propylene/1-hexene series, during cooling and heating, are shown in Figure 5.10(A) and 5.10(B). Here DSC curves are positioned according to the amount of higher α-olefin incorporated. The presence of a double melting peak for syndiotactic polypropylene is well documented and can be attributed to a recrystallisation process [25].

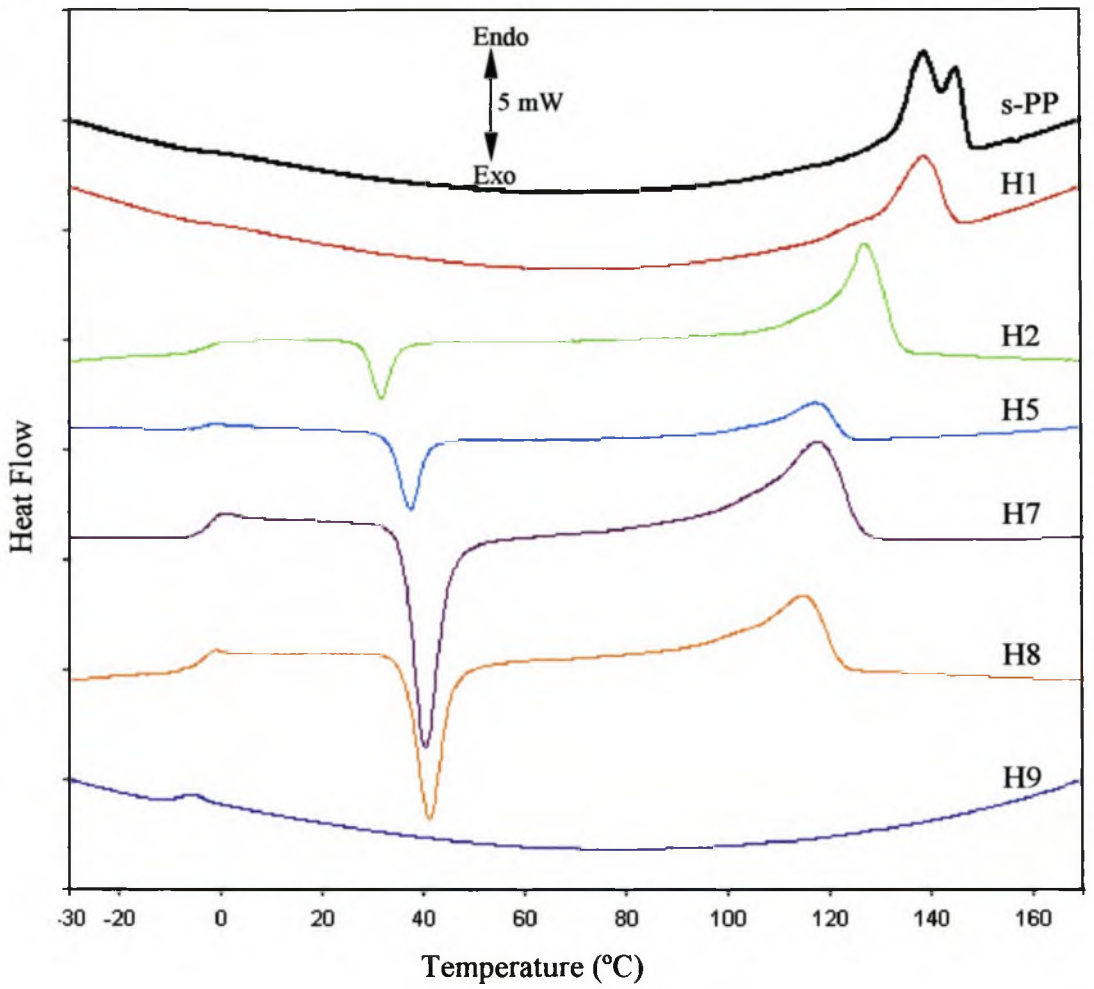

Figure 5.10A. DSC heating curves (2nd heating cycle, heating rate 10 °C/min) of syndiotactic propylene/1-hexene copolymers with varying (increasing from top to bottom) 1-hexene content.

The decrease in the endothermic $T_{m\ (DSC)}$ peak with increase in monomer content is shown in Figure 5.10(A). With the addition of comonomer, the characteristic double melting peak of the s-PP polymers disappears. An exothermic peak can also be seen in these runs, which correlates to crystallisation on heating, also called cold crystallisation. Thus $T_{c\ (DSC,\ heat)}$ increases with an increase in comonomer content. T_g (around –7 °C) can be observed for samples with higher amounts of comonomers, resulting from the higher amorphous polymer fraction. Figure 5.10(B) indicates the decrease in the $T_{c\ (DSC)}$ on cooling with a rise in comonomer content. The $T_{c\ (DSC)}$ peak broadens and the maximum peak height gets smaller with the addition of comonomer. This phenomenon is better explained with further experimentation at lower scanning speeds (see page 97).

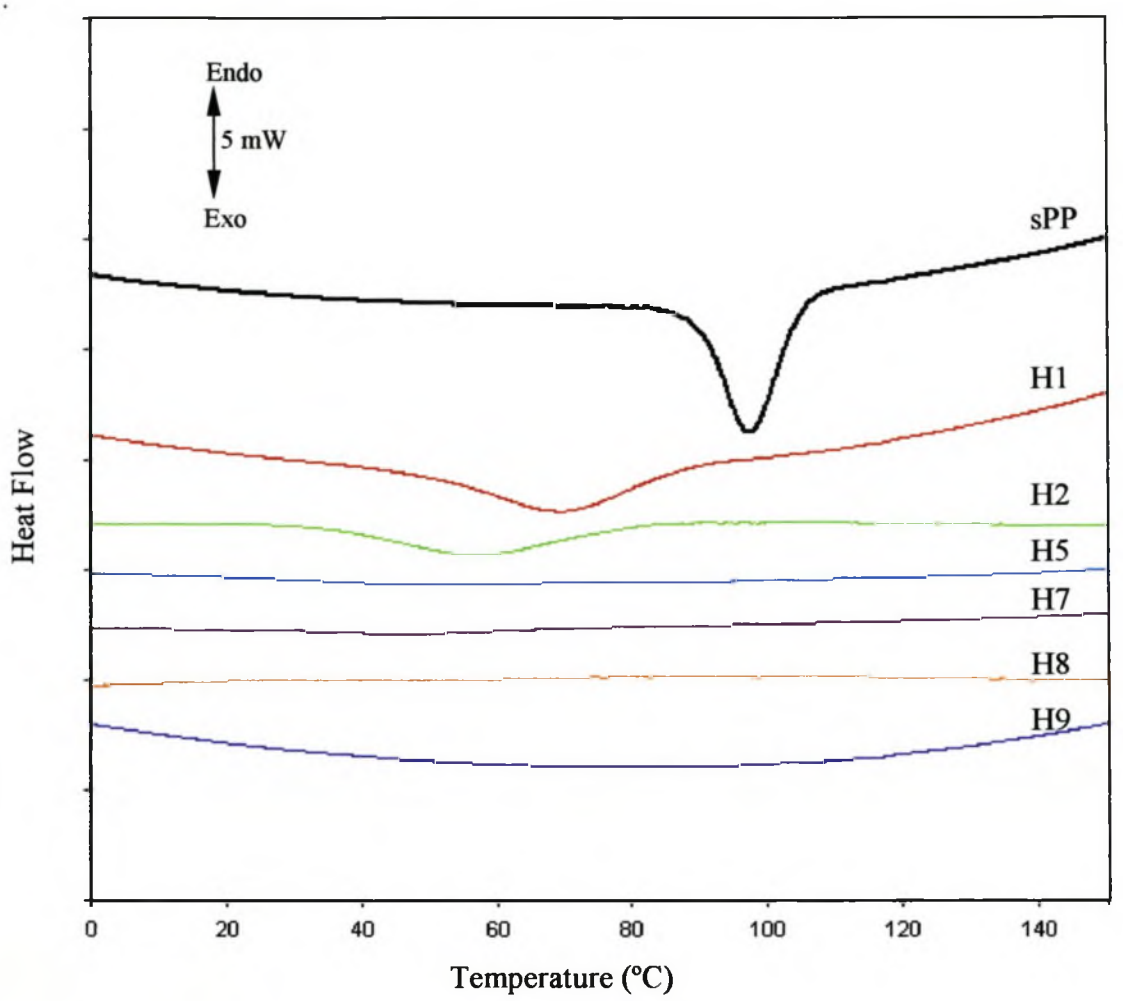

Figure 5.10B. DSC cooling curves (cooling rate 10 °C/min) of syndiotactic propylene/1-hexene copolymers with varying (increasing from top to bottom) 1-hexene content.

The melting peak temperatures, $T_{m\,(DSC)}$, of the syndiotactic propylene/higher α-olefin copolymers were plotted versus the corresponding comonomer content (Figure 5.11). According to the Flory theory, Equation 5.4 describes the melting behavior of random copolymers with low comonomer content.

$$T_m \cong T_m^o - \frac{R(T_m^o)^2}{\Delta H_u} X_{com} \qquad \textbf{(5.4)}$$

T_m and T_m^o are the equilibrium melting points of the copolymer and the homopolymer respectively; ΔH_u is the heat of fusion per crystallised unit; X_{com} is the fraction of

comonomer incorporated. Hence, for random copolymers the melting point depression is linearly related to X_{com}, irrespective of the nature of the non-crystallisable comonomer. Since the Flory theory describes an equilibrium state, it is in principle not applicable to the dynamic measurements presented here and the experimentally observed melting temperature of random copolymers will be lower than theoretically predicted by the Flory theory [26]. Naga *et al.* [13] studied the isothermal crystallisation behavior of syndiotactic propylene/α-olefin copolymers for which the equilibrium theory is directly applicable. To the best of my knowledge, no theory exists to describe the dynamic measurements presented here. Nevertheless, the results obtained for the metastable states during the dynamic measurements can at least qualitatively be rationalised according to the equilibrium theory. As expected from the equilibrium theory, this holds only true for comonomers that are bulky enough to be excluded from the lattice. Kakugo *et al.* [10] have shown that the melting points of syndiotactic propylene/1-butene copolymers are higher than those of propylene/1-pentene, and propylene/1-hexene copolymers.

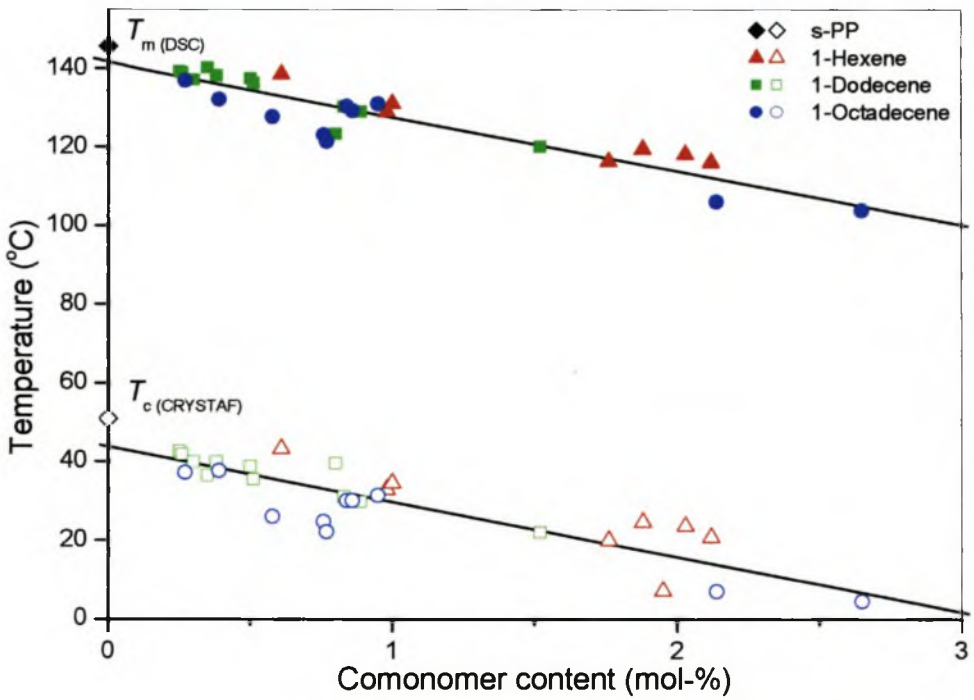

Figure 5.11. Melting temperature, $T_{m\ (DSC)}$, determined by DSC, and crystallisation temperature, $T_{c\ (CRYSTAF)}$, determined by CRYSTAF, of syndiotactic propylene/higher α-olefin copolymers synthesised with **1** as function of the comonomer content.

Thus far, only the comonomer amount was discussed as a contributing factor for the melting point depression. Differences in the stereoregularity of the samples have also to be considered. However, it is difficult to separate these variables and to quantify their contributions independently. Above we have shown that an increasing amount of comonomer has a strong influence on the stereoregularity of the copolymer. It is well known that the degree of tacticity influences the melting temperature. Assuming that the incorporation of a higher α-olefin into the growing chain enhances the possibility of skipped insertions, this subsequently leads to rrmr-stereoerrors due to the bulkiness of the comonomer around the catalyst centre. These errors are more likely to occur in the vicinity of the incorporated higher α-olefm. Therefore, the stereoerrors should not have a major effect on the crystallisable sequence of the copolymer.

It is striking to see that the samples with comonomer contents around 1 mol-% show an exothermic peak on heating which can be attributed to a crystallisation process. This phenomenon is well known for numerous polymer classes [27-29], but is hardly known to occur for polyolefins. In a comparable series of isotactic propylene/higher α-olefin copolymers with low comonomer content this crystallisation process was not observed. The peak crystallisation temperature on heating, $T_{c\,(DSC,\,heat)}$, increased with the amount of comonomer added (Figure 5.10A). The propylene/1-hexene series which included a copolymer with over 4 mol-% comonomer clearly revealed that the energy required for the crystallisation process goes through a maximum (Figure 5.10A). Samples with higher comonomer content are amorphous and consequently a crystallization process could not be observed. In Figure 5.10B, cooling curves from DSC are shown for the propene/1-hexene series. Samples with lower comonomer content tend to crystallise at higher temperatures, whereas copolymers with higher comonomer content are prevented from crystallising during cooling at a rate of 10 °C/min. The crystallisation behaviour on cooling is opposite to the behaviour on heating. Of course copolymers which are crystallised to a large extent during cooling, e.g. the syndiotactic polypropylene reference sample, cannot show crystallisation on heating. In general, the energy required for the melting

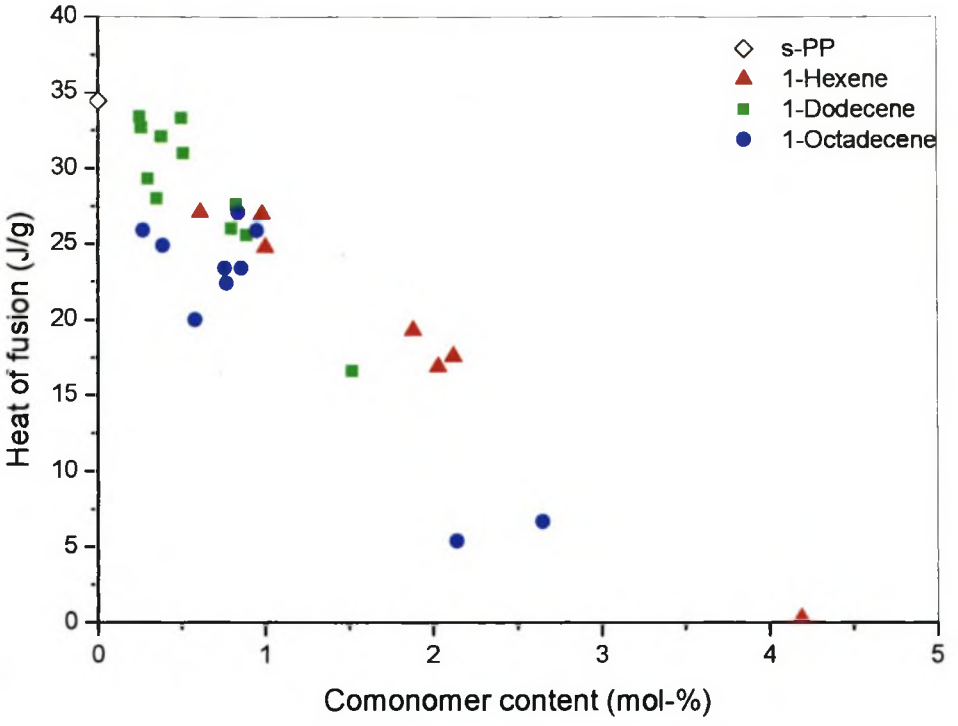

Figure 5.12. Heat of fusion for propylene/higher α-olefin copolymers synthesised with **1** as a function of the comonomer content.

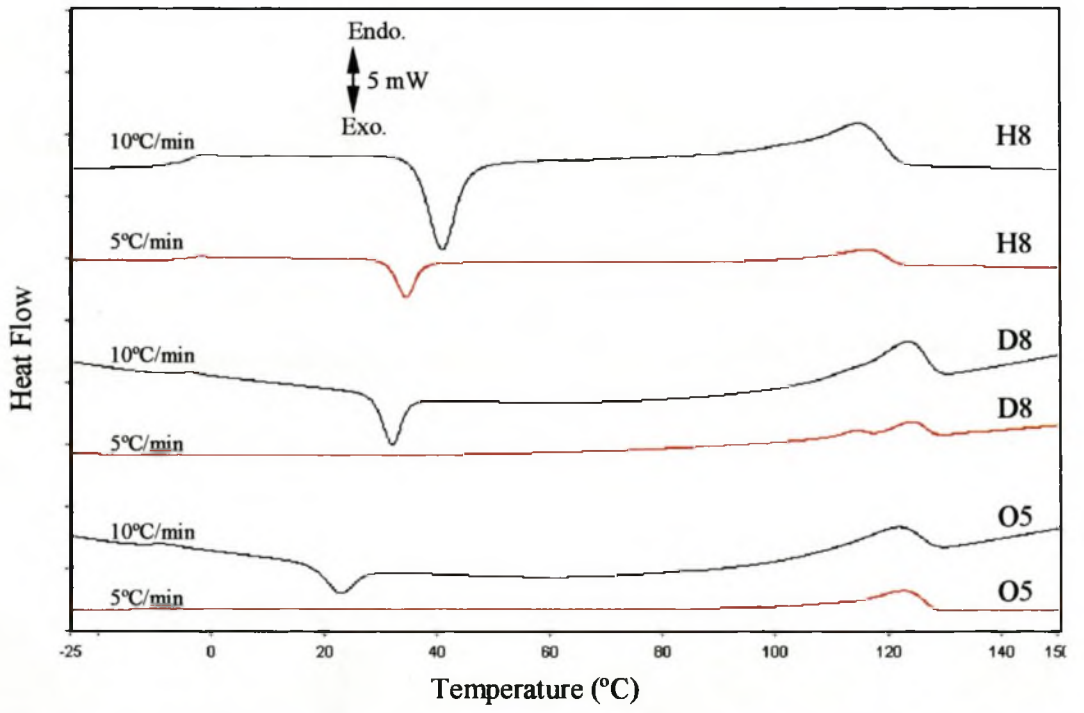

Figure 5.13. DSC heating curves (2nd heating cycle) of the propylene/1-hexene copolymer (H8), the propylene/1-dodecene copolymer (D8) and the propylene/1-octadecene (O5) copolymer at heating rates of 10 °C/min and 5 °C/min.

of the copolymers decreases with increasing comonomer content. This indicates the lower crystallinity of the materials with higher amounts of comonomer incorporated (Figure 5.12).

DSC curves are dependent on the applied heating and cooling rates. In Figure 5.13 samples H8, D8 and O5 represent examples of each copolymer series, which are compared at both heating and cooling rates of 10 °C/min and 5 °C/min. As expected, the peak melting temperatures are shifted to higher values at the slower heating rate. Furthermore, their crystallisation phenomena, as observed for the syndiotactic polypropylene reference sample, can now be observed. However, the exothermic peak indicating a crystallisation process during heating is less pronounced in the case of the propylene/1-hexene copolymer H8. It disappears completely for the propylene/1-dodecene and propylene/1-octadecene copolymers D8 and O5. This is due to the fact that the samples had sufficient time to crystallise during the preceding cooling cycle, conducted at a rate of 5 °C/min. Therefore, it can be concluded that the introduction of branches hinders the effective orientation of crystallisable polymer sequences efficiently at faster cooling rates.

In contrast to the melting temperatures, the glass transition temperatures depend not only on the amount but also on the nature of the comonomer. The incorporation of the longer chain 1-octadecene leads to a significantly lower glass transition temperature than the incorporation of 1-dodecene and 1-hexene at comparable comonomer amounts.

5.3.3 CRYSTAF

The crystallisation behaviour of the copolymers in dilute solution was studied with the crystallisation fraction analysis (CRYSTAF) technique developed by Monrabal [4]. The concentration of the polymer in solution is monitored by means of an IR-detector while cooling the solution at a rate of 0.1 °C/min. The principles of CRYSTAF are described in Chapter 4 [4]. An example of the first derivative of the concentration

Table 5.4. Melting temperatures, $T_{m\ (DSC)}$, and crystallisation temperatures, $T_{c\ (CRYSTAF)}$, of propylene/higher α-olefm copolymers synthesised with **1**, determined by DSC and CRYSTAF, respectively. $T_{c\ (DSC,\ heat)}$ and $T_{c\ (DSC)}$ are the exothermic peaks during the second heating cycle and the cooling cycle, respectively, ΔH the heat of fusion (J/g) and T_g the glass transition temperature. All temperatures are stated in °C.

Sample	Comonomer content in polymer (mol-%)	$T_{c\ (CRYSTAF)}$	$T_{c\ (DSC)}$	$T_{m\ (DSC)}$	$T_{c\ (DSC,\ heat)}$	ΔH	T_g
Polypropylene							
s-PP	n.a.[a]	50.8	97.5	145.6	n.o.[b]	34.4	-6.3
1-Hexene							
H1	0.61	43.3	69.7	138.6	n.o.	27.1	-7.2
H2	0.96	32.9	59.4	129.0	32.1	27.0	-4.5
H3	1.02	34.6	77.1	131.1	n.o.	24.8	n.d.[c]
H4	1.76	20.0	84.4	116.3	40.1	31.6	-10.3
H5	1.88	24.6	48.3	119.5	38.6	19.3	-5.9
H6	1.95	7.1	n.o.	n.o.	n.o.	n.o.	n.d.
H7	2.03	23.6	52.9	118.2	39.9	16.9	-4.5
H8	2.12	20.8	n.d.	116.2	42.2	17.6	-6.6
H9	4.19	3.2	n.d.	n.d.	22.7	0.3	-11.9
1-Dodecene							
D1	0.24	42.5	91.6	139.2	n.o.	33.4	-6.5
D2	0.27	41.8	89.5	138.9	n.o.	32.7	-6.3
D3	0.30	39.9	71.5	137.1	n.o.	29.3	-6.3
D4	0.35	36.4	80.5	140.1	n.o.	28.0	-5.9
D5	0.38	39.8	84.6	138.1	n.o.	32.1	-7.3
D6	0.49	38.7	82.6	137.4	n.o.	33.3	-7.0
D7	0.52	35.4	77.3	136.2	n.o.	31.0	-7.2
D8	0.80	39.5	32.2	123.4	32.2	26.0	-8.0
D9	0.83	31.0	72.4	130.3	n.o.	27.6	-7.5
D10	0.89	29.8	71.5	129.0	n.o.	25.6	-5.7
D11	1.52	22.0	52.3	120.0	33.7	16.6	-9.4
1-Octadecene							
O1	0.27	37.2	72.7	136.9	n.o.	25.9	-10.7
O2	0.39	37.6	66.5	132.1	n.o.	24.9	-10.3
O3	0.58	26.0	55.5	127.7	23.2	20.0	-17.4
O4	0.75	24.7	69.1	123.1	20.9	23.4	-21.4
O5	0.78	22.1	81.0	121.4	23.0	22.4	-14.3
O6	0.84	30.1	71.5	130.4	n.o.	27.1	-9.6
O7	0.87	30.1	70.9	129.3	n.o.	23.4	-12.8
O8	0.95	31.4	74.4	131.0	n.o.	25.9	-16.8
O9	2.14	6.9	23.7	106.0	24.4	5.4	-22.0
O10	2.65	4.4	81.2	103.8	31.0	6.7	-17.7

[a] not available
[b] not observed
[c] not determined

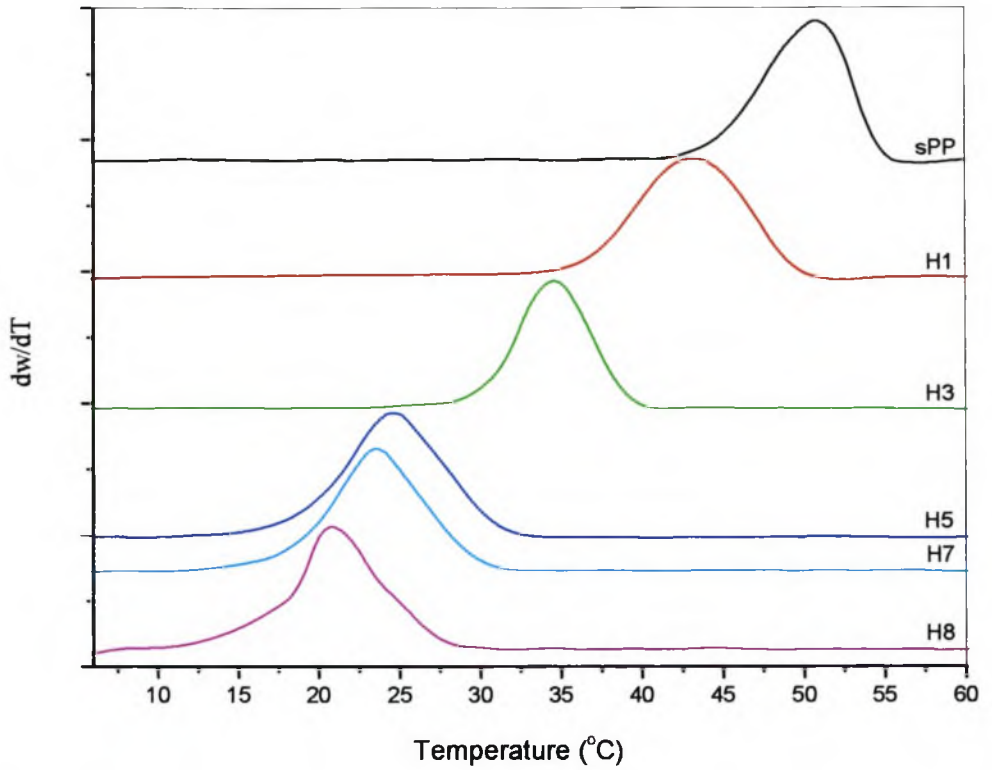

Figure 5.14. First derivative of the concentration profile for propylene/1-hexene copolymers, determined in the CRYSTAF experiment as a function of temperature.

versus temperature profile is shown for the propylene/1-hexene copolymers in Figure 5.14. The peak maxima of these curves were registered as crystallisation temperatures from solution, $T_{c\,(CRYSTAF)}$ (as seen in Table 5.4.). $T_{c\,(CRYSTAF)}$ values of the copolymers decreased with an increasing amount of comonomer incorporated. In a previous paper, concerning the melting and crystallization behavior of isotactic copolymers of propylene with higher α-olefins, we reported that all the melting temperatures determined by DSC and the crystallization temperatures determined by CRYSTAF from dilute solution are only separated by a constant factor [30]. Plotting $T_{m\,(DSC)}$ and $T_{c\,(CRYSTAF)}$ for the syndiotactic copolymers against the comonomer content reveals that this is also true for the syndiotactic copolymer series discussed in this chapter (Figure 5.11). However, closer inspection of the data obtained for $T_{c\,(CRYSTAF)}$ displayed a small, but discernible, difference between the 1-hexene and 1-octadecene copolymer series. The temperature difference between $T_{m\,(DSC)}$ and $T_{c\,(CRYSTAF)}$ for the pure syndiotactic polypropylene copolymer (s-PP) was 94.8 °C. In

Figure 5.15A, $T_{m\ (DSC)}$ and $T_{c\ (CRYSTAF)}$ of the propylene/1-hexene copolymers are overlaid in such a manner that the temperature difference of 94.8 °C obtained for the pure s-PP was cancelled out. As can be seen in Figure 5.15A, $T_{m\ (DSC)}$ and $T_{c\ (CRYSTAF)}$ for the propylene/1-hexene copolymers can be almost perfectly superimposed. Repeating the same procedure for the propylene/1-octadecene series displays a distinct difference between $T_{m\ (DSC)}$ and $T_{c\ (CRYSTAF)}$ (Figure 5.15B). This implies a small dependence of the comonomer type on the crystallisation process from solution, whereas the melting temperature can be regarded to be independent thereof. Syndiotactic propylene/1-dodecene copolymers show an intermediate behaviour. Copolymers with comparable comonomer amounts have a similar amount of non crystallisable units, as long as the comonomer cannot be incorporated into the crystal lattice. Therefore, it can be assumed that the copolymers gain a similar amount of lattice energy by forming crystals. Further details on this phenomenon will be given in section 6.3.3, with the additional data from the ethylene/higher α-olefins.

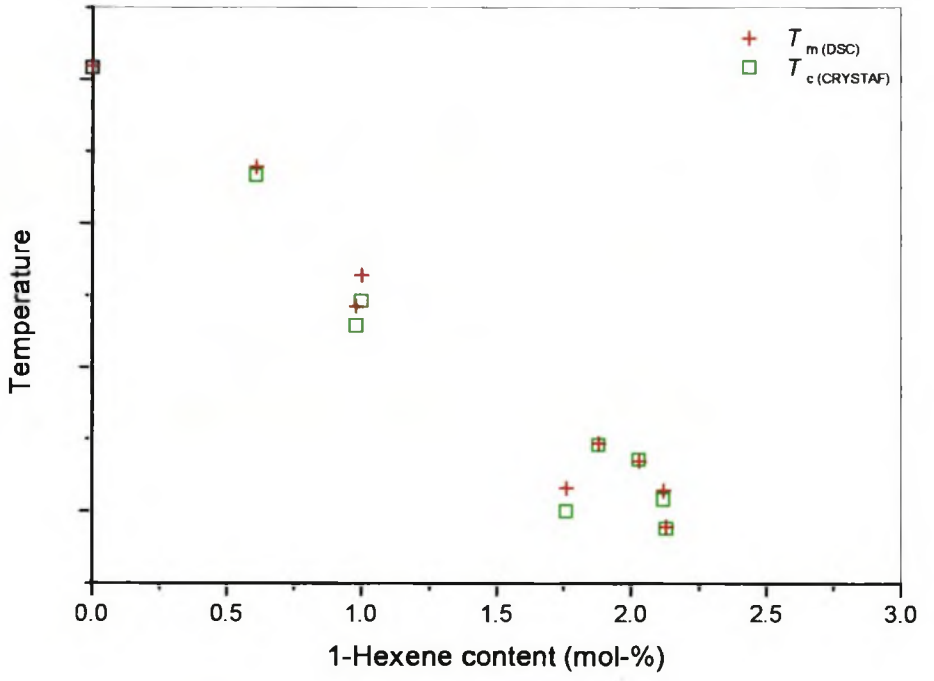

Figure 5.15A. Melting (T_m) and crystallisation (T_c) temperatures determined by DSC and CRYSTAF, respectively, overlaid in such a way that the temperature difference for the s-PP reference sample is cancelled out for propylene/1-hexene copolymers synthesised with **1**.

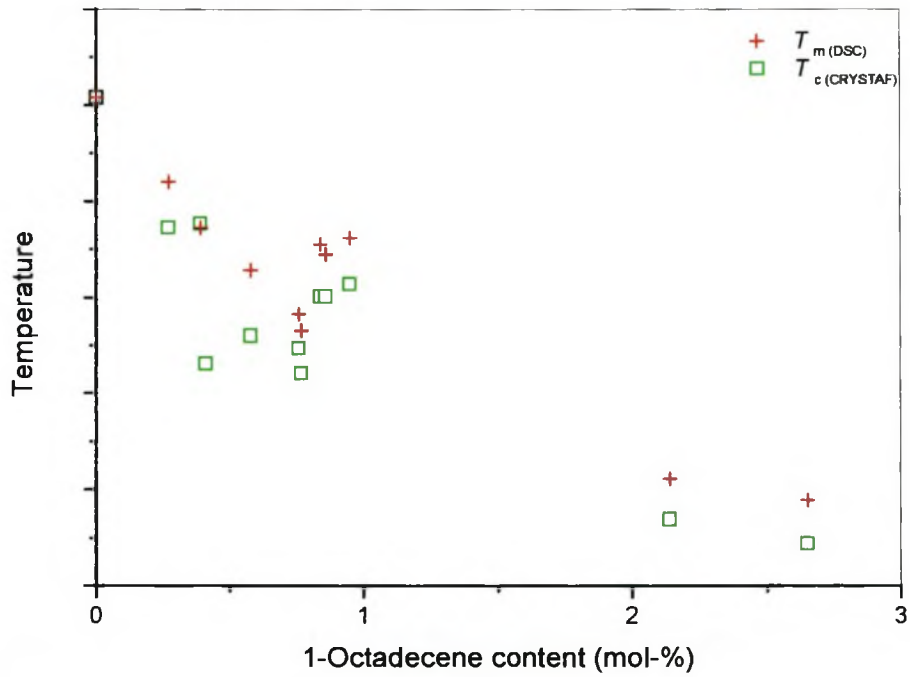

Figure 5.15B. Melting (T_m) and crystallisation (T_c) temperatures determined by DSC and CRYSTAF, respectively, are overlaid in such a way that the temperature difference for the s-PP reference sample is cancelled out for proplyene/1-octadecene copolymers synthesised with 1.

With increasing branch length the crystallisation process could be retarded due to an entanglement of the more mobile longer branches. In a recent study, Soares *et al.* [31] demonstrated that for polyethylene the CRYSTAF peak temperature is practically independent of the molar mass and that the influence thereof is only significant for samples with number-average molar mass below 5 000. Since the molar mass of all samples used in this study far exceed this molar mass, a significant influence of the molar mass on the lowering of the peak crystallisation temperature can be ruled out.

5.4 Summary

This chapter described the analysis of propylene/higher α-olefins (1-hexene, 1-decene and 1-octadecene) prepared with **1**. The catalyst **1** has a C_s-symmetry, thus allowing the stereoregular synthesis of syndiotactic polypropylene. In the microstructure identification of this samples it was observed that the site-chain controlled reversal of the enantiface selectivity error [rmmr] stayed constant with an increase in comonomer concentration, but the chain migration without olefin insertion error [rrmr] increased with higher concentrations of comonomer incorporated. This was attributed to the bulkiness of the comonomer around the active catalyst centre. For this reason the syndiotacticity also decreased with addition of comonomer.

During the thermal analysis by DSC a decrease in the $T_{m\,(DSC)}$ as well as an increase in both the peak area of the crystallisation on heating and the $T_{c\,(DSC,\,heat)}$ was seen with a rise in comonomer concentration. The observation of $T_{c\,(DSC,\,heat)}$ in polyolefins was seen here for the first time. This process of crystallization on heating was related back to the fact that crystallisation could not be completed during the cooling cycle. The $T_{c\,(DSC)}$ also showed a decrease in temperature with the addition of comonomer incorporated into the copolymer. It was observed that both DSC and CRYSTAF data give parallel lines when plotting the data on a temperature versus comonomer content scale. This confirms that DSC and CRYSTAF give similar results. Small differences were observed when the data of DSC and CRYSTAF were overlaid on the temperature scale. These small differences were larger in samples containing 1-octadecene than those containing 1-hexene.

5. References

1. Natta G, Pasquon I, Zambelli A, J. Am. Chem. Soc., 1962, **84**, 1488.
2. Zambelli A, Sessa I, Grisi F, Fusco R, Accomazzi P, Macromol. Rapid. Commun., 2001, **22**, 297.
3. Ewen J A, Jones R L, Razavi A, Ferrara J D, J. Am. Chem. Soc., 1988, **110**, 6255.
4. Monrabal B, J. Appl. Polym. Sci., 1994, **52**, 491.
5. Monrabal B, Blanco J, Nieto J, Soares J B P, J. Polym. Sci., Part A: Polym. Chem., 1999, **37**, 89.
6. Forlini F, Fan Z-Q, Tritto I, Locatelli P, Sacci M, Macromol. Chem. Phys., 1987, **198**, 2367.
7. Arnold M, Henschke O, Knorr J, Macromol. Chem. Phys., 1996, **197**, 563.
8. Arnold M, Bornemann S, Köller F, Menke, Kressler J, Macromol. Chem. Phys., 1988, **199**, 2647.
9. Fan Z-Q, Yasin T, Feng L-X, J. Polym. Sci., Part A: Polym. Chem., 2000, **38**, 4299.
10. Naga N, Mizunuma K, Sadatoshi H, Kakugo M, Macromolecules, 1997, **30**, 2197.
11. deRosa C, Talarico G, Caporaso L, Auriemma F, Galimberti M, Fusco O, Macromolecules, 1998, **31** (26), 9109.
12. Thomann R, Kressler J, Mülhaupt R, Polymer, 1998, **39** (10), 1907.
13. Naga N, Mizunuma K, Sadatoshi H, Kakugo M, Polymer, 2000, **41**, 203.
14. van-Reenen A J, Brull R, Wahner U W, Raubenheimer H G, Sanderson R D, Pasch H, J. Polym. Sci., Part A: Polym. Chem., 2000, **38** (22), 4110.
15. Randall J C, Polym. Charact. ESR NMR Symp., 1980, **6**, 93.
16. Kaminsky W, Macromol. Chem. Phys., 1996, **197**, 3907.
17. Busico V, Cipullo R, Talarico G, Caporaso L, Macromolecules, 1998, **31**, 2387.
18. Brüll R, Pasch H, Raubenheimer H G, Sanderson R D, Wahner U W, J. Polym. Sci., Part A: Polym. Chem., 2000, **38** (21), 2333.
19. Busico V, Cipullo R, Monaco G, Vacatello M, Segre A L, Macromolecules, 1997, **30**, 6251.

20. Resconi L, Cavallo L, Fait A, Piemontesi F, Chem. Rev., 2000, **100**, 1253.
21. Brintzinger H H, Fischer D, Mülhaupt R, Rieger B, Waymouth R M, Angew. Chem., Int. Ed. Engl., 1995, **34**, 1134.
22. Ewen J A, Elder M J, Jones R L, Haspeslagh L, Atwood J L, Bott S G, Robinson K, Makromol. Chem., Macromol. Symp., 1991, **48** (49), 253.
23. Herfert N, Fink G, Makromol. Chem., 1992, **193**, 1359.
24. Grant D M, Paul E G, J. Am. Chem. Soc., 1964, **86**, 2984.
25. deRosa C, Auriemma F, Viniti V, Galimberti M, Macromolecules, 1998, **31**, 6206.
26. Alamo R G, Mandelkern L, Thermochim. Acta., 1994, **238**, 155.
27. Tanaka M, Motomura T, Ishii N, Shimura K, Onishi M, Mochizuki A, Hatakeyama T, Polymer International, 2000, **49** (12), 1709.
28. Cho J W, Woo K S, J. Polym. Sci. Part B: Polym. Phys., 2001, **39** (16), 1920.
29. Qiu Z, Mo Z, Zhang H, Shouri S, Song C, J. Appl. Polym. Sci., 2000, 77 (13), 2865.
30. Brüll R, Pasch H, Raubenheimer H G, Sanderson R D, vanReenen A J, Wahner U M, Macromol. Chem. Phys., 2001, **202**, 1281.
31. Nieto J, Oswald T, Blanco F, Soares J B P, Monrabal B, J. Polym. Sci., Part B: Polym. Phys., 2001, **39**, 1616.

CHAPTER 6

COPOLYMERISATION OF ETHYLENE WITH HIGHER α-OLEFINS IN THE PRESENCE OF THE METALLOCENE CATALYST $Et(Ind)_2ZrCl_2$ / MAO

6.1 Abstract

The catalyst system $Et(Ind)_2ZrCl_2$/MAO was utilised to synthesise random copolymers of ethylene and 1-decene, 1-tetradecene and 1-octadecene as comonomers. Determination of the comonomer content was done by ^{13}C-NMR spectroscopy. The melting- and crystallisation temperatures of the copolymers, as measured by DSC, decreased linearly with increasing comonomer content. The depression of the crystallisation temperature with an increase in comonomer content was also observed in CRYSTAF data. Results show a small but significant dependence of crystallisation temperature from CRYSTAF on the nature of the comonomer. CRYSTAF results proved the presence of gradient copolymerisation during the reaction. Crystallisation and melting curves from DSC gave matching results to CRYSTAF curves when superpositioned relative to the peak maximum. Chemical heterogeneity was only seen in the chemical composition distribution measurable with CRYSTAF. The molar mass distribution measured with GPC, coupled to FTIR spectroscopy (LC-Transform), did not reveal a significant change in the relative amounts of comonomer incorporated versus chain lengths.

6.2 Introduction

Until recently, three types of polyethylenes have been commercially available: low-density polyethylene (LDPE), high-density polyethylene (HPDE) and linear low-density polyethylene (LLDPE).

Dow and Exxon developed a new class of polyethylene copolymers by the copolymerisation of ethylene with long α-olefins (1-hexene, 1-octene and 1-decene) via so-called CpA catalysts [1-3]. Substantially linear polymers with the strength and toughness of LLDPE, as well as the processability of LDPE were obtained [4, 5]. The theory behind this is that the open catalyst structure, combined with high temperature and a critical level of β-H elimination, leads to the formation of vinyl-terminated macromonomers that are reinserted into the growing polymer chain [6].

Further research by Exxon showed that higher α-olefins, ranging from 1-decene (C_{10}) up to 1-octadecene (C_{18}), could be copolymerised with ethylene, in the presence of $Me_2Si(Me_4Cp)(NC_{12}H_{23})]TiCl_3$, with incorporation levels as high as 11 % and molar masses of 80 kD [7]. When the comonomer content exceeds 10 %, the polymers exhibited melting behaviour suggestive of side chain crystallisation. These polymers are of interest for applications in shock-adsorbing and vibration-damping materials.

In this chapter, the synthesis and analysis of ethylene/higher α-olefm copolymers is discussed in a similar manner to the propylene/higher α-olefin copolymers discussed in Chapter 5. Focus will also be placed on the chemical composition heterogeneity regarding the comonomer content in both GPC and CRYSTAF analyses.

6.3 Results and Discussion

6.3.1 Synthesis

Copolymers of ethylene with various amounts of higher linear α-olefins (1-decene, 1-tetradecene and 1-octadecene) were synthesised in batch mode with the single site precatalyst $Et(Ind)_2Zr\ Cl_2$ (**1**) (Scheme 6.1 and Figure 6.2). The conversion was kept below 20 % in all cases so that statistical random copolymers could be synthesised. All of the copolymers had molar mass between 28 000 and 87 000 g/mol and exhibited polydispersities around 2, as expected for metallocene catalysts (Table 6.1). Samples ED1-3 (Table 6.1) had polydispersities greater than 2. This stems from the fact that the reactor was only cooled down to the desired temperature after the addition of the ethylene gas. During the few seconds that thermal regulation was not maintained (inside a water bath), the temperature inside the reactor increased dramatically causing the broader polydispersity.

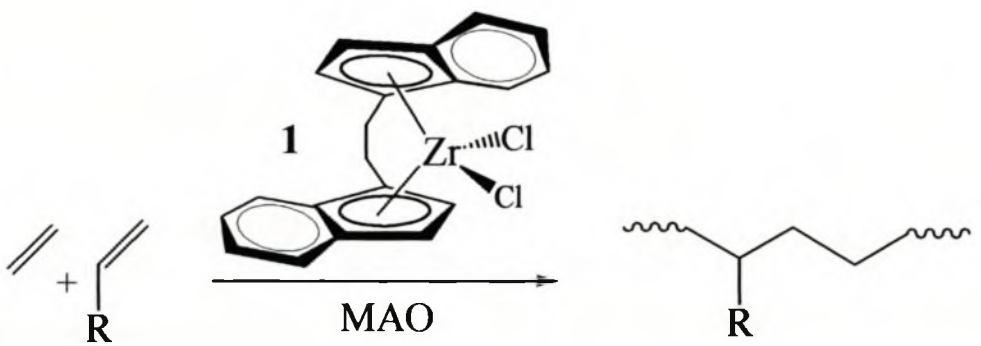

R = *n*-octyl, *n*-dodecyl, *n*-hexadecyl

Scheme 6.1. Reaction diagram for the synthesis of ethylene/1-decene, /1-tetradecene or /1-octadecene copolymers via the **1**/MAO catalyst system.

The incorporation of comonomer into the copolymer by catalyst **1** follows a linear relationship under the experimental conditions where low comonomer concentrations

were used (Figure 6.2). Metallocene catalysts show constant reactivity ratios for the polymerisation of ethylene with higher α-olefins [8].

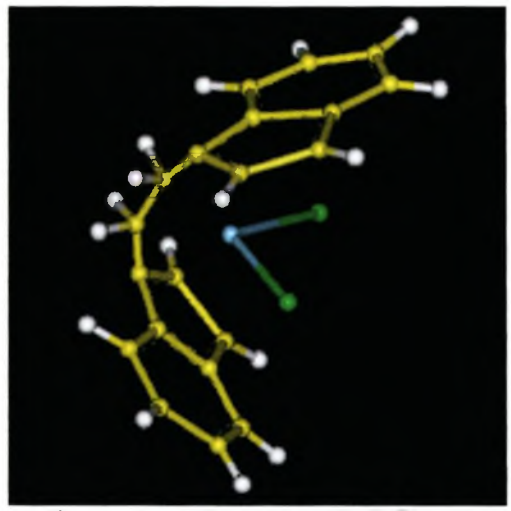

Figure 6.1. 3-Dimensional illustration of *rac*-Et(Ind)$_2$ZrCl$_2$ pre-catalyst (white = hydrogen atoms, yellow = carbon atoms, cyan = zirconium atom and green = chlorine atoms).

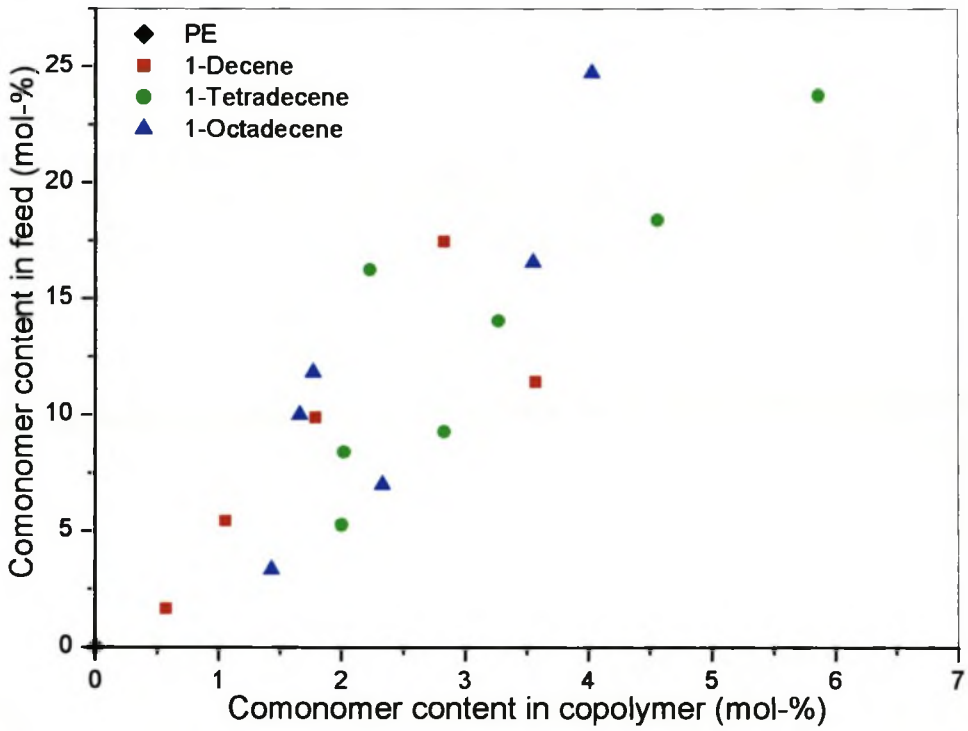

Figure 6.2. The amount of comonomer added under feed conditions as a function of the comonomer incorporation in the copolymer, as determined by ^{13}C NMR spectroscopy.

Table 6.1. Reaction conditions for the preparation of ethylene copolymers, with reference to the quantities of (co)monomers added during the polymerisation process, as well as data regarding the subsequent analysis of the copolymers. Values regarding comonomer content (^{13}C NMR spectroscopy), crystallization temperature $T_{c\,(CRYSTAF)}$, melting temperature $T_{m\,(DSC)}$, crystallisation temperature $T_{c\,(DSC)}$, ΔH the heat of fusion (DSC), T_g (DMA), M_n and M_w/M_n are given.

Sample code	Comonomer content in polymer (mol-%)	Volume comonomer (mL)	Ethylene weight (g)	Comonomer content in feed (mol-%)	$T_{c\,(CRYSTAF)}$ 0.1°C/min (°C)	$T_{c\,(CRYSTAF)}$ 0.05°C/min (°C)	$T_{m\,(DSC)}$ (°C)	$T_{c\,(DSC)}$ (°C)	ΔH (J/g)	M_n (g/mol)	M_w/M_n
Polyethylene											
PE	0	0	17.6	0	86.3	88.5	134.5	115.6	189.7	53800	2.1
1-Decene											
ED1	0.57	2	17.6	1.66	84.5	86.8	130.0	113.2	141.7	34630	4.5
ED2	1.05	6	15.5	5.43	81.4	83.7	124.8	111.2	157.5	28170	6.3
ED3	1.79	12	16.2	9.89	78.8	82.2	121.3	107.9	130.2	30860	3.1
ED4	2.83	18	12.6	17.47	73.4	74.9	117.0	101.7	99.2	70460	1.8
ED5	3.57	6	6.9	11.42	72.5	74.6	116.5	96.4	99.8	70800	1.9
1-Tertadecene											
ET1	2.00	12	14.5	8.39	79.1	82.3	121.8	107.7	106.5	30800	2.2
ET2	2.05	6	12.0	5.25	81.9	83.7	123.5	109.4	97.8	58120	2.1
ET3	2.23	6	6.5	9.27	78.8	82.1	121.3	106.2	91.6	64130	1.9
ET4	2.83	18	12.2	14.04	73.2	75.1	117.5	102.5	86.8	53650	1.9
ET5	3.27	24	13.7	16.24	72.4	71.2	116.8	101.5	58.3	43650	2.2
ET6	4.56	12	5.9	18.38	62.8	57.2	110.3	92.6	41.2	58910	2.0
ET7	5.86	18	6.4	23.74	57.0	58.2	107.2	87.9	51.3	76740	1.7
1-Octadecene											
EO1	1.43	6	15.2	3.34	78.8	84.3	125.5	108.5	121.0	52460	2.1
EO2	1,50	12	14.1	6.94	76.5	82.6	125.5	89.0	105.0	47500	2,8
EO3	1.66	18	14.2	10.00	76.5	78.9	124.1	105.0	92.6	65120	2.2
EO4	1.77	6	7.0	6.99	78.9	78.2	121.8	105.7	80.4	86770	1.9
EO5	2.33	24	15.7	11.82	65.8		117.0	101.4	80.1	66450	1.8
EO6	3.55	12	5.3	16.56	63.7	59.0	111.5	101.4	66.1	80300	1.7
EO7	4.03	24	6.4	24.74	59.8	61.9	109.3	91.0	60-8	76790	1.8

6.3.2 Microstructure

The publication of Randall [9] was used for the chemical shift assignments of copolymers containing little or no comonomer clustering. The assignments shown in Table 6.2 were used to label the C-atoms shown in the structure in Figure 6.3. Verification for the relaxation peak assignments (Figure 6.3) was compared with the chemical shifts predicted by the additivity rules described by Grant and Paul [10] (Table 6.2).

Table 6.2. Chemical shifts (ppm) for ethylene/higher 1-olefin (1-decene, 1-tetadecene and 1-octadecene) copolymers synthesised with **1** and the shift predictions, as obtained by Paul Grant calculations. Code numbering is the same as in Figure 6.3.

	Grant and Paul predictions				
Code	Backbone carbons	Side chain carbons	Ethylene/ 1-decene	Ethylene/ 1-tetradecene	Ethylene/ 1-octadecene
Br	38.00		38.14	38.18	38.18
$^{\alpha}C + {}^{8}C$	34.89	34.89	34.50	34.51	34.52
^{3}C		32.52	32.28	32.26	32.27
$^{\gamma}C$	30.44		30.58	30.58	30.58
$^{\varepsilon}C + {}^{5,6}C$	30.01	30.01	30.09	30.09	30.09
^{4}C		29.65	29.70	29.67	29.67
$^{\beta}C + {}^{7}C$	27.56	27.50	27.30	27.31	27.31
^{2}C		22.68	22.96	22.95	22.95
^{1}C		14.07	14.16	14.12	14.13

The comonomer content [C], in mole percent (mol-%), for all ethylene/α-olefin (1-decene, 1-tetradecene and 1-octadecene) copolymers was calculated according to the following formula [11]:

$$[C] = 200\ Br / (TBC) \qquad \textbf{(6.1)}$$

Br is the intensity of the methine branching peak, as indicated in the spectrum in Figure 6.3. The TBC (total backbone carbon content) is determined by the intensity obtained from the sum of the methyl branching carbons and the α-, β-, γ-, δ-, ε-methylene integrals. The value of 200 is related to the factor 2 for the second carbon of the comonomer which is situated in the backbone and the factor 100 for the

calculation of the percentage comonomer. Backbone carbons separated by more than five carbons from the branching carbon converge towards the same chemical shifts value (30 ppm) in order to get a correct value for the total branch carbon content. In cases where the chemical shift of the side chain C-atoms equals that of the backbone C-atoms, the intensity of the methyl branching was subtracted from these carbon intensities.

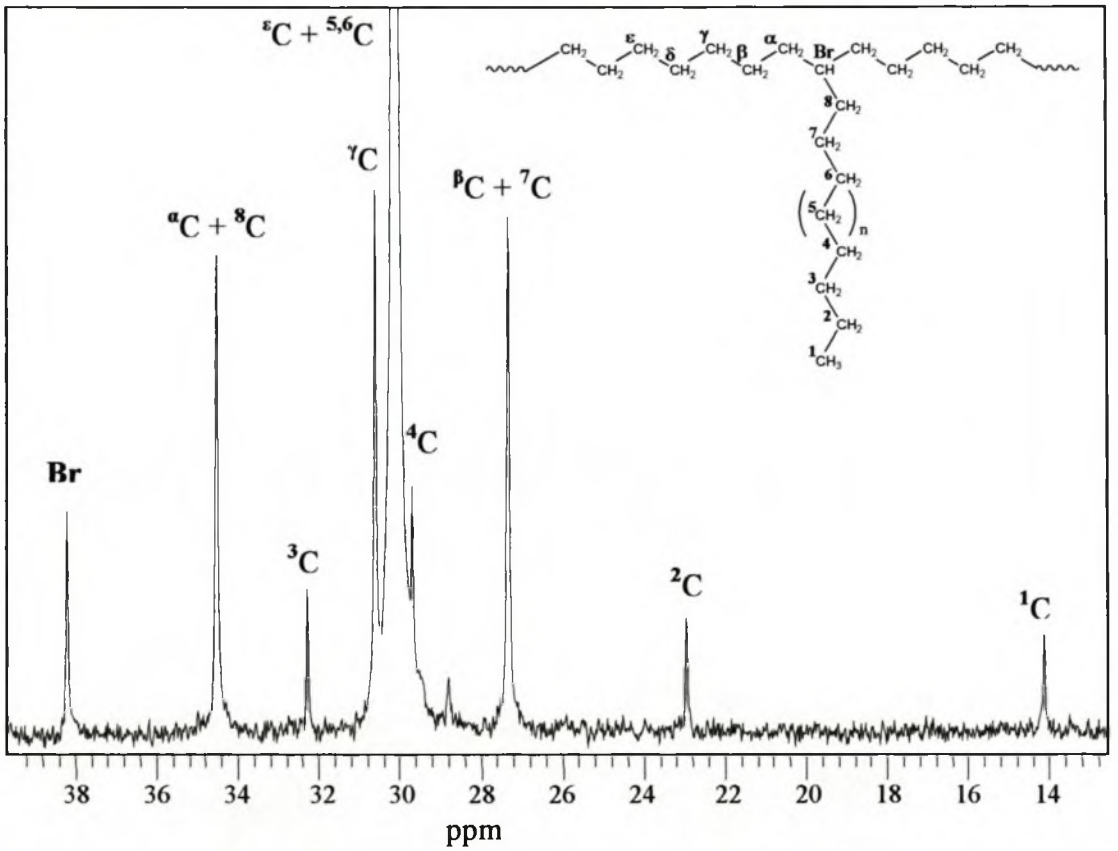

Figure 6.3. ^{13}C NMR spectrum of the ethylene/1-octadecene copolymer (EO6) synthesised with **1**. The designated numbers refer to C-atoms of the long chain branches, while the Greek symbols refer to C-atoms in the backbone. Branched C-atoms are indicated by the letters Br.

6.3.3 Thermal analysis

The thermal behaviour of the ethylene/higher α-olefin (1-decene, 1-tetradecene and 1-octadecene) copolymers synthesised with **1** was investigated by DSC, at a heating and cooling rate of 10 °C/min. In order to obtain accurate and comparable data with no thermal history, only the results of a second heating cycle and the first cooling runs

were considered for the discussion of the thermal behaviour. The curves recorded by DSC for the ethylene/1-tetradecene series during cooling and heating are shown in Figures 6.4 and 6.5. Here DSC curves are positioned according to the amounts of the higher α-olefm incorporated.

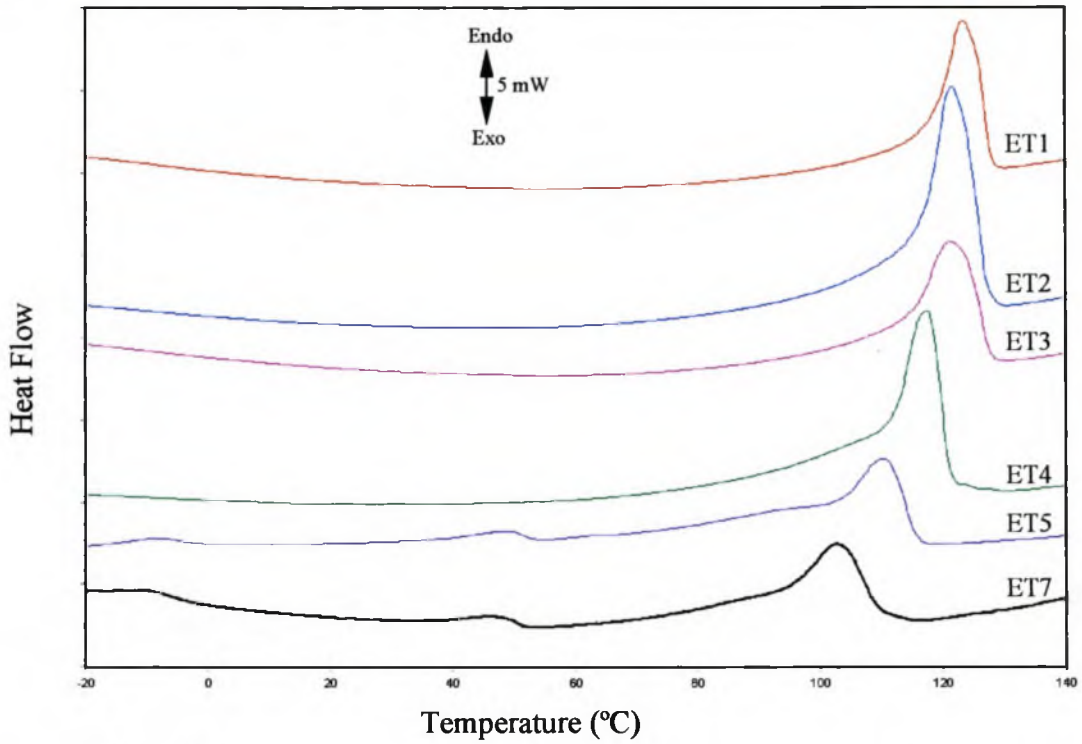

Figure 6.4. DSC heating curves (2nd heating cycle, heating rate 10 °C/min) of ethylene/1-tetradecene copolymer samples with varying 1-tetradecene content (increasing from top to bottom).

Goderis *et al.* observed the presence of two crystallisation peaks in the DSC cooling cycle for an ethylene/1-octadecene copolymer synthesised with a vanadium based catalyst [12]. He stated that the primary crystallisation (large peak in cooling cycle of DSC) is related to the spherulite growth formation. The secondary crystallisation occurs after the spherulite growth front has impinged, taking place in and around these spherulites. This involves lamellar insertion in the nano-confinement between existing crystals, as well as the creation of the new stacks in large amorphous spherulite inclusions. The presence of a second exothermal crystallisation peak at 19.22 °C (ET5) and 16.11 °C (ET7), in Figure 6.5, can thus be related to secondary crystallisation. The melting of the second crystallisation could not be seen in the heating cycle done by Goderis *et al.* [12], although these endothermal peaks are observed in this work (Figure 6.4) at 50.51 °C (ET5) and 46.40 °C (ET7).

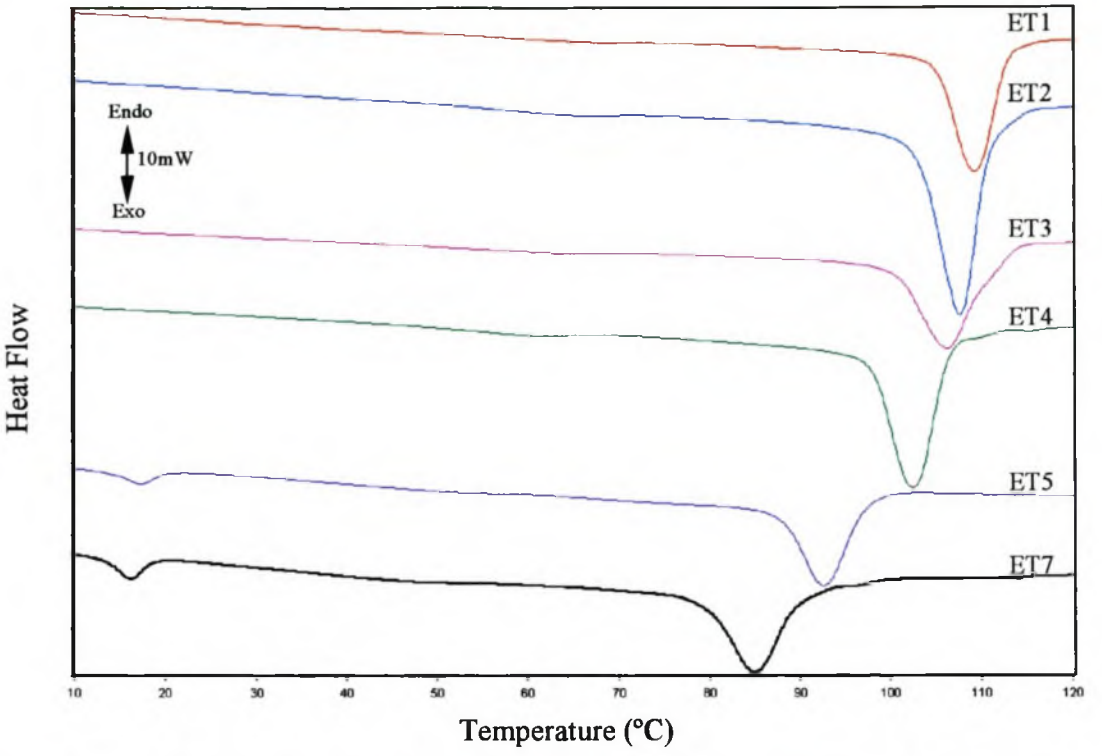

Figure 6.5. DSC cooling curves (cooling rate 10 °C/min) of ethylene/1-tetradecene copolymer samples with varying 1-tetradecene content (increasing from top to bottom).

The $T_{m\,(DSC)}$ on the 2nd heating cycle, as well as the $T_{c\,(DSC)}$ on cooling clearly show declines in the melting and crystallization temperature with an increase in comonomer content. This is expected for copolymers where the comonomer content increases and thus the amorphous part as well.

The melting peak temperatures, $T_{m\,(DSC)}$, and the $T_{c\,(DSC)}$, of the ethylene/higher α-olefin copolymers were plotted against the corresponding comonomer content (Figure 6.6). According to the Flory theory, Equation 6.2 (see chapter 5) describes the melting behaviour of random copolymers with low comonomer content.

$$T_m \cong T_m^o - \frac{R(T_m^o)^2}{\Delta H_u} X_{com} \qquad \textbf{(6.2)}$$

T_m and T_m^o are the equilibrium melting points of the copolymer and the homopolymer respectively; ΔH_u is the heat of fusion per crystallised unit and X_{com} is the fraction of comonomer incorporated.

Hence, for random copolymers, the melting point depression is linearly related to X_{com} irrespective of the nature of the non-crystallisable comonomer. Since the Flory theory describes an equilibrium state, it is in principle not applicable to the dynamic measurements presented in this chapter and the experimentally observed melting temperature of random copolymers will be lower than theoretically predicted by the Flory theory [13].

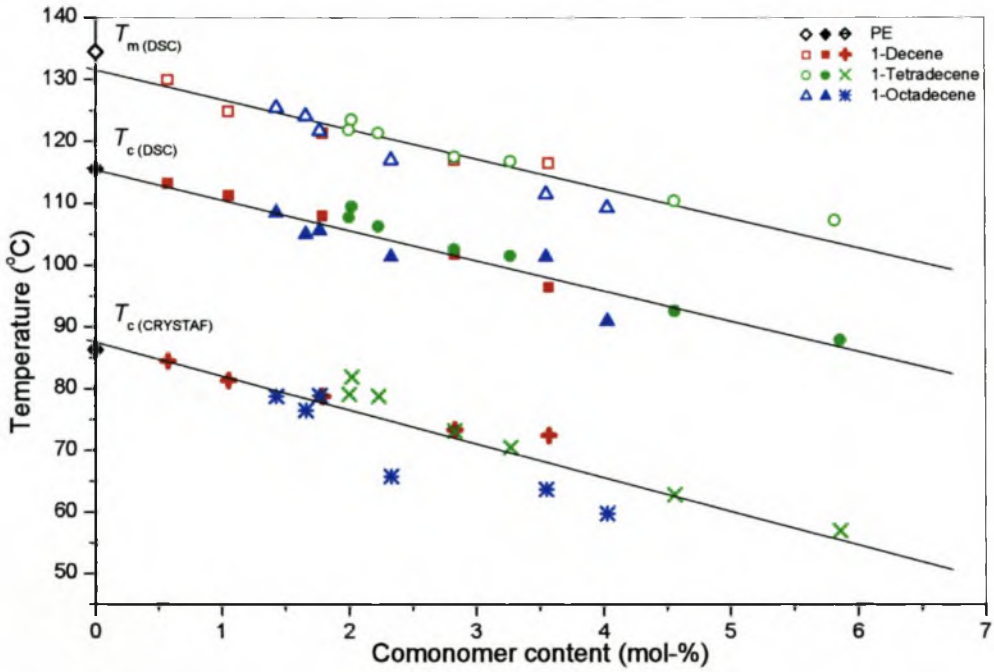

Figure 6.6. Melting temperature $T_{m\,(DSC)}$, and crystallisation temperature, $T_{c\,(DSC)}$, determined by DSC, as well as the crystallisation temperature $T_{c\,(CRYSTAF)}$, determined by CRYSTAF, of ethylene/higher α-olefin copolymers synthesised with **1**, as function of the comonomer content.

As expected, the lines drawn through the $T_{m\,(DSC)}$ and $T_{c\,(DSC)}$ are parallel to one another due to the close relationship between the crystallisation and melting processes (Figure 6.6). $T_{c\,(CRYSTAF)}$, as measured by CRYSTAF, shows a slight deviation from the results obtained in the DSC and CRYSTAF analyses done on propylene/higher α-olefin copolymers (Chapter 5). The latter gave parallel lines between the $T_{m\,(DSC)}$ and $T_{c\,(CRYSTAF)}$, whereas the line through $T_{c\,(CRYSTAF)}$ gave a steeper slope compared to $T_{m\,(DSC)}$ for the ethylene/higher α-olefins copolymers.

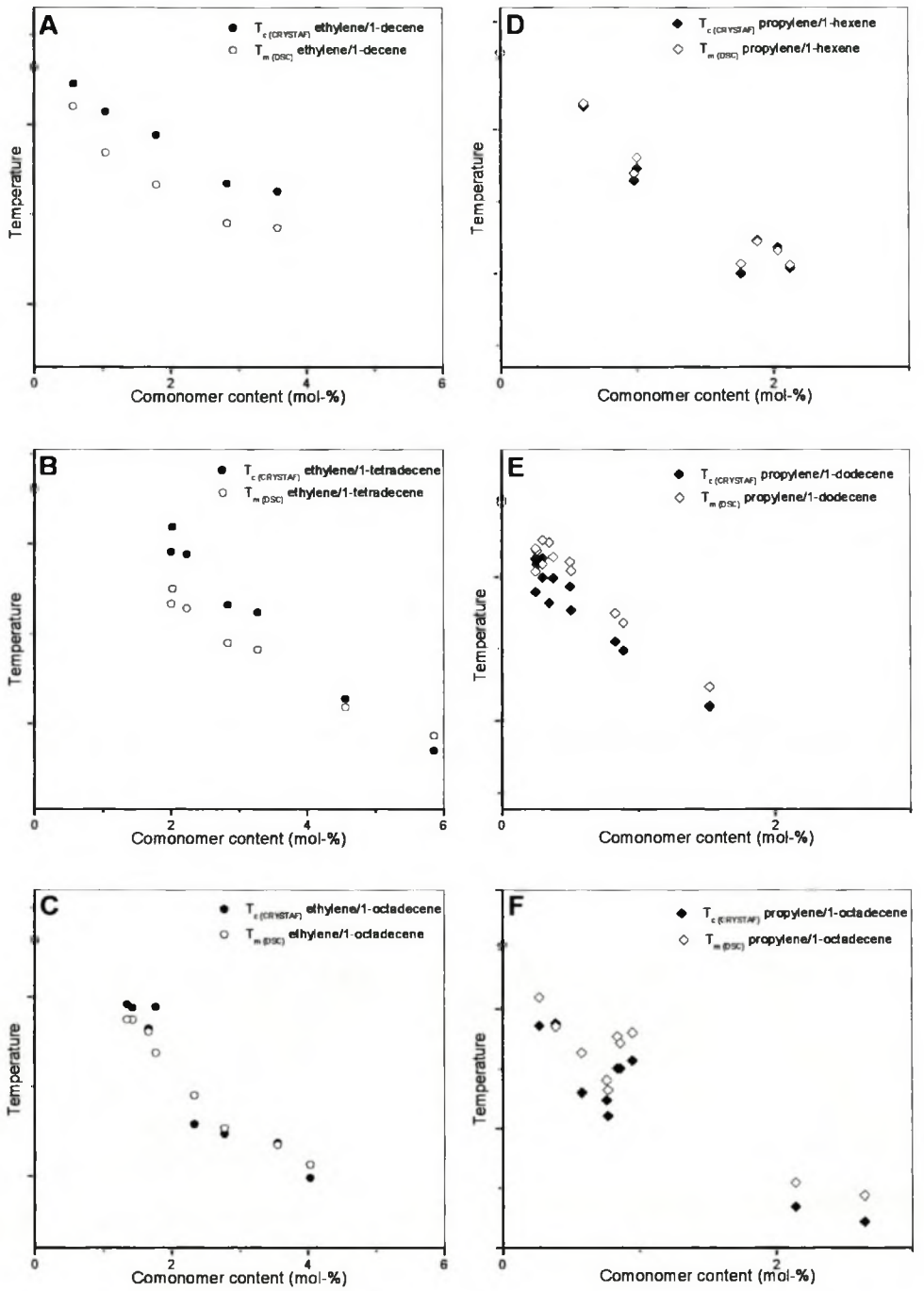

Figure 6.7. Melting and crystallisation temperatures determined by DSC and CRYSTAF, respectively, overlaid in such a way that the temperature difference for the s-PP or PE reference samples are cancelled out.
Copolymers: ethylene/1-decene (A), ethylene/1-tetradecene (B), ethylene/1-octadecene (C), propylene/1-hexene (D), propylene/1-dodecene (E) and propylene/1-octadecene (F).

A possible explanation for this is given in Figure 6.7, where the data for both the DSC and the CRYSTAF for each of the s-PP and PE copolymers series are overlaid with a

vertical data shift to compensate for the supercooling effect. The difference between the DSC and the CRYSTAF results decreased as the chain length of comonomer inserted increases for the PE series (Figure 6.7 (A-C)). The PE series contradicts the results of the s-PP series where the shorter pendant chain length shows very little difference compared to the longer comonomer chains. In the PE series, the CRYSTAF data points lie above the DSC data points and for the s-PP the CRYSTAF data points lie below the DSC data points.

The reason for this observation may be due to the difference in entropy resulting from the copolymers moving from the solution to a solute. The randomness entropic effect in the melt is smaller than that of the same molecule in solution. Polymers with similar MM and comonomer content, but with different comonomers, will have different dissolution entropy levels and therefore ΔS in solution making the copolymer soluble to a larger or smaller extent, resulting in different $T_{c\,(CRYSTAF)}$. For a copolymer to crystallise from solution the system temperature in CRYSTAF must be lower then a certain minimum crystallisation temperature. Therefore copolymers with higher dissolution entropy (easier dissolved) will need lower system temperatures before the copolymer crystallises from solution [14]. 1-Decene or 1-hexene as comonomers will have lower dissolution entropies than the same amount of 1-octadecene in propylene and ethylene copolymers. This difference yields a steeper negative slope (bigger differences in the data of DSC and CRYSTAF) for copolymers of 1-octadecene than with 1-hexene or 1-decene. In the s-PP the added effect of the methyl groups of the propylene will further increase solubility of the copolymers, leading to the CRYSTAF data points appearing below the DSC data points. DSC results can be used as a standard indicator to relate to the CRYSTAF results as no solvent is used, ensuring minimal entropy effects. The assumption was also made that the enthalpy effect is smaller than the entropy effect in this system.

A more exhaustive study should be done regarding the thermodynamic process taking place in the CRYSTAF compared to that in the DSC. This was however not a goal of this study and therefore only a plausible explanation regarding the change in dissolution entropy of different copolymers is given. Kinetics may also play a role during crystallisation in solution.

6.3.4 CRYSTAF

Gradient copolymer formation

An explanation for the broadening of the $T_{c\,(CRYSTAF)}$ in CRYSTAF data can be given by the consideration of the longest ethylene sequence (LES). The LES is the number of carbon atoms between two comonomer units. The higher the number of carbon atoms, the thicker the crystalline lamella structure and thus an increase in the melting or crystallisation temperature of the samples is observed.

In a polymerisation system with constant feed stream conditions no changes in comonomer concentration will take place during the copolymerisation. This will lead to homogeneous comonomer incorporation. The monomer to comonomer ratio determines the critical LES, where the ethylene sequence length starts to influence the T_c. Above this critical point, the sequence length will have no influence on the T_c. In the thermodynamic model of Flory, the degree of crystallinity at a given temperature is fully determined by the crystallisable ethylene sequence length distribution [15]. It can thus be said that sequences that do not have the minimum length required for crystallisation at a given temperature do not crystallise even though they can do so at

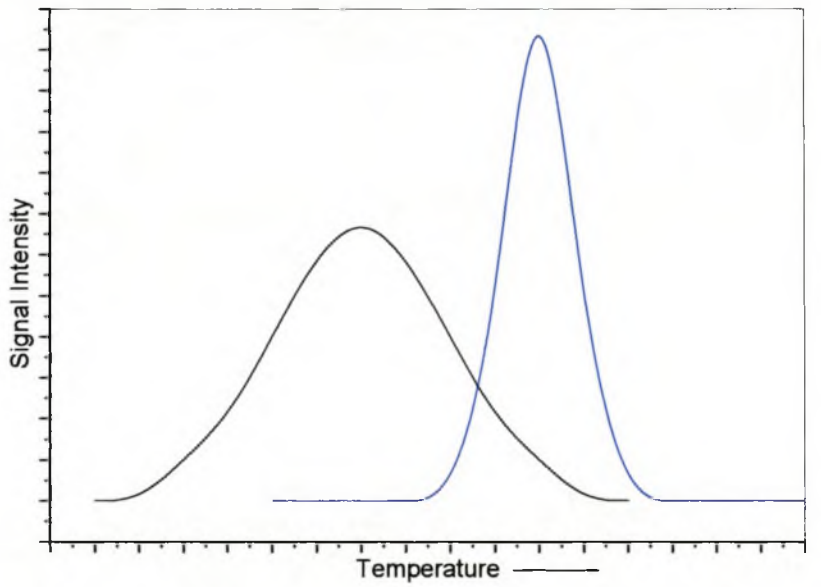

Figure 6.8. Hypothetical illustration of a broad and narrow chemical composition distribution, as observed from CRYSTAF analysis.

lower temperatures. All sequences of similar lengths are supposed to merge into crystallites of related thickness.

At high monomer to comonomer ratios, the critical LES is surpassed and a narrow distribution will be observed in a CRYSTAF run (Figure 6.8). In the case of low ratios the LES will have an influence on the crystallisation process, giving a broad distribution in CRYSTAF.

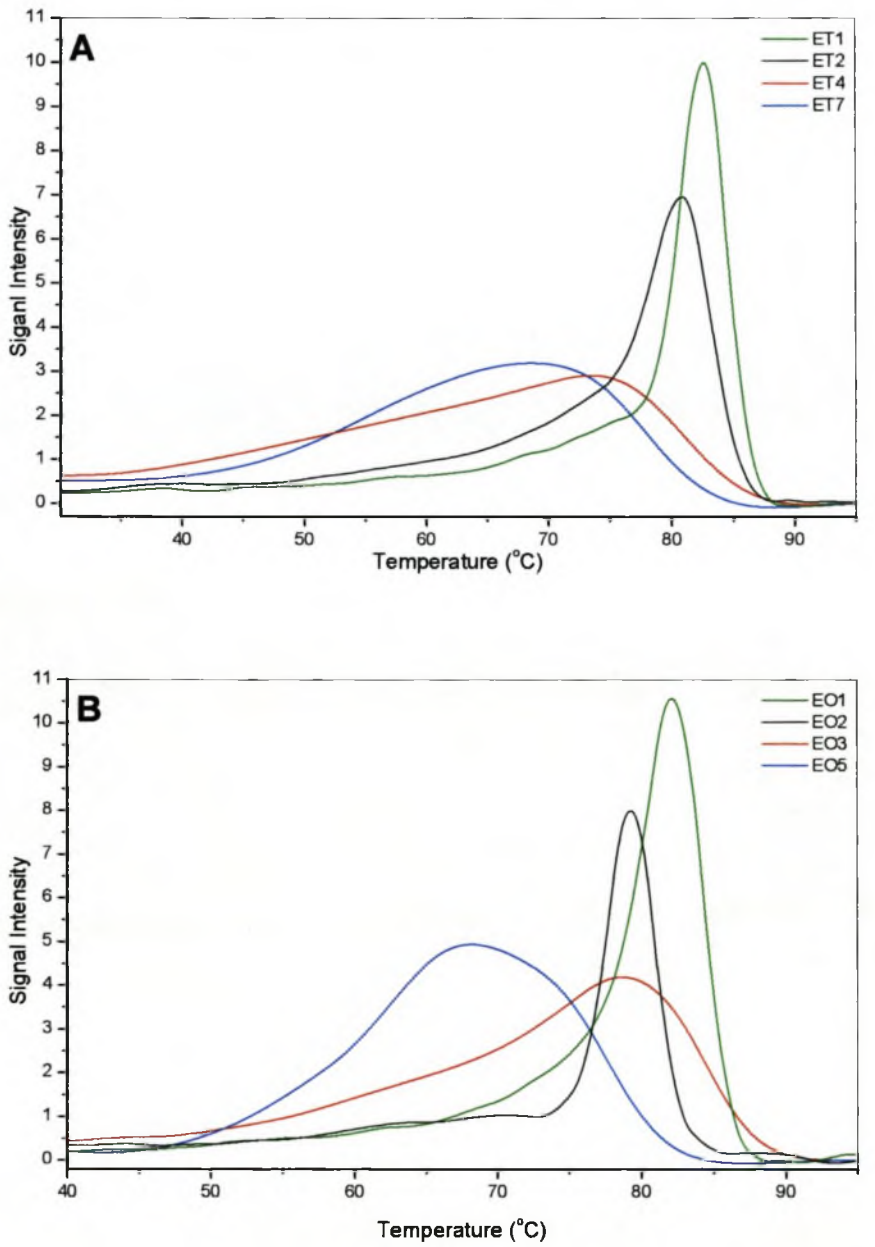

Figure 6.9. CRYSTAF curves of ethylene/1-tetradecene (A) and ethylene/1-octadecene (B) copolymers synthesised with **1**, containing different amounts of comonomer (see Table 6.1).

Soares *et al.* have shown that it is possible to obtain information on the different activities and compositional products in a Ti^{3+} catalyst system [16] and on different catalyst support treatments of metallocene catalyst respectively [17, 18] via CRYSTAF analysis. Figure 6.9 shows that the homogeneous catalyst **1** produces a heterogeneous copolymer. As mentioned above, an increase in the comonomer content results in a decrease in $T_{c\,(CRYSTAF)}$. Clearly seen here is the broadening of the peak with higher comonomer content. Upon closer investigation, the tailing can already be observed in the samples with lower comonomer incorporation content. ET1 and EO1 only show tailing towards the low temperature side. In the case of EO2, this tail changes to a small shoulder and for ET4 and EO3 the shoulder has become a pronounced part of a broad peak.

The formation of the peaks ET7 and EO5 may be associated with gradient copolymerisation, due to the reaction conditions where no monomer is added after the initiation of the reaction. A considerable difference in the reactivity ratios for the two monomers is observed for the copolymerisation with **1** ($r_1 = 2.57$ and $r_2 = 0.39$) [19]. This difference in reaction ratios implies that, in a closed system, the ethylene monomer will be consumed more rapidly. This will lead to an increase in the relative concentration of the comonomer in the reactor. A copolymer with gradient composition is thus produced where an increase in comonomer is observed in the polymer chain during the reaction. Low comonomer content copolymers have thus only a few regions in the polymer chain that have sufficiently high amounts of comonomer (LES under the critical value) to influence the $T_{c\,(CRYSTAF)}$ resolution in tailing (ET 1 and EO1 Figure 6.9). Higher comonomer concentrations will allow the shift in $T_{c\,(CRYSTAF)}$ to become more pronounced (ET2, ET4, EO2 and EO3). A striking resemblance can be observed in the curves of the 1-tetradecene and the 1-octadecene series. Clustering of the comonomer cannot be excluded in these copolymers, but no concrete proof can be shown that this does take place, even with NMR spectroscopy.

Comparison of CRYSTAF and DSC analysis

A monomodal chemical composition distribution (CCD) would be expected for the copolymers synthesised with **1**. This homogenous morphology results from the uniform incorporation of the comonomers.

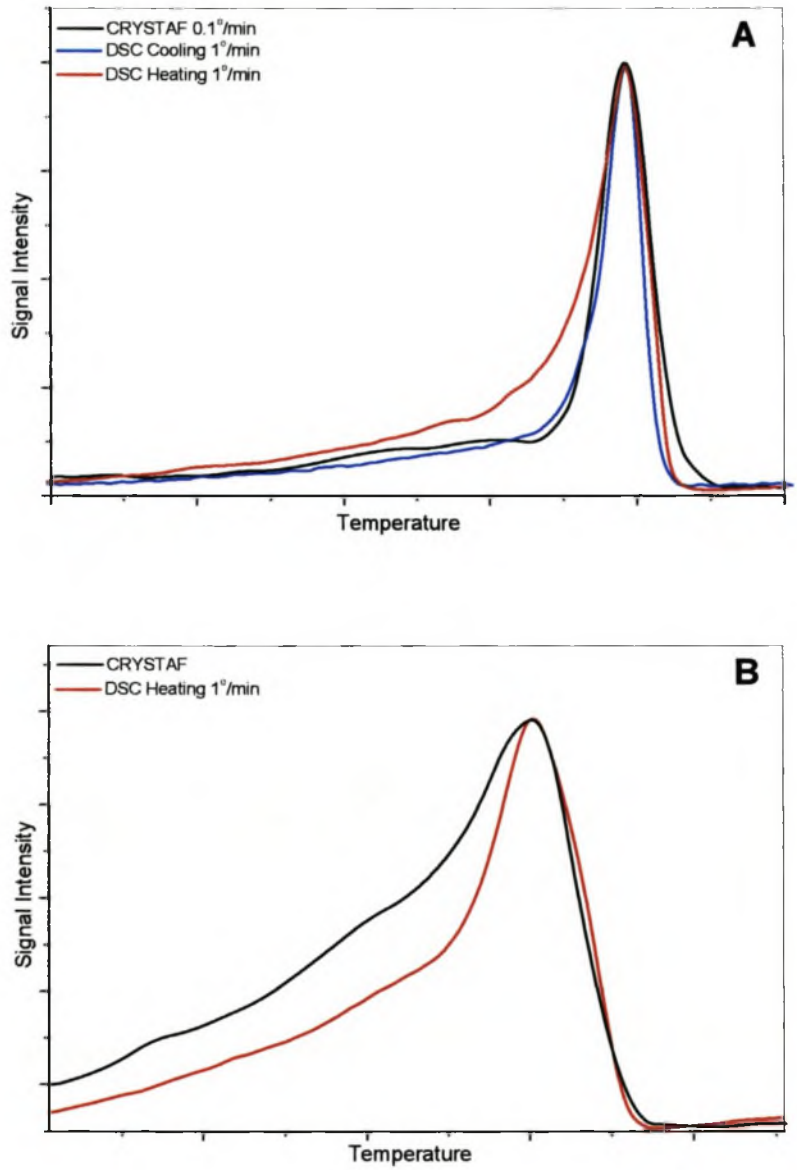

Figure 6.10. Comparison of the curves of A = EO2 (1.50 mol-%) and B = EO6 (3.55 mol-%), as obtained by CRYSTAF and DSC analysis.

In order to compare the results obtained from CRYSTAF and DSC analysis, the DSC curves can be shifted along their temperature axis to be superimposed with the peak maximum of the CRYSTAF data. The peak heights were normalised, hence no

numbers are shown. A similar approach was reported by Gabriel and Lilge [20], who compared copolymers synthesised by Ziegler-Natta catalyst, with reference to DSC, TREF and CRYSTAF as analytical tools.

Figure 6.10 clearly shows that the different experimental methods agree well in a qualitative manner. The curves have similar shapes and give good fits regarding the short-chain branching distribution of copolymers with different 1-octadecene contents. Also shown in Figure 6.10 is that the DSC cooling curve gives a good fit for the copolymer with low comonomer content. The slow cooling- and heating rates of 1 °C/min were used to give the system sufficient time to melt and crystallise, as these parameters can be influenced by the cooling- and heating rates.

The drawback of DSC is that the distribution curve cannot be directly converted into a weight percentage of the comonomer content distribution as it can with CRYSTAF. This is explained by the fact that the heat flow depends on the amount of sample melting at a certain temperature, as well as the temperature dependent heat capacity [21].

6.3.5 FTIR spectroscopy

As with NMR spectroscopy, attenuated total refractance (ATR) FTIR spectroscopy can also be used for the determination of the comonomer content. Although this method of comonomer concentration detection was not used here, FTIR spectroscopy could give valuable information on a sample's compositional distribution when combined with a suitable separation technique. Figure 6.11 shows the characteristic peaks at 2915 cm^{-1} (1) an asymmetric CH_2 stretching, 2847 cm^{-1} (2) a symmetric CH_2 stretching, 1471 cm^{-1} (3) a CH_2 scissoring, 1462 cm^{-1} (4) an asymmetric CH_3 bending at 1377 cm^{-1} (5) a symmetric CH_3 bending, as well as the split peaks at 731 cm^{-1} (6) a CH_2 rocking and 721 cm^{-1} (7) a CH_2 rocking in the crystalline and amorphous part, respectively. These data can be used for further structural differentiation [22]. By using the intensity of peak (5) and comparing this to that of peaks (3) and (4) the comonomer content of the sample or a fraction thereof can be determined. These are

also the peaks that were used in the determination of the comonomer content by coupling the FTIR spectrometer to the high temperature GPC with the aid of LC-Transform.

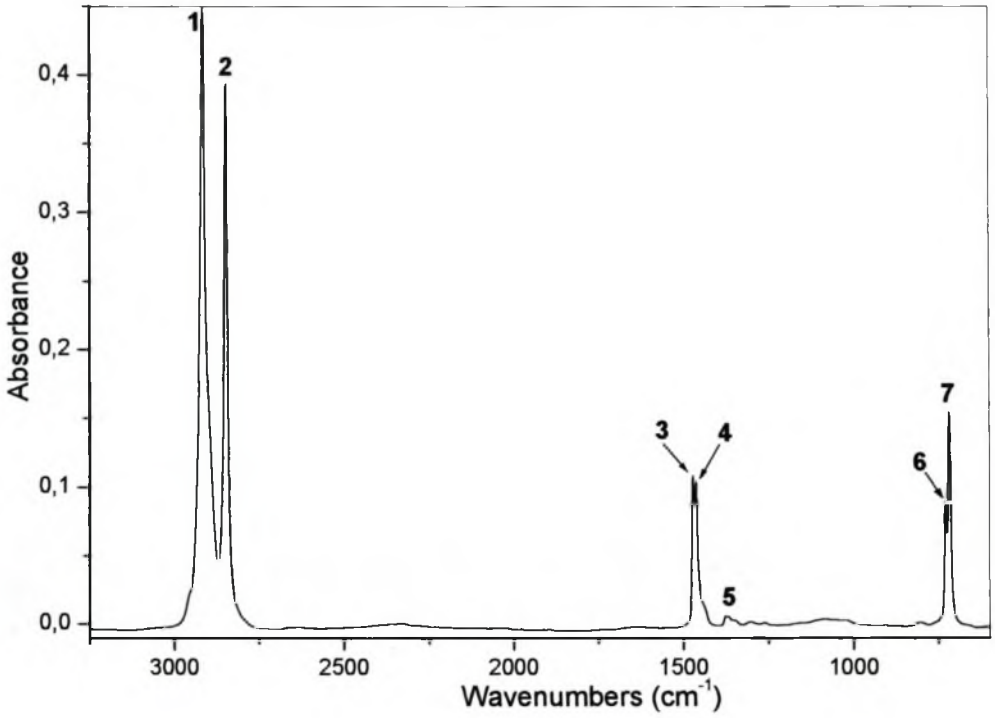

Figure 6.11. The ATR-FTIR spectrum of ET4, with peaks of interest allocated numbers (1) 2915 cm^{-1}, (2) 2847 cm^{-1}, (3) 1471 cm^{-1}, (4) 1462 cm^{-1}, (5) 1377 cm^{-1}, (6) 731 cm^{-1} and (7) 721 cm^{-1}. For a more detailed description see text.

6.3.6 GPC coupled to FTIR spectroscopy via LC-Transform

GPC analysis on its own cannot give information on the chemical composition of a sample, but in combination with a second technique like FTIR spectroscopy (through the use of a LC-Transform interface), predictions on the structural composition can be made perpendicular to the MM axis. The LC-Transform (FTIR interface) was coupled to the GPC for the analysis of the polyethylene copolymers. The areas under the peaks at 1410-1490 cm^{-1} and 1340-1390 cm^{-1} were evaluated, regarding the

composition in the form of chemigrams. As mentioned above, the two peaks in the IR spectrum (Figure 6.11) represent the total carbon (CH_2+ CH_3) and methyl carbon content in the samples.

Figure 6.12 shows chromatograms as seen in normal high temperature GPC, where the black line represents the Gram-Schmidt. The Gram-Schmidt is the sum of the intensities of the individual bands in an IR spectrum, taken at multiple points during the scanning of the germanium disc. The Gram-Schmidt shows thus the MMD of the samples. The red line shows the carbon atom content (CH_n) in both the backbone, as well as the side branches in the polyethylene copolymer. This red line should match the Gram-Schmidt since the samples only contain carbon atoms. The blue line, on the other hand, represents the CH_3 content resulting from main chain and branched chain ends. This line can however change in intensity within a MMD curve, resulting from non-homogeneous incorporation of the comonomer.

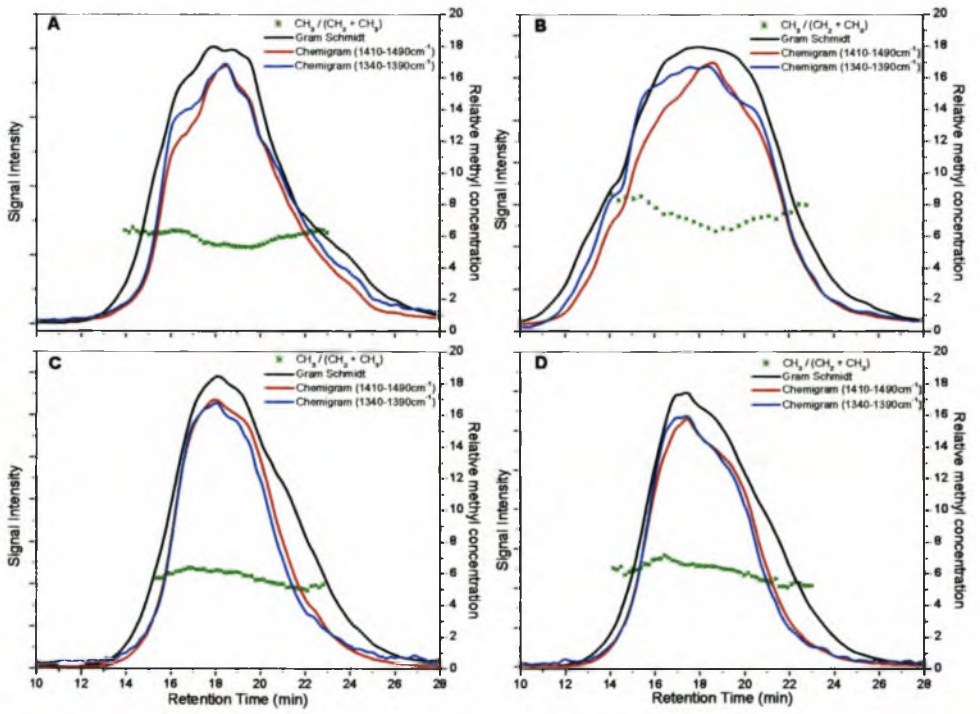

Figure 6.12. Chromatograms produced by the coupling of FTIR to GPC via LC-Transform where peaks at 1462-1471 cm^{-1} and 1377 cm^{-1} were used to plot the area chemigrams and this data was used to determine the percentage methyl groups in the samples.
(A = EO1 (1.43 mol-%), B = EO2 (1.50 mol-%), C = EO3 (1.66 mol-%) and D = EO5 (2.33 mol-%))

The percentage methyl groups shown as data points in Figure 6.12 prove that there is no significant chemical heterogeneity along the MM axis as would be expected with Ziegler-Natta copolymers. A small decline in the methyl content can be seen to the end of (B), (C) and (D). These small changes would not contribute much too the gradient composition expected from peak tailing in CRYSTAF. The small variations in the percentage methyl groups could also be due to limitations of the detection method. Reasoning for this statement can be seen in the small size of the CH_3 peak (5) in the IR spectrum (Figure 6.11). All chains have thus more or less the same amount of comonomer incorporated in relationship to their chain length. The differences in the CRYSTAF (Figure 6.9) must thus result from intramolecular changes.

Summary

The focus of this chapter was on the analysis of ethylene/ higher α-olefins (1-decene, 1-tertadecene and 1-octadecene) prepared with **1**. A linear correlation was obtained between the amount of comonomer added under feed conditions and the amount incorporated into the polymer.

The DSC analysis showed a decrease in the $T_{m\,(DSC)}$ with an increase in comonomer addition. At higher concentrations of comonomer a secondary crystallisation could be seen. This secondary crystallisation forms after the primary spherulite growth. On cooling, the $T_{c\,(DSC)}$ also decreased with comonomer addition. Similar to the polypropylene copolymers the data of DSC and CRYSTAF gave parallel lines on a plot of temperature versus comonomer content. Differences in the overlaid plots for the DSC and CRYSTAF data obtained from both polyethylene as well as polypropylene copolymers could be related to the entropy of the copolymers in solution. The entropy of a copolymer is higher if the side branches are longer or if there are smaller side branches, as is the case of polypropylene compared to polyethylene. By superimposing the diagrams obtained by DSC and CRYSTAF it could be shown that these two analytical techniques give similar curves.

CRYSTAF results showed that copolymer samples are not homogeneous mixtures. Samples with low comonomer content gave a well-defined peak containing a tailing. As the comonomer content increased the peak base got broader and the peak height became smaller. When analysing the samples regarding their comonomer content along the MM axis it could be seen that there was no change in the comonomer distribution in the MMD axis. It was concluded that there is an equal spread of LES for all hydrodynamic volumes on the MM axis. But these spreads in LES are so large that they result in tailing and broadening of the CCD in CRYSTAF.

6.4 References

1. Canich J A M, (Exxon). Eur. Pat. Appl. 0 420 436 A1, 1991.
2. Stevens J C, Timmers F J, Wilson D R, Schmidt G F, Nickias P N, Rosen R K, Knight G W, Lai S Y, (Dow). Eur. Pat. Appl. 0 416 815 A2, 1991.
3. Canich J A M, (Exxon). US Patent 5,096,867, 1992.
4. Lai S Y, Wilson J R, Knight G W, Stevens J C, (Dow). PCT Int. Appl. 93/08221, 1993.
5. Lai S Y, Wilson J R, Knight G W, Stevens J C, (Dow). USA Patent 5,278,272, 1994.
6. Stevens J C, Stud. Surf. Sci. Catal., 1996, **101**, 11.
7. Brant P, Canich J A M, (Exxon). PCT Int. Appl. WO 93/12151, 1993.
8. Brintzinger H H, Fischer D, Mülhaupt R, Rieger B, Waymouth R M, Angew. Chem., Int. Ed. Engl., 1995, **34**, 1134.
9. Randall J C, Long-Chain Branching in Polyethylenes in Polymer Characterization by ESR and NMR, 1980, **6**, 93.
10. Grant D M, Paul E G, J. Am. Chem. Soc., 1964, **86**, 2984.
11. Joubert D, *Ph D thesis (confidential)*, 2002, University of Stellenbosch, Stellenbosch.
12. Goderis B, Reynaers H, Koch M H J, Macromolecules, 2002, in print.
13. Alamo R G, Mandelkern L, Thermochim. Acta., 1994, **238**, 155.
14. Morawetz H, *Macromolecules in solution*. Vol. Second print, 1966, New York, London, Syndney, John Wiley & Sons, 33.
15. Flory P J, Trans. Faraday Soc., 1955, **51**, 848.
16. Chu K J, Soares J B P, Penlidis A, Ihm S K, Macromol. Chem. Phys., 1999, **200**, 1298.
17. Kim D J, Soares J B P, Macromol. Rapid. Commun., 1999, **20**, 347.
18. Chu K J, Shan C L P, Soares J B P, Penlidis A, Macromol. Chem. Phys., 1999, **200**, 2372.
19. Chien J C W, He D, J. Polym. Sci. Part A:, 1991, **29**, 1585.
20. Gabriel C, Lilge D, Polymer, 2001, **42**, 297.

21. Mathot V B F, *Calorimetry and thermal analysis of polymers*. Chapter 4, Ed. Mathot V B F, 1994, New York, Vienna, Munich, Hanser/Gardner Publications, 91.

22. Chanunpanich N, Ulman A, Strzhemechny Y M, Schwarz S A, Janke A, Braun H G, Kratzmüller T, Langmuir, 1999, **15**, 2089.

CHAPTER 7

ETHYLENE AND METHYL METHACRYLATE BLOCK COPOLYMERS SYNTHESISED BY $Me_2C(Cp)(Ind)ZrMe_2/B(C_6F_5)_3$ THE CATALYST SYSTEM

7.1 Abstract

The first block copolymers of ethylene and methyl methacrylate (MMA) were successfully synthesised with zirconocene-based catalysts, through a collaboration with scientists at Aachen University. The active catalyst species is generated *in situ* from the reaction between $Me_2C(Cp)(Ind)ZrMe_2$ and $B(C_6F_5)_3$ in toluene. The block structure is achieved by sequential addition of ethylene, followed by MMA after a predetermined time interval. ^{13}C- and ^{1}H- NMR spectroscopy revealed the isotactic stereoregularity of the MMA block in the system. Molar mass distributions (MMD) from GPC and melting temperature diagrams from DSC gave the first indications of an inhomogeneous system. Interpretation of data obtained from CRYSTAF analysis was the key in understanding the suggestions of a block copolymer given by chromatograms obtained from the coupling of GPC to FTIR spectroscopy. The conclusive proof that block copolymers were indeed synthesised was given by data obtained from further CRYSTAF analysis that allowed the detection of MMA monomer units in the polymer chain. This was only possible after modification of the available instrument with a special carbonyl infrared filter. A new method, high temperature gradient HPLC, was developed for the separation of samples into different chemical composition fractions. FTIR spectroscopy was also used as a

detector in high temperature gradient HPLC separation, owing to its selective detection of individual compounds.

7.2 Introduction

Success in the polymerisation of MMA by transition metal catalysts was achieved in the early 1990's, as reported by Collins *et al.* [1]. Many reports on the synthesis of isotactic and syndiotactic PMMA followed shortly thereafter, as explained in Chapter 2. The following question to be answered was what polymerisation conditions would be required for the synthesis of ethylene/MMA copolymers. This breakthrough in the copolymerisation of ethylene and MMA was achieved by the group of Höcker *et al.* [2].

The research covered in this chapter was done in collaboration with the research group under the guidance of Höcker at the Institut für Technische Chemie und Makromolekulare Chemie der RWTH Aachen, Germany. Poly(ethylene-co-MMA) samples (provided for this study) were synthesised with precatalyst $Me_2C(Cp)(Ind)ZrMe_2$ **2** and $B(C_6F_5)_3$ as cocatalyst (Scheme 7.1). The chain propagation mechanism for **2** was developed by Höcker *et al.* [3] and is illustrated in Scheme 7.1.

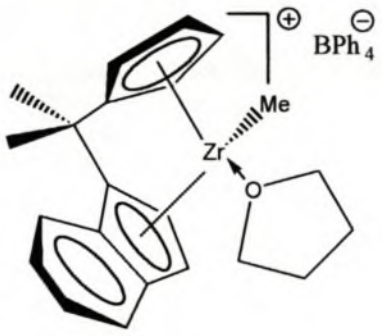

1

Figure 7.1. The active catalysts species for the synthesis of isotactic PMMA, discussed in Chapter 2, as reported by Höcker *et al.* [3].

Through collaboration with colleagues at this Institute (S. Balk and H. Keul, members of the group of Höcker), it was established that the reaction mechanisms for $Me_2C(Cp)(Ind)ZrMeTHF$ **1** (Figure 7.1) and **2** are the same. Figure 7.1 is the precatalyst for which the original chain propagation mechanism was proposed from as seen in Scheme 7.1. The reaction mechanism in Scheme 7.1 is a combined model of Yasuda's [4, 5] eight membered ring structure and Collins's [6, 7] two catalyst propagation mechanism.

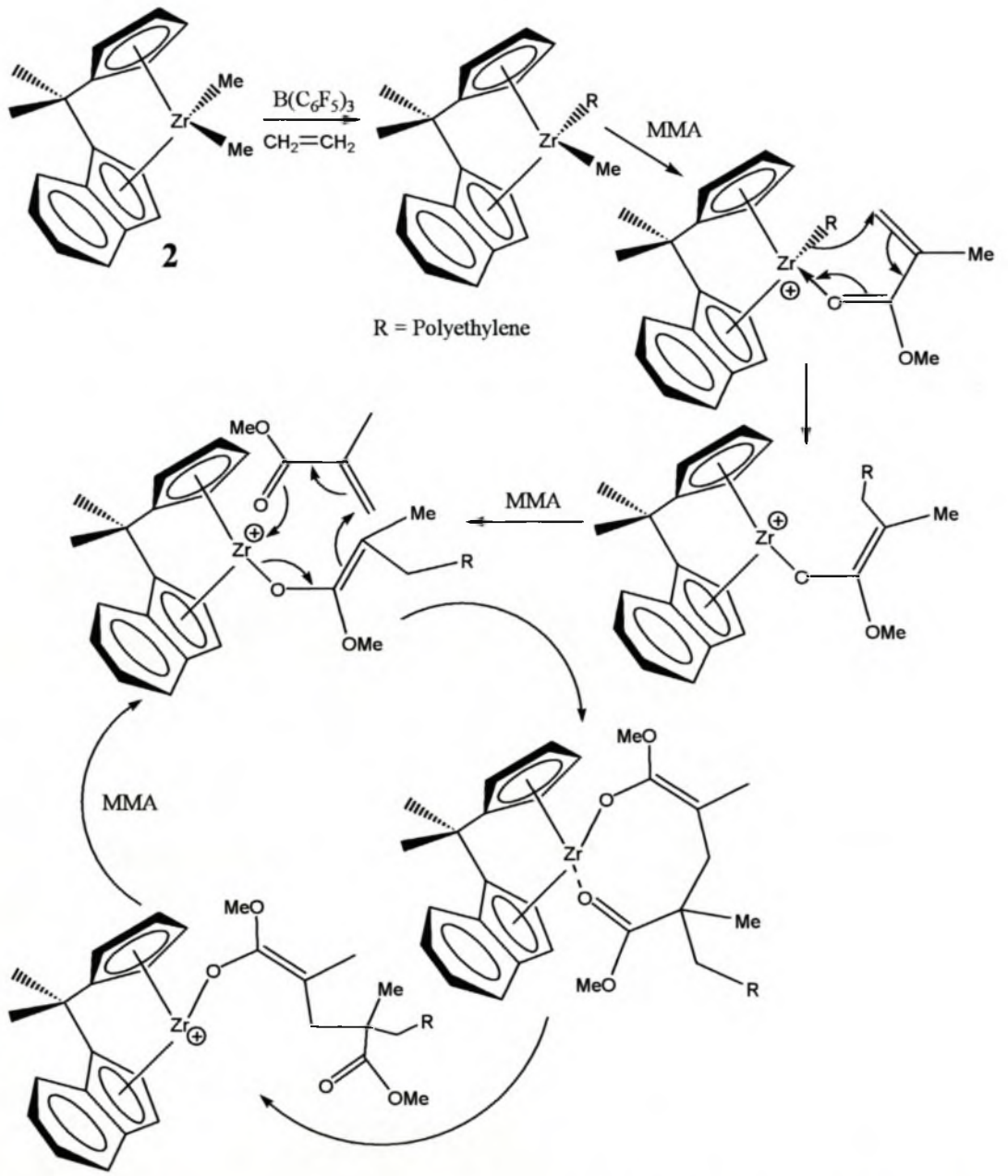

Scheme 7.1. Reaction scheme as proposed by Höcker *et al.* [3], for the copolymerisation of ethylene and MMA with **2**.

Catalyst **2** has a C_1-symmetry with an enantiomorphic site controlled isospecific polymerisation step. Consequently, after each polymerisation step a fast active-site epimerisation reaction must occur, with a strong preference for the chain oriented to one side of the complex.

This chapter will concentrate on the analysis of ethylene and methyl methacrylate copolymers synthesised with **2**, in Aachen, Germany. GPC, DSC, DMA and NMR spectroscopy were used as basic analytical techniques. These techniques only give information about the general microstructure and compositional trends in the samples. For the identification of the block structure more unique and innovative techniques were used and developed. These techniques included GPC-FTIR spectroscopy coupling, CRYSTAF (using a 5.82 micron wavelength filter) and the newly developed high temperature gradient HPLC and high temperature liquid chromatography under critical conditions.

7.3 Theory of chromatographic separation

7.3.1 Gradient HPLC

General

Separation of any two compounds showing up as bands in a chromatogram can be varied substantially by changing the experimental conditions. The resolution R_s can be expressed in terms of the parameters k, α and N [8]. These three parameters are directly related to the experimental conditions:

$$R_s = 1/4(\alpha - 1) \quad N^{1/2} \quad \frac{k}{1+k} \qquad (7.1)$$

Here the parameters relate to the selectivity for separation (α), column efficiency (N) and the retention (k). k is the average retention factor for the two bands (also referred to as the capacity factor, k'), N is the plate number of the column and α is the

separation factor, $\alpha = k_2/k_1$. In the calculation of the separation factor, k_1 and k_2 are the values of k for neighbouring bands. Equation 7.1 simplifies the method development through the use of the three parameters. For convenience, the three parameters (α, N and k) are regarded as independent of one another, meaning that changes can be made to each variable without influencing the other two. This is, however, only a simplified manipulation of the data, especially when looking at k and α.

The retention factor k is given as a function of t_R (the peak retention time) and t_0 (the column dead time), as given in Equation 7.2. The column dead time is related to the column dead volume (volume of the mobile phase inside the column) and the flow rate.

$$k = \frac{t_R - t_0}{t_0} \qquad \textbf{(7.2)}$$

By making k bigger, the resolution usually improves and when α is increased the two bands move apart, thus giving a better resolution (Equation 7.1). When the column efficiency is increased, the bands get narrower and are better separated, although their relative positions do not change.

Factors contributing to parameters k and α are variables that affect the retention or the equilibrium distribution of the samples between the mobile- and stationary phases:

- Composition of the mobile phase
- Composition of the stationary phase
- Temperature

These changes will however have a lesser effect on N. The column plate number N is primarily dependent on column quality and can be changed by varying the column conditions:

- Flow rate
- Column length
- Particle size

Changes in these conditions will not affect k and α, unless the mobile- and stationary phases are changed.

Gradient steepness

The gradient steepness can be defined as the rate at which the gradient is applied, i.e. the change in % of solvent A as a function of time.

Gradient steepness is represented by ϕ' where

$$\phi' = (change\ in\ volume\ fraction\ A)/time \qquad \textbf{(7.3)}$$

Thus for 0 – 100% A,

$$\phi' = 1/t_G \ (\text{min}^{-1}) \qquad \textbf{(7.4)}$$

where t_G = time from beginning to the end of the gradient.

Another way to represent gradient steepness is

$$\phi'' = (change\ in\ volume\ fraction)/(t/t_0) \qquad \textbf{(7.5)}$$

$$= \phi' t_0 \qquad \textbf{(7.6)}$$

$$= t_0/t_G \qquad \textbf{(7.7)}$$

where t_0 is the column dead time.

Gradient separation (Linear Solvent Strength (LSS) Model)

The fundamental equation of gradient elution is based on a stepwise gradient due to its easy mathematical manipulation. However, if an infinite number of steps are to be taken, then a continuous gradient can be modeled using this equation. The equation for gradient elution is:

$$\int_0^{V_R'} \frac{1}{V_m} \frac{dV}{k_a} = 1 \qquad \textbf{(7.8)}$$

The equation is based on the integration of solute retention volumes from 0 to V_R' where V_R' is the solute retention volume corrected for V_m (column dead volume). V_R' can be expressed as the cumulative volume of mobile phase that has passed through the column and k_a is the instantaneous value of k for the solute band at any time during the gradient. Due to each volume element dV of the mobile phase passing through the band center, the band will undergo band migration $dx = dV/V_m k_a$. The sum of all the band migrations must be equal to 1 ($\sum dx = 1$) if the total volume of mobile phase passing through the band center equals the corrected retention volume.

Therefore, if k is known as a function of V_t or t where $t = V_t/F_{rate}$ (F_{rate} = flow rate), then Equation 7.8 can be solved for the solute retention volume or solute retention time $t_R = V_R/F_{rate}$.

Before going further, it is important to note that a linear gradient for a gradient elution system can be represented by

$$\phi = \phi_0 + \left(\frac{\Delta\phi}{t_G}\right)t \qquad \textbf{(7.9)}$$

where ϕ_0 is the value of ϕ at $t = 0$, $\Delta\phi$ is the change in ϕ during the gradient run and t_G is the duration of the gradient.

The capacity factor k_i for different compounds can be expressed as

$$\log k_i = \log k_0 - S\phi \qquad \textbf{(7.10)}$$

where k_i is the capacity factor at a given time after a gradient separation begins, k_0 is the capacity factor at the beginning of the gradient, ϕ is the volume fraction of solvent and S is a constant for a gradient elution system. The above equation holds for reverse-phase (RP) gradient elution systems.

For normal phase (NP) gradient elution systems, Equation 7.10 will have the form

$$log\, k = c - n\, log\, X_B \qquad \textbf{(7.11)}$$

where c and n are constants and only the mole fraction X_B of strong solvent (e.g. solvent B) varies. Note that the capacity factor can change linearly with time due to the linear increase of solvent strength. By utilizing all of the above equations it is therefore possible to do a mathematical presentation of gradient elution through the LSS model [9, 10].

This model makes it possible to derive equations for retention, bandwidth and resolution of a gradient elution system. Although equations will be derived for a RP system, a NP system LSS model can also be derived by using Equation 7.11 instead of Equation 7.10.

7.3.2 Liquid chromatography under critical conditions (LCCC)

The distribution coefficient (K_d) for a chromatographic process is associated with the change in free energy (ΔG). ΔG is dependent on the size of the polymer, the pore size of the stationary phase, the interaction potential of the monomer unit and the surface of the stationary phase. The critical point (CP) of a polymer sample can be determined either by changing the solvent mixture at a constant temperature or by changing the temperature at a constant solvent mixture [11-14]. The CP is the point where the polymer elutes from a column, independent of its MM. There is a decrease in entropy of the polymer molecule when it goes from an unbounded space, like the mobile phase, into a limited volume, like that of the pores. This is compensated by a change in energy, resulting from the interaction of the polymer molecule with the

surface of the stationary phase, the so-called adsorption energy or enthalpy. These two forces are present at the CP, but they are in equilibrium ($\Delta G = 0$). The fact that ΔG is zero at the CP, irrespective of the size of the polymer, explains why the retention time is only dependent on the heterogeneity of the polymer. One can separate graft- and block copolymers according to one of the building blocks [15, 16].

$$\Delta G_{AB} = \Sigma (n_A \Delta G_A + n_B \Delta G_B) \qquad \Rightarrow \Delta G_A = 0 \qquad \textbf{(7.12)}$$

$$\Delta G_{AB} = \Sigma n_B \Delta G_B \qquad \textbf{(7.13)}$$

$$K_d^{AB} = K_d^{B} \qquad \textbf{(7.14)}$$

At the CP, the distribution coefficient of the polymer sample will only depend on the distribution coefficient of polymer B ($K_d^{AB} = K_d^{B}$) at critical conditions of A. If polymer B is at the critical point, then it means that the distribution coefficient is only governed by polymer A. By using this approach at the CP, one can analyse the copolymer according to one of the two monomer units [17]. By choosing the right solvent mixture and stationary phase, the so called visible polymer can be separated in either size exclusion mode or adsorption mode.

7.4 Results and Discussion

Here we will prove, with the aid of different analytical techniques, the presence of PE and PMMA homopolymers as well as block copolymers synthesised with **2** as catalyst precursor. The combination of ethylene and a polar monomer (MMA) in one polymer chain has led to new challenges in polymer analysis. These challenges proved to be difficult, not only due to the insolubility of the samples at room temperature and subsequent limited separation possibilities, but the detection and identification after separation also required some unique analytical tools. PE is a semi-crystalline polymer that is only soluble at high temperatures in a limited number of solvents. The

solubility problem of the PE part in all the samples led to the exclusive use of high temperature analytical techniques. A further challenge resulting from the use of high temperature analytical techniques was the simultaneous detection of the ethylene and the methyl methacrylate. Detectors must be capable of detecting the difference between the two types of monomers, while also withstanding the high temperatures of the solvents. The only detector that can be used for this analytical work is the FTIR coupled to GPC via LC-Transform, which allows the coupling between a chromatographic separation technique and the FTIR detection technique.

7.4.1 ^{13}C- and ^{1}H-NMR spectroscopy

NMR-spectroscopy was used for the determination of the microstructure of the copolymer samples. Emphasis was placed on the determination of the tacticity in the PMMA part, the comonomer content of the samples and the existence of branched units in the PE part.

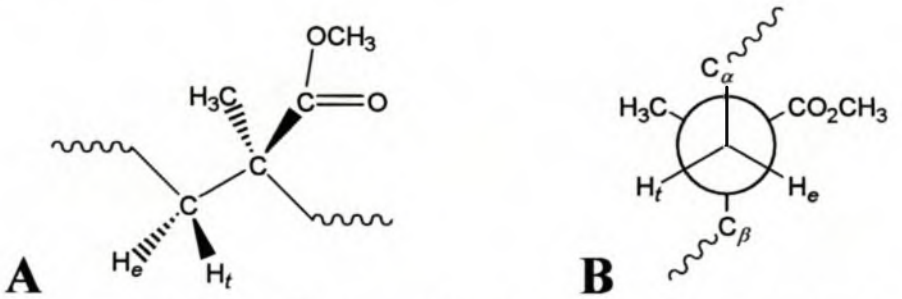

Figure 7.2. An illustration of A) the three dimensional projection and B) Newman-projection of a MMA unit in an isotactic PMMA homopolymer. (The methylene protons H_e and H_t are not in the same chemical environment.)

In isotactic PMMA a very large chemical shift separation is observed between the non-equivalent methylene protons labeled *e* and *t* (Figure 7.2(A)). The *e* and *t* notations for the methylene protons refer to *erythro* and *threo* configurations. These are *syn* and *anti*, respectively, to the ester group in the *trans-trans* conformation. [18, 19] This observation in molecular symmetry, or rather the lack of symmetry, depends upon the fact that similar nuclei surround a geometrically non-equivalent site. In general, these will be magnetically non-equivalent (Figure 7.2(B)). For this reason,

the protons will exhibit different chemical shifts and different coupling to neighbouring nuclei [18].

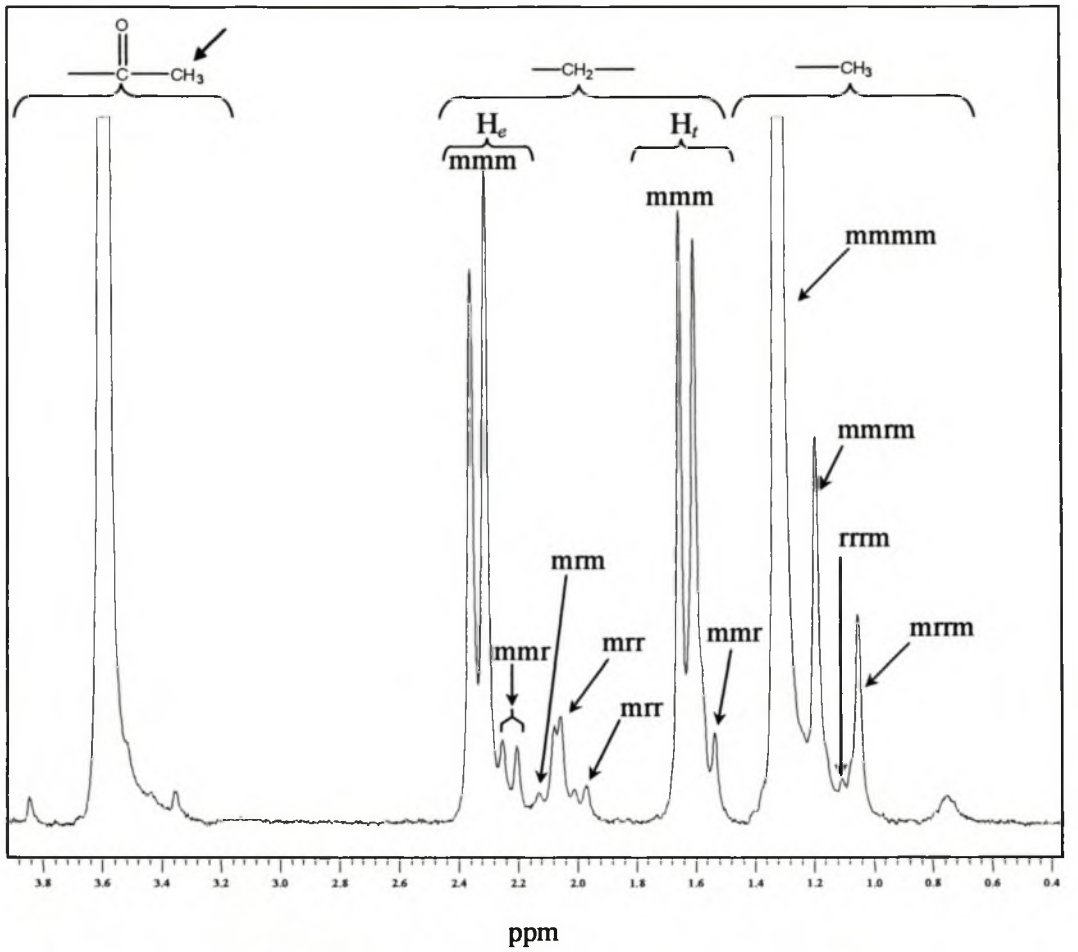

Figure 7.3. The 300-MHz proton NMR spectrum of isotactic PMMA, where the peak shift can be attributed to the tacticity of the polymer.

Table 7.1. Tetrad and pentad assignments of the synthesised PMMA compared to Ferguson's predictions [20].

Tetrad	Configuration	Methylene group values Ferguson (ppm)	Methylene group values T8 (ppm)	Pentad	Methyl group values Ferguson (ppm)	Methyl group values T8 (ppm)
mmr	*t*	1.59	1.55	mrrm	1.09	1.07
	e	2.25	2.25	mrrr	1.10	1.13
mmm	*t*	1.67	1.63	mmrm	1.20	1.21
	e	2.37	2.36	mmmm	1.34	1.34
rrr		2.00	1.99			
mrr		2.05	2.07			
		2.10	2.10			
mrm		2.15	2.15			

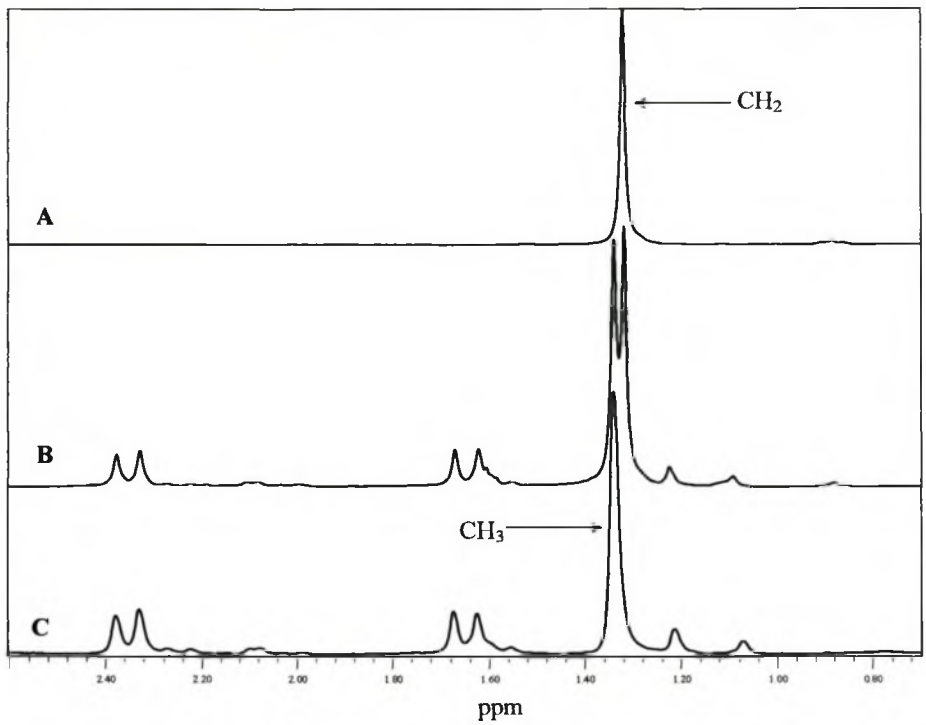

Figure 7.4. 300 MHz proton spectra of A) polyethylene, B) an ethylene and MMA copolymers (T8) and C) PMMA.

The magnetically non-equivalent state of isotactic PMMA can also be seen in the proton NMR spectrum of PMMA (Figure 7.3), synthesised in the presence of **2** as catalyst precursor. From the ^{1}H NMR spectrum, it can be seen that **2** predominantly results in the synthesis of isotactic PMMA. The tacticity, according to the methyl pentads, is [mmmm] = 82.9, [mmrm] = 10.4 and [mrrm] = 6.4. The peak assignment was done according to R.C. Ferguson [20]. There is a rather good relationship between the values obtained by Ferguson and data obtained from our polymers, even though they were working in another solvent (chlorobenzene). These values are depicted in Table 7.1. The rest of the tetrads and pentads are not shown here since they are also not observed in the NMR spectrum due to overlapping of the peaks.

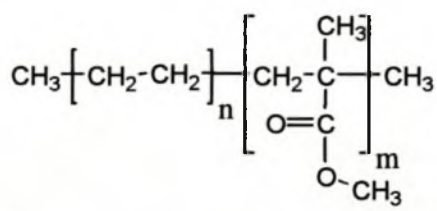

Figure 7.5. Representation of an ethylene and methyl methacrylate block copolymer.

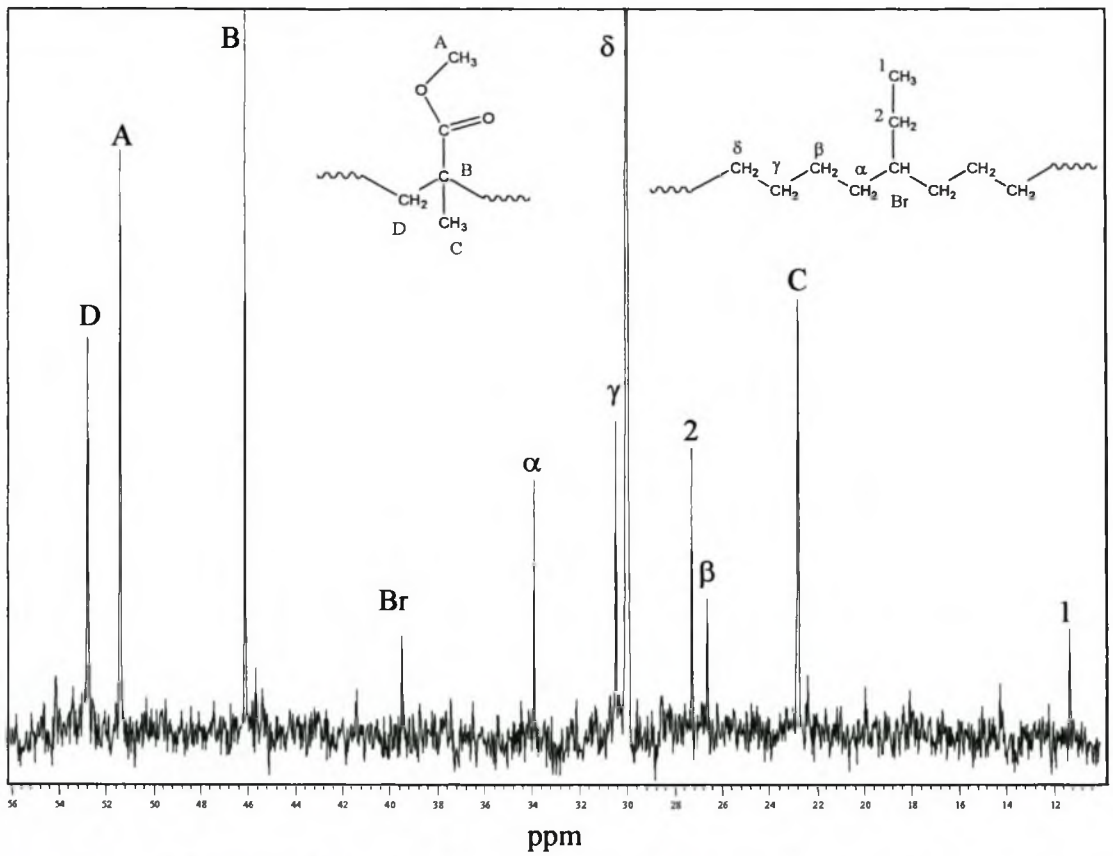

Figure 7.6. ^{13}C NMR spectrum of sample T8 where both the poly(methyl methacrylate) and the poly(ethylene) can be seen.

It was found that the differences in chemical shift between relaxation peaks for the methylene protons of the polyethylene and the methyl protons of the PMMA were very small. This small difference can be seen in the biggest peak (Figure 7.4 (B)), which has a bimodal distribution with no baseline separation. The relative heights of the two peaks will vary, depending on the monomer content. For this reason, normal integration could not be used to determine the monomer content in the samples. A mathematical integration manipulation was used to calculate the monomer content. The methyl relaxation peak of –O-CH_3 (at 3.58 ppm) was given an integral value of three, due to the three protons that this species possesses. Thereafter, the integrals of all the remaining peaks were taken and five was subtracted from the sum of the integrals. The value of five is derived from the remaining five protons on the MMA monomer unit (Figure 7.5). The sum of these calculations was divided by four (the number of protons in an ethylene unit). The product of this depicted the molar ratio of

ethylene to 1 mol of MMA in the polymer samples. Table 7.2 gives the amount of MMA in the samples.

The carbon relaxation peaks (10 ppm-56 ppm) of the ethylene and MMA can be seen in Figure 7.6. The relaxation peak for the carbonyl carbon, not shown here, was observed at 176.2 ppm. The catalyst promotes the formation of oligomers and branches in the ethylene backbone, as observed in the above NMR spectrum. Chemical shift assignments for the carbon relaxation peaks to arrive at possible configurations of the polymer structure were made after consideration of the Grant and Paul rules [21]. These predicted values correlated well with the obtained values (Figure 7.6). The presence of the ethyl side branches is a known structural defect that is observed in the polymer backbone when ethylene is synthesised by precatalyst **2.** 1-Butene units are formed in situ and incorporated into the polymer.

7.4.2 GPC

GPC is one of the more basic laboratory analytical techniques. Nonetheless, with sound interpretation of the available data and the use of specialised detectors, good deductions can be made on the structural composition of a sample. The PMMA homopolymer (T0), synthesised with **2**, shows a non-uniform distribution curve. The non-uniformity is seen as a sudden drop in molar mass at $1x10^5$ g/mol (Figure 7.7). MMA polymerised with **2** is a slow reaction, which takes several hours to reach completion. Under the present reaction conditions where the reaction is terminated after 2 hours, sufficient time was not given to allow for the completion of this reaction [2]. This meant that the chains were terminated during their growth, giving polymer chains with a predefined maximum length.

Figure 7.8 and the data in Table 7.2 (peaks 1 to 3) show that some samples display a bimodal or trimodal MMD, whereas others give only monomodal MMD. Data given in Table 7.2 (with reference to the bi- and trimodal MMD) do not represent molecular

Table 7.2. The MMA content of the ethylene/MMA copolymers synthesised via **2**, as well as their peak maximum molar mass values (M_p) and further results obtained from thermal analysis.

Sample code	[^{1}H] MMA content (mol-%)	GPC Peak 1 [M_p]	GPC Peak 2 [M_p]	GPC Peak 3 [M_p]	$T_{m\,(DSC)}$ [1] (°C)	$T_{m\,DSC)}$ [2] (°C)	$T_{m\,(DSC)}$ [3] (°C)	$T_{c\,(CRYSTAF)}$ (°C)	T_g (°C)
T0	100.0		81500		64.6			0	55.9
T1	70.1	48600		1230000	64.2		133.0	85.8	49.5
T8	25.0	24400	46500		66.6	109.5	130.3	84,1	43.0
T11	18.5	18800				110.5	127.9	81.8	25.5
T9	16.7	21100				114.3	127.1	83.1	

[1] Peaks appearing at low melting points

[2] Peaks appearing at intermediate melting points

[3] Peaks appearing at high melting points

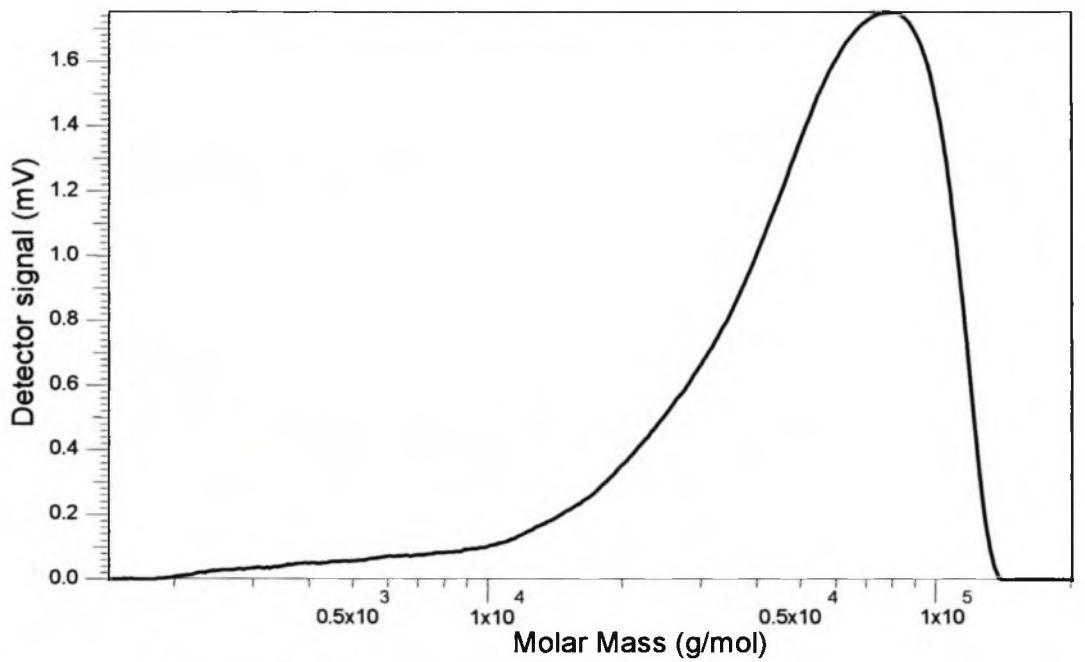

Figure 7.7. Molar mass distribution of T0 synthesised via **2**.

mass distribution data, but can only be quoted in terms of peak maxima. The multimodality is an indication of a non-homogenous system. (Consisting of a mixture with different polymer species, which can comprise PMMA and polyethylene homopolymers together with the copolymer of ethylene/MMA.) The trimodal chromatogram could depict the synthesis of ethylene homopolymer in the first step and, with the addition of MMA, MMA homopolymer, as well as the block copolymer

of ethylene and MMA in the second reaction step. Unfortunately no proof can be given for these statements when using the Refractive Index (RI) detector in the Waters 150C.

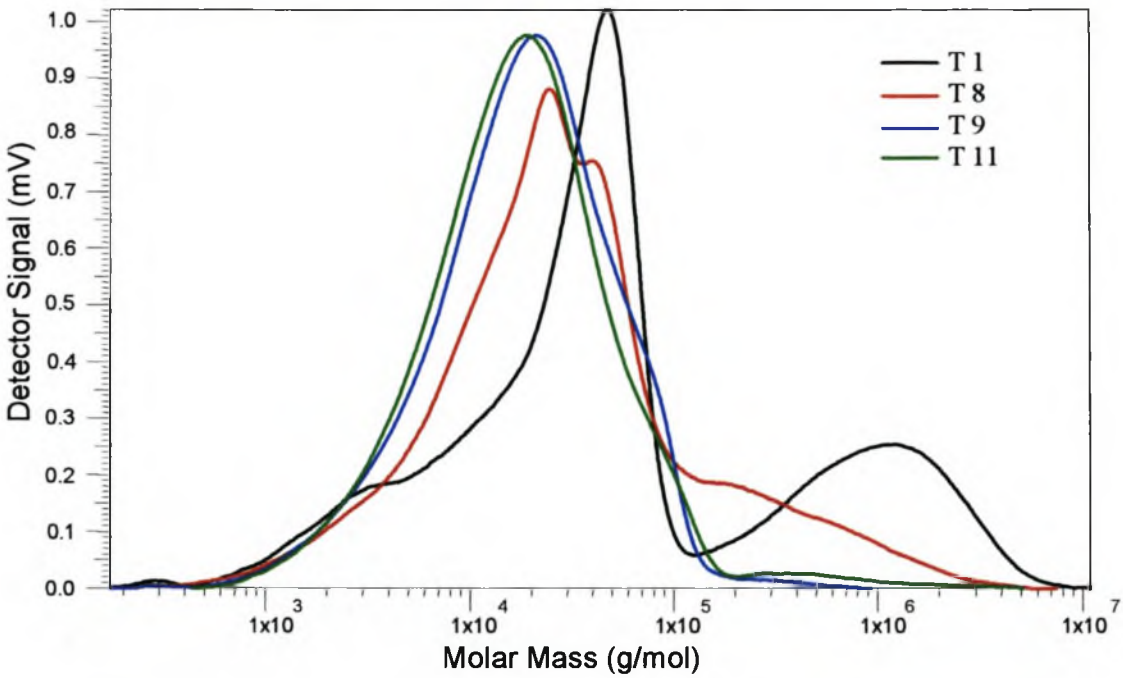

Figure 7.8. Mono-, di- and trimodal molar mass distribution GPC curves for samples T1, T8, T9 and T11.

7.4.3 Thermal analysis

Thermal analyses of the polymer samples by means of DSC are shown in Figure 7.9, where four samples are compared to the PMMA homopolymer. For the sample T1, a distinctly large endothermal peak can be seen at a temperature of 133.0 °C, while a second peak is also observed at 64.2 °C. Peaks noted at lower temperatures correspond to the endothermal peak of PMMA homopolymer, while the peaks at higher temperatures appear in the region of slightly branched polyethylene melts. The peaks observed at high temperatures have shoulders that seem to become more prominent as ethylene addition increases and the peak shifts to lower temperatures (Table 7.2).

Also seen in Figure 7.9 are the T_g's of the samples. These values become less defined in the series from T1 to T11. T_g measured by DMA also shows a decrease in temperature with a decrease in PMMA (Table 7.2). The T_g for the sample T0 (isotactic PMMA homopolymer) has a similar T_g as observed in literature (Y. Grohens *et al.* [22] at 61 °C or J.-J. Kim *et al.* [23] at 51 °C).

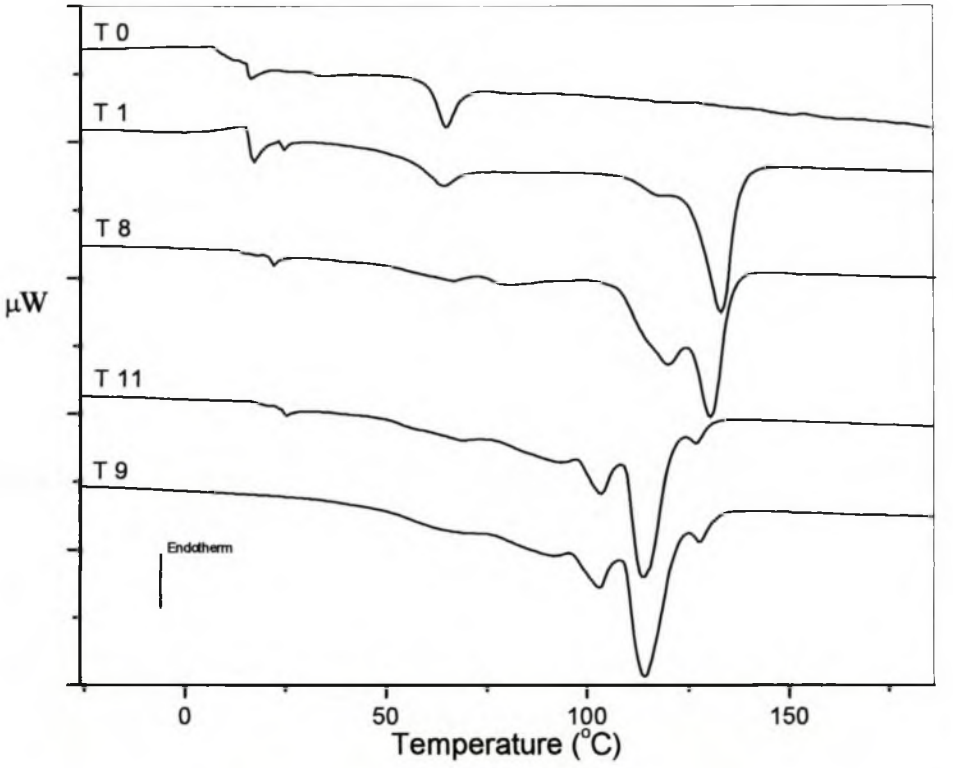

Figure 7.9. DSC heating curves of the copolymer samples T0 (homopolymer), T1, T8, T9 and T11.

The appearance of a shoulder and the shift in the melting peak to a lower temperature are indications that changes have taken place in the system during the different ethylene feed times in the individual reactions. It can be argued that these changes are due to the synthesis of copolymers or the decrease in MMA for these samples or it can be due to the increase in branch distribution of the polyethylene. The DSC gives no proof that a copolymer has been formed. Considering that most of the reaction parameters stay constant, changes are most likely due to the amount of the copolymer present in the samples and not due to the branches produced by the catalyst. Further

analytical work has to be done on these samples to show the existence of block copolymer structures.

7.4.4 Infrared spectroscopy

Identification of MMA in an IR spectrum (Figure 7.10) containing PMMA and polyethylene is quite easy due to the characteristic carbonyl band at 1730 cm^{-1}, which is not influenced by the absorbance bands of the polyethylene. The analysis of the polyethylene part is not as simple, there are less characteristic adsorption bands and most of them lie underneath the bands of the PMMA. The only bands that are useful

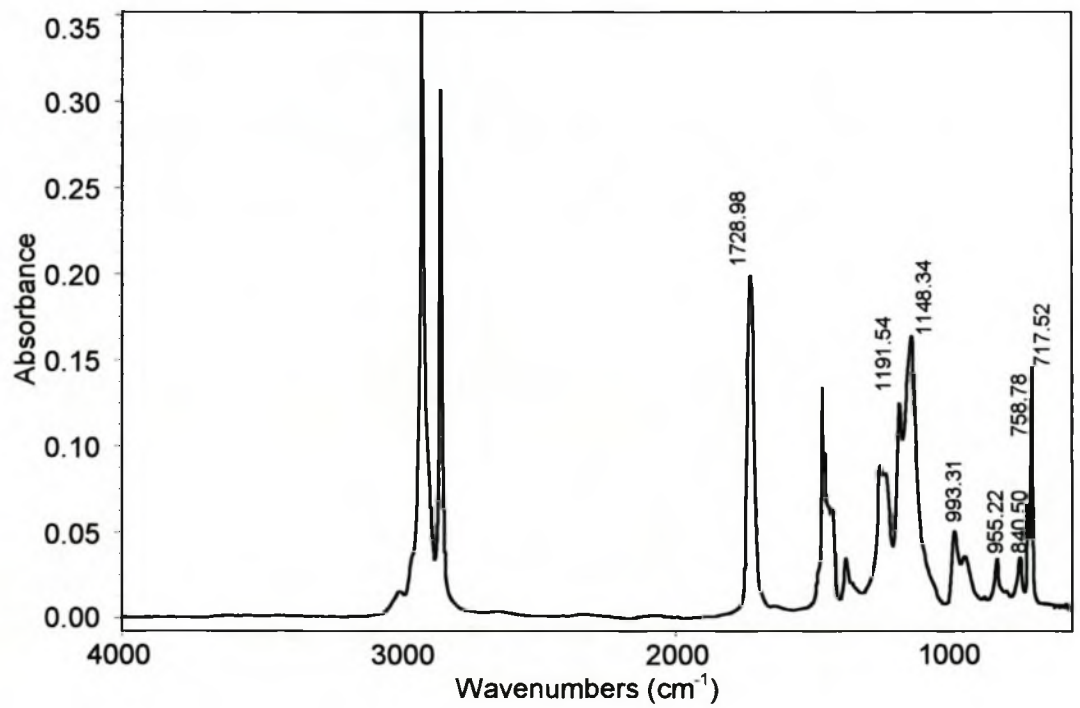

Figure 7.10. Peak identification of IR spectra for the poly(ethylene/MMA) sample T8.

for the identification of polyethylene in these samples are the bands at 730 cm^{-1} and 720 cm^{-1}, which are the bands of the crystalline and amorphous parts respectively [24]. The bands at 730 cm^{-1} and 720 cm^{-1} are associated with the $-CH_2$ vibrations in the rocking mode and the band at 760 cm^{-1} is characteristic of the

vibration for ethyl side branches, also in the rocking mode [25]. In the following sections we will only mention the peak at 720 cm^{-1}, since the two peaks cannot be baseline separated and the peak at 720 cm^{-1} is also the predominant peak.

7.4.5 GPC coupled to FTIR spectroscopy (LC-Transform)

Separation was achieved with a standard GPC column before the sample was sprayed onto the Germanium disk in the collection module (LC-Transform). Results of these separations can be seen in Figure 7.11, where the Gram-Schmidt plots are compared to the wavenumber height chemigrams. (Further information regarding the exact calculations for producing a Gram-Schmidt and chemigram can be seen in the section that covers GPC coupled FTIR spectroscopy in Chapter 3.) This was done for the carbonyl band at wavenumber 1730 cm^{-1} and the ethylene band at wavenumber 720 cm^{-1}. This figure further illustrates the relative of ethylene to MMA content at several points along the retention time scale.

Gram-Schmidt chromatograms represent the intensity of the IR spectrum for the entire time span and therefore show the molar mass distribution of the samples. The Gram-Schmidt (black line in Figure 7.11(A) for T1) shows a similar bimodal distribution as seen in the GPC chromatograms (Figure 7.8). The red line in the chemigram (for the peak at 720 cm^{-1}) indicates the presence of ethylene in the samples. A bimodal composition can also be seen here, where the first part of the bimodal distribution shows a good fit with the Gram-Schmidt peak at earlier retention times. The second peak in the chemigram (720 cm^{-1}) lies off-centre from the second peak maximum in the Gram-Schmidt bimodal distribution towards a higher retention time. The blue line represents the chemigram at 1730 cm^{-1} for the detection of MMA. This chemigram (1730 cm^{-1}) shows only one MMD chromatogram at a high retention time, exactly fitting the peak maximum of the Gram-Schmidt curve at high retention time. The green stars in Figure 7.11(A) are the ethylene ratios in the samples during a chromatographic run, giving thus a summary of the chemigrams at 1730 cm^{-1} and 720 cm^{-1}.

In Figure 7.11(A) one can clearly observe the bimodal MMD of T1, where the high MM (short retention time) part only contains PE and the low MM part (long retention time) has predominantly PMMA. As seen in the ethylene/MMA ratio, the ethylene content increases slightly in the very low MM region (15 minutes and longer). For sample T8, as seen in Figure 7.11(B), a reduction in the high MM PE part is observed and the ethylene is more evenly distributed over the entire PMMA region. The presence of PE homopolymer can, however, still be observed in the high MM shoulder (low retention time).

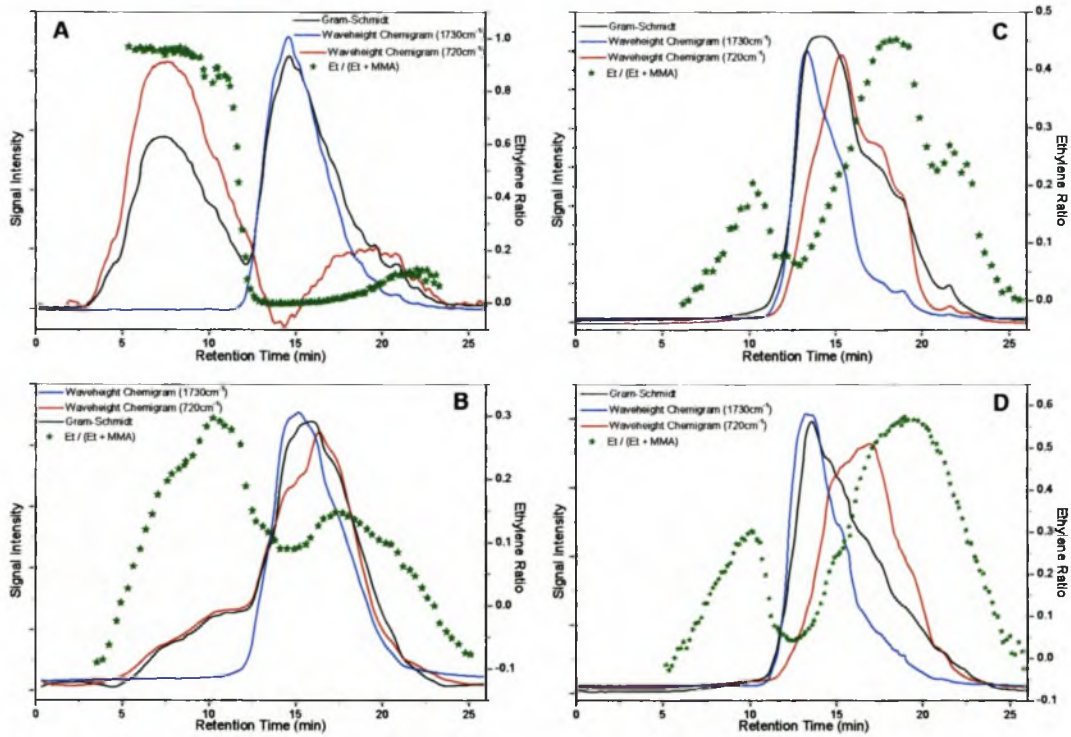

Figure 7.11. LC-Transform chromatograms for (A) T1, (B) T8, (C) T9 and (D) T11, with data given in the form of Gram-Schmidt chromatograms, wavenumber height chemigrams at 1730 cm^{-1} and 720 cm^{-1}, as well as the relative amount of ethylene in the samples.

The overlapping of the PE and PMMA does not indicate the presence of block copolymers. In this separation system samples are only separated according to their hydrodynamic volume and not according to their chemical composition. In other words, a PE sample and PMMA sample could have the same hydrodynamic volume

and could therefore elute at the same retention time. Although the synthesis of ethylene/MMA block copolymer with **2** is a prerequisite when looking at the reaction mechanism, where the activation of the catalyst by alkylation is a requirement before MMA polymerisation, GPC will thus not prove block formation.

T 9 and T11, in Figure 7.11(C) and (D), show similar trends to T1 and T8. The main difference is the absence of the high MM PE homopolymer peak. As with the previous two examples, T9 and T11 also show a higher concentration of ethylene in the low MM region of the PMMA.

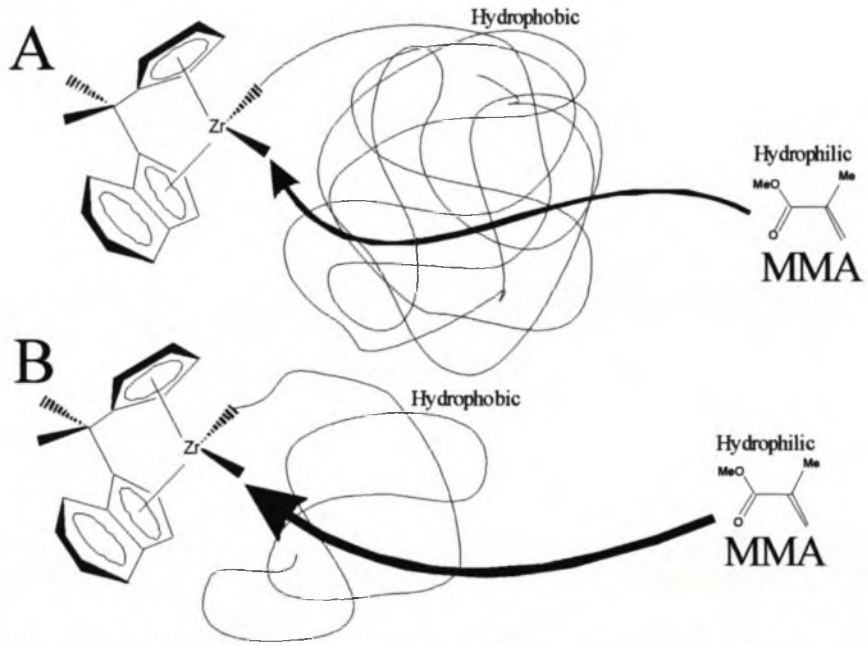

Figure 7.12. An illustration of the proposed monomer shielding through the formation of hydrophilic ethylene chains around the active catalyst site. A) depicts the effect of long ethylene sequences, while B) represents the effect of shorter ethylene sequences.

CRYSTAF and gradient HPLC analyses confirmed the presence of block structures (see later in CRYSTAF and high temperature gradient HPLC sections 7.4.6 and 7.4.7). This information was used to create a hypothesis regarding the data obtained by GPC coupled to FTIR spectroscopy (LC-Transform). Figure 7.12(A) illustrates that the longer hydrophobic ethylene chains shield the active catalyst site from MMA monomer units. The chance of a hydrophilic MMA unit reaching the active catalyst site is greater if the hydrophobic ethylene chain is shorter. This theory is illustrated in Figure 7.12(B). The hydrophobic shielding effect would give an explanation for the

higher concentration of PE on the lower MM side of the PMMA MMD curve in Figure 7.11.

7.4.6 CRYSTAF

The analysis of the samples by CRYSTAF yields information on the different crystalline fractions. Highly crystalline fractions crystallise at high crystallisation temperatures and non-crystallising fractions remain in the soluble part. The diagram obtained by CRYSTAF is a representation of the chemical composition of the samples.

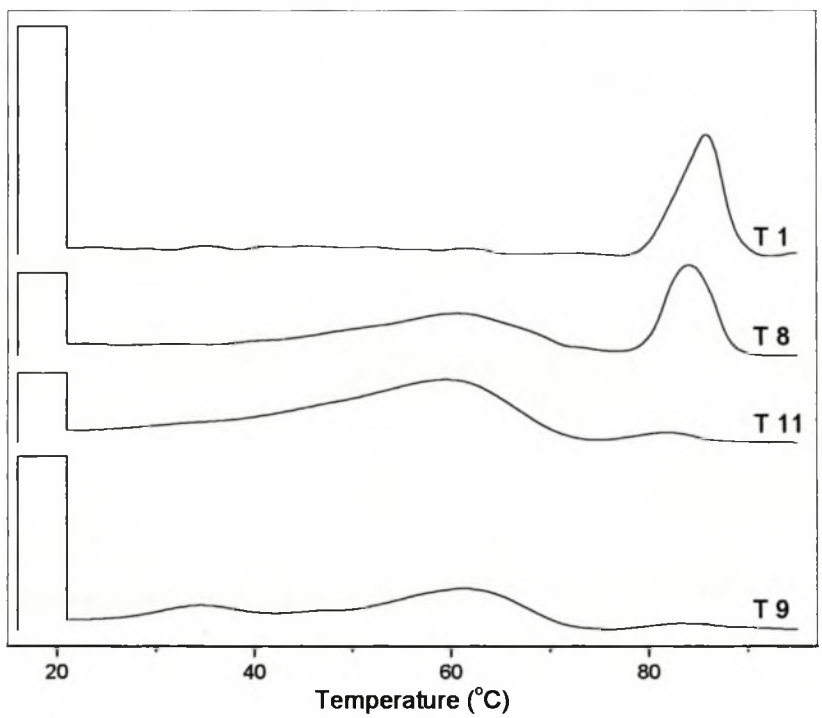

Figure 7.13. CRYSTAF curves for ethylene/MMA copolymers, containing increasing amounts of ethylene from T11, T9, T8 to T1. (Information on the different comonomer amounts can be found in Table 7.2.)

Looking at the chemical composition distribution in respect to the crystalline structure by means of CRYSTAF, certain changes can be seen in the samples, as illustrated in

Figure 7.13. All the runs showed a soluble fraction, indicated by a square peak (profile) in the first derivative chromatogram at low temperatures. A large percentage of this square peak is PMMA homopolymer. This polymer may be largely amorphous and will not crystallise in solution. In the temperature region of 85 °C, a crystallization peak is visible for T1. This peak decreases with temperature, decreases in signal intensity and broadens at the base of the peak in the order T1, T8, T11 and T9 samples. This $T_{c\ (CRYSTAF)}$ region correlates well with slightly branched polyethylene analysed in TCB [26-28]. All samples show crystalline fractions between the soluble and the highly crystalline fraction at 85 °C. This crystalline part becomes more pronounced from T1, T8, T11 through to T9. Due to the limitation of the CRYSTAF detector to a single wavenumber, the individual detection of MMA is not possible.

The combination of using 1,1,2,2-tetrachloroethene (TClEt) as solvent with a 5.82 micron wavelength filter, allowed the detection and identification of the MMA in a CRYSTAF diagram. TClEt is a symmetrical molecule and therefore has few IR bands in its IR spectrum, making it an ideal solvent for the IR detection of carbonyl groups. As already mentioned in the experimental chapter, the 5.82 micron wavelength filter is a customised filter for the selective filtration of all wavelengths except the wavelengths around 1730 cm^{-1}. The transmitted wavelengths lie in the same region as the IR adsorption bands of the carbonyl group for MMA, thus allowing the detection PMMA in a CRYSTAF chromatogram. Similarities between the chromatograms run in TCB (Figure 7.13) and TClEt (Figure 7.14) can be observed with a shift to a lower $T_{c\,(CRYSTAF)}$ for the TClEt runs. There are two lines in every chromatogram shown in Figure 7.14. The black lines are the detection signals of the carbon in the backbone, giving thus the total concentration of the samples at different crystallisation temperatures. For the detection of the backbone carbons the normal IR filter is used. The blue lines are the detection signals from the 5.82 micron filter and show thus the presence of MMA in the crystalline region.

Figure 7.14(A) and (B) clearly shows that the fraction that crystallises at high $T_{c\,(CRYSTAF)}$ contains no detectable MMA units of PMMA, thus corresponding to PE homopolymer. Cleary seen in all the chromatograms in Figure 7.14 is the presence of MMA units in the crystalline part below 65 °C. For the purpose of clarification the

following is repeated, the reaction mechanism only allows the formation of clearly defined ethylene and MMA blocks, only polymerising in order from ethylene to MMA (starting with an ethylene block, followed by the MMA part).

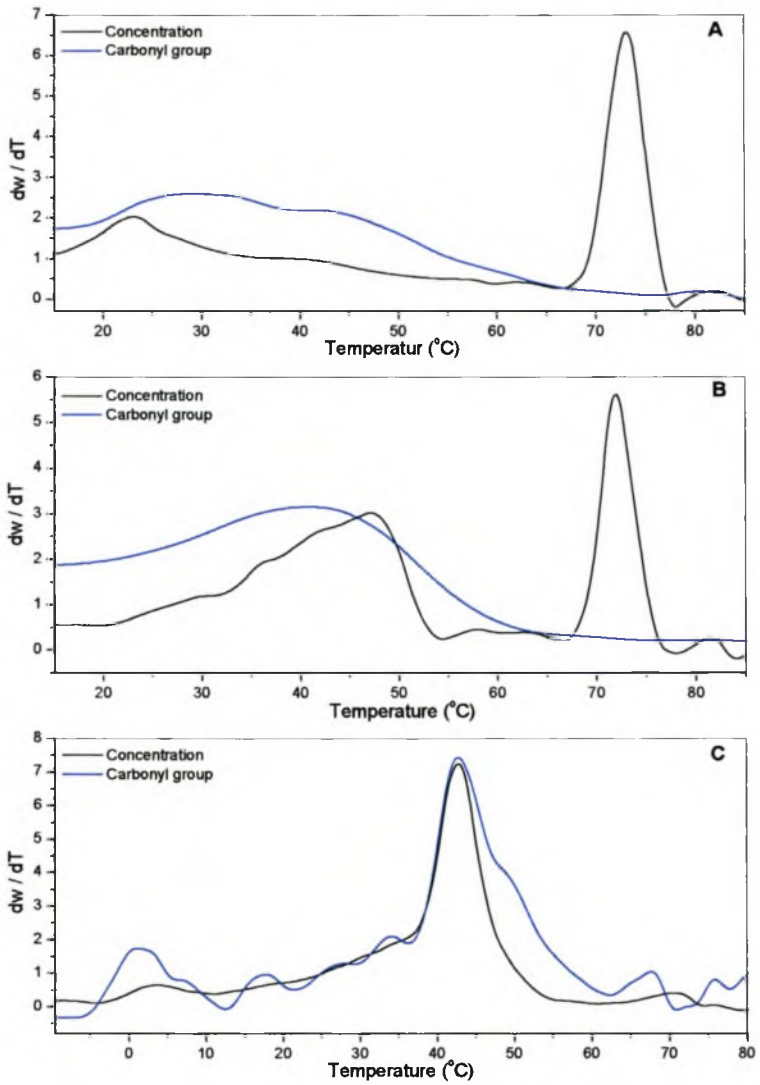

Figure 7.14. Carbonyl and total concentration detection for T1 (A), T8 (B) and T9 (C), with a 5.82 micron filter (in perchloroethylene as solvent).

Parallel comparisons can thus be drawn between the LC-Transform results and the results of the carbonyl detection method. In the LC-Transform method both samples T1 and T8 show PE homopolymer peaks at high retention times (Figure 7.11(A) and (B)). These PE homopolymers can also be seen in the CRYSTAF chromatograms at 72.5 °C (Figure 7.14(A) and (B)). T1 and T8 both contain high percentages of PE

homopolymer. T9 in Figure 7.14(C) has no $T_{c\ (CRYSTAF)}$ at high temperature. The only $T_{c\ (CRYSTAF)}$ observed is the peak at lower temperature, where the PMMA is also present. The CRYSTAF chromatogram shows that T9 has no PE homopolymer in the system, but block copolymers are detected. The noise in T9 is due to the lower concentration of the carbonyl groups in the sample. The same phenomenon as for CRYSTAF is seen in the GPC coupled to FTIR spectroscopy (LC-Transform) data (Figure 7.11(C)) where no PE homopolymer peak is observed. The only ethylene peak observed in the GPC chromatogram is the one lying in the same region as the MMD for MMA, indicating a copolymer structure. This clearly confirms that chemigram peaks for ethylene, that are observed in the same region as the chemigram (1730 cm^{-1}) for MMA, indicate the presence of a copolymer in the GPC coupled FTIR spectroscopy.

A second interesting factor, regarding the fraction crystallising at lower temperature, can be observed when comparing the chromatograms of the GPC coupled FTIR spectroscopy and CRYSTAF. Sample T1, in Figure 7.14(A), shows only a small crystallisation peak at a temperature around 23,1 °C. A similar small fraction for PE was detected in the chemigram (720 cm^{-1}) (Figure 7.11(A) at long retention times). The long retention time of this fraction indicates short chains that will result in low crystallisation temperatures. In T8 the opposite is seen, with the largest PE part in the same region as the MMA at a lower retention time (higher MM (Figure 7.11(B)). The diagram of T8 (Figure 7.14(B)) shows a crystallisation peak of higher intensity and with a peak maximum at 47.5 °C. CRYSTAF also shows that T1 contained shorter chain PE units than T8 in the block copolymer.

This analytical technique, with the 5.82 micron filter, clearly shows the presence of PE homopolymer, as well as that of a PE-block-PMMA copolymer.

7.4.7 High temperature gradient HPLC (HTG-HPLC)

To my knowledge, this is one of the first successful separations of a copolymer at higher temperatures by means of gradient HPLC. Lyons *et al.* [29] have done some

work on the separation of ethylene/styrene copolymers via gradient absorption conditions in cyclohexane and chloroform on a silica column at 100 °C. The separation of copolymers at high temperatures using a solvent gradient is limited to a solvent that can be used at these temperatures. The analysis temperature of 140 °C used here is significantly higher than the boiling point for most conventional solvents used in gradient HPLC.

In this work, the reversed phase separation (RP) system [30, 31] was adopted where the gradient was run from a more polar non-solvent solvent (DMF) to a less polar solvent (TCB) in a non-polar (C_{18}) column. The polarity of the gradient in RP decreases with time. The C_{18} column is packed with a non-polar stationary phase made from silica, with the silica beads having C_{18} carbon chains attached to their surface [32]. Hydrophobic interaction with the stationary phase and polar interaction with the mobile phase drive the retention in this process. So, in this process, retention is not so much governed by adsorption, but rather by precipitation/re-dissolution of polyethylene [31, 33]. Only the PMMA shows adsorption in this system. In general the RP-HPLC is dominated by the molar mass of the polymer molecules and, to a lesser extent, influenced by the chemical composition of the polymer, meaning that homopolymers will elute in order from lowest to highest MM. For this reason one should remember that RP is a versatile qualitative tool, because it shows the observed differences in the high MM part. But it still seems, without a doubt, that it does not show any sensitivity to the microstructural difference between copolymers. In the RP a change in the stationary and mobile phases will have a definite influence on the retention of a sample.

DMF is a polar solvent, able to dissolve PMMA homopolymers up to a high MM in the temperatures range where these experiments were carried out. Contrary to this, DMF can only dissolve PE homopolymer up to a few thousand molar mass units at the analysis temperature 140 °C. The opposite is true for TCB, which dissolves PE homopolymer, but does not dissolve higher molar mass PMMA homopolymer at elevated temperatures. An opposing solvent system regarding the solubility of the polymers, is thus required. The choice of the stationary phase, in the form of a C_{18} column, was made to achieve adsorption of the PE on the column. It was also found

that a silica gel column shows total adsorption of the PMMA on the column with the DMF/TCB gradient.

The only gradient for this analytical instrument reported in literature is a temperature gradient [12-14]. This type of separation was only used up a temperature range of 70 °C. This separation is not a temperature rising elution fractionation system since standard HPLC columns were used for the separation of the samples. In temperature gradient analysis the sample is precipitated on a column and with a rise in temperature the polymers start to elute from the column. In HTG-HPLC, the temperature was set well above the crystallisation temperature of the samples in the solvents at 140 °C, to prevent incomplete elution of the samples. In this system the temperature of the instrument was also set at 140 °C to prevent polymer crystallisation in the column.

The standard run clearly showed that the PMMA standards elute in the order of highest to lowest MM. This mechanism is known as size exclusion (Figure 7.15(A)). In the case of PE, the sample elutes from the lowest to highest MM, thus precipitation is observed as the predominant mechanism for separation. The low MM standards of PE, Peak 4 in Figure 7.15(A), elute in 100 % DMF solution (in the region of the PMMA). For the standard M_n = 12 000 g/mol, two peaks (5 (a) and (b)) are seen in Figure 7.15(A). This is referred to as the borderline, where a small amount of standard is soluble in DMF and the rest will only elute at a solvent concentration close to 100 % TCB. The high MM PE standard elutes at the highest retention time and shows no sign of elution at lower retention times in DMF.

Chromatograms obtained from T1, T8 and T9 via HTG-HPLC show resemblance in the part eluted in the region of the PMMA, but striking differences are observed in the PE region. Looking at peaks eluting at the regions marked 9 and 10, in Figure 7.15(B), a clear similarity can be seen between these results for samples T1, T8 and T9 and those obtained with GPC coupled FTIR spectroscopy (LC-Transform) (Figure 7.11 (A-C)). The PE homopolymer peak (T1) showed a separate peak, as seen in the LC-Transform data. Only PE was present at the high MM side of the T1 elugram (Figure 7.11(A)). A peak of T1 in the region 9 (as depicted in Figure 7.15(B)) elutes also in the same area as the PE standard. This correlates well with the data obtained from CRYSTAF, using the 5.82 micron filter, where a PE

homopolymer peak was detected during crystallisation. The chemigram (720 cm^{-1}) of T8 shows a PE homopolymer peak and another peak where the PE is more evenly distributed over the entire PMMA elugram (as depicted in Figure 7.11(B)). Figure 7.15 (B) also showed two peaks for this sample. One is situated in the region marked 9, wereas the second one appears in the region marked 10, at a retention time of 19.0 minute (which is 1 minute before the lowest PE standard retention time). Here too, the CRYSTAF (5.82 micron filter) chromatogram shows a PE homopolymer and a crystalline region of high MMA concentration (Figure 7.14(B)). In T9, no PE homopolymer was visible in the GPC coupled FTIR spectroscopy (LC-Transform) (Figure 7.11 (C)) and PE is only distributed over the PMMA elugram. The HTG-HPLC chromatogram of T9 has only one peak in the region marked 10, with a retention time of 18.9 minutes. The CRYSTAF chromatogram in Figure 7.11(C) also shows no PE homopolymers.

It can thus be deduced that T1 contains no PE-block-PMMA with large PE blocks; T8 contains PE homopolymers as well as PE-block-PMMA, where the PE block has a MM grater than M_n = 12 000 g/mol; T9 has no PE homopolymers, only PE-block-PMMA with sufficient block length. Proof for the statements made here can only be verified by a detection method that is selective for one of the two compounds in the samples.

The only selective component detector that can be used under these analytical conditions is HTG-HPLC coupled FTIR spectroscopy (LC-Transform). This detector, however, also has its limitations; one of them is separation resolution. Separation resolution relates to the quality of separation that allows for the identification of two closely eluting species. Due to the spraying of the sample onto the disc, closely eluting compounds will overlap and will thus reduce the resolution in the LC-Transform.

The same wavenumbers were used for the detection of the ethylene in PE and the methyl methacrylate in PMMA as in the GPC separations (for PE it was 720 cm^{-1} and for PMMA it was 1730 cm^{-1}). In Figure 7.16, the numerical notations at the wavenumber 720cm^{-1} represents the number of times that the chemigram was enlarged in relationship to the PMMA chemigram at 1730 cm^{-1}.

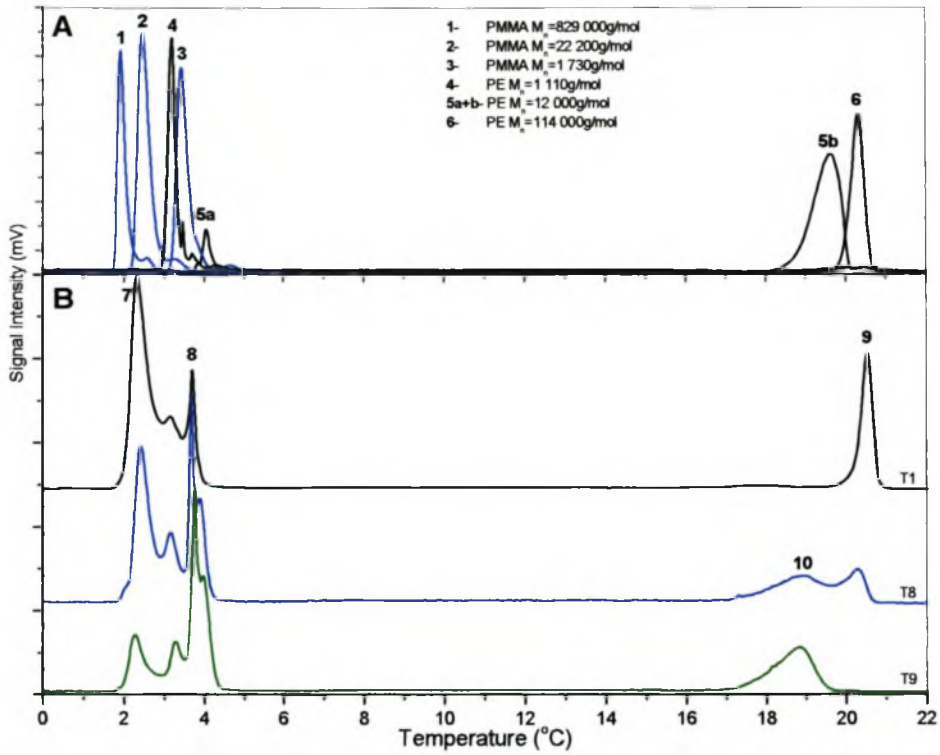

Figure 7.15. A) Chromatogram for PE and PMMA standards with MM as outlined in the legend, as well as B) Chromatograms of T1, T8 and T9 with different elution regions marked 7-10. (Method: Gradient: 100% DMF to 100% TCB, column: Nucleosil C_{18}, flow speed 0.5mL/min, ELSD-PL detector.)

Peak 1 in Figure 7.16(A) shows almost no detectible PE in the PMMA part. Peak 1 is thus PMMA homopolymer. The presence of ethylene in the form of oligomers or polymers can not by excluded even though PE is not detected, since PE forms an integral part in the activation of the catalyst. Mentionable PE contents are seen in peaks 2 and 3 for sample T1. The low signal intensity and the position of peak 2 on the retention time scale correlates well with analytical data obtained previously (sections 7.4.5 and 7.4.6). The data from GPC coupled FTIR spectroscopy and 5.82 micron filter for CRYSTAF, showed clearly that T1 contains only a small amounts of block copolymer with short ethylene chains. Figure 7.15(A), shows that PE standards with M_n lower than 12 000 g/mol elute in the region of PMMA and those with higher M_n will elute at high retention time. This thus gives the explanation for the presence of PE at the low retention time of peak 2 (Figure 7.16). The PE block length is

smaller than 12 000 g/mol. Peak 3 contains only PE homopolymer, since no PMMA can be detected under this peak.

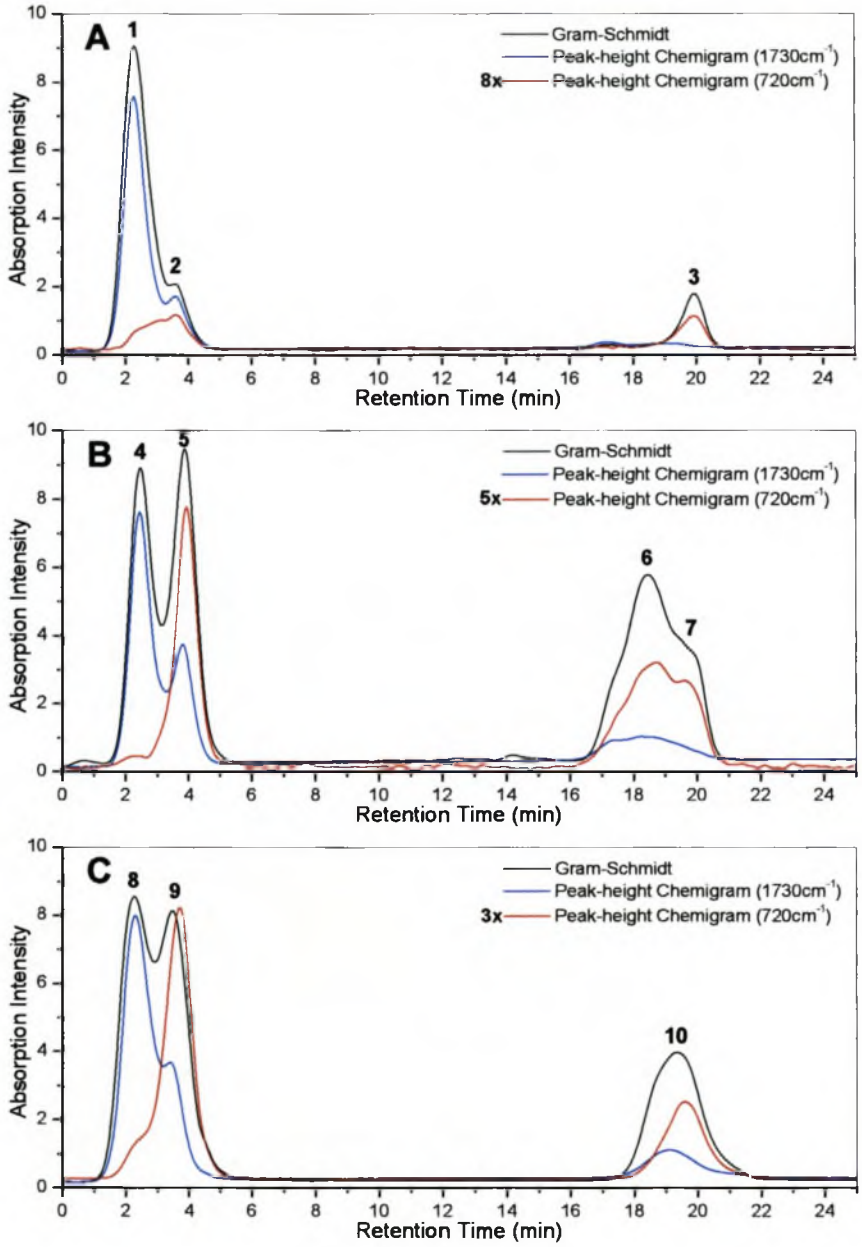

Figure 7.16. High temperature gradient HPLC, with LC-Transform as detector, for samples T1 (A), T8 (B) and T9 (C). Peak-height chemigrams were chosen for wavenumbers 1730 cm^{-1} (carbonyl group) and 720 cm^{-1} (ethylene group). The factors 8× (A), 5× (B) and 3× (C) are the ratios by which the cheimgrams at 720 cm^{-1} were enlarged.

Figure 7.16(B) shows that PMMA homopolymer is present in T8 (peak 4) and both peaks 5 and 6 contain PE-block-PMMA. Shoulder 7 contains high amounts of PE

homopolymer. The small breach of the 1730 cm^{-1} PMMA line into the shoulder region is the result of the spraying process. The same argument can be used for the interpretation of peaks 5 and 6 regarding the chain length and quantity of sample as was done for peak 2 with the aid of GPC coupled FTIR spectroscopy and the 5.82 micron filter in CRYSTAF data (seen previous paragraph). Greater amounts of high MM PE block fractions were seen with the LC-Transform (Figure 7.11(B)) and CRYSTAF (Figure 7.14(B)) analysis of T8 than for T1. Since both peaks 5 and 6 contain ethylene as well as MMA, it can be concluded that peak 5 contains lower MM PE blocks and peak 6 higher MM PE blocks of the copolymers.

T9 in Figure 7.16(C) shows a complete distribution of both PE and PMMA over the entire chromatogram, meaning that this sample is only composed of block copolymers with varying block sizes. (Even though the PE appears only as a shoulder under peak 8.) Peak 10 also results from the block copolymer, as was suggested in Figure 7.15(A), region 10.

Results from Figure 7.16 correspond well to the chromatograms in Figure 7.15. Assumptions made with reference to Figure 7.15 were confirmed with the results from the GPC coupled FTIR spectroscopy (LC-Transform) detection method.

7.4.8 Higher Temperature Liquid Chromatography under Critical Conditions (HT-LCCC)

LCCC is a special type of chromatographic method; its relation to size exclusion mode and adsorption mode can be seen in Figure 7.17. This figure is only a schematic representation for the separations in the three modes. The region of critical separation is a narrowly defined region controlled by the solvent ratio and the temperature of the system. Deviation in either the solvent composition or the temperature will result in separation being done in the exclusion or adsorption mode [34, 35].

The system used for the separation of ethylene/MMA was optimised to allow the elution of PMMA at the CP. (This means that elution is independent of the MM with regards to the PMMA.) The PMMA chains are thus chromatographically "invisible" for the separation and will therefore elute at the same retention time. At the CP, separation is based on differences in chemical groups of the modified PMMA. These chemical groups can either be single molecules that are situated at the ends of the chain, or they can be larger oligomers or polymers that are attached to the PMMA chain through graft or block formation.

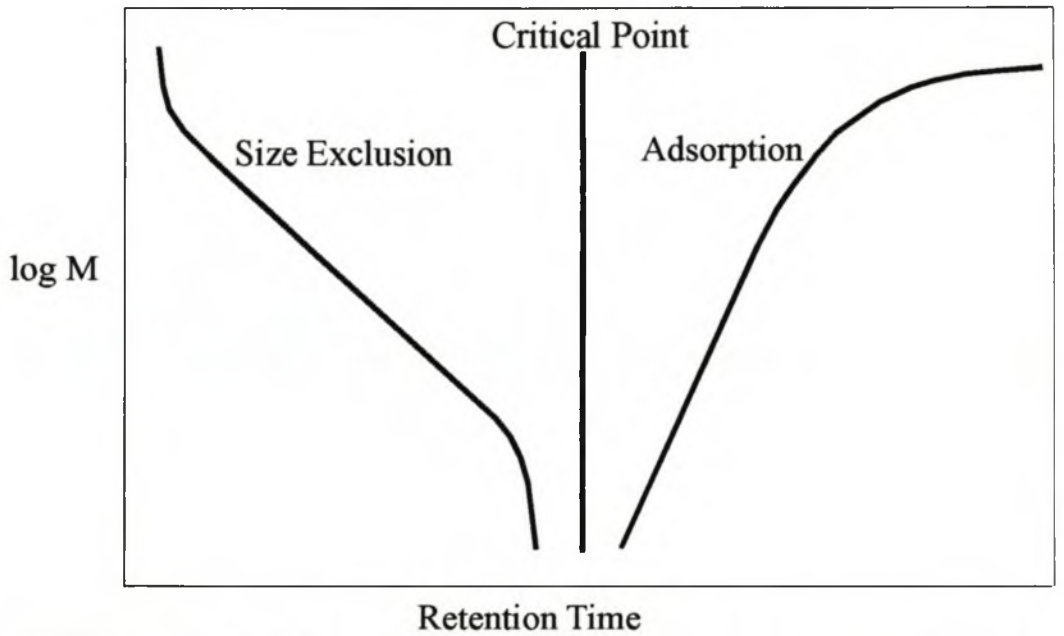

Figure 7.17. Illustration of the separation of different MM samples by changing the solvent composition to show size exclusion-, critical- and adsorption modes respectively.

The advantage of working at the CP of PMMA is that the second monomer type in the copolymer, whether graft or block in structure, can be separated in either size exclusion- or adsorption mode depending on the choice of column and solvent mixture. In the case where a good solvent, with reference to the second monomer type, is used then separation is achieved through size exclusion. The opposite is true when a weak solvent is used; separation is achieved through adsorption mode. The former mode forms the basis of separation in this study.

The determination of the CP for any polymer is the most time consuming and labour intensive process in critical chromatography. Determination of the CP for PMMA is done with a series of different PMMA standards. Different isocratic modes of solvent/non-solvent mixtures are used as eluents for the separation of the standards, which are dissolved in the same isocratic solvent mixtures. Data obtained by this method is shown in Figure 7.18. The different lines in Figure 7.18 represent separations under different isocratic conditions. The figure clearly shows that the PMMA standards are eluted under size exclusion conditions at a concentration of 33/67 (V/V%) TCB/CH. At a concentration of 34.5/65.5 (V/V%) TCB/CH, the CP for PMMA was reached. The CP is characterised by the elution of all PMMA standards at the same retention time. Solvent concentrations of 39/61 (V/V%) TCB/CH and higher elute in the adsorption mode. There is however a maximum value for the solvent/non-solvent ratio where no adsorption will take place, only precipitation. At the point of precipitation the polymer is retained permanently on the column and will therefore not elute.

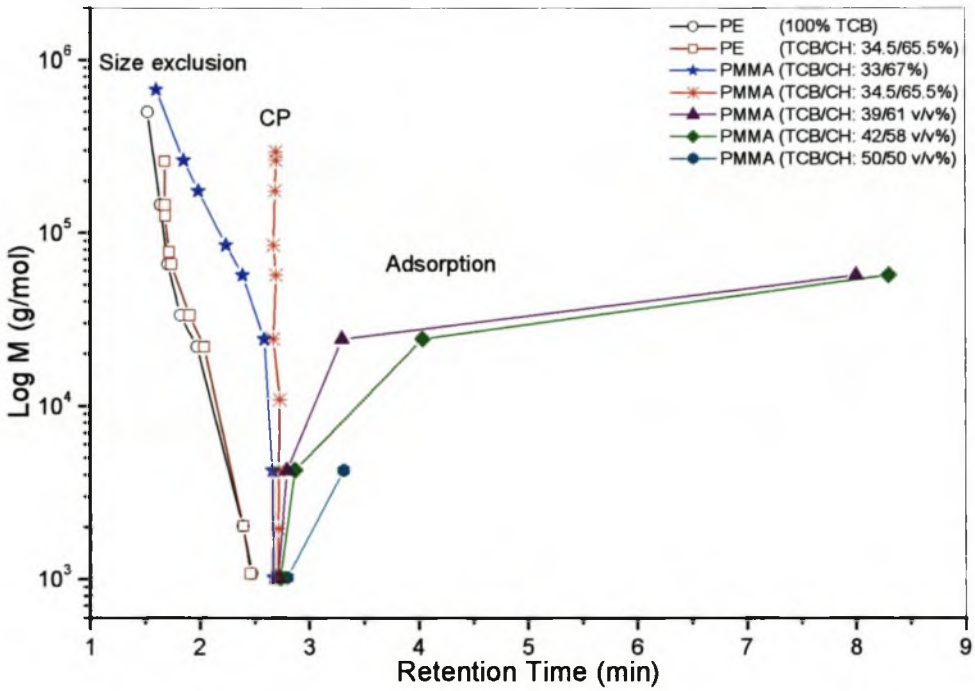

Figure 7.18. Critical diagram of MM vs retention time for PMMA and PE standards under different solvent/non-solvent conditions. Stationary phase: Nucleasil 300 Å silica gel; mobile phase TCB and CH; separation temperature 140 °C.

PE standards were also analysed, using the same experimental set-up as described in section 7.4.7. When using 100% TCB as eluent the PE standards elute in the characteristic size exclusion mode as seen for normal GPC. The separation of the PE standards gives a standard calibration curve, with a maximum and a minimum separation of high and low MM samples at short and longer retention times respectively (Figure 7.17). This shows that the separation of PE follows the size exclusion separation when using the Nucleosil silica gel column. At the critical condition of 34.5/65.5 (V/V%) TCB/CH the PE standards still elute under size exclusion conditions. Results prove therefore that when working at the CP of PMMA, the PE elutes according to its MM (from highest to lowest).

The separation of PMMA standards under critical conditions using TCB and CH are shown in Figure 7.19. The chromatogram shows the overlying of the peaks for the different PMMA standards at the same retention time. The retention time of PMMA under critical conditions of 34.5/65.5 (V/V%) TCB/CH at 140°C is 2.7 minutes.

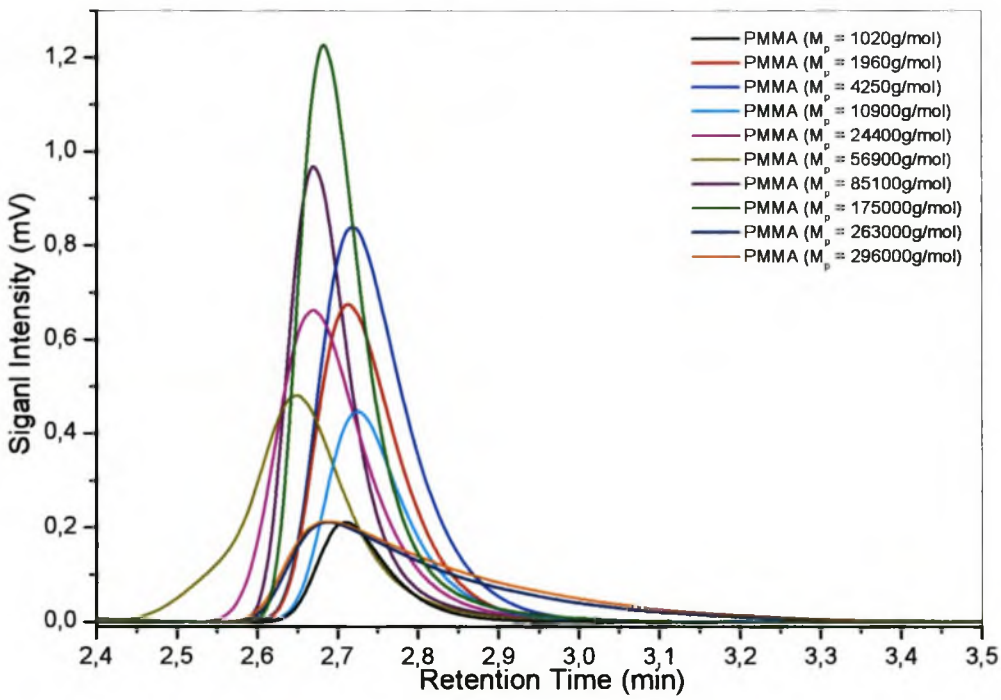

Figure 7.19. Critical chromatograms for a range of PMMA standards at the CP of 34.5/65.5 (V/V%) TCB/CH.

Only after the determination of the critical solvent composition for either of the two components in the system and the identification whether the component (not eluted under critical conditions) elutes in the size exclusion or adsorption mode can compositions of unknown samples be determined.

Two PE standards and a dashed line were added to the data obtained in Figure 7.20 (A) for easier identification and interpretation of the samples (T1, T8, T9 and T11). The two standards, M_p =2030 g/mol and M_p = 22000 g/mol, were introduced to show where in the chromatogram PE elutes under critical conditions. The dashed line is placed at 2.7 minutes to represent the CP, as determined previously.

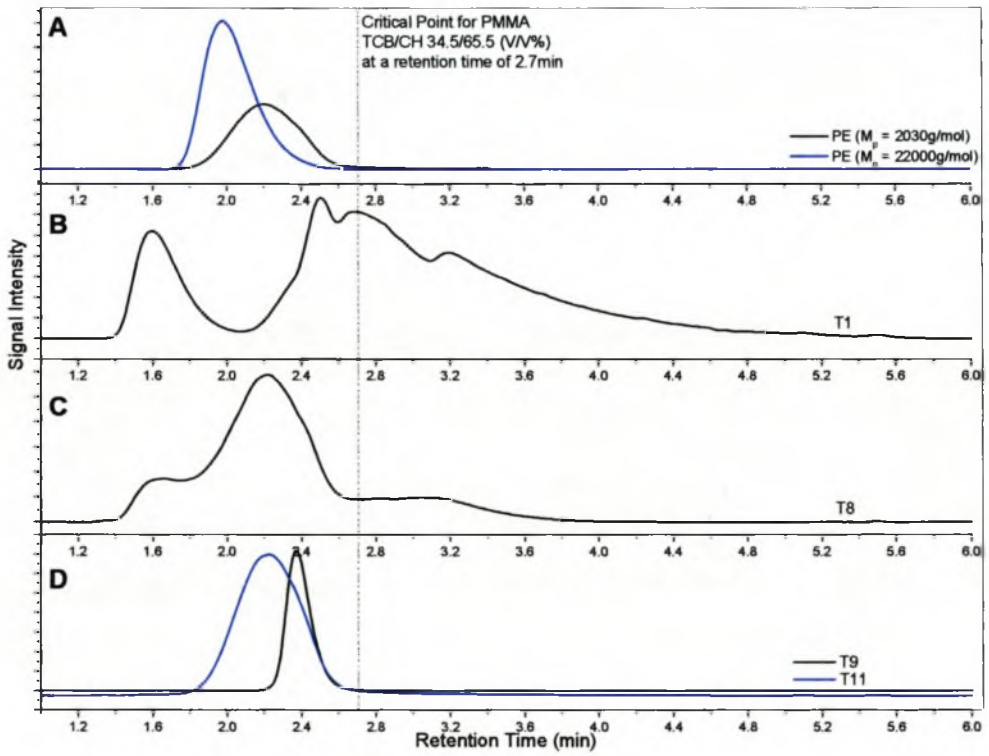

Figure 7.20. Chromatogram under critical conditions of PE standards (M_p = 2030 g/mol and 22000 g/mol) (A), T1 (B), T8 (C) and T9 as well as T11 (D). Stationary phase: Nucleosil 300 Å silica gel; mobile phase 34.5/65.5 (V/V%) TCB/CH; analysis temperature 140 °C.

T1 in Figure 7.20 (B) has a clearly defined peak at 1.6 minutes. This peak represents the PE homopolymer in the sample. The presence of PE homopolymer in this sample has already been proven on several occasions in this chapter, see sections on GPC coupled FTIR spectroscopy (LC-Transform), CRYSTAF using a 5.82 micron filter and HTG-HPLC (sections 7.4.5 – 7.4.7). The PE peak at a retention time of 1.6 minutes is lower than the PE standard (M_p = 22000 g/mol). This is expected, given that the M_p of the PE peak (T1), as determined by high temperature GPC, is 1 230 000 g/mol (Table 7.2). Further peaks in the chromatogram show rather a trimodal distribution with no base line separation. No information can be given concerning the composition of these peaks. The reason for this is that the ELSD detector is not selective in the detection of the individual monomers. The presence of low MM PE block can thus not be seen as in the previous analyses.

The chromatogram for T8 appears to be a single peak with different size shoulders on either side of it (Figure 7.20 (C)). The shoulder to the left of the peak is PE homopolymer, which was already shown by other analytical techniques (seen in sections 7.4.5 – 7.4.7). In these analytical techniques it was also seen that the PE hompolymer content is lower in T8 than in T1. The previous findings correspond very well with the LCCC data obtained in that the PE peak is much smaller in T8 than in T1. The shoulder to the right of the peak represents polymers with very high percentages of MMA, thus eluting under critical conditions. In the analysis of T8 with HTG-HPLC coupled to FTIR spectroscopy it was also shown that this sample contains PMMA homopolymer (Figure 7.16 (B)). These results indicate thus that the main peak would mainly consist of Et/MMA block copolymer.

The peaks of samples T9 and T11 in the chromatograms, shown in Figure 7.20 (D), have retention times of 2.4 minutes and 2.2 minutes, respectively. These retention times are similar to the retention times of the low MM PE standard (M_p = 2030 g/mol), but these two samples have a M_ps of 21 100 g/mol (T9) and 18 800 g/mol (T11), respectively, as measured by high temperature GPC (Table 7.2). The great difference in MM between the two samples and the PE standard (Figure 7.20 (A)) suggests that the peaks must contain not only PE homopolymer, but also PMMA. The presence of a block copolymer, as previously suggested, is therefore also confirmed by these data.

7.5 Summary

In this chapter different analytical techniques were used to prove the presence of ethylene/MMA block copolymers synthesised with **2**. ^{1}H NMR spectra were only used to verify that the catalyst **2** synthesises isotactic PMMA. In the ^{13}C NMR spectra no chemical shifts could be observed for the relaxation peaks resulting from the interaction of neighbouring ethylene and MMA units. This means that these carbons are percent in low concentration, thereby excluding the possibility of a random or gradient copolymer.

Standard GPC detection showed that these samples are not homogeneous but rather have a bi- or trimodal distribution. The DSC results also gave an indication that the system was heterogeneous, since the melting temperature of the samples with increasing MMA content shifted towards a lower temperature. T_g could also be observed for samples with high MMA concentration.

Identification of the different peaks in GPC chromatograms could only be made after the use of FTIR spectroscopy as a detector. This detection method revealed that some samples contain PE homopolymer whereas others have PE peaks overlapping the PMMA peaks. Since GPC separation resulted from exclusion (hydrodynamic volume), overlapping peaks in a chromatogram do not prove that the two compounds (ethylene and MMA) are block copolymers.

Standard CRYSTAF runs showed that some samples had $T_{c\,(CRYSTAF)}$ at temperatures of PE homopolymers and others had a crystallisation peak at lower temperature. By using a 5.82 micron filter as a detector, the presence of MMA could be detected in the crystallisation peaks at lower temperature. This proved the formation of block copolymers since only the PE part of an ethylene/MMA block copolymer can crystallise.

High temperature gradient HPLC and high temperature LCCC also proved that some samples contain PE homopolymers and that all samples contain block copolymer. Furthermore, GPC coupled to FTIR, CRYSTAF (using an 5.82 micron filter), HTG-HPLC and HT-LCCC all gave the same results regarding the samples analysed, thus

showing that the samples were correctly analysed. A second point to be noted is that the results obtained from the two newly developed techniques HTG-HPLC and HT-LCCC corresponded well with the results of the analyses of the other two techniques. This showed that these new techniques could be used for the separation and identification of these types of copolymers.

Sample T1 contained large amounts of high MM PE homopolymer and only low concentration of block copolymer. The PE block length in T1 was relatively short, as seen from the low crystallisation temperature. T8 also contained both PE homopolymer and block copolymer. In T8 the PE block length was longer then all other samples when comparing the $T_{c\ (CRYSTAF)}$. T9 and T11 were quite similar in composition, having no PE homopolymer and only block copolymer. These block lengths were longer than that of T1.

7.6 References

1. Collins S, Ward G, J. Am. Chem. Soc., 1992, **114**, 5460.
2. Frauenrath H, Balk S, Keul H, Höcker H, Macromol. Rapid. Commun., 2001, **22**, 1147.
3. Frauenrath H, Keul H, Höcker H, *Single component Zirconocene catalysts for the stereospecific polymerization of MMA*. in Organometallic Catalysts and Olefin Polymerization, Ed. Blom R, Follestad A, Rytter E, Tilset M, Ystenes M, 2000, Berlin, Springer Verlag, 97.
4. Yasuda H, Yamamoto H, Yamashita, Yokota K, Nakamura A, Miyake S, Kai Y, Kanehisa Y, Macromolecules, 1993, **26**, 7134.
5. Yasuda H, Yamamoto H, Yokota K, Miyake S, Nakamura A, J. Am. Chem. Soc., 1992, **114**, 4908.
6. Collins S, Ward D G, Suddaby K H, Macromolecules, 1994, **27**, 7222.
7. Li Y, Ward D G, Reddey S S, Collins S, Macromolecules, 1997, **30**, 1875.
8. Snyder L R, Kirkland J J, Glajch J L, *Practical HPLC method development*. Second ed, 1997, New York, Chichester, Weiheim, Brisbane, Singapore, Toronto, John Wiley & Sons, Inc.
9. Snyder L, High-performance Liquid Chromatography, 1980, **1**, 207.
10. Snyder L R, Dolan J W, Adv. Chromatography, 1998, **38**, 115.
11. Mori S, J. Appl. Polym. Sci.: Appl Polym. Sym., 1989, **43**, 65.
12. Chang T, Lee H C, Lee W, Macromol. Symp., 1997, **118**, 261.
13. Lee H C, Chang T, Macromolecules, 1996, **29**, 7294.
14. Lee H C, Chang T, Polymer, 1996, **37** (25), 5747.
15. Pasch H, Macrmol. Symp., 1996, **110**, 107.
16. Gorshkov A V, Much H, Becker H, Pasch H, Evreinov V V, Entelis S G, J. Chromatogr., 1990, **523**, 91.
17. Skvortsov A M, Gorbunov A A, J Chromatogr., 1990, **507**, 487.
18. Bovey F A, Acc. Chem. Res., 1968, **1**, 175.
19. Schilling F C, Bovey F A, Bruch M D, Kozlowski S A, Macromolecules, 1985, **18** (7), 1418.
20. Ferguson R C, Macromolecules, 1969, **2** (3), 237.

21. Grant D M, Paul E G, J. Am. Chem. Soc., 1964, **86**, 2984.
22. Grohens Y, Hamon L, Carriere P, Holl Y, Schultz J, Mat. Res. Soc. Symp., 2000, **629**, 171.
23. Kim J J, Jung S D, Hwang W Y, ETRI Journal, 1996, **18** (3), 195.
24. Chanunpanich N, Ulman A, Strzhemechny Y M, Schwarz S A, Janke A, Braun H G, Kratzmüller T, Langmuir, 1999, **15**, 2089.
25. Subramaniam C, *Morphology, crystallization and melting behaviors of random copolymers of ethylene with 1-butene, 1-pentene and 1-hexene*. Chapter 7, Ed. Thesis P, 1999, Virginia, Virginia Polytechinc Institute & State University, 199.
26. Pasch H, Brüll R, Wahner U, Monrabal B, Macromol. Mater. Eng., 2000, **279**, 46.
27. Monrabal B, J. Appl. Polym. Sci., 1994, **52**, 491.
28. Monrabal B, International GPC Symp., 1996, **San Diego**, 415.
29. Lyons J W, Poche D, Wang F C-Y, Smith P B, Adv. Mater., 2000, **12** (123), 1847.
30. Teramachi S, Sato S, Shimura H, Watanabe S, Macromolecules, 1995, **28**, 6183.
31. Glöckner G, J. Appl. Polym. Sci.: Appl. Polym. Sym., 1989, **43**, 39.
32. Lewis J J, Rogers L P, Pauls R E, J. Chromatogr., 1983, **264**, 339.
33. Glöckner G, Stickler M, Wunderlich W, J. Appl. Polym. Sci., 1989, **37**, 3147.
34. Pasch H, Brinkmann C, Gallot Y, Polymer, 1993, **34** (19), 4100.
35. Pasch H, Zammert I, J. Liquid Chrom., 1994, **17** (14&15), 3091.

CHAPTER 8

Conclusions

8.1 CRYSTAF

CRYSTAF is a new technique for the analysis of semi-crystalline polymers. The analysis speed and the quality of data obtained were better than could be achieved with TREF. By changing the instrumental parameter settings for the analysis of standard samples it was found that the only instrumental parameter that influenced the $T_{c\,(CRYSTAF)}$ was the cooling rate. The amount of sample tared and the solvent used for analysis also changed the $T_{c\,(CRYSTAF)}$. Through the use of PP copolymer samples of known comonomer content, calibration curves could be drawn from which the comonomer content distribution of unknown samples could be determined.

8.2 Copolymers of propylene/higher α-olefins

In the copolymerisation of propylene and higher α-olefins with *i*-Pr(Cp)(9-Flu)$ZrCl_2$/MAO, an increase in stereoerrors with an increase in comonomer concentration was observed by NMR spectroscopy. The chain migration misinsertions increased whereas the reversed enantioface misinsertions remained constant, with incorporation of higher concentrations of comonomer into the copolymer. This increase in stereoerrors came about as a result of the sterical hindrance on the active site of the catalyst centre by the larger comonomer units. ^{13}C NMR spectra and subsequent calculations, proved that these comonomers were randomly distributed throughout the copolymer, with no cluster formation.

On the 2nd heating cycle in the DSC analysis cold crystallisation was observed. This crystallisation peak on heating could be reduced by slower cooling rates. This is the first time that such a process is reported for polyolefins. The phenomenon is a result of thermodynamical incomplete packing of the polymer chains during cooling. Good relationships between the linear decline in the $T_{c\ (CRYSTAF)}$ and the $T_{m\ (DSC)}$ with an increase in the comonomer content was observed for propylene copolymers, thereby showing that the CRYSTAF gives representative results regarding crystallisation.

8.3 Copolymers of ethylene/higher α-olefins

DSC analysis of the ethylene and higher α-olefin copolymers, synthesised with $Et(Ind)_2ZrCl_2$/MAO, showed the usual linear decline in $T_{m\ (DSC)}$ with increase in comonomer concentration. At high comonomer incorporation both heating and cooling curves revealed a second melt- and crystallisation peak, respectively. The occurrence of a second crystallisation peak can thus be related to a secondary crystallisation process after spherulite formation. Linear relationships were also seen here between the $T_{c\ (CRYSTAF)}$, $T_{c\ (DSC)}$ and $T_{m\ (DSC)}$ for the ethylene copolymer series as was seen for the polypropylene copolymers. The entropy effect of polymer chain mobility (dissolution entropy) was used to explain the difference between the 1-decene, 1-tetradecene and 1-octadecene copolymer series for the data obtained by DSC and CRYSTAF. This was done by comparing results obtained from CRYSTAF with DSC. Copolymers with longer comonomer chains per amount of comonomer incorporated require a lower system temperature in CRYSTAF analysis to obtain crystallisation.

Through comparison of various CRYSTAF diagrams of different copolymer series and with knowledge of the reaction conditions, the formation of copolymers with a gradient composition was detected. For the first time the heterogeneity of the metallocene synthesised copolymers was shown by overlaying DSC and CRYSTAF curves. This was done by compensating for the supercooling effect for that solvent by superpositioning the CRYSTAF and DSC (heating and cooling peak) results. This superpositioning of the data illustrated that DSC and CRYSTAF gave similar heating

and cooling profiles. In the coupling of the GPC to a FTIR via LC-Transform, homogeneity regarding the comonomer distribution throughout the MMD curve was observed.

8.4 Block copolymers of ethylene and methyl methacrylate

NMR-spectroscopy showed the expected isotacticity of PMMA prepared with the use of the $Me_2CCpIndZrMe_2/B(C_6F_5)_3$ catalyst system. Through the GPC analysis it was seen that the PMMA polymerisation was terminated before completion of the chain growth reaction. MMD chromatograms with di- and trimodal distribution, as well as shifts in the melting peak to lower temperature in the DSC, gave indication that the samples contain block copolymers. GPC coupled to FTIR via LC-Transform proved that peaks at lower retention time (higher MM) contained only PE homopolymers. It was also detected that ethylene was present in the same region as where the PMMA eluted.

For conclusive proof of the existence of block structures in the samples of ethylene/MMA copolymers, three new methods for high temperature separations were developed. The use of a 5.82 micron filter (for detection of MMA) in CRYSTAF gave a clear indication that MMA was included in the crystalline fraction. The appearance of MMA in the diagram is only possible if the MMA forms part of the block structure. In some samples T1 and T8 PE homopolymer, as seen in GPC coupled FTIR via LC-Transform, were again noted. Separation done by high temperature gradient HPLC (HTG-HPLC) gave chromatograms where the samples were separated into different compounds, thereof the composition could not be determined. Detection by FTIR via LC-Transform revealed the individual composition of these peaks. The homopolymers were thus separated from the block copolymer peaks. As for HTG-HPLC, high temperature liquid chromatography under critical conditions (HT-LCCC) was also a technique invented during the course of my research. Separations were done at the critical point of PMMA in 34.5/65.5 (V/V%) TCB/CH, with PE eluting under size exclusion conditions. Identification of block copolymers and PE homopolymer could also be shown by LCCC.

It was shown by numerous analytical techniques that the $Me_2CCpIndZrMe_2/B(C_6F_5)_3$ catalyst system renders itself suitable for the synthesis of ethylene/MMA block copolymers.

8.5 Recommendations for future studies

The use of a 5.82 micron filter in CRYSTAF for the identification of carbonyl group in other copolymers systems will have endless possibilities. Analysis of the products of oxidation of polyolefins would be one of the fields of interest, especially for industry, since this is of great economic value when manufacturing products for outdoor use.

The HTG-HPLC and the HT-LCCC are both still in the development stages in terms of their separation potential. In both cases separation conditions can be improved through the use of different solvent/non-solvent mixtures and the selection of the type of columns used. Hereafter, the separation of more complex samples could be considered.